NTNU
Norwegian University of
Science and Technology

Analysis of the Systems for Thermal Energy Supply at the Living Lab

Analyse av systemer for termisk energiforsyning ved Living Lab

Stian Johansen Lillevåg

Master of Energy and Environmental Engineering
Submission date: June 2016
Supervisor: Jørn Stene, EPT
Co-supervisor: Hans Martin Mathisen, EPT

Norwegian University of Science and Technology
Department of Energy and Process Engineering

NTNU
Norwegian University
of Science and Technology

Department of Energy
and Process Engineering

EPT-M-2016-79

MASTER THESIS

for

Student Stian Johansen Lillevåg

Spring 2016

Analysis of the Systems for Thermal Energy Supply at the Living Lab

Analyse av systemer for termisk energiforsyning ved Living Lab

Background

The Living Laboratory (Living Lab) is a Norwegian test facility that has been developed within The Research Centre on Zero Emission Buildings (ZEB). The test facility is a single-floor single-family house with a gross volume of approximately 500 m^3 and a heated surface (floor area) of approximately 100 m^2. The passive house or zero energy building has been designed for experimental investigations at different levels of the building envelope, ventilation system, heating systems, PV system and different building equipment. The highly insulated and leak-proof building has been optimized through a set of extensive preliminary simulations.

A 3.2 kW ground-source heat pump connected to a horizontal ground collector, a 4.2 m^2 façade-integrated solar heater panels and electrical heaters cover the demands for space heating, heating of ventilation air and heating of domestic hot water. Space heating is distributed by means of tempered ventilation air, radiators and/or floor heating systems. 48 PV modules with a total installed power of 12.5 kW$_P$ have been installed on the two roofs facing south. In order to maintain an acceptable room temperature during the four seasons, the building has been equipped with an automatic integrated shading system in the window of the living room. A group of windows are equipped with motors to allow automated opening for cross-ventilation (cooling) of the house.

The extensive Data Acquisition (DAQ) system monitors the most important environmental quantities such as indoor air temperature, humidity ratio, pressure and CO_2 concentration as well as outdoor air temperature, humidity ratio, pressure, wind velocity, global solar irradiance on different planes and illuminance. The DAQ also record users patterns and occupants' habits (rooms occupancy, windows/shading systems opening/displacement; use and control of appliances and lighting system), and measures electrical/thermal power/energy use/supply for space heating and heating of ventilation air, distribution of ventilation air, hot water heating, artificial lighting and various electrical appliances. The DAQ also quantifies the solar energy exploitation (PV and solar thermal panels) and electrical power/energy from the grid as well as the efficiency regarding conversion and storage of thermal energy for different applications.

Objective

The main objective is to document the performance for the prevailing thermal energy system in the Living Lab, and to analyse alternative possibly more optimum designs and operational strategies based on a technical/LCC analysis.

The following tasks are to be considered:

1. Presentation of the heating system of Living Lab incl. the extensive monitoring system
2. In-depth analysis of the heating system with special focus on the design, dimensioning, control and performance of the ground-source heat pump system in combination with the solar thermal panels. Measuring data should comprise an important part of the analysis.
3. Suggestions for alternative designs and operation of the heat pump system
4. Recommendations for design, dimensioning and operation for combined heat pump and solar heating systems for single-family houses of passive house or ZEB standard

-- " --

Within 14 days of receiving the written text on the master thesis, the candidate shall submit a research plan for his project to the department.

When the thesis is evaluated, emphasis is put on processing of the results, and that they are presented in tabular and/or graphic form in a clear manner, and that they are analyzed carefully.

The thesis should be written in English and formulated as a research report with summary both in English and Norwegian, conclusion, literature references, table of contents etc. During the preparation of the text, the candidate should make an effort to produce a well-structured and easily readable report. In order to ease the evaluation of the thesis, it is important that the cross-references are correct. In the making of the report, strong emphasis should be placed on both a thorough discussion of the results and an orderly presentation.

The candidate is requested to initiate and keep close contact with his/her academic supervisor(s) throughout the working period. The candidate must follow the rules and regulations of NTNU as well as passive directions given by the Department of Energy and Process Engineering.

Risk assessment of the candidate's work shall be carried out according to the department's procedures. The risk assessment must be documented and included as part of the final report. Events related to the candidate's work adversely affecting the health, safety or security, must be documented and included as part of the final report. If the documentation on risk assessment represents a large number of pages, the full version is to be submitted electronically to the supervisor and an excerpt is included in the report.

Pursuant to “Regulations concerning the supplementary provisions to the technology study program/Master of Science” at NTNU §20, the Department reserves the permission to utilize all the results and data for teaching and research purposes as well as in future publications.

The final report is to be submitted digitally in DAIM. An executive summary of the thesis including title, student’s name, supervisor's name, year, department name, and NTNU's logo and name, shall be submitted to the department as a separate pdf file. Based on an agreement with the supervisor, the final report and other material and documents may be given to the supervisor in digital format.

☐ Work to be done in lab (Water power lab, Fluids engineering lab, Thermal engineering lab)
☒ Field work – study of the technical installation at the Living Lab.

Department of Energy and Process Engineering, 14th January 2016

Olav Bolland
Department Head

Jørn Stene
Academic Supervisor

Research advisor: prof. Hans Martin Mathisen

Preface

This Master's Thesis was written at the Norwegian Univeristy of Science and Technology during the spring semester of 2016. It represents my concluding works at the five year study program *Energy and Environmental Engineering*, and comprises 30 ECTS credits.

I would like to thank my academic supervisor, Jørn Stene, for providing me with an interesting topic, and for insightful guidance and feedback along the way. I would also like to thank my research advisor, Hans Martin Mathisen, for helpful support and advices. A special thanks goes to Torgeir Viking Skiple, for valuable feedback and support during my work on this report.

At last, I would like to express my gratitude towards the employees at the Department of Energy and Process Engineering, who have made contributed in making field measurements and data acquisition possible. In particular, Reidar Tellebon and Inge Håvard Rekstad, for help with external measuring equipment, and Stein Kristian Skånøy, for help with LabVIEW controls.

Trondheim, 22.06.2016

Stian J. Lillevåg

Stian Johansen Lillevåg

Abstract

The main purpose of this Master's Thesis has been to analyze the systems for thermal energy supply at the ZEB Living Lab, at NTNU, Trondheim. The 102 m^2 single-family house is designed and built in accordance with the Norwegian passive house standard, as a *Zero Emission Building*. Efficient utilization of on-site renewable heat sources, such as ground and solar heat, are thus essential means to reach this ambitious goal.

The thermal energy supply system comprises a 3.2 kW ground-source heat pump unit, 4.2 m^2 of south façade-mounted solar panels, a 400 l integrated water tank, including two 3.0 kW back-up heaters, and an hydronic heat distribution system. A combination of theoretical and experimental approaches have been applied in the analyze. Thermal energy and power demands from SIMIEN simulations, resulted in a heat pump power coverage factor of 54 %, at 0/35 °C. Energy coverage factors were 70 % and 85 %, with and without DHW heat supply. Corresponding SPF values were 2.56 and 3.52. Polysun simulations of the solar thermal system gave an annual solar fraction of 0.37, and a value of 0.6 for DHW heating during the summertime.

Results and observations from measurements have revealed a potential for improvement of system operating strategies, performance, design and dimensioning. The heat pump system is designed for alternate operation between space and DHW heating, but is currently incapable of the latter. Direct-acting electricity is thus an important heat producer in the system. The solar thermal system is designed for combined space and DHW heating, but is operated too intermittently to provide significant heat input. Low-temperature solar heating is furthermore prioritized by the integrated water tank, which restricts the potential for high-temperature DHW heating during the summer. Field measurements have shown a significant electric power consumption for operation of pumps. The electric power input to the ground circuit pump, for instance, corresponded to 15 % of the power input to the heat pump compressor. This contributed to a 13.5 % reduction in the heat pump system COP. Replacement of the brine solution is one of the suggested measures to redeem this deficiency.

In order to obtain the energy savings necessary to reach the ZEB goal, it is essential that the electric energy input to pumps and electric heaters is minimized. Meanwhile, the operating time for the heat pump unit and solar thermal system has to be extended. It is also essential that the measuring equipment is fully functional, so that the system energy performance can be documented.

Sammendrag

Formålet med denne masteroppgaven har vært å analysere systemene for termisk energiforsyning av ZEB Living Lab, ved NTNU i Trondheim. Den 102 m^2 store eneboligen er designet og bygget som et *nullutslippshus*, i henhold til kravspesifikasjoner i den norske passivhusstandarden. Effektiv utnyttelse av lokale fornybare varmekilder, som jord- og solvarme, er derfor essensielle tiltak for å nå dette ambisiøse målet.

Systemene for termisk energiforsyning består av en 3,2 kW jordvarmepumpe, 4,2 m^2 solfangere montert på sørvendt vegg, en 400 l integrert varmtvannstank inklusiv to 3 kW varmekolber, og et vannbårent varmeanlegg. En kombinasjon av teoretiske og eksperimentelle framgangsmåter har blitt benyttet gjennom analysen. For varmepumpen har SIMIEN-beregninger av termiske energi- og effektbehov, resultert i en teoretisk effektdekningsgrad på 54 %, ved 0/35 °C. Energidekningsgrader ble beregnet til henholdsvis 70 % og 85 %, med og uten dekning av tappevannsbehovet. Dette ga resulterede SPF-verdier på henholdsvis 2,56 og 3,52. Gjennom simuleringer av solfangersystemet i Polysun®, ble den årlige solfraksjonen estimert til 0,37. For tappevannsoppvarming gjennom sommerhalvåret ble en solfraksjon på 0,6 estimert.

Resultater og observasjoner fra målinger har avdekket et potensiale for utbedring av systemets driftsstrategier, ytelser, design og dimensjonering. Varmepumpesystemet er designet for vekslende drift mellom rom- og tappevannsoppvarming. Sistnevnte er imidlertid ikke funksjonelt på nåværende tidspunkt. Oppvarming av tappevann løses derfor i hovedsak ved hjelp av direktevirkende elektrisitet. Solfangersystemet er designed som et kombinert romoppvarmings- og tappevannsanlegg, men driftes for periodisk til å kunne levere betydelige varmemengder. Videre prioriteres tilskudd av lavtemperatur solvarme i varmtvannstanken, noe som begrenser muligheten for ettervarming av tappevann gjennom sommerhalvåret. Feltmålinger har påvist et betydelig elektrisk effektforbruk til pumpedrift. Eksempelvis trekker brine-pumpen i jordkretsen en elektrisk effekt tilsvarende 15 % av forbruket til varmepumpe-kompressoren. Dette har bidratt til en 13,5 % reduksjon av effektfaktoren til varmepumpe-systemet. Utskifting av frostvæsken er ett av flere foreslåtte tiltak for å rette opp i dette.

For å oppnå de nødvendige energibesparelser som skal til for å nå nullutslipps-målet, er det essensielt at det elektriske energiforbruket til drift av pumper og varmekolber minimeres. Samtidig må det gjøres tiltak for å utvide driftstiden til både varmepumpen og solfangersystemet. Det er også essensielt at alt måleutstyr fungerer som tiltenkt, slik at energiytelsen til anlegget kan dokumenteres.

Contents

Preface i

Abstract ii

Sammendrag iv

List of Figures xiii

List of Tables xvii

Nomenclature xix

1 Introduction 1
- 1.1 Background 1
- 1.2 Objectives 3
- 1.3 Limitations 3

2 The Living Laboratory 5
- 2.1 Zero Emission Buildings 5
- 2.2 Architecture and Building Physics 8
- 2.3 Technical Installations 10
  - 2.3.1 Heating and Ventilation 12
  - 2.3.2 Electricity Production 13
  - 2.3.3 Monitoring and Control 14

3 Residential Heat Pump Technology 15
- 3.1 System Solutions 15
  - 3.1.1 Air-to-water 16
  - 3.1.2 Exhaust air-to-water 16
  - 3.1.3 Brine-to-water 18
- 3.2 Ground Collector Systems 19
  - 3.2.1 Vertical Ground Heat Exchangers 19
  - 3.2.2 Horizontal Ground Heat Exchangers 22
  - 3.2.3 Aqueous Antifreeze Solutions 25
- 3.3 The Heat Pump Cycle 25
- 3.4 Working Fluids 26
  - 3.4.1 Selection Criteria 26
  - 3.4.2 Synthetic Working Fluids 28

3.4.3 Natural Working Fluids 29
3.5 Components 31
3.5.1 Scroll Compressors 31
3.5.2 Brazed Plate Heat Exchangers 32
3.5.3 Throttling Valves 32
3.5.4 Process Improvements 33

4 Solar Assisted Heat Pump Systems 37
4.1 Solar Energy Potential 37
4.2 Solar Collector Systems 38
4.2.1 Collector Technologies 39
4.2.2 Building Integration and Orientation 42
4.3 Development of Solar Assisted GSHP Systems 44
4.4 Optimal Utilization of Solar Heat in GSHP Systems 46
4.4.1 Thermal Depletion and Recharging 47
4.4.2 Operation Strategies 48
4.5 Key Design Parameters for the Multikomfort ZEB 49

5 Thermal Energy Supply at the Living Laboratory 53
5.1 Heat Pump Circuits 53
5.1.1 Ground Source Heat Pump Unit 53
5.1.2 Ground Collector Circuit 55
5.2 Solar Thermal Circuit 56
5.3 Heat Accumulation and Storage 57
5.4 Heat Distribution 59
5.4.1 Primary Circuit 59
5.4.2 Secondary Circuit 60
5.5 Monitoring and Data Acquisition 60
5.5.1 Thermal Energy Metering in Hydronic Circuits 62
5.5.2 Thermal Energy Metering in Brine Circuits 63
5.5.3 Electric Energy Metering 63
5.5.4 Temperature Metering in the Main Ventilation Ducts 63
5.5.5 Temperature Metering in the Integrated Water Tank 64
5.5.6 Indoor Environmental Quantities 64
5.5.7 Outdoor Environmental Quantities 64

6 Analytical Approach 67
6.1 Operation and Control 67
6.2 Performance and Control 69
6.2.1 GSHP System 69
6.2.2 Heat Pump Cycle 71

6.2.3 STC System 73
6.3 Design and Dimensioning 75
6.3.1 GSHP System 75
6.3.2 STC System 76

7 Thermal Power and Energy Demands 79
7.1 Gross vs. Net Power Demand 79
7.2 Domestic Hot Water Demand 80
7.3 Simulation Input Data 80
7.4 Calculated Net Thermal Power and Energy Demand 81
7.5 Relating Theoretical and Actual Thermal Demands 83

8 Preliminary Performance and Control 85
8.1 Energy Performance Measurements 86
8.1.1 Driving Factors 86
8.1.2 Energy Supply and Use 87
8.2 SPF Calculations 89
8.3 System Control Strategies 91
8.3.1 GSHP: Space Heating 93
8.3.2 GSHP: Domestic Hot Water Heating 96
8.3.3 STC: Water Heating 97
8.3.4 IWT IEHs: Peak Load Heating 99

9 Complementary Field Measurements 101
9.1 Measuring Devices 101
9.1.1 IMI Hydronics TA-SCOPE 101
9.1.2 Ultraflux UF 801-P 102
9.1.3 Analog Manometers 102
9.1.4 Handheld Analog Refractometer 103
9.2 Test 1 and 2: GSHP and STC Performance 104
9.2.1 Test 1: GSHP Standalone Operation 104
9.2.2 Test 2: GSHP and STC Combined Operation 108
9.3 Test 3 and 4: IWT and STC Performance 112
9.3.1 Test 3: IWT Discharging 112
9.3.2 Test 4: STC Standalone Operation 114
9.4 Summary of Measurements 116
9.5 Error Sources and Comments 119

10 System Design and Dimensioning 121
10.1 GSHP Power and Energy Coverage Potential 121
10.2 GSHP Unit 123

10.2.1 Cycle Comparison with Alternative Working Fluids 126
10.3 Ground Collector Circuit 128
10.4 Hydronic Heat Accumulation and Distribution 132
10.4.1 Space Heat Accumulation Tank 132
10.4.2 Hydronic Heating System 134
10.5 Actuators 135
10.5.1 Circulator Pumps 135
10.5.2 Modulating Valves 137
10.6 Solar Thermal Circuit 138
10.6.1 Energy Coverage Potential 138
10.6.2 Heat Accumulation 142
10.7 Domestic Hot Water Tank 145

11 Suggested Improvements **147**
11.1 Alternative Operation 147
11.1.1 GSHP 147
11.1.2 STC 148
11.1.3 IWT: Peak Load Heating 149
11.1.4 Seasonal System Operation 150
11.2 Alternative Designs 152
11.2.1 Heat Pump Unit 152
11.2.2 Ground Collector Circuit 153
11.2.3 Heat Distribution System 154
11.2.4 Solar Thermal System 155
11.2.5 Monitoring and DAQ System 156

12 Recommendations for Future Installations **159**
12.1 System Design and Dimensioning 159
12.2 System Operation 161
12.3 Comments 161

13 Conclusions **163**

Bibliography **165**

Appendices **173**
A Thermal System Monitoring and Control 174
B Calorex WW3500 Ground Source Heat Pump 176
C OSO Hotwater Optima Triple Coil - EPTRC 400 183
D Working Fluids Comparison 184
E Smedegaard Pump Characteristics 185

F Hewalex KS2000 SP Solar Keymark Certification 186
G Additional Field Measurements 188
H DAQ Measuring Data 192
I Ground Collector Performance 194
J Alternative System Designs 196

List of Figures

2.1 Connections between a Net ZEB and energy grids [1] 6
2.2 Illustration of the Net ZEB balance concept [1] 7
2.3 Exterior view from the south-west corner. 8
2.4 Floorplan of the Living Lab [2] 9
2.5 Flow scheme of the technical installations in the Living Lab [3] 11
2.6 Principle flow scheme of the thermal energy system at the Living Lab [4] . 13

3.1 Illustration of an air-to-water system [5]. 16
3.2 Illustration of an exhaust air/water system [5]. 17
3.3 The Nilan Compact P Geo 3 ventilation, heating and cooling device [6]. . . 18
3.4 Illustration of a vertical ground collector system [5]. 20
3.5 The three system arrangements assessed [7] 21
3.6 Illustration of a horizontal ground collector system [5]. 22
3.7 Vertical temperature profiles at the centre of the surface collector field and in neutral ground [8]. 23
3.8 Measurements are done at 0, 0.1, 0.2, 0.4 and 0.8 m distance from the collector tube, after the heat pump [8]. 24
3.9 Basic vapor compression cycle. 26
3.10 Working principle of the scroll compressor [9]. 31
3.11 Improved heat pump cycle with added DSH, EEV and VSD. 33
3.12 Improved heat pump cycle with added DSH, SGHX, EEV and VSD. 34
3.13 Improved heat pump cycle with added SC, DSH, SGHX, EEV and VSD. . . . 35

4.1 Solar energy on an horizontal surface in January and July, respectively [10]. 37
4.2 Distribution installed solar thermal capacity by type [11]. 40
4.3 Principle drawing of the PV/T modules [12]. 41
4.4 Principle flow scheme of the GEOSOL combined GSHP and STC system [13] 45
4.5 HYSS - Hybrid Solar System operating modes [14]. 46
4.6 Principle flow scheme of the integrated thermal energy system at the Multikomfort ZEB[15, 16] 50

5.1 Principle flow scheme of the Calorex heat pump unit. 54
5.2 Operating range for the scroll compressor. 55
5.3 Principle layout of the horizontal collector circuit. 56

5.4 Cross sectional view of the Hewalex KS2000 SLP solar thermal collector [17]. 57
5.5 Principle flow scheme of the thermal energy system at the Living Lab [4] . 58
5.6 Capacity control of the radiator circuit. 59
5.7 Capacity control of the heating battery. 59
5.8 Capacity control of the floor heating circuits. 60
5.9 Zoning of the underfloor heating circuits. 61

6.1 Principle Calorex GSHP vapor compression cycle. 72

7.1 Net thermal power-duration curve for the Living Lab. 82
7.2 Thermal energy demand of the Living Lab relative to the prevailing standards. 83

8.1 Thermal heat recovery efficiency during the second DAQ period. 87
8.2 Comparison of electrical energy use. 88
8.3 Principle flow-scheme of the thermal energy system. 92
8.4 TEA closing valve positions during testing. 94
8.5 Heat pump operation during testing. 95
8.6 Modulating valve positions during testing. 96
8.7 DHW temperature and flow development during testing. 97
8.8 Variation of the STP inlet and outlet temperatures during testing. 98
8.9 Temperature development in the IWT during testing. 99

9.1 Setup of volumetric flow meters. 102
9.2 Manometer measurements. 103
9.3 Handheld refractometer used to determine the PG concentration. 103
9.4 Brine circuit temperature and flow development - Test 1. 105
9.5 Water circuit temperature and flow development - Test 1. 105
9.6 COP development - Test 1. 107
9.7 Relative energy saving potential - Test 1. 107
9.8 STC temperature and flow development - Test 2. 108
9.9 Brine circuit temperature and flow development - Test 2. 109
9.10 Water circuit temperature and flow development - Test 2. 109
9.11 COP development - Test 2. 111
9.12 Relative energy saving potential - Test 2. 111
9.13 SHT temperature and flow development - Test 3. 113
9.14 DHWT temperature and flow development - Test 3. 113
9.15 IWT power and energy development - Test 3. 114
9.16 Outdoor environmental quantity development - Test 4. 115
9.17 STC temperature and flow development - Test 4. 116

9.18 STC power and energy development - Test 4. 117

10.1 Theoretical energy coverage at t_{w-o} = 35 °C. 122
10.2 Principle flow scheme of the Calorex heat pump unit. 124
10.3 Overall volumetric efficiency curves for the R407C compression process. . 125
10.4 Overall isentropic efficiency curves for the R407C compression process. . 126
10.5 Hydrodynamic and thermodynamic performance of the collector tube. . . 131
10.6 Ground collector circuit during the second DAQ period. 132
10.7 Capacity control of the floor heating circuits. 135
10.8 Illustration of the Smedegaard Magneta circulation pump [18]. 136
10.9 Flow direction of the Siemens 2-port and 3-port valves. 137
10.10 Schematic drawing of the Polysun model. 139
10.11 Solar thermal energy coverage potential. 140
10.12 Solar fraction at different panel areas. 141
10.13 Solar fraction at different panel tilt angles. 141
10.14 Outdoor environmental quantities during the second DAQ period. 143
10.15 STC operation during the second DAQ period. 144
10.16 STC heat input to the IWT during the second DAQ period. 144

11.1 EV5 condition before and after 6 weeks of operation. 154

1 Relative thermophysical properties of subcritical working fluids. 184
2 Pump characteristics for the Magneta circulation pumps. 185
3 Circulator pump power use: 2x 60 min test. 188
4 Brine circuit temperature and flow development: 0 - 60 min. 189
5 Water circuit temperature and flow development: 0 - 60 min. 189
6 COP development: 0 - 60 min. 190
7 Brine circuit temperature and flow development: 60 - 120 min. 190
8 Water circuit temperature and flow development: 60 - 120 min. 191
9 COP development: 60 - 120 min. 191
10 Principle flow-scheme of system design option 1. 197
11 Principle flow-scheme of system design option 2. 198

List of Tables

2.1 ZEB definitions as given by The Research Centre on Zero Emission Buildings [19]. 7
2.2 Properties of building envelope components [2]. 9

3.1 Overview of some low-capacity ground source heat pump units. 19
3.2 Thermophysical properties at -10 °C freezing point and 0 °C operating temperature. 25
3.3 Overview of local safety classifications and environmental properties. 27

4.1 Relative effect of change in design parameters [15] 51

5.1 WW3500 performance data at 0 °C brine inlet temperature. 54
5.2 Overview of underfloor heating circuits and zones. 61
5.3 Overview of thermal energy meters and connected sensors. 62
5.4 Indoor temperature control sensors. 64

6.1 Parameters addressing system performance. 69
6.2 Parameters addressing system design and dimensioning. 75
6.3 Recommended dimensioning of solar thermal systems for single-family houses [20, p. 138]. 76

7.1 Overview of building performance input data [21, 22, 2] 80
7.2 Overview of net specific power and heat gain input data [23] 81
7.3 Calculated thermal energy and power demand. 82
7.4 Comparison of calculated and measured energy use at Miljøbyen Granås. 83

8.1 Quantities governing the thermal energy use. 86
8.2 Energy use during the selected DAQ periods. 88
8.3 SPF input data at different system boundaries. 89
8.4 SPF values at different system boundaries. 90
8.5 Overview of sensors used for the preliminary control scheme. 91
8.6 Overview of floor heating zones, control sensors and valves. 94

9.1 External measurements and readings - Test 1. 106
9.2 DAQ system recordings - Test 1. 106
9.3 Performance measurements - Test 1. 107
9.4 External measurements and readings - Test 2. 110
9.5 DAQ system recordings - Test 2. 110

9.6 Performance measurements - Test 2. 112

10.1 Heating capacities for the WW3500 at different operating conditions. . . . 122
10.2 Theoretical performance of the GSHP system. 123
10.3 Comparison of cycle characteristics for alterneative working fluids. 127
10.4 Thermophysical properties of propylene glycol-water. 128
10.5 Collector tube properties. 129
10.6 Intermittency of operation for the GSHP. 134
10.7 Overview of circulator pumps. 136
10.8 Overview of actuator valves in the system. 137
10.9 Hewalex KS 2000 series technical data. 140
10.10 Annual SF for 1 to 7 panels mounted at 90°. 141
10.11 Annual SF for 2 panels mounted at 0 to 90 °. 142

1 External measurements and readings - 2x 60 min test. 188
2 DAQ recordings - 2x 60 min test. 189
3 Performance measurements: 2x 60 min test. 189
4 Average temperatures and total circulated volumes. 192
5 Outdoor and indoor thermal environment. 193

Nomenclature

Latin Letters

Q	Thermal energy	kWh
E	Electric energy	kWh
$\dot{Q}$	Thermal power	kW
$\dot{E}$	Electrical power	kW
$\dot{W}$	Work input	kW
P	Power	kW
c_p	Specific heat capacity	kJ/kgK
C_p	Specific heat capacity	$kWh/(dm^3K)$
k	Thermal conductivity	W/mK
L	Length	m
p	Pressure	bar
U	Overall heat transfer coeffcient	W/m^2K
Re	Reynolds number	-
Pr	Prandtl number	-
$\dot{m}$	Mass flow rate	kg/s
$\dot{V}$	Volumetric flow rate	m^3/s

Greek Letters

ρ	Density	kg/m^3
μ	Dynamic viscosity	kg/ms
η	Efficiency	-
λ	Conductivity	W/mK

Subscripts

b	Brine	-
w	Water	-
i	Inlet	-
o	Outlet	-
C	Carnot	-
vap	Vapor	-

th	Thermal	-
el	Electrical	-
m	Mean	-
a	Ambient	-
aux	Auxiliary	-
C	Condenser	-
E	Evaporator	-
$Comp$	Compressor	-

Abbreviations

ZEB	Zero emission/energy building	-
HVAC	Heating, ventilation and air conditioning	-
GSHP	Ground source heat pump	-
HP	Heat pump	-
STC	Solar thermal circuit	-
STP	Solar thermal panel	-
SCF	Surface collector field	-
PV	Photovoltaic	-
PVR	Photovoltaic roofs	-
DHW	Domestic hot water	-
DHWT	Domestic hot water tank	-
BT	Buffer tank	-
IWT	Integrated water tank	-
IEH	Immersed electrical heater	-
AHU	Air handring unit	-
SH	Space heating	-
SHT	Space heating tank	-
UHP	Underfloor heating panels	-
HTR	High temperature radiator	-
BMV	Balanced mechanical ventilation	-
AWO	Automated windows operations	-
EUA	Electricity use for applications	-
EUO	Electricity use other	-
LLS	LED lighting system	-
MAC	Monitoring and control	-
TEM	Thermal energy meter	-
EEM	Electrical energy meter	-
PEM		-

GWP	Global warming potential	-
ODP	Ozone depleting potential	-
COP	Coeffcient of Performance	-
SCOP	Seasonal Coefficient of Performance	-
SPF	Seasonal Performanc Factor	-
EES	Engineering Equation Solver	-
HX	Heat exchanger	-
VSD	Variable speed drive	-
LMTD	Logarithmic mean temperature difference	-
VHC	Volumetric heating capacity	-

Chapter 1

Introduction

1.1 Background

In Norway, the total annual energy use has grown from 600 to 890 PJ between 1976 and 2013 [24]. The 50 % increase is largely a result of economic, as well as population growth. 40 % of the total national use is allocated to the building sector, of which 22 and 18 % points are ascribed to residential and non-residential buildings, respectively [25]. In 2012 the total energy use in the Norwegian household sector amounted to 48 TWh. This energy quantity is allocated between energy carriers as 38 TWh electricity, 8 TWh firewood and 1 TWh fuel oils. As a mountainous country with large hydroelectric resources, the Norwegian energy market is characterized by a strong dependency on high-quality electrical energy. Measured per capita, Norway is the worlds second largest electricity user, and at 23 700 kWh this is almost three times higher than the OECD average [24].

The most common combinations of heating technologies in Norwegian dwellings include direct electrical equipment, alone or in combination with heat pumps and/or wood burning stoves [26]. Positive opinions regarding the environmental benignity of electrical heating may explain why electrical space heating still is the primary solution in households. In recent years, however, regulatory requirements, informational campaigns, subsidies, as well as cost and income levels has initiated a shift in the type of heating equipment.

In the Norwegian household sector the prevalence of air-to-air heat pump installations have grown from 3 % in 2004 to 24 % in 2012 [26]. The corresponding statistic for brine-to-water installations is less drastic, with an increase from 1 to 4 % between 1997 and 2012. The share of households with ventilation air heat recovery equipment has increased from 5 % in 2006 to 9 % in 2012. Meanwhile, the share of electrical heating equipment has been stable around 97 % between 1993 and 2012. The transition from electrical heating to more efficient solutions thus appear to be reluctant.

The 20/20/20 goals of the EU aim for a collective reduction in CO_2 emissions and primary energy use of 20 % within 2020. During the same period, the renewable energy share shall be increased by 20 %. The abundance of hydro-electric energy has resulted in a 94.8 % renewable energy share in the Norwegian building sector [27]. Hence, the potential for a further increase is limited. The potential for improved energy efficiency, however, is significant.

The recast of the EU Directive on Energy Performance of Buildings (EPBD) has established the *nearly Zero Energy Building* (nZEB) as the building target from 2018 for all non-residential buildings. Within the end of 2020, this target is also extended to residential buildings [28]. Buildings codes of the future specifically aim to eliminate the net energy use in buildings, or even obtain a positive balance. Improvements to the building envelope are nevertheless not sufficient to reach this goal. Hence, systems for on-site energy utilization and efficient coverage of the thermal energy demands become increasingly important.

Realizing such projects require the use of innovative and smart technologies, that have not been widely implemented in the residential buildings of today. Hence, test projects have been initiated in several European Countries. One example is The Living Laboratory in Trondheim, Norway. This is a residential test facility, realized as a collaborative project between The Research Centre on Zero Emission Buildings and NTNU/SINTEF [29].

The Living Lab is a single floor single-family house, with a heated air volume and floor area of approximately 450 m^3 and 100 m^2, respectively. The building is designed and built according to the Norwegian passive house standard [22], and is thus characterized by a highly insulated and leak-proof building envelope. Heat recovery rates of ~85 % are achieved by means of a rotary heat wheel, and balanced mechanical ventilation. Thermal energy supply for ventilation, space and domestic hot water heating is covered by means of a combined ground-source heat pump and solar thermal system. Peak load heating is covered by electrical heaters.

The 3.2 kW heat pump is coupled with a horizontal ground heat exchanger, and the solar thermal system integrates 4.2 m^2 façade-mouted solar collectors. Space heat is distributed by means of an hydronic system, which combines a ventilation heat exchanger, a single radiator and eight underfloor heating circuits. On-site electricity production is achieved by means of 48 roof-mounted PV modules, with a total installed power of 12.5 kW_p. The current report deals with experiences related to design, dimensioning, operation and performance of the combined heat pump and solar thermal system at the Living Laboratory.

1.2 Objectives

The main objectives of this master thesis are summarized as following:

- To investigate the design and dimensioning of the prevailing thermal energy system at the Living Laboratory, and to assess its performance experimentally from measuring data. The potential for renewable thermal energy coverage shall be assessed theoretically.

1.3 Limitations

The major limitations imposed on this assessment are as following:

- The heat pump system was put into operation on March 18, and operated during the residual part of the heating season. As a result, it has not been possible to perform measurements on the heat pump during the least ideal conditions. Furthermore, as the heat extraction from the ground during the measuring period has been considerably lower than what is expected for the winter period. This means that the temperature decline in the ground has been modest, yielding unrealistically high evaporator inlet temperatures and thus higher COP values.

- The detail level and accuracy of energy measurements is limited due to a partially flawed or inoperable functionality of the monitoring and control system. Specifically, the thermal energy meters in the heat pump and domestic hot water circuits (TEM1 and TEM2) have been inoperable. This is a result of flawed configuration or communication with the DAQ system.

- The detail level and accuracy of solar circuit energy measurements is limited due to partially flawed communication between the flow meter (EFS2) and the DAQ system. This problem was not resolved until early May.

- Communication errors between the monitoring and DAQ systems have resulted in a significant prevalence of corrupted log files. This has put limitations on relevant log data for the analysis.

- Automated switching between heat pump space and DHW heating modes is currently not operational. Operation of the heat pump is thus limited to space heating mode only.

- Thermal energy supply from the combined heat pump and solar thermal system is the main focus of this report. Systems for electrical power supply and generation, as well as monitoring and control are thus briefly discussed, but not devoted a detailed analysis.

Chapter 2

The Living Laboratory

2.1 Zero Emission Buildings

The Living Laboratory has been designed as a *Zero Emission Building* (ZEB). This is a topic which, despite a lack of internationally consistent definitions, has gained increasing attention in recent years. As a partial solution for the mitigation of CO_2 emissions and reduced energy use in the building sector, the *Zero Energy Building* (ZEB) is now considered a realistic target for future building design internationally [30]. The recast of the EU Directive on Energy Performance of Buildings (EPBD) has established the *nearly Zero Energy Building* (nZEB) as the building target from 2018 for all buildings that are either publicly owned or occupied by public authorities, and by December 31^{st} 2020 for all new buildings in general [28]. It is the responsibility of the member states to draw up plans for increasing the number of nearly zero energy buildings.

Evidently, the term ZEB has been used commercially without consistent definitions in place, and countries are enacting policies and national targets without a clear understanding of the concept [1]. Still, there is a general understanding of a ZEB as an energy efficient building capable of local energy generation, primarily electricity, to compensate for its demand. While the term ZEB is general and may include off-grid autonomous buildings, the term Net ZEB can be used to refer to grid-connected buildings that maintain a balance between the energy taken from and supplied back to the grid over a period of time [1, 30]. Grid connected ZEBs enable the possibility to exploit local renewable energy sources, and to feed surplus electric energy from on-site generation to the grid. This strategy contributes to an increase in the share of renewable energy in the grid, and thereby reduces carbon emissions associated with resource consumption, such as fossil fuel combustion.

Sartori et al.[1] defines the Net ZEB balance as satisfied when weighted supply meets or exceeds weighted demand over a period of time. In this context the *supplied* energy refers to the electric energy fed *to* the grid *from* the building. This balance can be determined with respect to one of two system boundaries, known as the delivered/exported balance and the load/generation balance. The broader the system boundary, the stricter the requirement. For instance, by using the delivered/exported balance, the efficiencies of building systems are counted in. Fig.2.1 illustrates the building system boundary in relation to the grid.

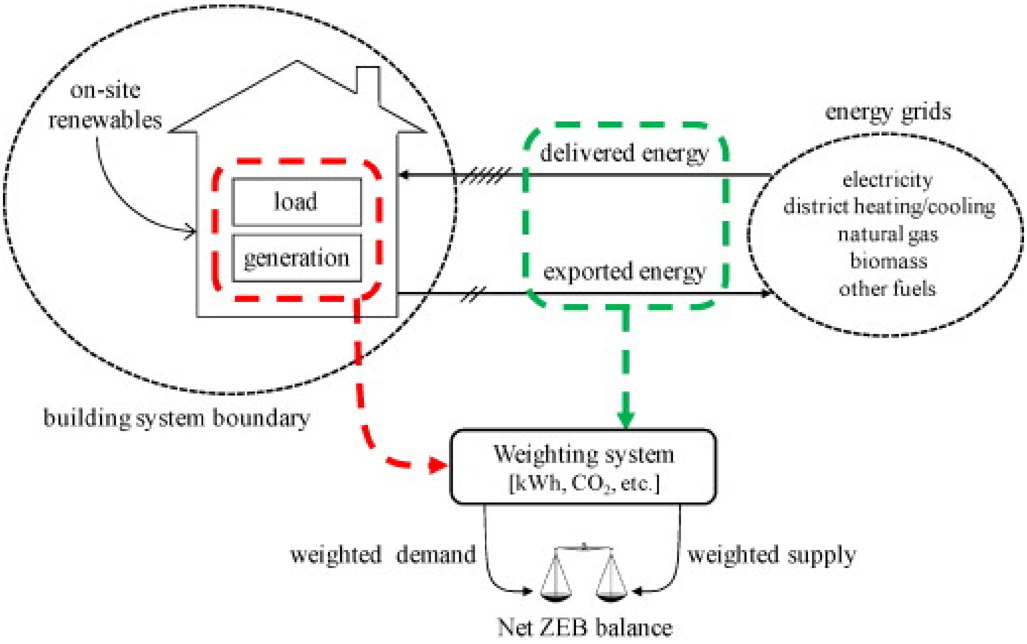
on-site
renewables
load
generation
building system boundary
delivered energy
exported energy
energy grids
electricity
district heating/cooling
natural gas
biomass
other fuels
Weighting system
[kWh, CO$_2$, etc.]
weighted demand
weighted supply
Net ZEB balance

Figure 2.1: Connections between a Net ZEB and energy grids [1]

Weighted demand is the sum of the load or all delivered energy, obtained by summing all energy carriers, each multiplied by their respective weighing factors. The same methodology applies to the weighted supply, which is the sum of all generated or exported energy. Using a weighing system it is possible to compare the physical units of different energy carriers and evaluate the entire energy chain. This includes the properties of natural energy resources, and losses associated with the conversion from primary to secondary energy, transmission and distribution. The weighing system may be based on one of several metrics, where energy [kWh] or carbon emissions [kg CO_2] are broadly applied. Depending on the choice of weighing system, the term ZEB may be used to refer to either zero energy buildings or zero emission buildings. The Net ZEB balance is illustrated in fig. 2.2 a compared to that of a reference building, which may be designed according to the minimum requirements of the prevailing building code, for instance TEK10 [21] in Norway. Compared to the ZEB, it is evident that the on-site electricity generation required to compensate for its demand, is much larger for the reference building.

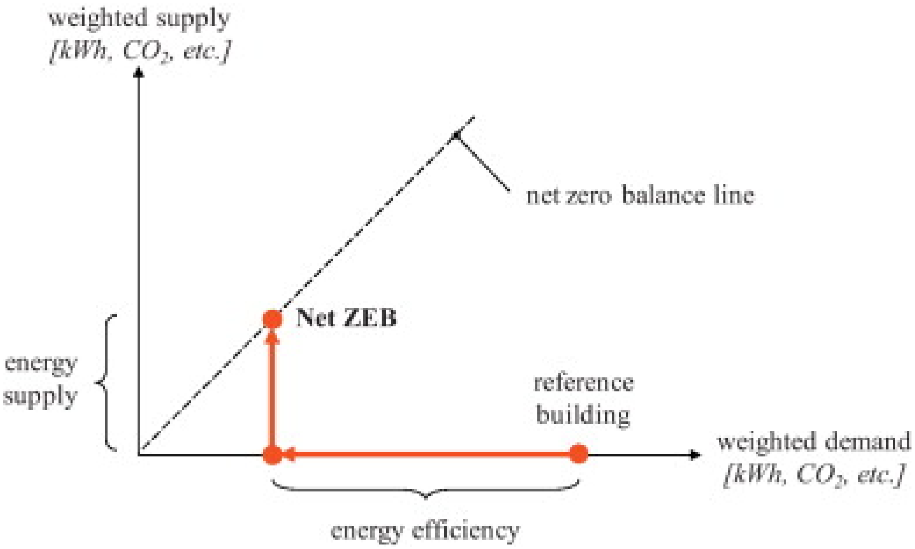

Figure 2.2: Illustration of the Net ZEB balance concept [1]

In Norway, the ZEB definition adopted by the Research Centre on Zero Emission Buildings, is that of a building which produces enough thermal and electric *renewable energy* to compensate for its greenhouse gas emissions during its lifespan [19]. In this relation, a total of five ambition levels have been defined, depending on the scope of which the building's phases of life are included. The prevailing definitions are listed in table 2.1.

Table 2.1: ZEB definitions as given by The Research Centre on Zero Emission Buildings [19].

ZEB Definition	The building's renewable thermal and electric energy production compensate for greenhouse gas emissions from:
O	Operation of the building.
O - EQ	Operation of the building minus the energy use for equipment (plug loads).
OM	Operation and production of its building materials.
COM	Construction, operation and production of building materials.
COMPLETE	The entire lifespan of the building. Building materials, construction, operation and demolition/recycling.

The ZEB Living Laboratory, or Living Lab, in Trondheim, has been designed and built according to the OM ambition level [31]. That is, during its lifespan the building shall produce sufficient amounts of renewable energy to compensate for greenhouse gas emissions from operation and production of its building materials. Carbon emissions related to the construction and demolition phases are not accounted for.

2.2 Architecture and Building Physics

The Living Laboratory is a ZEB test facility within the Research Centre on Zero Emission Buildings at The Norwegian University of Science and Technology, designed to carry out experimental investigations at different levels. These range from investigations on the building envelope to building equipment components, from ventilation strategies to action research where the ways users interact with buildings characterized by high indoor comfort conditions and low energy demand is studied [3]. The exterior of the building is as illustrated in fig. 2.3.

Lab.jpg

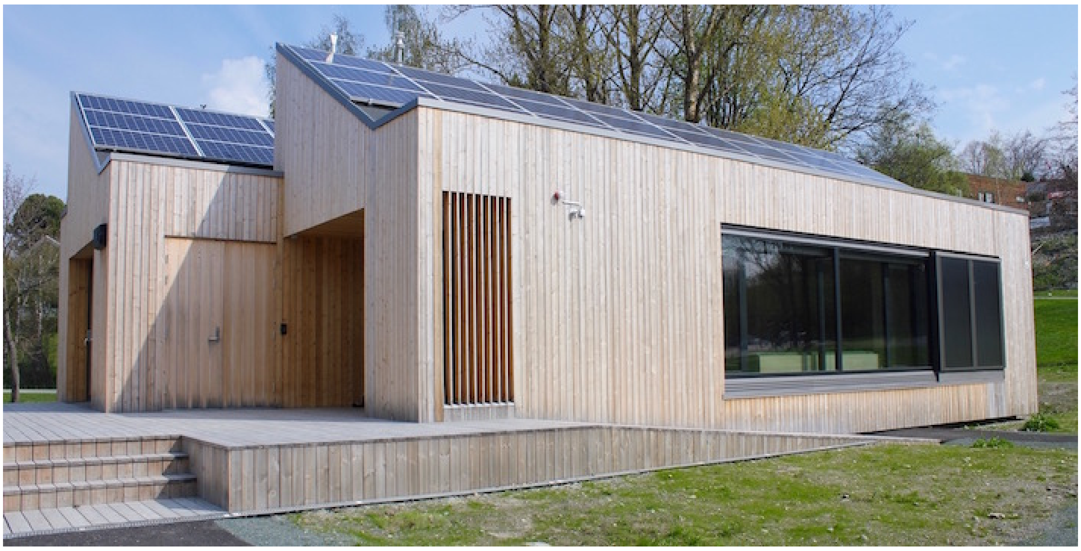

Figure 2.3: Exterior view from the south-west corner.

Initially, the building was designed as an autonomous energy positive mountain cabin, but has later been re-designed as a detached, single-family house, representative of the Norwegian residential building stock. The Living Lab is a single-storey building with a heated floor area of approximately 100 m^2 and a volume of approximately 450 m^3 [2, 3]. The building design is compact but space efficient, and may be regarded as two main zones, divided by the west/east axis running through the center of the building, as shown in fig. 2.4. The south-facing zone includes an entrance/wardrobe at the southwest corner, a bathroom, and a living room connected to the kitchen at the southeast corner. The south façade of the living room integrates a large double skin window for maximum daylight utilization and solar heat gain during the fall, winter and spring. This window also include a vented area for intended use in hybrid ventilation mode, as well as adjustable solar shading to control solar gains during the summertime.

The north-facing zone is characterized as a working/sleeping area, comprising a studio room, which separates the two bedrooms found at each of the north-facing corners

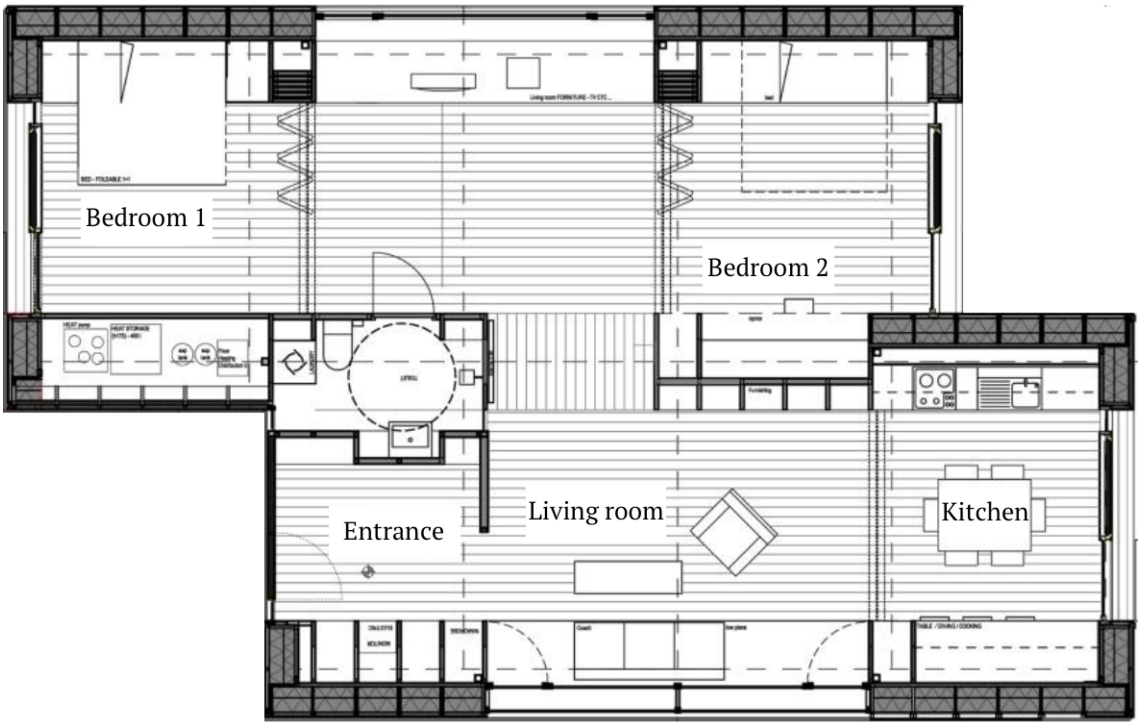

Figure 2.4: Floorplan of the Living Lab [2]

of the building. A small mezzanine is placed above the west bedroom. Additionally, a technical room excluded from the heated area of the building is found at the west end, adjacent to the bathroom. The technical room is accessible from the outside, and is located in the spine of the building, thus optimizing the length of ventilation ducts and the distribution of technical installations in general.

Table 2.2: Properties of building envelope components [2].

U-value wall	W/m^2K	0.11
U-value floor	W/m^2K	0.10
U-value roof	W/m^2K	0.10
U-value windows (south façade)	W/m^2K	0.65/0.69 (when ventilated)
U-value windows (north façade)	W/m^2K	0.97
U-value windows (east-west façade)	W/m^2K	0.80
U-value skylight	W/m^2K	1.0
g-value	-	0.5
Infiltration	ach	0.5
Normalized thermal bridge	W/m^2K	0.03

The building envelope has been designed according to the overall goal of very low transmission and infiltration losses. As a result, the construction components are both highly insulated and air-tight, and comply with the Norwegian requirements for residential buildings of passive house standard, specified in the standard NS3700 [22].

Building envelope properties, as documented by Finocchiaro et al. [2], are listed in table 2.2. The glazed area of the façades constitute approximately 40 % of the heated floor area, and is characterized by low U-values. Both the north and and south-facing windows have automated openings to comply with strategies for hybrid ventilation. The sloped ceilings integrate 90 m^2 PCM-panels, thus reducing the risk of overheating during summertime.

2.3 Technical Installations

Interaction with the external environment is decisive for minimization of the net energy demand and carbon footprint of the building, and ultimately fulfillment of the ZEB O&M ambition. State-of-the-art technologies for energy conservation and renewable exploitation are therefore an integrated part of the building design. In this regard, the monitoring system is a key feature. It records the most relevant indoor and outdoor environmental quantities, the thermal energy supply for space heating and ventilation, as well as the electrical energy supply for lighting and appliances. On-site generation of solar thermal and photovoltaic electrical energy is also monitored.

The monitoring system has been designed to assess the energy and environmental balance of the building, and the interaction between the users and it, according to the relevant technical standards for energy performance and comfort assessments. The primary goal is nevertheless to evaluate the total energy behavior of the building. Measuring data is recorded to an integrated data acquisition and control system. The system can be adapted so that occupants have limited control of building features, while access to more comprehensive control features are available for remote research purposes.

In the following an overview of the major technical building systems is given, while the systems for thermal energy supply are thoroughly described in chapter 5. Fig. 2.5 presents the energy flows for both thermal and electrical systems [3]. The thermal energy systems, indicated by the brighter arrows are henceforth emphasized. The reader is refered to the nomenclature for an overview of the abbreviations used.

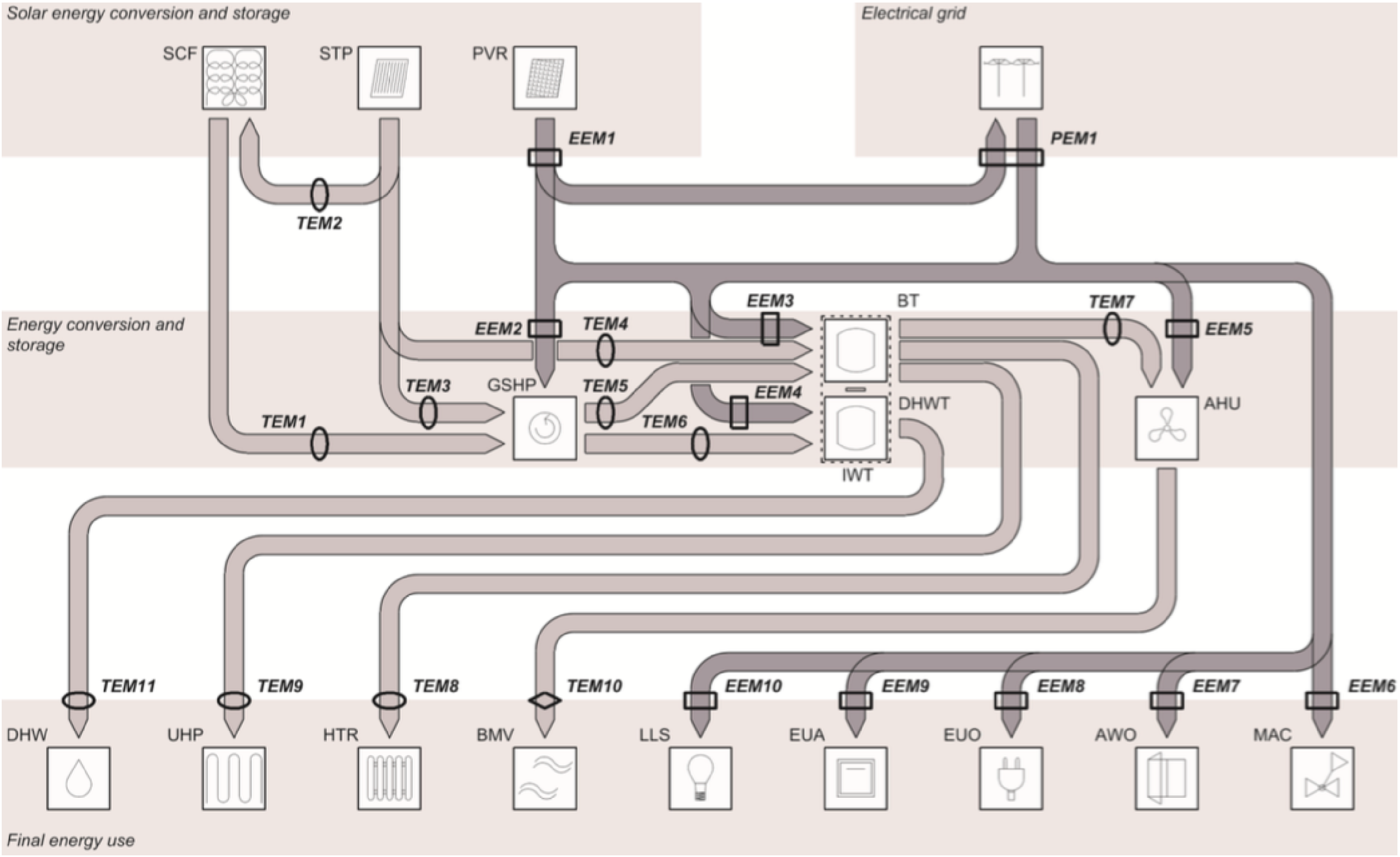
Solar energy conversion and storage
Electrical grid
SCF
STP
PVR
EEM1
PEM1
TEM2
Energy conversion and storage
EEM2
TEM4
EEM3
BT
TEM7
EEM5
TEM3
GSHP
TEM5
EEM4
DHWT
AHU
TEM1
TEM6
IWT
TEM11
TEM9
TEM8
TEM10
EEM10
EEM9
EEM8
EEM7
EEM6
DHW
UHP
HTR
BMV
LLS
EUA
EUO
AWO
MAC
Final energy use

Figure 2.5: Flow scheme of the technical installations in the Living Lab [3]

2.3.1 Heating and Ventilation

The systems for thermal energy supply at the Living Lab are designed with the aim to cover the majority of the thermal energy demand by means of renewable energy. A 3.2 kW **ground source heat pump** (GSHP) is installed to cover the demands for space heating, heating of ventilation air and production of domestic hot water (DHW). The heat pump is coupled to a horizontal surface collector field (SCF), located on the north side of the building.

A **solar thermal system** is installed in combination with the GSHP system. It comprises 4.2 m^2 south façade-mounted solar thermal panels (STP). The solar thermal circuit (STC) is designed primarily to cover space heating and DHW requirements. Solar heat is delivered to, and accumulated in, an **integrated water tank** (IWT), by means of a coil in the bottom section. The solar thermal system is additionally coupled to the GSHP collector circuit by means of a 0.18 m^2 brazed plate heat exchanger (BPHX). This design enables alternative utilization of the solar heat.

The 400 l IWT comprises a 160 l **space heating buffer tank** (BT/SHT) and a 240 l **DHW storage tank** (DHWT). In addition to the STC coil, the BT also accommodates a coil for DHW preheating, as well as a 3 kW **immersed electrical** heater (IEH). The DHWT integrates a large HP-coupled reheat coil, and an additional IEH. Fig. 2.6 shows the principle layout of the system with connections to the IWT.

The hydronic system has been designed for both low-temperature heat distribution via **underfloor heating circuits**, and medium/high temperature heat distribution via a **wall-mounted radiator** and **ventilation heat exchanger**. This facilitates distinct strategies for space heating, that are likely to affect both thermal efficiency and comfort. Two main strategies for heat distribution have been projected:

1. Low-temperature heat distribution via the living room, bedrooms and bathroom underfloor heating circuits.
2. A combination of low- and medium/high-temperature heat distribution via bathroom underfloor heating circuit, and the wall-mounted radiator.

Fresh air supply is achieved by means of **balanced mechanical ventilation system**. In accordance with the Norwegian standard NS3031 [23], the nominal capacity is set to 120 m^3/h, corresponding to approximately 1.2 m^3/m^2h [2]. The air handling unit (AHU) has a maximum capacity of 360 m^3/m^2h. Fresh air is supplied via diffusers in the living room, studio room and in the bedrooms at either sides. Extracts are located in the kitchen and in the bathroom. The latter account for the majority of the extracted

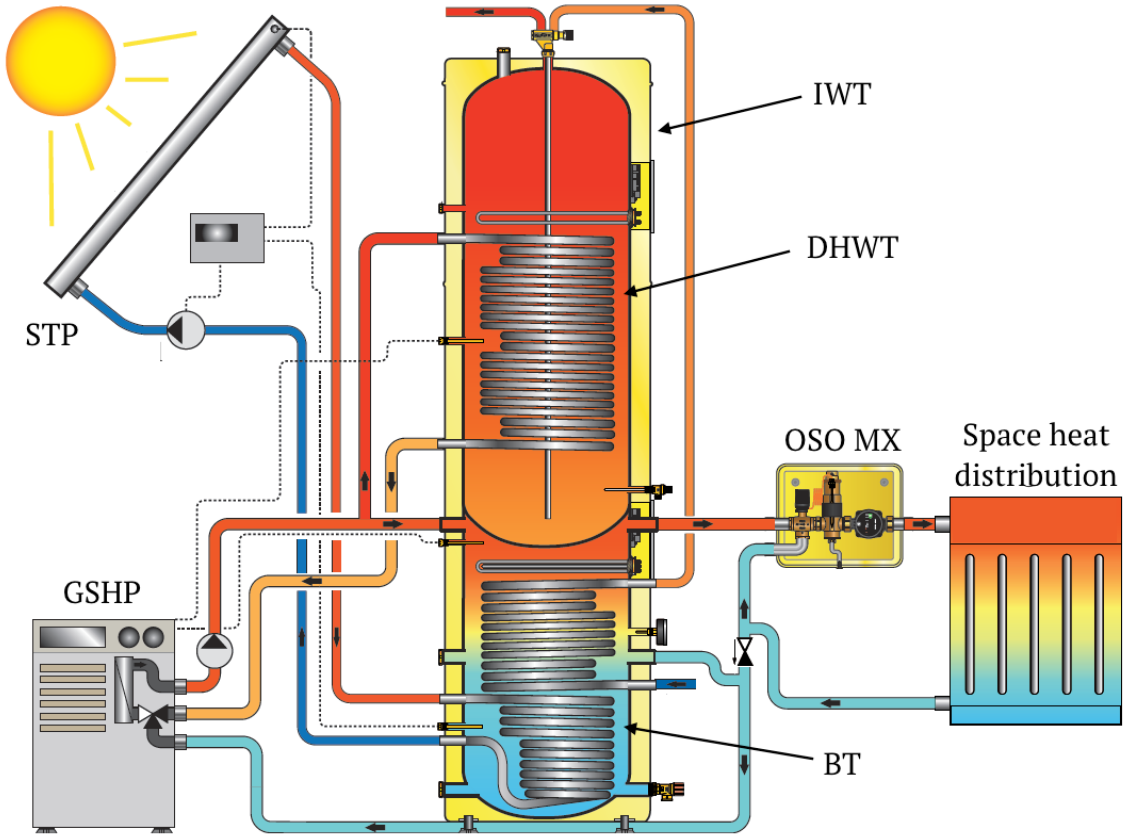

Figure 2.6: Principle flow scheme of the thermal energy system at the Living Lab [4]

air. The AHU integrates a rotating heat recovery wheel, with a nominal thermal efficiency of 85 %. Two main strategies for heating of the supply air have been projected:

1. Direct electrical heating via a 1.2 kW electric coil. The coil has a temperature limitation of 40 °C.
2. Hydronic heating by means of a 2.5 kW heat exchanger.

Both options are limited to sensible heat control, meaning that it is not possible to control the relative humidity of the supply air. The combined heating capacity of these units facilitate space heating via overheated supply air as a third option.

2.3.2 Electricity Production

As part of reaching the ZEB goal, the Living Lab integrates a photovoltaic electricity system. The system comprises two photovoltaic roofs (PVRs in fig. 2.5), each with 24 polycrystalline PV modules. The modules are aligned with the roof surface at 30° incline and have a nominal power of 260 W each. Hence, the total installed power is 12.5 kW_p. The nominal output power is specified for standard test conditions (STC), which involve an air mass (AM) of 1.5, an irradiance of 1000 W/m^2 and a 25 °C cell temperature. It is expected, however, that 96 % of the specified efficiency of 16 % is achieved even at an irradiance of 200 W/m^2 [2]. Power conversion from DC to AC output is done by means of one inverter connected to each PVR. These have a rated output power of 4.6 kW and an efficiency of 96.5 %. As indicated by fig. 2.5 the PV system is designed to function as power supply for the GSHP, IWT, AHU and other electricity specific appliances in the building.

2.3.3 Monitoring and Control

The monitoring and data acquisition (DAQ) system is designed to collect data for use in various scientific assessments, such as demographical profiles and building energy performance [3]. Room occupancy, opening and closing of windows and doors, as well as use of windows shading systems and electrical appliances are monitored to map **occupants behavior and user patterns**. Indoor environmental quantities, such as air temperatures and relative humidity, CO_2 concentration and diffuse illuminance are monitored, in order to facilitate evaluations of the **indoor climate and thermal environment**.

Outdoor environmental quantities, such as air temperatures, relative humidity, barometric pressure, wind velocity and direction, illuminance, and global solar irradiance are also moitored. The latter is measured on the vertical, horizontal and PV planes, and is directly related to the local energy production from the solar thermal and PV systems.

Building systems energy performance is monitored as thermal energy use for heating, ventilation and production of domestic hot water. This is achieved by means of extensive use of thermocouples, flow sensors and thermal energy meters in the heating plant. Electrical energy meters are used to monitor the electricity use for operation of the heat pump, circulation pumps, actuators and auxiliary heating. Electricity specific energy use for artificial lighting and appliances is also monitored.

Chapter 3

Residential Heat Pump Technology

The next generation of residential passive houses and ZEBs are characterized by a highly insulated building envelope, as well as high efficiency heat recovery. As a result, the thermal power and energy demands to compensate for transmission, infiltration and ventilation heat losses are very low. This means that the equivalent operating time for the heating system is reduced, typically to 5-7 months per year [32, 33]. As a result, the DHW heating demand accounts for a larger share of the total annual heating demand. Experience show that values range between 40 and 85 % in residential buildings, depending on user patterns. Consequently, the strategies for investment, design, dimensioning and operational strategies are heavily affected.

3.1 System Solutions

Residential heat pumps may be characterized by either of three categories, depending on the application for which the seasonal energy efficiency is optimized [34, Chapter 8]:

1. Space heating heat pumps.
2. Heat pump water heaters.
3. Combined space and water heating heat pumps.

For passive house and ZEB buildings the combined solutions are favorable, because the annual heating demand decreases, while the relative DHW demand increases. Cost effective solutions for coverage of the DHW heating, in combination with the space heating demand, thus become more important. Combined systems are henceforth assumed.

Distinctions between the design of the heat collector and heat distribution system may also be used. Specifically, the secondary heat transfer mediums are addressed. Combined systems are preferably coupled with low-temperature hydronic systems, in order to optimize operating conditions [32]. Hydronic heating systems are therefore assumed, making the heat source the only variable.

Typical heat sources for low-capacity residential heat pumps systems include ambient air, exhaust air, bedrock, soil, groundwater, seawater, freshwater and grey water. The main heat source properties are availability and practicality, cost of use, temperature level and stability, thermal conductivity, and specific heating capacity. Jointly due to availability and practicality, costs and thermodynamic system performance, the most interesting alternatives for passive house and ZEB residential buildings include ambient air, exhaust air, bedrock and soil.

3.1.1 Air-to-water

Air source heat pump units are available for combined space and water heating applications, or as pure water heater solutions. These units typically use R410A, R407C, R744 (CO_2) or R290 (propane) as working fluid, and can reach water temperatures in the range of 35-85 °C [32]. Ambient air is the most widely used heat source for residential heat pump systems, largely as a due to low initial investment costs and minimum required effort during installation [35]. Air-source heat pumps are nevertheless affected by reduced heating capacities and COPs at low ambient air temperatures. In general, the heating capacity is in antiphase with the demand. Due to low evaporating temperatures and excessive discharge gas temperatures, full stop at ambient air temperatures below -20 °C should be expected. This reduces the operating time for the heat pump and consequently its energy coverage factor. In terms of DHW production, the conventional heat pumps usually require some top-up electricity heating, which further deteriorate the overall system performance.

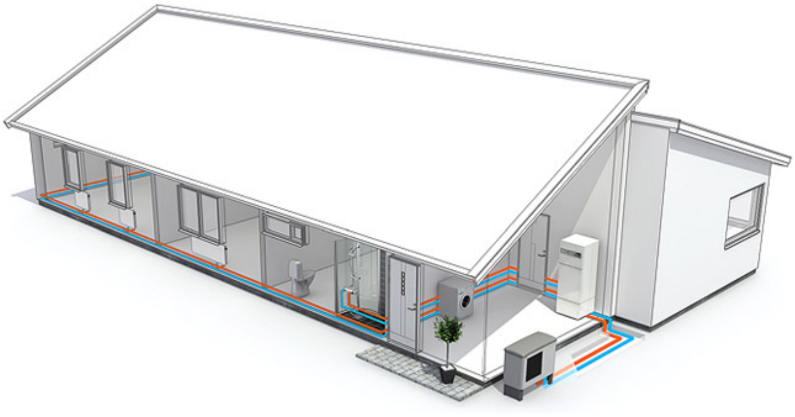

Figure 3.1: Illustration of an air-to-water system [5].

3.1.2 Exhaust air-to-water

Exhaust air heat pumps (EAHPs) can be applied for heat recovery in combination with balanced ventilation, which is an integrated part of the residential passive house and

ZEB design. This is possible by fitting the evaporator in the ventilation exhaust air duct. The heat pump can operate alone, or be combined with a cross-flow heat exchanger for passive heat recovery. EAHPs can provide DHW heating, space heating and heating of ventilation air, and usually apply R410A, R407C or R290 as working fluid. While the exhaust air acts as the primary heat source, ambient air or ground heat may be utilized additionally to increase heating capacity. Due to the low temperatures following the heat recovery unit, this is usually a beneficial solution in such systems. As an optional improvement, the ambient air is passed through a ground/air heat exchanger prior to the heat pump or heat recovery unit. As a result, the intake air temperature can be kept above the freezing point throughout the year, thus improving the heat pump COP or avoiding frosting of the heat recovery unit [32].

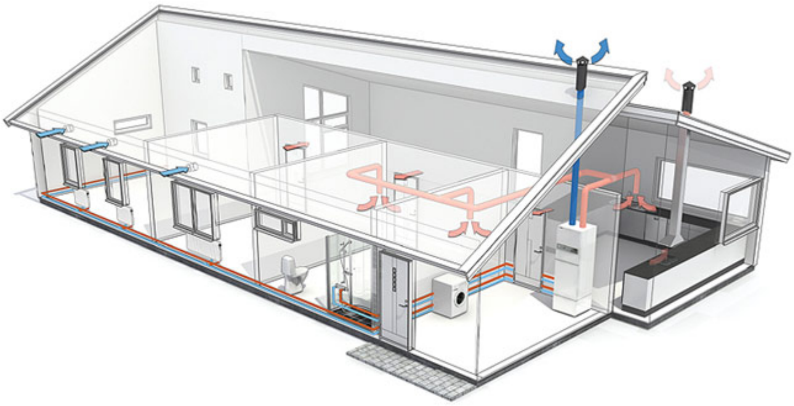

Figure 3.2: Illustration of an exhaust air/water system [5].

An integrated solution for balanced ventilation, DHW heating, space heating and heating of ventilation supply air, is the *combined ventilation and heating device* (CVHD). These units, which are made for high performance residential buildings, include supply and exhaust air fans, a cross-flow heat recovery unit, air filters, an EAHP, a DHWT, and IEHs for water reheating. An example of a CVHD is the *Nilan Compact P* series, which can be adapted for additional heat sources, such as ground heat [6]. A disadvantage of EAHPs in residential passive houses or ZEBs is that the airflow rate and temperature decrease of the exhaust air is relatively limited, thus restricting the heating capacity of these units. An advantage is that these systems, if necessary, can be used for space cooling during the summer.

Fig. 3.3a illustrates as an example, the *Nilan Compact P Geo 3* combined ventilation and heating device (CVHD). This unit combines ventilation with passive and active heat recovery, space heating and cooling, as well as DHW production and storage [6]. The EAHP is mounted after the heat recovery unit as an integrated part of the AHU. Heat recovery is achieved with a counterflow polystyrene heat exchanger, with a nominal thermal efficiency of 85 %. The heat recovery unit is shown in fig. 3.3b.

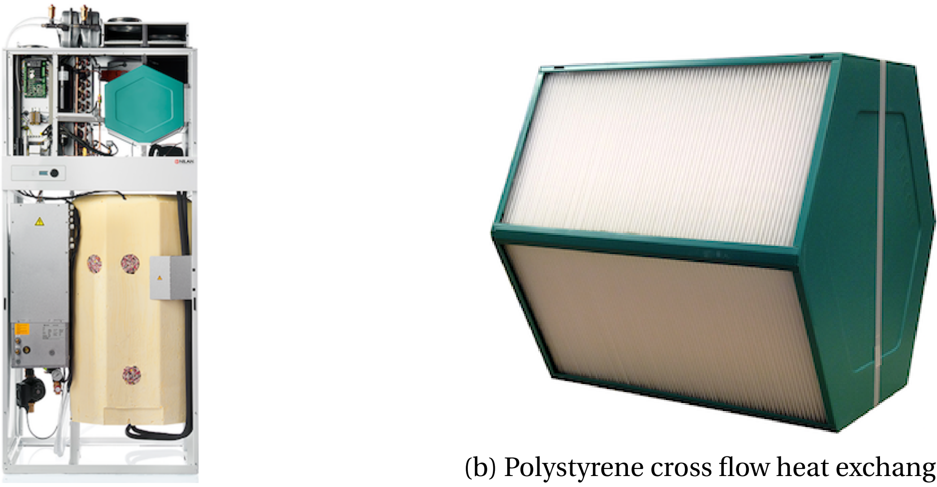

(b) Polystyrene cross flow heat exchanger.

(a) Front view of the integrated unit.

Figure 3.3: The Nilan Compact P Geo 3 ventilation, heating and cooling device [6].

It is charged with 1.1 kg of R410A, and has a nominal heating power of 3 kW (0/35 °C). High performance at off-design conditions is achieved by means of VSD compressor control, which allows step-less capacity control down to 20 %. As a result, a seasonal coefficient of performance (SCOP) of 5.17 is achievable.

3.1.3 Brine-to-water

These systems are characterized by indirect designs, meaning that an antifreeze brine is circulated between the heat source and the evaporator in a secondary circuit. While brine-to-water systems may use seawater or freshwater as heat source, the current presentation include ground source systems. Typically, the soil in the upper layer of the ground, or vertical boreholes are used as heat source. The added complexity of the heat collector system results in higher initial investment costs, compared to air-based systems. An advantage of the extra investment, however, is a higher and more stable temperature level on the heat source. The results are longer possible operating times and a stable heating capacity throughout the year. Hence, a larger share of the annual heating demand is covered, yielding larger potential energy savings and longer technical lifetimes.

Low-capacity brine-to-water units for residential space heating and DHW production are available with heating capacities from about 4 kW. Typical working fluids are R410A, R407C or R134a as working fluid. R290 is also used, but these units are presently less available. Table 3.1 provides a sample overview of ground-source heat pump units from four leading manufacturers. The table include information about the type of working fluid (WF), maximum supply water temperature ($T_{w,max}$) and minimum heating capacity ($\dot{Q}_{c,min}$). It is also specified if the unit has an integrated DHW tank (DHWT), and/or desuperheater (DSH), and/or compressor VSD control.

Table 3.1: Overview of some low-capacity ground source heat pump units.

	WF	$T_{w,max}$ [°C]	$\dot{Q}_{c,min}$ [kW]	DHWT [liter]	DSH	VSD
Nibe F1255	R407C	65	1.5-6	180		✓
Nibe F1245	R407C	65	6.3	180		
Thermia Diplomat Inverter	R410A	65	5	180	✓	✓
Thermia Diplomat Optimum	R407C	60	4	180		
Thermia Diplomat G2	R407C	60	6	180	✓	
IVT PremiumLine HQ	R410A	62	4.5	185		
Nilan Compact Geo 3	R410A		0.5-3	180		✓
Calorex WW3500	R134a	65	2.61			

3.2 Ground Collector Systems

3.2.1 Vertical Ground Heat Exchangers

These systems comprise a collector tube, which is lowered into a 80-200 m deep borehole. The major advantages are high efficiencies and a minimum requirement of site area [35]. Technical lifetimes up to 50 years also contribute to a high reliability. An illustration is shown in fig. 3.4. The depth depends on the capacity of the heat pump system, and hence the necessary heat extraction. The latter depends on the bedrock type, the temperature level and the presence of ground water. **Typical design values range between 20 and 40** W/m. Water increases the convection heat transfer between the collector tube and the bedrock, and is therefore essential. Additional advantages of BHE collector systems is that they can be used for thermal storage and passive cooling during the summer. Typically, the borehole temperature is in the range between -3 to 8 °C [20].

A relatively high initial investment cost is the only major disadvantage of BHE-coupled systems. G. Nielsen [7] carried out a theoretical LCC analysis, in which BHE-coupled and air-source heat pump systems were compared with respect to energetic and economic performance. With the site locations Bergen, Oslo, Røros, Karasjok and Tromsø, the following parameters were considered:

1. Climatic data for the location.

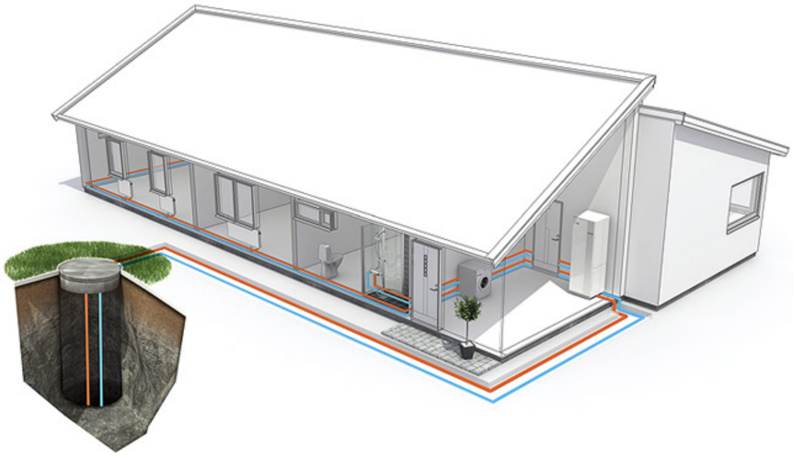

Figure 3.4: Illustration of a vertical ground collector system [5].

2. Design power and heat demand for the actual building.
3. Internal loads of the building (daily, weekly and annually).
4. Compressor efficiency at different running conditions.
5. Variation in evaporation temperatures (climatic data).
6. Variation in condensation temperatures (space heating system).

The heat collector arrangements evaluated are illustrated in fig. 3.5. The borehole installation is shown in fig. 3.5a, while the indirect and direct air-to-water arrangements are shown in figs. 3.5b and 3.5c, respectively. The following assumptions were applied:

- Minimum evaporator temperature difference: 3 K.
- Brine temperature difference: 3 K.
- Annual energy coverage factor for the borehole: 95 %.
- Average borehole temperature equal to the annual mean ambient temperature.
- BHE conductivity: 5 W/mK.
- Design heat extraction for the BHE: 30 W/m.

For the BHE system (fig. 3.5a) a mean temperature difference of 6 K between the bedrock and brine resulted from the design heat extraction and conductivity. This gave an evaporator outlet temperature 7.5 K below the borehole temperature. Including the minimum temperature difference of the evaporator, the average evaporation temperature was assumed equal to 10.5 K below the borehole temperature.

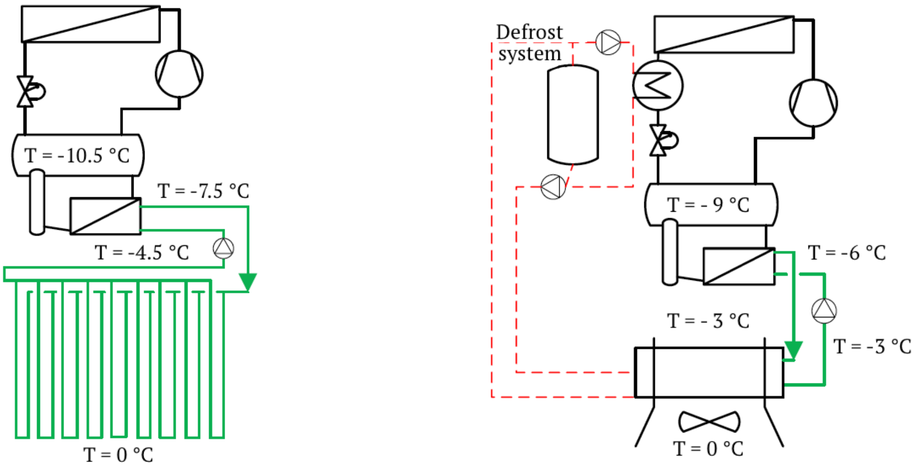

(a) Borehole brine-to-water system.

(b) Indirect air-to-water system.

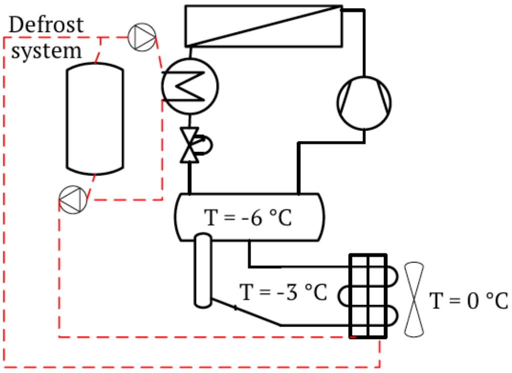

(c) Direct air-to-water system.

Figure 3.5: The three system arrangements assessed [7]

For the indirect air-to-water arrangement (fig. 3.5b) with the dry-cooler it was assumed that the cooling of the air and the heating of the brine is equal to 3 K. Thus the inlet brine temperature to the evaporator is equal to the air temperature, which gives an evaporation temperature 9 K below the ambient temperature. **For the direct air-to-water system** (fig. 3.5c) the temperature difference due to the brine circuit is omitted, and the evaporation temperature is 6 K below the ambient.

Despite added heat exchange losses for the borehole systems, the evaporation temperature is typically higher relative to the air-based systems, due to a higher mean annual temperature in the ground. As a result, the performance and the annual relative energy savings for these systems are better for all climates, though marginal in the case of high design ambient and mean annual temperatures. This applies, for instance, to Bergen and Tromsø.

The economic efficiency of these systems were evaluated by means of their respective payback periods [7]. Annual capital costs were calculated with an interest rate of 7 % and a technical lifetime of 25 years. For the BHE installations the collector system account for 75 % of the total investment, whereas the dry cooler and air evaporators account for 40 % and 25 %, respectively. As a result, the payback periods for the borehole-based systems were significantly longer compared to the air-based systems. From an economical perspective, the air-based systems were regarded preferable to borehole-based systems in mild climates.

3.2.2 Horizontal Ground Heat Exchangers

Compared to BHE-coupled systems, this design is less documented in the literature. Nevertheless, it represents a compromise between high efficiency and initial costs, and is therefore a competitive alternative to vertical ground heat exchangers [35]. In this case, it is the solar energy stored in the upper layer of the ground, which is utilized, and hence a larger site area is required. For residential applications, however, this is a minor barrier since the required area is moderate.

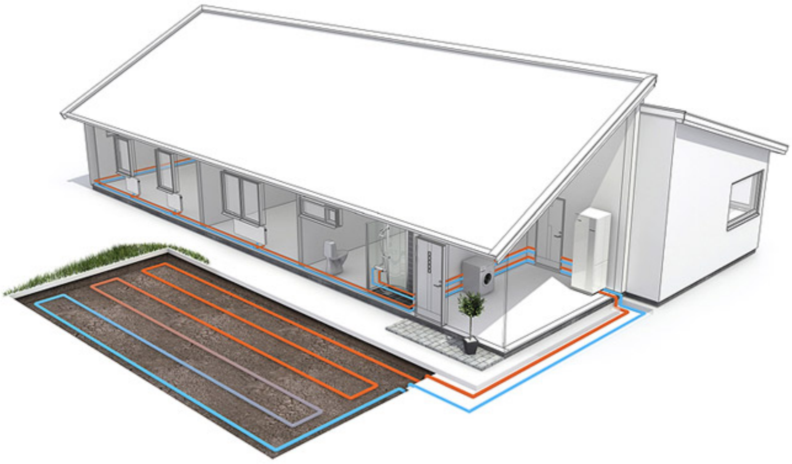

Figure 3.6: Illustration of a horizontal ground collector system [5].

Of the three basic configurations; linear, spiral and slinky, the linear type HGHE, as illustrated by fig. 3.6 represent the most common type. Collector tubes typically have an external diameter between 30 and 50 mm, and are buried at 1-2 m depth. At this depth the temperature is steady, with slight variation around the annual mean temperature of the location. Typically, the temperature is in the range between -3 and 10 °C. As for BHE systems, the maximum heat extraction is dependent on soil conditions. **Design values typically range between 8 and 30** W/m [36]. Congedo et al. [37] analyzed the performance of HGHEs, and concluded that the ground thermal conductivity and the heat transfer coefficient between the heat transfer fluid pipe wall are the two most important parameters. Meanwhile, the installation depth and tube configuration were of minor importance.

During the 1980s, a residential heat pump test project was conducted for a residential area in Trondheim [8]. A horizontal ground collector system was compared to five other systems with respect to thermo-economical performance. The heat pump system was designed to cover the entire heating demand for both space heating and DHW production. The heat distribution system was a radiator circuit with a maximum supply temperature of 55 °C. The surface collector field covered a ground area of 400 m^2. A 300 m PE 40 tube, circulating a water/glycol brine, was buried at 0.75 m depth and with 1.3 m mutual distance in moist soil (marsh).

Heat extraction from the ground was largely due to latent heat transfer as the water surrounding the PE tubes froze. The temperature development in the SCF was recorded at different vertical and horizontal positions. Below 0.5 m depth it was observed that the average temperature decrease in the SCF was 2 °C. Fig. 3.7 gives the vertical temperature profiles for the ground at the centre of the SCF (measuring string A, solid line) and in neutral ground (measuring string B, dashed line). At the centre of the SCF the temperature at 1 m depth ranged between approximately 1.5 and 6.5 °C throughout the year. A shift in the temperature variation was also observed, noting that the ground temperature in April was lower, compared to January. Likewise, the ground temperature in October was higher compared to July. For an increasing depth below the collector tube the vertical temperature profile in the SCF approached that of the neutral ground.

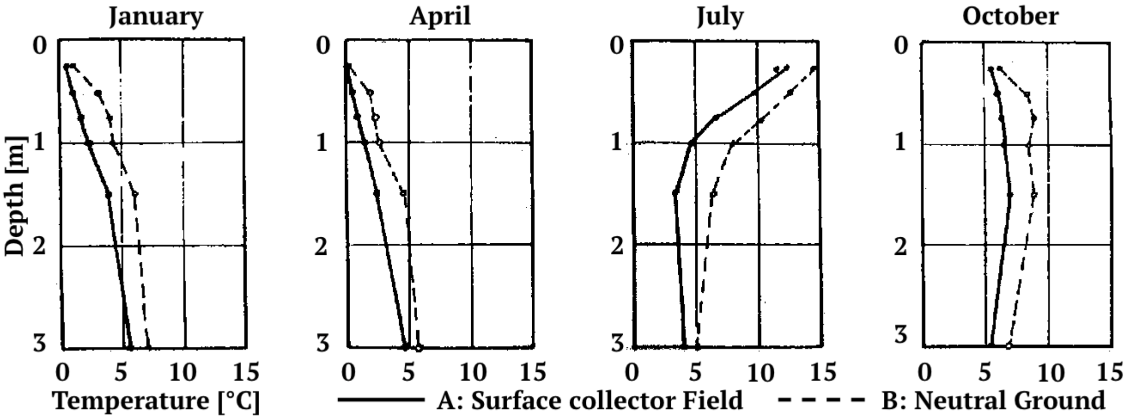

Figure 3.7: Vertical temperature profiles at the centre of the surface collector field and in neutral ground [8].

Fig. 3.8 shows the horizontal temperature development after the heat pump, over a 2 year period from August 1982 to July 1984. Temperature sensors were placed at 0, 0.1, 0.2, 0.4 and 0.8 m distance from the collector tube. In accordance with fig. 3.7 the lowest ground temperatures were measured at the end of the heating season in April/May. After natural thermal recovery during the summer, peak temperatures were observed in August/September. Peak temperatures after the first year of operation were somewhat lower, compared to the temperatures at start-up. A noticeable increase ground temperature was observed for short distances from the collector tube. However, by moving from 0.4 to 0.8 m distance from the tube, only a slight increase in ground temperature was observed. This indicated that a 1.3 m mutual distance between the tubes is sufficient to prevent them from thermally influencing one another.

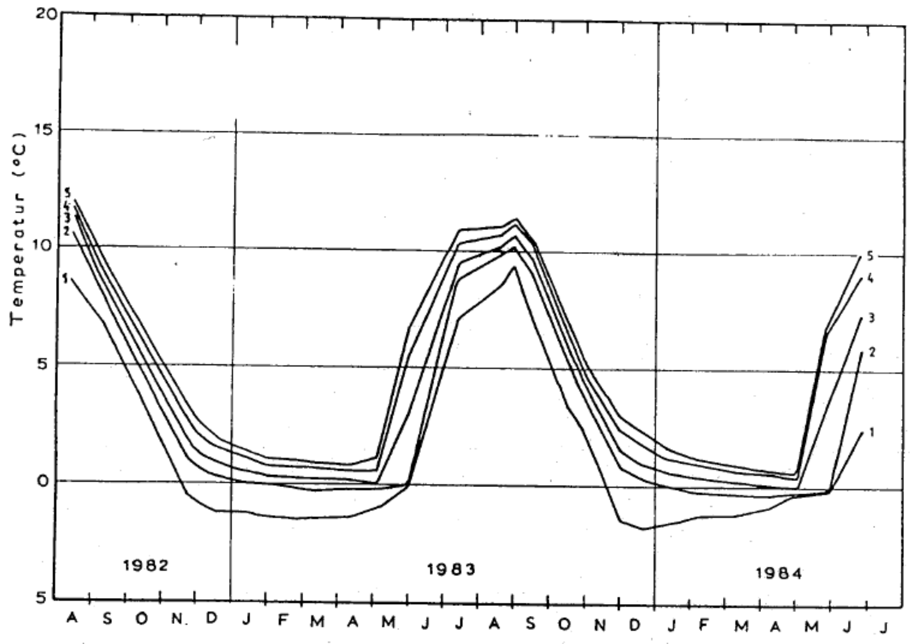

Figure 3.8: Measurements are done at 0, 0.1, 0.2, 0.4 and 0.8 m distance from the collector tube, after the heat pump [8].

By comparing annual electricity savings it was concluded that the brine-to-water system, despite higher investment costs, was superior compared to the air-to-water and air-to-air systems.

3.2.3 Aqueous Antifreeze Solutions

To maintain effective heat transfer between the ground source and the heat pump evaporator at sub-zero temperatures, an aqueous antifreeze solution is usually used as heat transfer fluid. Common additives are ethyl acohol (EA), ethylene glycol (EG) and propylene glycol (PG). While the first and the latter are non-toxic, the opposite is true for ethylene glycol. From an environmental aspect, ethylene glycol is a less preferable option, since the absence of leakages can not be guaranteed. Table 3.2 list the relevant thermophysical properties of the three options, for a freezing point of -10 °C and an operating temperature of 0 °C. Data is attained from the International Institute of Refrigeration [38].

Table 3.2: Thermophysical properties at -10 °C freezing point and 0 °C operating temperature.

	Concentration Weight-%	ρ $[kg/m^3]$	c_p $[J/kgK]$	λ $[W/mK]$	μ $[kg/ms]$	Pr [-]
Water	0	1000	4217	0.562	1.78	13.4
EA	18.8	977	4355	0.454	5.02	48.2
PG	25.0	1025	3975	0.451	5.45	48.0
EG	23.6	1035	3820	0.471	3.52	28.5

Compared to PG-water and EG-water solutions, a lower EA concentration is required to achieve the same freezing point. EA also offer a lower density and higher specific heat, compared to pure water, and a lower dynamic viscosity than PG. The thermal conductivity is also marginally higher. This benefits friction losses and heat transfer efficiency. PG offer properties in between those of EA and EG, but has a higher flame point. Compared to EG, PG is also non-toxic. According to J. Acuña [39], the choice of antifreeze solution has a large impact on both hydrodynamic and thermal performance of the system. In this regard, ethanol-water solutions are considered a better alternative.

3.3 The Heat Pump Cycle

The conventional heat pump technology is represented by the **subcritical vapor compression cycle**, which is also the most prevalent configuration encountered in low-capacity residential systems. Based on the ideal reversed Carnot cycle, four basic processes - evaporation, compression, condensation and expansion - are undertaken, entirely below the critical point of the working fluid. The ideal reversed Carnot cycle is characterized by isothermal heat absorption and rejection processes, and isentropic compression and expansion processes [40]. By contrast, the vapor compression cycle employs some modifications in order to make practical implementation possible. Fig. 3.9 gives a principle flow scheme of the basic cycle, including the main components: evaporator, compressor, condenser and throttling valve. Additionally, a liquid receiver is included, which primary function is to offset fluctuations in the working fluid mass flow.

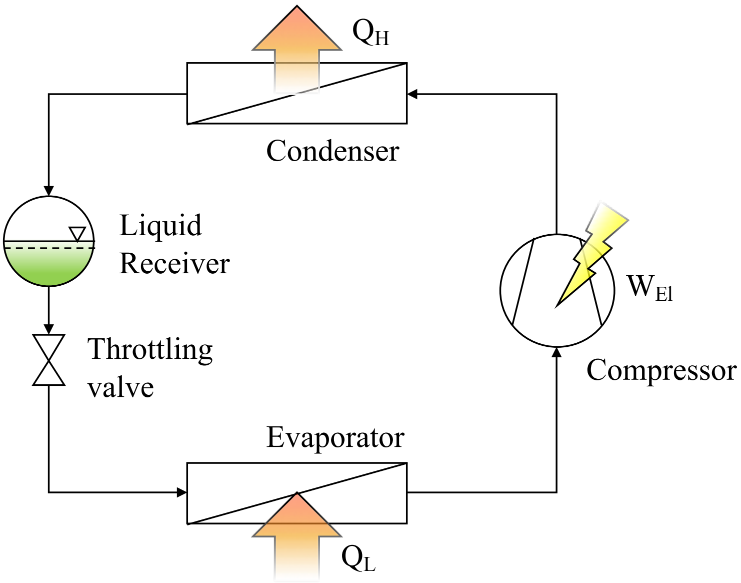

Figure 3.9: Basic vapor compression cycle.

The vapor compression cycle employs dry compression in the vapor region, rather than wet compression in the two-phase region. Due to second law losses, the real compression process is non-isentropic and, if accounting for heat losses to the ambient, also polytropic. Another deviation from the Carnot cycle is found at the opposite side of the cycle, where depressurization occur as isenthalpic throttling, rather than isentropic expansion. Furthermore, temperature driving forces and inherent necessary temperature differences between the working fluid and the secondary fluid, induce additional losses in the evaporator and condenser.

3.4 Working Fluids

3.4.1 Selection Criteria

Selection of environmentally benign working fluids, that concurrently allow competitive system performance, is vital part of heat pump design. Working fluid selection necessarily involve some degree of compromise between environmental benignity, local safety, thermodynamic and physical performance, practicality of use, as well as costs

[34, Chapter 2]. The following lists some of the most typical working fluid selection properties:

- Local safety, including flammability and toxicity.
- Global environmental impact, including zero ODP and low GWP values.
- Thermophysical properties.
- Chemical stability.
- Miscibility with lubrication oils.
- Material compatibility.
- Price and availability.

In practice, the perfect working fluid does not exist. Thermophysical and practical deficiencies are still largely offset by taking specific properties into account during the heat pump design phase. For apparent reasons, local safety and global environmental impact are the first properties to be considered. Local safety classifications and environmental properties of the most relevant working fluids are presented in table 3.3. Each working fluid is assigned a two-component safety label describing its degree of toxicity and flammability. The first letter, A or B, indicates a lower or higher degree of toxicity, respectively. The number and the occasional last letter indicate the degree of flammability, where 1 means no flame propagation, 2L means lower flammability, 2 means flammable and 3 means higher flammability [34, Chapter 2].

Table 3.3: Overview of local safety classifications and environmental properties.

	Safety Class	GWP_{100}
R134a	A1	1360
R1234yf	A2L	< 1
R407C	A1	1700
R410A	A1	2100
R32	A2L	704
R744	A1	1 (0)
R290	A3	5 (0)

To a varying extent, the HFCs have significant *global warming potentials*, GWPs, owing to the presence of fluorine. The 100 year GWP value, expresses the integrated radiative forcing over a 100-year time period of 1 kg of working fluid emitted to the atmosphere [34]. The short time global warming effects of these substances are, however, even more significant. Per definition the GWP of CO_2, R744, is equal to 1. As a result, the global warming potency of R410A, for instance, is 2100 times higher by comparison.

3.4.2 Synthetic Working Fluids

HFC working fluids are widely used in heat pumps, and are commercialized worldwide. Today, the most common HFCs for domestic heat pump applications are R134a, R407C and R410A. As indicated by table 3.3, all three contribute significantly to the global warming effect, in case of unintended leakages to the atmosphere. A less harmful option is R32, which is found as a component in both R410A and R407C.

R134a is a single-component HFC, which is both non-toxic and non-flammable. Compared to alternative HFC fluids, it has a relatively low GWP value. It is classified as an A1 working fluid and is, due to critical temperature of 101 °C, well-suited for high-temperature applications. R134a is commonly used in medium and large-capacity installations. Due to a low volmetric heating capacity, R134a units require a relatively large filling charge and mass flow rate. This has a consequence on components, such as the compressor, since the required dimensioning becomes larger [41].

R1234yf and R1234ze are HFO working fluids that have gained recent interest for low and high temperature applications, respectively. While the latter is still at a trial stage, R1234yf is already commercialized in the automotive industry. R1234yf has similar properties to R134a, and can be used as a replacement in heat pump applications where the water outlet temperature is less than 50 °C [42]. Due to price competitiveness, however, it is disputed whether pure R1234yf is an option for future heat pump system [34, Chapter 8]. For domestic applications the filling charge is nevertheless minimal, and the conclusion might be different.

The indirect ecological effects of HFOs are still uncertain due to scarce research. For instance, the varying halogenation is a trade-off between flammability associated with la higher degree of stability, and low GWP values associated with a lower degree of stability. The low GWP HFOs are inherently both flammable and unstable, which in turn makes them unsafe and reactive when leaked to the ambient [34]. These substances are equally foreign to nature as their artificially synthesized predecessors, and there are no known biologically degrading processes in the atmosphere.

R407C has been used in existing systems as a replacement for the ozone-adverse HCFC-22. Their properties are similar, resulting in minimum required system modifications. R407C is a three-component mixture, which contains nearly 25 % R32 and nearly 50 % R134a. The remaining component, comprising 23 %, is R125. Due to its mixture composition, R407C is characterized as a **zeotropic** working fluid. This implies approximately 7 K temperature glide during evaporation and condensation, which is significant compared to other zeotropic mixtures. As seen in table 3.1, R407C is used as a working fluid in residential brine-to-water heat pumps by both Nibe and Thermia.

R410A is a two-component zeotropic blend, containing 50 % R32 and R125. By contrast to R407C, the temperature glide of the R410A blend is less pronounced. The operating pressures of R410A are higher compared to R407C, and require more system modifications to fully utilize the properties of the working fluid [34, Chapter 8]. Nevertheless, R410A is the typical choice for new systems as is allows more compact and efficient designs, when optimized. As seen in table 3.1, R410A is used as working fluid in residential brine-to-water heat pumps by Nibe, IVT and Thermia.

R32 is not yet commercialized as a pure substance for water heating applications on a larger scale. It has higher operating pressures and discharge temperatures than R410A, and requires more accurate throttling devices for temperature control. This applies particularly to high temperature water heating, when the heat source temperature is low. The maximum permitted condensing temperature is nevertheless restricted by a critical temperature of 78 °C. Both heat transfer and transport properties are superior to the HFC blends, resulting in higher theoretical system efficiencies. A high vapor density and specific heat of vaporization implies higher volumetric efficiencies. A as result, components dimensions is reduced, making R32 units potentially cheaper than the commercialized HFC units. Concerns towards local safety is currently the main barrier for wide use.

3.4.3 Natural Working Fluids

Carbon dioxide, R744, was the dominating refrigerant for air conditioning and marine refrigeration until the 1950s, but as the CFCs was introduced a market shift occurred. Prior to the Montreal Protocol about 60 % of the CFC emissions originated from mobile refrigeration systems [43]. Consequently, CO_2 was reintroduced in the search for ozone-friendly refrigerants [44].

R744 has zero ODP and a GWP, which per definition is 1. Nevertheless, since it is a by-product of industry, its actual GWP as a technical gas is zero. One of the main assets of R744 is its very high vapor density, allowing low compressor swept volumes and compact equipment in general. In turn, system costs are reduced. The advantages of CO_2 are further extended with its non-toxic and fire-suppressing characteristics, thus placing it in the A1 safety group. As CO_2 is 2.2 times denser than air, leakages in confined spaces may result in air displacement and a theoretical risk of asphyxiation [45]. However, because the filling charge in low capacity systems is modest, this represents a negligible hazard towards local safety [46].

At 31.1 °C the critical temperature of R744 is very low. Consequently, practically all CO_2 heat pumps are operated as **transcritical vapor compression cycles**. These are based on the reversed Lorenz cycle, and differs from the subcritical cycles in that heat is rejected at constant pressure and gliding temperature above the critical pressure. The high pressure heat exchanger is referred to as a *gas cooler*, due to the absence of phase-change. In order to achieve competitive performances the temperature glide during heat rejection has to be large. As a result, the transcritical cycle is ideally matched with a similarly large temperature glide on the secondary fluid. A typical example is the CO_2 heat pump water heater (HPWH), allowing temperature glides of 80 °C in a single stage. A low inlet water temperature is a prerequisite for achieving high COPs in the transcritical cycle, making them ideal for DHW heating. Units have been developed both for DHW heating only, and for combined DHW production and space heating [47, 48].

Propane, R290, is a non-toxic, environmentally benign working fluid, which is well suited for use in low-capacity residential heat pump units. R290 heat pumps installed in Austrian low energy houses have achieved minimum SPFs of 4. In addition to a GWP value 3, it offers excellent thermophysical properties. The main barriers restricting wide use, however, are local savety concerns related to flammability.

R290 has a lower explosion limit (LEL) of 2.1 vol-% or 39 g/m^3 in air. The upper explosion limit (UEL) is 9.5 vol-% or 177 g/m^3 [49]. It is however physically impossible to obtain an explosive mixture within a pumping process. The main explosion hazards are therefore related to leakages to the surroundings, in the presence of ignition sources.

Because it is heavier than air, R290 is also characterized as a simple asphyxiant. In case of leakages the vapor may accumulate in low-laying areas, where air is displaced. The heat pump room should therefore be sufficiently large and have sufficient natural ventilation. Separate VAV ventilation should activated by leakage detectors, mounted near the floor. Ignition sources are prohibited, and the heat pump unit should be installed in a gas-tight casing with all electrical components on its exterior.

Charge minimization is also crucial point in R290 heat pump design. Compact equipment is thus necessary to minimize the internal volume of the units. Cavallini et al.[50] was able to reduce the propane charge of a 100 kW unit by 25 % from 3 to 2.2 kg, by using a customized tube-in-shell mini-channel condenser. With a 65 % reduction in the internal volume, the COP was reduced by just 2 %. In this case the working fluid charge was just 0.022 kg/kW, although values may range between 0.06 and 0.15 kg/kW

[49].

Propane is compatible with most typical materials, such as iron, steel, stainless steel, aluminum, copper and zinc. The methods for design and construction of HFC units are therefore applicable to R290 units. Due to low mass flow rates, densities and viscosities, the required dimensions for components are smaller, compared to the HFCs.

Despite the gradually increasing interest and psychological acceptance for HC working fluids [51], there are still some barriers that impede wide use. Presently, the main barriers are a lack of economically viable methods to make systems safe and foolproof.

3.5 Components

In the following, the most common type of equipment encountered in low-capacity residential heat pump applications is presented.

3.5.1 Scroll Compressors

This is the most widely used compressor technology in low-capacity heat pump applications. This compressor type, which is hermetically sealed, is constructed by two identical spirals, or scrolls, fixed onto separate plates. The spirals are mounted eccentrically to each other, so that they interlock at several positions. While one of the spirals has a fixed position, the other orbits to change the volume of the pockets in between the interlocking parts. Fig. 3.10 illustrates how the low pressure suction gas (SG) enters at the perimeter of the compressor, where the volume between the interlocking scrolls is large. As the orbiting scroll changes position the volume is reduced, and as a consequence the gas trapped pocket between the scrolls is compressed. After a series of compression cycles the high pressure discharge gas (DG) leaves the compressor at the center of the scrolls.

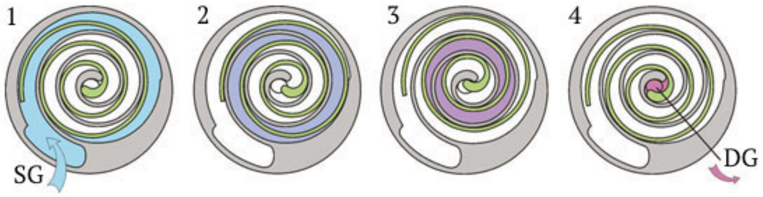

Figure 3.10: Working principle of the scroll compressor [9].

Leakage and heat losses are the dominating loss factors of the scroll compressor [40]. In addition, friction between the interlocking scrolls and in bearings contribute to minor losses. Due to the lack of valves, the scroll compressor has built-in volumetric and pressure ratios. As such, care should be taken when selecting the compressor size in order to avoid additional compressor work due to over or under compression. The only volumetric losses are related to internal leakages, or back-flow, from higher to lower pressure pockets. Nevertheless, volumetric efficiencies are typically high. Additionally, the scroll compressor include few movable parts, has a small volume, low levels of noise and vibrations, as well as a high tolerance for contaminants in the working fluid.

Intermittent capacity control means that the compressor is turned on and off according to the required load. As a result, heat is supplied at a higher temperature during on-time to cover the heating load during off-time [52]. Frequent on/off-cycling also increases the wear and tear on the heat pump compressor, due to significant friction losses and low suction pressures at start-up. As a rule of thumb, the compressor should be limited to 3-4 start-ups per hour, which implies that a certain heat accumulator volume is necessary. However, with **variable speed drive (VSD)** control, the heating capacity can be adjusted dynamically according to the load by varying the frequency or the voltage to the electric motor. An analysis performed by Karlsson and Fahlen [53] concluded that the COP of an on/off controlled GSHP unit could be improved by 7-15 % by mean of VSD operation.

3.5.2 Brazed Plate Heat Exchangers

To achieve compact designs, brazed plate heat exchangers are commonly used as evaporators and condensers in low capacity heat pump units. These heat exchangers compress a large heat transfer area into a very limited volume, and contribute to favorable heat transfer characteristics as well as reduced working fluid charges.

3.5.3 Throttling Valves

These devices ensure control of the evaporating pressure and mass flow in the heat pump cycle. This device, which is either mechanical or electronic, ensures that the suction gas to the compressor is superheated. Typically, the throttling valve is adjusted to allow a 2-5 K superheating of the suction gas.

Thermostatic expansion valves (TEVs) are mechanically controlled devices, which typically adjust the valve opening according to a pre-set degree of superheating. A thermostatic phial is mounted on the suction line subsequent to the evaporator, where it senses the temperature and acts as *feedback control* to the TEV. Pressure variations inside the phial translate to the TEV, which then opens or closes accordingly. An advantage of this control strategy is that evaporator pressure losses are accounted for.

Electronic expansion valves (EEVs) are commonly used in modern heat pump units. The valve opening is controlled electronically according to temperature or pressure sensors at the evaporator inlet and outlet. Compared to TEVs, the EEV adjusts the evaporating temperature more accurately at varying operating conditions. It is thus the recommended alternative, especially in combination with VSD compressor control.

3.5.4 Process Improvements

The COP and heating capacity of the basic heat pump cycle can be enhanced by better utilizing the working fluid properties. For water heating applications a higher outlet water temperature is an important incentive. For low-capacity residential heat pump units the most relevant options are additional heat exchangers.

The desuperheater (DSH) is placed between the compressor outlet and the condenser inlet. It allows cooling of the superheated gas prior to condensation, and is ideally applied to cover heating duties at higher temperature requirements than the condensation temperature, such at DHW reheating. By cooling the superheated gas in a separate heat exchanger, the condenser heating capacity and logarithmic mean temperature difference are reduced. Consequently, the condensing temperature decreases, which also implies a lower condensing pressure. This, of course, results in a lower pressure ratio and reduced compressor work.

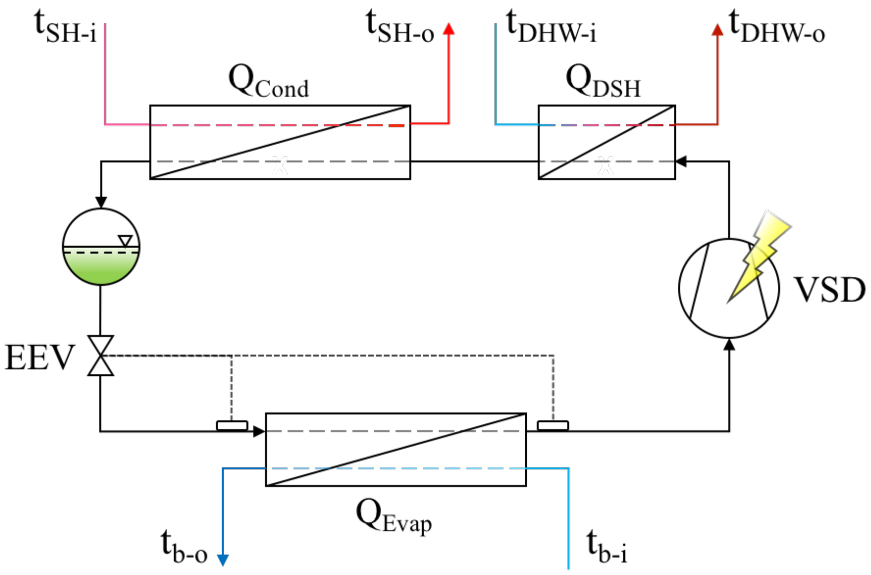

Figure 3.11: Improved heat pump cycle with added DSH, EEV and VSD.

The suction gas heat exchanger (SGHX) enables internal heat transfer between the liquid line and the vapor line, and thus provides subcooling and superheating simultaneously. This improves the evaporator capacity, as the specific enthalpy difference is increased. Meanwhile, the necessary evaporator heat transfer area for superheating is reduced. As a result, the evaporator LMTD is reduced, and the working conditions for the compressor are improved. Despite a lower vapor density and reduced mass flow rate, a higher isentropic and volumetric efficiency typically results in a net improvement. Increased superheating at the compressor inlet, results in an increased discharge temperature at the outlet. The SGHX is therefore ideally combined with the DSH for DHW heating purposes.

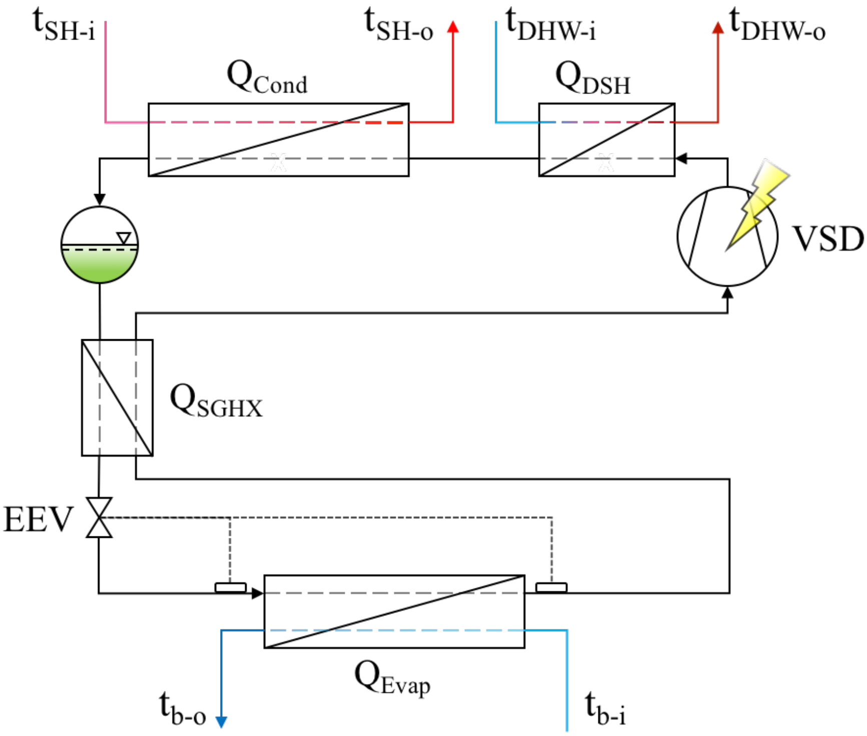

Figure 3.12: Improved heat pump cycle with added DSH, SGHX, EEV and VSD.

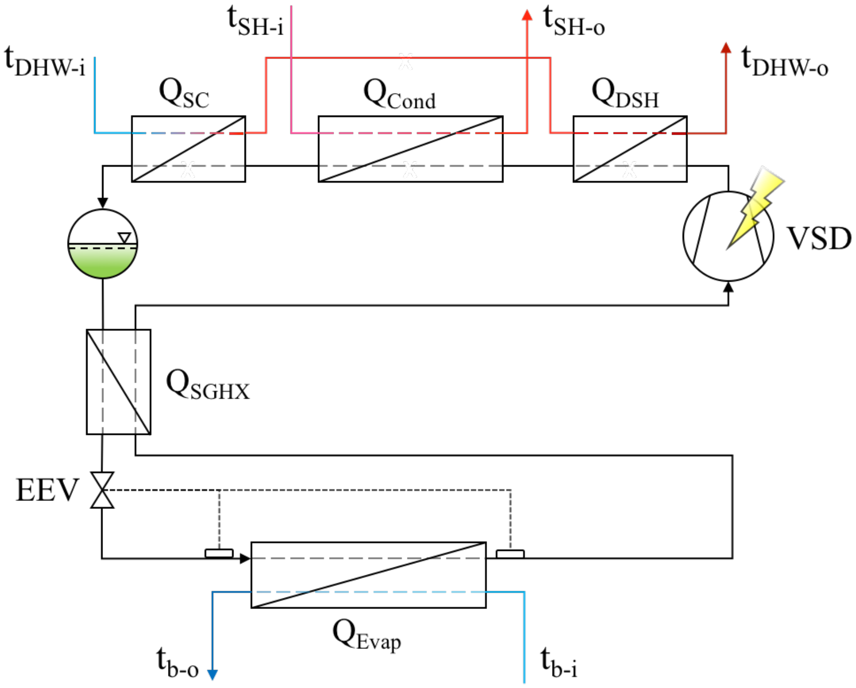
$t_{SH\text{-}i}$
$t_{SH\text{-}o}$
$t_{DHW\text{-}i}$
$t_{DHW\text{-}o}$
Q_{SC}
Q_{Cond}
Q_{DSH}
VSD
Q_{SGHX}
EEV
Q_{Evap}
$t_{b\text{-}o}$
$t_{b\text{-}i}$

Figure 3.13: Improved heat pump cycle with added SC, DSH, SGHX, EEV and VSD.

The subcooler (SC) is a third option, which is placed between the condenser outlet and the liquid receiver inlet. It may be applied in combination with a low-temperature heating demand, such as for DHW preheating. Subcooling of the working fluid reduces its specific enthalpy prior to throttling, which results in lower throttling losses and a larger specific enthalpy difference in the evaporator. This is especially beneficial for working fluids that otherwise experience a large vapor formation during throttling. Either way, the evaporator heat transfer area must be increased in order to maintain a constant LMTD and avoid a drop in the evaporation temperature.

Chapter 4

Solar Assisted Heat Pump Systems

4.1 Solar Energy Potential

The potential for solar energy harvesting is enormous, even at higher latitudes. Nevertheless, the prevalence of systems to utilize this energy is modest. The specific solar irradiation perpendicular to the outer layers of the the atmosphere is on average 1367 W/m^2 near the equator. Due to reflection and absorption of energy in the atmosphere, the *direct* solar radiation that reaches the surface of the earth is about 1000 W/m^2 [20]. Fig. 4.1 illustrates the incident solar energy per day in Norway, for January and July, respectively.

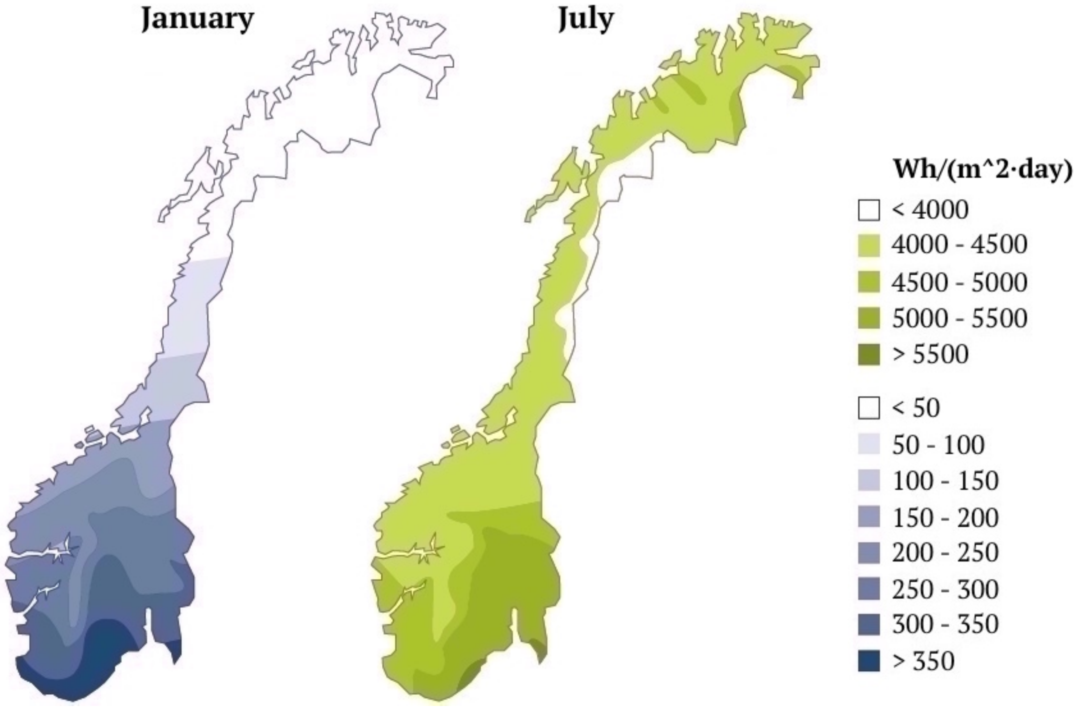

Figure 4.1: Solar energy on an horizontal surface in January and July, respectively [10].

The annual solar irradiation on a horizontal surface ranges between about 600 kWh/m^2 in the north, to 1000 kWh/m^2 in the south [10]. It is evident that the potential solar energy production in January is marginal. In the northern part of Norway, where the sun is below the horizon roughly between November and February, the potential for solar energy utilization is negligible during this period. By contrast, the opposite conditions are prevailing during the summertime. In July, the solar energy intensity in the north of Norway is comparable to that of the central and western regions. Naturally, the largest solar energy potential is found at the southern part of Norway.

The flux of the solar irradiation is also dependent on local weather conditions and latitude. Overcast weather will cause more absorption and reflection of solar radiation in the atmosphere. As a result, the *diffuse* radiation can be much lower than the direct. Solar energy utilization at higher latitudes implies that the solar radiation has to travel further through the atmosphere. Consequently, more radiation is scattered and the flux on the earth's surface is reduced.

4.2 Solar Collector Systems

Utilization of solar thermal energy may be distinguished as either *passive* or *active*. Passive solar heat utilization implies thermal gains through glazed building surfaces, such as windows. These gains contribute to reducing the net heating demand of the building. Active solar heat utilization refers to solar collector systems, in which the solar energy is absorbed by a heat transfer fluid and transferred to a secondary fluid. Depending on the solar collector type and operational conditions, overall efficiencies may range from 50 to 90 % [20].

As a rule of thumb, a typical solar collector system in Norway delivers between 300 and 450 kWh/m^2 annually. In the south and east of Norway, solar collector systems may cover as much as 25-35 % of the annual space heating demand and 50-60 % of the DHW demand in residential buildings [32]. The exact quantities are nevertheless dependent on many factors, such as design and application of the system, latitude and weather conditions.

Residential solar collector systems are typically distinguished as one of two categories:

1. DHW heating systems.
2. Combined space and DHW heating systems.

According to the IEA, the most important application for solar thermal systems is DHW heating. In Europe, small scale residential systems accounted for 84 % of the total solar heat DHW production in 2013 [11]. The collector yield corresponded to 37 TWh, or roughly equivalent to the total energy use of the Norwegian building stock. In Norway, the energy yield from such systems was approximately 15 GWh, corresponding to a 5

084 tonne reduction in CO_2 emissions.

The main components in a solar collector system are the solar collector, or solar panel, the heat distribution system and the thermal energy storage tank. As solar collector systems are largely used for domestic hot water production, water-based distribution system are the most common. Air-based heat distribution via the ventilation system is a less common option. The storage tank is designed for short-term heat accumulation on an hourly, daily or weekly basis. Hence, the system may still provide heat when the irradiation is negligible or the demand is higher. The storage vessel should be designed for a large thermal stratification between the top and bottom, to allow for low-temperature solar heat input near the bottom.

4.2.1 Collector Technologies

Worldwide installed solar thermal capacity, including the contribution to the energy supply and reduction of CO_2 emissions, is reported by the Solar Heating and Cooling Programme (SHC) of the International Energy Agency (IEA) [11]. Here, it is reported that by the end of 2013 the vast majority of the total capacity was installed in China (262.3 GW_{th}) and Europe (44.1 GW_{th}). This capacity is further divided into flat plate collectors (89.3 GW_{th}), evacuated tube collectors (264.1 GW_{th}), unglazed water collectors (25.0 GW_{th}), as well as glazed and unglazed air collectors (1.7 GW_{th}). Evidently, on a worldwide scale the evacuated tube collectors (70.5 %) are most widely used. In Europe and Norway, however, the flat plate collectors are by far most prevalent with shares of 83.8 % and 78.7 %, respectively. The relative shares on a worldwide, European and Norwegian scale are illustrated by fig. 4.2.

Flat Plate Collectors

Flat plate collectors are used in liquid based systems and are the most widely used technology for active solar thermal utilization in Norway and Europe. In general, the simple construction of these collectors comprise an absorber plate, metal tubing, a transparent cover and insulation. A heat transfer fluid is circulated through the metal tubes, that are fixed to the absorber plate. The absorber plate is usually coated with a material which absorbs most of the visible light, while emitting very little infrared radiation [32]. The cover plate reduces the heat losses via long wave radiation from the collector, while being transparent to short wave solar irradiation.

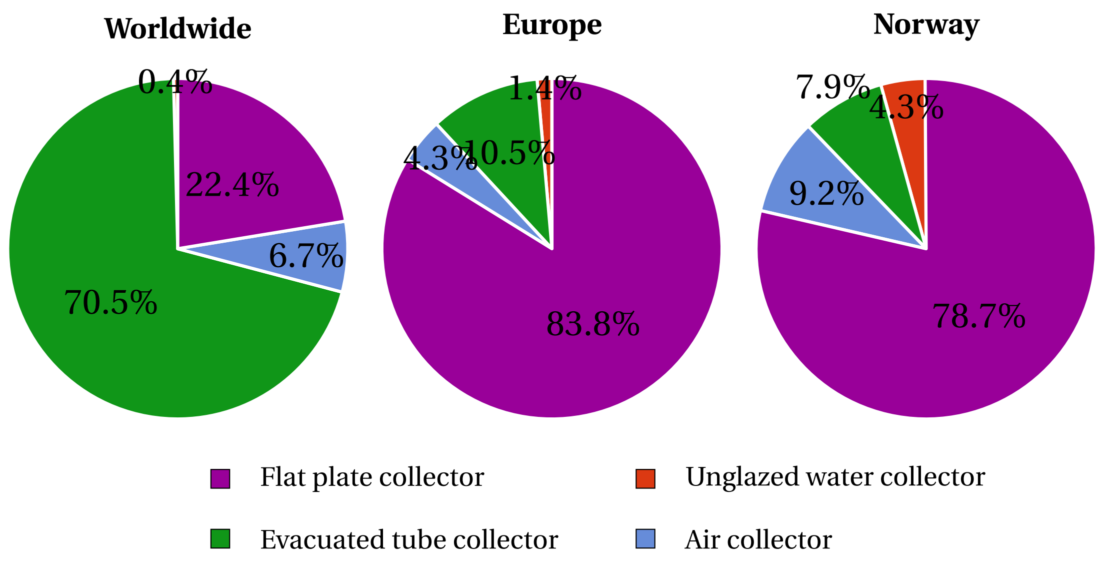

Figure 4.2: Distribution installed solar thermal capacity by type [11].

Evacuated Tube Collectors

This is a less common option for liquid-based solar thermal systems in Europe and Norway. The construction is more complicated compared to flat plate collectors, and consists of several coaxial glass tubes, placed in a vacuum. The inner tube is coated with an absorbing material, and a metal absorber is placed within this tube. The vacuum between the tubes ensure minimal convection heat losses to the ambient, compared to flat plate collectors. Compared to flat plate collectors, the specific cost of these collectors is typically 2.5 times higher. Although the thermal efficiency of evacuated tube collectors is superior at large temperature differences between the absorber and the ambient, the heat yield is typically lower [54].

PV/T Collectors

This is a third option, which has not yet had a commercial breakthrough comparable neither to that of photovoltaic (PV) technologies nor the pre-mentioned solar collector technologies. Lately however, there has been a growing interest in this technology in relation to low and zero energy buildings. For projects with ambitious energy targets or limited available area for local solar energy utilization, solar thermal and PV systems will eventually compete for space on roofs and facades. The possibility of architectural uniformity is the underlying motivation for using PV/T panels, rather than PV and solar thermal panels separately.

Additionally, a typical PV module has an efficiency between 10 and 20 %, which decreases with increasing panel temperatures. This is because a large share of the solar energy is either reflected or dissipated as heat. The latter may be utilized by the

PV/T technology to improve the efficiency of electricity production. Fig. 4.3 depicts the principal construction glazed and unglazed PV/T modules, repsectively. Whereas the unglazed PV/T modules are characterized as *PV panels with cooling*, the glazed modules are described as *solar thermal panels with PV panels added*. The latter produces a higher thermal output than the unglazed modules, and are therefore the preferred choice in thermal systems.

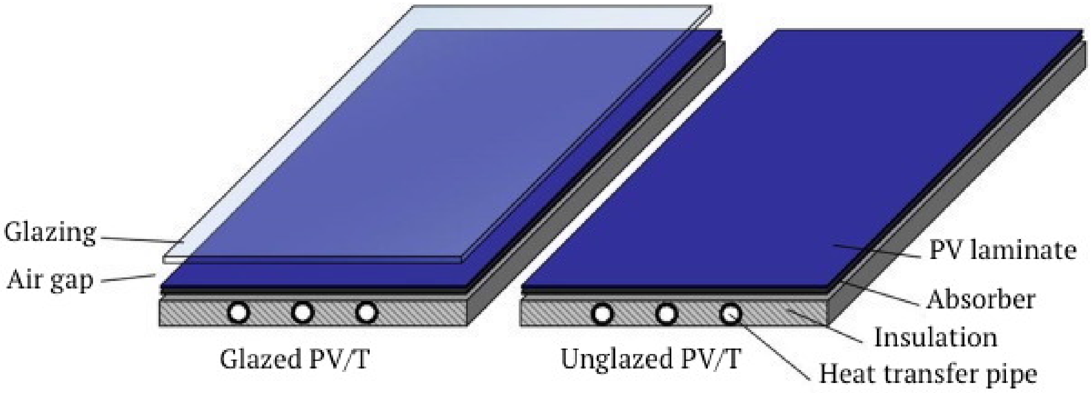

Figure 4.3: Principle drawing of the PV/T modules [12].

Good et al. [12] assessed the performance of PV/T modules, in combination with various PV and solar thermal technologies, for a residential nZEB building in Oslo climate. Comparisons were made using the dynamic simulation tool Polysun [55]. The annual solar fraction, which in the literature is typically thermal energy specific, was highlighted as an important design parameter. Since PV/T panels combine thermal and electrical energy production, an electricity-specific solar fraction was defined additionally. These are given by eq. 4.1 and eq. 4.2.

$$SF_{th} = \frac{Q_{sol}}{Q_{sol} + Q_{aux}} \tag{4.1}$$

where:

SF_{th} : thermal solar fraction $[-]$
Q_{sol} : thermal energy from the solar energy system $[kWh]$
Q_{aux} : thermal energy from the auxiliary energy source $[kWh]$

$$SF_{el} = \frac{E_{sol}}{E_{need}} \tag{4.2}$$

where:

SF_{el} : thermal solar fraction $[-]$

E_{sol} : electricity from the solar energy system $[kWh]$

E_{need} : electricity-specific energy energy demand $[kWh]$

The results indicated that the combination high thermal efficiency (glazed) PV/T modules and average efficiency PV modules may yield solar fractions, both thermal and electrical, intermediate to those of average efficiency and high efficiency combinations, respectively. The largest differences related to module efficiency were nevertheless observed for the electricity-specific solar fraction. For thermal energy production the solar fraction was more or less constant, regardless of whether average or high-end modules were used.

4.2.2 Building Integration and Orientation

Solar panels are commonly façade or roof integrated, due to esthetics and practicality of installation. Nevertheless, to utilize the full potential of the incident solar irradiation, more optimal orientation of the panels is possible. Firstly, the panels should be facing south, with an allowable deviation of ± 45° in the east-west direction. Secondly, the **optimal tilt angle** should be used. This is the fixed angle between the solar panel and the horizontal plane that result the maximum annual accumulated energy quantity [20]. In Trondheim, the optimal tilt angle for solar thermal panels is 44°. For any given location the optimal tilt angle is calculated according to eq. 4.3.

$$\psi_{opt} = \frac{\sum_{n=1}^{n=365} (\psi_n \cdot q_n)}{\sum_{n=1}^{n=365} q_n} \tag{4.3}$$

where:

n : number of the day $[-]$

ψ_{opt} : optimal tilt angle at day n $[°]$

q_n : average incident energy quantity at day n $[kWh/(m^2 day)]$

In practice, however, it might be more beneficial to deviate from the theoretical optimum when fixing the solar thermal panels. For instance, a less steep angle might be more optimal if the collector system is used to heat an outdoor swimming pool during the summertime. The same methodology applies if the DHW demand is large during this period [20]. By contrast, since the angle of the incident solar irradiation is low during the wintertime, a steeper angle might improve the energy coverage factor for space heating systems. Moreover, since a steeper angle permits snow to slide off the collector surface, this this contributes to reduced losses in terms of shading.

Façade mounted collectors typically result in a larger annual heat production, due to better utilization of the solar irradiation during the wintertime. Nevertheless, the capacity of the solar thermal system is low during the wintertime as a result of limited solar irradiation. The opposite conditions are prevailing during the summertime, and typically there is a surplus heat production. A better balance between demand and supply might be seen during the spring and fall, when the solar irradiation is intermediate. Hence, there is a trade-off between annual delivered heat and peak power production. Consequently, the **recommended tilt angle** may deviate from the optimal, and is dependent on whether the system is used for DHW production alone, or for combined space heating.

4.3 Development of Solar Assisted GSHP Systems

Since the late 70s there has been an increasing interest in GSHP systems coupled with STPs, as a means of improving the overall system performance. Although the technology has yet to become widely adopted, the prevalence of such systems is increasing [56]. Driving factors for this development are primarily technological improvements and declining costs. Increasing electricity costs and a political focus on improved energy efficiency and a larger renewable energy share in the building sector are additional incentives.

During the 80s, international research work sprouted from the IEA (International Energy Agency) with the "Solar Heating and Cooling Program", "Energy Storage Program" and the "Advanced Heat Pump Program" [57]. Projects largely focused on borehole based systems and seasonal storage. The main purpose of the STC systems was to increase the borehole temperature, and consequently it was found equally advantageous to simply increase the borehole depth.

In the late 90s, there were about 100 000 GSHP systems in Europe, of which 50 % were located in Sweden [57]. The solar assisted systems, however, were located in central Europe. In Austria a combined GSHP and STP system with 20 m^2 collector area was able to cover 29 % of the total heating demand of a 218 m^2 single family dwelling by solar heat. In Germany, similar systems in larger buildings were able to cover up to 75 % of the DHW demand and 15 % of the total annual heating demand, respectively.

In the early 00s, both theoretical and experimental research was carried out on a combined GSHP and STP system in a 180 m^2 French single-family house [56, 13]. The heat pump was a 15.5 kW reversible unit, coupled with two 90 m deep double U-pipe BHEs. The solar thermal system integrated 12 m^2 of solar thermal panels and a 500 l storage tank. Fig. 4.4 illustrates the principle layout of the system. In particular, the system consisted of one continuous hydraulic circuit, circulating a glycol-water mixture by means of seven pumps. Hence, flow directions were decided by sequential pump operation, rather than by three-way valves. Consequently, increased electricity use due to longer operating times for the circulation pumps had dramatic effect on the overall performance. Careful control of the system thus proved very important.

Measurements on system behavior revealed, as expected, that the performance declined as the heating season advanced. Compared to the start-up in November 2004, the COP in April 2005 was reduced by 14 %, from 4.05 to 3.5. In this case, the solar thermal system was deliberately oversized with respect to the total DHW demand, so that excess solar heat could be directed to the BHEs or the floor heating circuit. By coupling

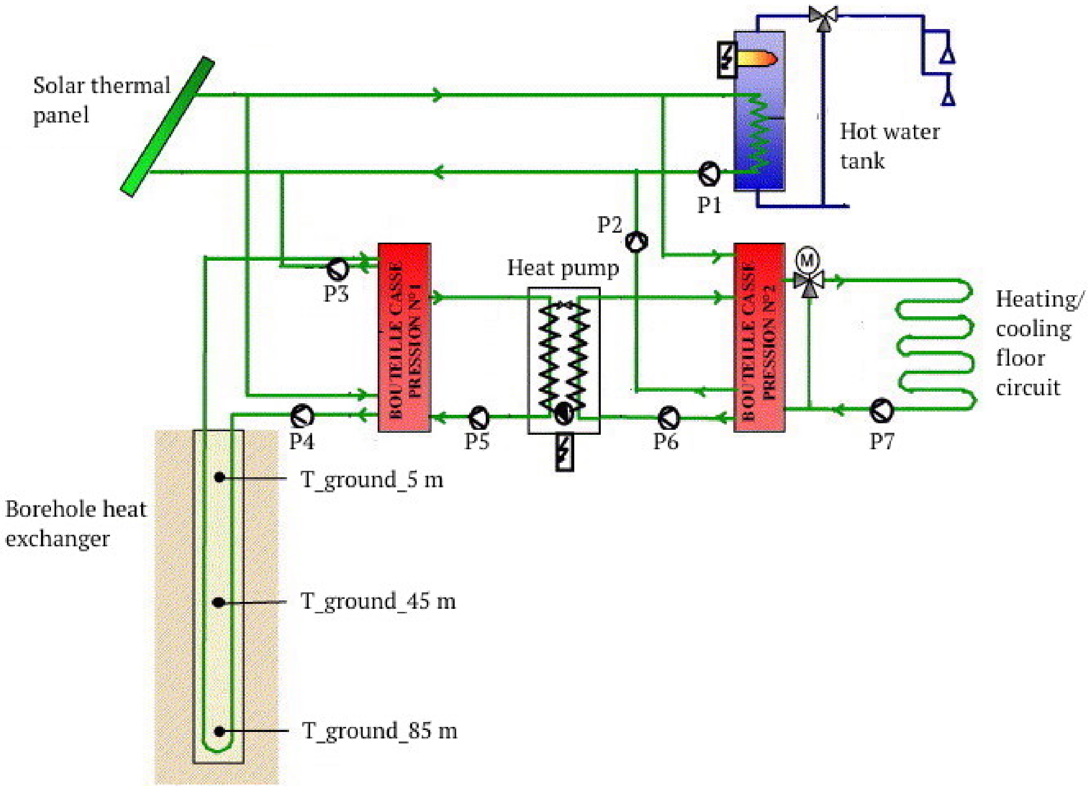
Solar thermal panel
Hot water tank
P1
P2
Heat pump
P3
BOUTEILLE CASSE PRESSION N°1
BOUTEILLE CASSE PRESSION N°2
M
Heating/ cooling floor circuit
P4
P5
P6
P7
Borehole heat exchanger
T_ground_5 m
T_ground_45 m
T_ground_85 m

Figure 4.4: Principle flow scheme of the GEOSOL combined GSHP and STC system [13]

the solar thermal and heat pump systems, it was argued that the required capacity of the heat collector system could be reduced as a means to cut system costs.

Today, solar assisted heat pump systems for single-family houses have been commercialized, and are available as plug-and-play solutions. One such example is the *HYSS - Hybrid Solar System* [14]. This is an integrated system, in which interaction between a solar thermal circuit, a brine-to-water heat pump and a thermal storage system is optimized to give SCOP values between 6 and 8 [58]. The heat pump integrates a VSD-controlled compressor, which is designed to cope with brine temperatures up to 40 °C. Solar heat is utilized according to two main strategies:

1. To reduce the operating time for the heat pump.
2. To optimize the operating conditions for the heat pump.

The HYSS system is operated in three distinct modes, designed to maximize the solar heat utilization. Switching between these modes is dictated by the temperature level in the solar thermal circuit. **At high temperatures (40-75 °C)**, solar heat is exchanged directly to produce DHW at more than 60 °C. This mode can be operated during 4-6 months of the year, and render supplementary heat unnecessary. **At medium temperatures (15-40 °C)**, solar heat is used to elevate the brine temperature to the heat pump evaporator. Hence, the heat pump COP is increased, contributing to a higher annual SCOP. **At low temperatures (5-15 °C)**, the solar heat is used for short-term energy storage by recharging the borehole or ground collector field. This reduces the net heat extraction from the ground, and contributes to a higher COP and SCOP.

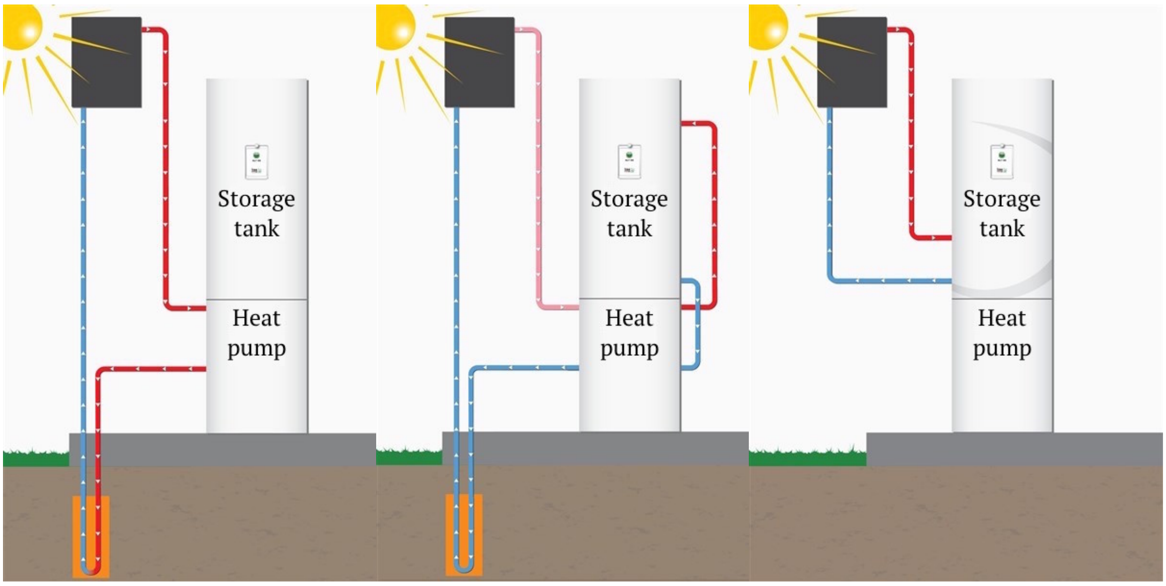

(a) 5-15 °C (b) 15-40 °C (c) 40-75 °C

Figure 4.5: HYSS - Hybrid Solar System operating modes [14].

4.4 Optimal Utilization of Solar Heat in GSHP Systems

A theoretical study, carried out at Lund University in Sweden, assessed the dynamics of solar assisted heat pump systems in dwellings [57, 59]. Several system configurations combining STPs and GSHPs, coupled with vertical BHEs, were simulated dynamically using TRNSYS [60]. The goal of this research was to optimize integration of the STPs in GSHP systems, in order to maximize the overall performance. Compared to a standalone GSHP systems, a large electricity saving potential was found. The results also indicated that the relative energy saving potential by utilization of solar heat, increased as the dimensioning of the BHE circuit decreased. The motivation behind integration of STPs with BHE-coupled GSHP systems is summarized as following:

1. To decrease the electricity use in the overall system.
2. To raise the average temperature in the borehole.
3. To decrease the net heat extraction from the borehole.

In combined systems both the solar collectors and the heat pump can get new operating conditions that ultimately improve the overall system performance [59]. For instance, the solar collectors might be used to increase the evaporation temperature of the heat pump, in which case the efficiency of the heat pump would improve. The solar collector system can cover the entire DHW demand during the summertime, thus reducing the operating time for the heat pump. This coincide with the HYSS methodology [14]. For intermittently (ON/OFF) controlled heat pumps, wear and tear of the compressor is furthermore reduced, as short operation periods are eliminated.

4.4.1 Thermal Depletion and Recharging

In France, Trillat-Berdal et al. experimentally investigated the effect of borehole recharging on the system COP [56]. Between November 2004 and September 2005 the power extracted from the ground had an average value of 40.3 W/m. Simultaneously, the power of solar heat injected to the ground had an average value of 39.5 W/m. By recharging the borehole with solar heat during summertime, the long-term loss in performance was practically redeemed. At the second start-up in the fall of 2005, the measured COP was equivalent to the measured value in the previous year.

Long-term thermal depletion was studied theoretically by means of TRNSYS simulations [13, 60]. It was found that thermal depletion of the ground is relatively rapid during the first year of operation, and then decreases at an increasingly slower rate. Over a 20-year period the simulated temperature decrease in the ground was 2 °C on average, although a steady state condition was not reached. The long-term temperature decrease was found to be more or less depending on the following parameters:

- Bedrock characteristics (conductivity, specific heat capacity, etc.)
- Initial ground temperature.
- Water content.
- Building loads.
- Borehole spacing.
- Borehole fill material.

E. Kjellsson et al. [59] concluded that long-term thermal recharging is of primary interest for borehole-coupled systems. However, if the heat collector system is properly sized, it might be more efficient to produce DHW during the summertime. This is because the natural recharging from the surroundings is large during the summer, when the heat extraction is low. Meanwhile, heat supplied to the borehole is quickly dissipated to the ambient, and gives almost no annual savings in electricity. These arguments are even more relevant for horizontal collector systems. Hence, thermal recharging was regarded most advantageous if closely timed to the heat extraction. **The sooner the recharged heat is extracted, the better**. If there is almost no need for auxiliary electric heating, the advantage of recharging is low. These findings are summarized as following:

1. For systems with undersized borehole systems, the savings in electricity may be large, especially if the solar heat can replace electricity from auxiliary electric heaters.

2. If the boreholes are oversized, then the potential savings from thermal recharging are negligible.

3. Solar heat for DHW heating is always replacing electricity, as the equivalent operating time for the GSHP decreases. This is valid, irrespective of the borehole depth.

Increased electricity use to circulation pumps, due to longer operating times, is a another disadvantage of solar thermal recharging. If the solar collector and borehole systems are permitted to run whenever solar heat is available, the increased electricity use to the circulation pumps may easily exceed the savings in electricity for the heat pump [59]. This emphasizes the importance of **high-efficiency circulator pumps**. If the system is well-designed and dimensioned with respect to GSHP heating capacity, borehole depth or collector length, and building load, while presuming all subsystems are working well, then the best use of solar heat is for DHW production during the summertime (March-October) and for borehole recharging during the wintertime (November-February). The optimum periods for this control strategy depend on the size of the heat load and the actual DHW demand.

4.4.2 Operation Strategies

It is recommended that solar assisted heat pump systems are designed and controlled so that solar heat can be utilized in alternative ways when the temperature is insufficiently high for DHW production [59]. Typical examples include low-temperature space heating, DHW preheating, increase of the evaporator inlet brine temperature, or recharging of the ground. E. Kjellsson et al. [57, 59] and Trillat-Berdal et al. [56, 13] suggested the following methodology for optimized utilization of solar thermal energy in combined systems:

At high temperatures (> 50°C) , the solar collectors should be used to produce or preheat DHW. In this case the heat pump is not in operation. This reduces the operating time for the heat pump, as well as the net heat extraction from the borehole.

At medium temperatures (20-50 °C) , the solar collectors should be used in combination with the space heating system. The overall system efficiency is improved as the solar collector operating time is increased, while the heat pump operating time is reduced. Simultaneously, the net heat extraction from the ground is reduced.

At low temperatures (5-20 °C) , there are two optional uses for the solar collectors. **Alternative 1** is to increase the brine temperature to the heat pump evaporator. This results in improved operating conditions and a higher COP for the GSHP. Meanwhile, the operating time for the solar collectors is increased. Improved operating conditions for the GSHP results in increased heat production and a reduced operating time. Due to the brine temperature increase, the net heat extraction from the ground is also reduced.

Alternative 2 is to use the solar heat to recharge the ground. In this case the heat pump is not in operation, implying that there must be no other heating demand in the building. This operation strategy result in both increased efficiency for the overall system and a longer operating time for the solar collectors. Heat injection to the ground results in a short-term increase in the ground temperature, and improved operational conditions for the heat pump. Meanwhile, long-term heat depletion of undersized ground collector systems may be counteracted.

4.5 Key Design Parameters for the Multikomfort ZEB

The *Multikomfort* ZEB is a pilot project, located in Larvik in the south of Norway [61]. It is a two-story single-family dwelling with a heated floor area of 202 m^2, and is designed and built according to the ZEB O&M ambition level. The system is relatively complex, and integrates state-of-the-art technologies for energy conservation and utilization of on-site renewable energy sources. A *Nilan Compact P Geo 3* combined GSHP and an exhaust air heat pump (EAHP) works together with a solar thermal system to cover the thermal energy demand. Additionally, heat is recovered at moderate temperatures from the exhaust air and from low-temperature grey water.

The calculated energy demand for DHW production in the building constitutes 60 % of the total thermal energy demand, while SH and heating of ventilation air account for the remainder [62]. The GSHP is designed for 80 % thermal energy coverage, and collects heat from one of two optional circuits: 1) a 150 m horizontal loop (SCF), or 2) a 100 m vertical loop (BHE). The remaining 20 % of the heating demand is covered by the solar thermal system. This system comprises 16 m^2 of *Hewalex* flat plate STPs that are mounted at 19° incline on the roof, facing southeast. Solar heat is accumulated in a space heating tank in the bottom section of an *OSO EPTRC 400* IWT, identical to that found at the Living Lab. Hence, solar energy is used for preheating of DHW, as well as for low-temperature underfloor heating. Additionally, one large radiator by *Lyngson* is located on each floor [62]. The top section of the IWT comprises a DHWT. A principle flow scheme of the system is given in fig. 4.6.

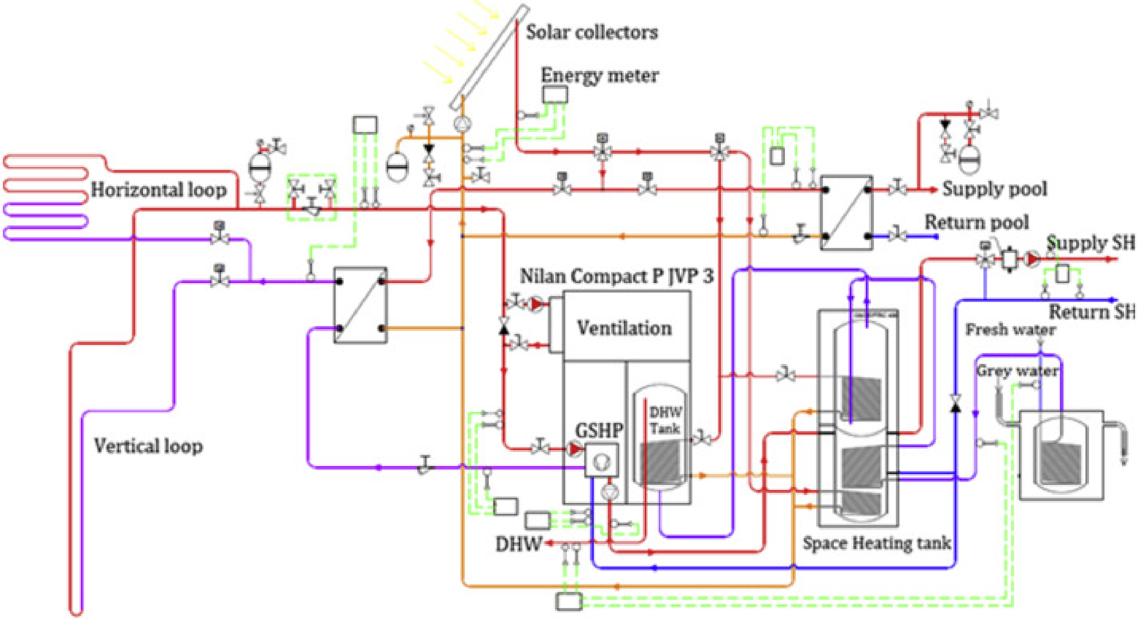
Solar collectors
Energy meter
Horizontal loop
Supply pool
Return pool
Supply SH
Nilan Compact P JVP 3
Ventilation
Return SH
Fresh water
Grey water
Vertical loop
GSHP
DHW Tank
DHW
Space Heating tank

Figure 4.6: Principle flow scheme of the integrated thermal energy system at the Multikomfort ZEB[15, 16]

As the DHW demand comprises a major part of the total heating demand, the system has been designed accordingly, and about 50 % of this heat is recovered after end use. This is achieved by means of heat exchangers in the drains, after which the entire volume of grey water is passed through an *OSO Energy Saver* heat recovery tank. After preheating with recovered heat, the DHW is passed through the bottom section of the IWT. Here, subsequent heating is achieved by means of a solar thermal coil, before reheating either by means of the GSHP (wintertime) or by the EAHP (summertime). Reheating by means of a 3 kW IEH is also possible. DHW is then transferred to the top section of the IWT, which accommodates a high temperature solar thermal coil, before being transferred to the auxiliary DHWT in the *Nilan Compact P* unit. A third solar thermal coil in this tank enables additional renewable energy input.

Nord et al. theoretically assessed the performance of the combined GSHP and STC system in the *Multikomfort* ZEB [15]. The sensitivity on the total energy use was assessed by simulating the system in the dynamic software IDA ICE, while changing one design parameter at a time. The effect in change of a given design parameter was quantified as the percentage change in total system electrical energy use (ΔE), relative to the percentage change of the parameter (ΔX). The results are summarized in table 4.1.

Table 4.1: Relative effect of change in design parameters [15]

	Parameter	$k = \frac{\Delta E}{\Delta X}$ [%]
1	Distribution supply temperature	38.5
2	Supply air volume rate	25.2
3	Storage volume, DHW	5.5
4	Storage volume, SH	4.6
5	Solar collector area	1.7

Solar collector areas between 8 and 16 m^2 were investigated to see the influence on system performance and electricity use. For each case the solar fraction was calculated and compared to the specific delivered solar energy on a monthly and annual basis. The solar fractions, which include the solar energy used to recharge the borehole, were highest for the largest collector areas, although only small changes were seen by reducing the area from 16 to 12 m^2. For 16 m^2 collector area the simulated annual solar fraction was 35.9 % with a total annual specific delivered energy of 35.5 kWh/m^2. By comparison, the simulated values for 8 m^2 collector area were 22.3 % and 36.1 kWh/m^2, respectively. From May to August, a STC area of 16 m^2 was able to cover 60 % of the DHW demand, whereas an area of 8 m^2 was able to cover 45-50 % of the demand. Simulations showed that by directing the collector surface towards the south, while increasing the tilt angle from 19° to the optimum of 55°, the annual solar fraction increased by 18 %. An oversized STC area of 16 m^2, compared to a moderate 8 m^2, could result in a reduced electricity use of 1.6 %. Optimized tilt angle and orientation of the STCs also contribute to reduced losses.

The effect of the DHWT volume on the annual solar fraction and specific delivered energy was also simulated by increasing the volume from 180 to 300 l. As a result, the solar volume was less affected by heat input from other heat sources. Due to better stratification, a lower temperature could be maintained at the bottom of the tank, thus improving the thermal efficiency. The inlet temperature to the STCs was consequently reduced by 3-4 K, giving an increase in the annual solar fraction of 3 %, and a decrease in the specific delivered energy for 3.7 %.

For the SH tank , no dependency between the height/diameter (h/d) ratio and the specific delivered energy was observed. There was however some correlation with the annual solar fraction. Reducing the h/d ratio from the initial 2.08 to 1.5 decreased the annual solar fraction by 0.6 %, whereas an increase from 2.08 to 2.6, gave an increase in the annual solar fraction of 0.3 %. Storing solar energy in the DHW tank is thus advised, as this increases the annual solar fraction more effectively with an increasing tank volume. The DHW tank volume is thus regarded as an important design parameter.

The volumetric flow rate and temperature of the ventilation supply air, as well as zone set-point temperatures had a slightly greater effect on the delivered electrical energy. By reducing the air volume flow rate from 1.2 to 1.0 m^3/hm^2, the electricity use was reduced by 4.2 %, while keeping the CO_2 concentration below the recommended limit of 1000 ppm. Reducing the supply air and zone set point temperatures from 20 to 19 °C resulted in a 3.6 % reduction in delivered electricity. By decreasing the supply temperature in the SH system from 35 to 32 °C, the system performance was improved as the COP of the GSHP increased.

An important point for consideration is that when a change in parameter leads to increased component sizes, the amount of saved energy must be weighted against the additional investment cost [15]. In general, the simulations indicated that the **supply air volume and temperature**, as well as the **zone set-point temperature** had the greatest relative impact on the specific delivered electricity. Variations in the IWT volume, and STC area, had a lower impact, due to smaller percentage changes in these parameters.

Chapter 5

Thermal Energy Supply at the Living Laboratory

The thermal energy supply system at the Living Laboratory [29] is designed to maximize the energy yield from on-site renewable energy sources. As a result, the system integrates both a ground-source heat pump and a solar thermal collector system. Both subsystems are coupled with an integrated water tank (IWT) for space heat accumulation and domestic hot water storage. The IWT incorporates one immersed electrical heater in each tank section, to ensure peak load coverage.

The overall system may be divided into several subsystems. In the following, these are distinguished as a heat pump subsystem, a solar thermal subsystem, a heat accumulation and storage subsystem, and a heat distribution subsystem. The latter may further be separated into primary and secondary circuits. In this context however, the heat pump, solar thermal, and thermal storage subsystems are the main focus.

5.1 Heat Pump Circuits

5.1.1 Ground Source Heat Pump Unit

A Calorex WW3500 brine-to-water heat pump unit has been installed to cover the majority of the demand for space heating, heating of ventilation air and domestic hot water production [63]. According to manufacturer test data the nominal heating capacity is 3.17 kW at 0 °C brine inlet temperature, and 35 °C outlet water temperature (0/35 °C). At these conditions the input power to the compressor is rated at 0.86 kW, resulting in a nominal COP of 3.69. At 0/55 °C, the heating capacity is reduced to 2.61 kW. At this condition the nominal compressor input power is given as 0.87 kW, which give a resulting COP of 3. Performance data as reported by the manufacturer is summarized in table 5.1.

Table 5.1: WW3500 performance data at 0 °C brine inlet temperature.

t_{w-o} [°C]	Q_{cond} [kW]	W_{el} [kW]	COP [-]	ε_C [-] [-]	η_C [-]
35	3.17	0.86	3.69	8.80	41.9
55	2.61	0.87	3.00	5.97	50.3

Fig. 5.1 the principle design of the Calorex heat pump unit, which is fairly simple. The unit incorporates the five basic components; an evaporator, a compressor, a condenser, a liquid receiver and a thermostatic throttling valve. The compressor is a fixed-speed hermetic scroll type, which is designed for operation with HFC working fluids, such as R134a, R404A and R407C. The heat pump unit is charged with 2.5 kg of R134a, and uses a polyolester (POE) lubricant.

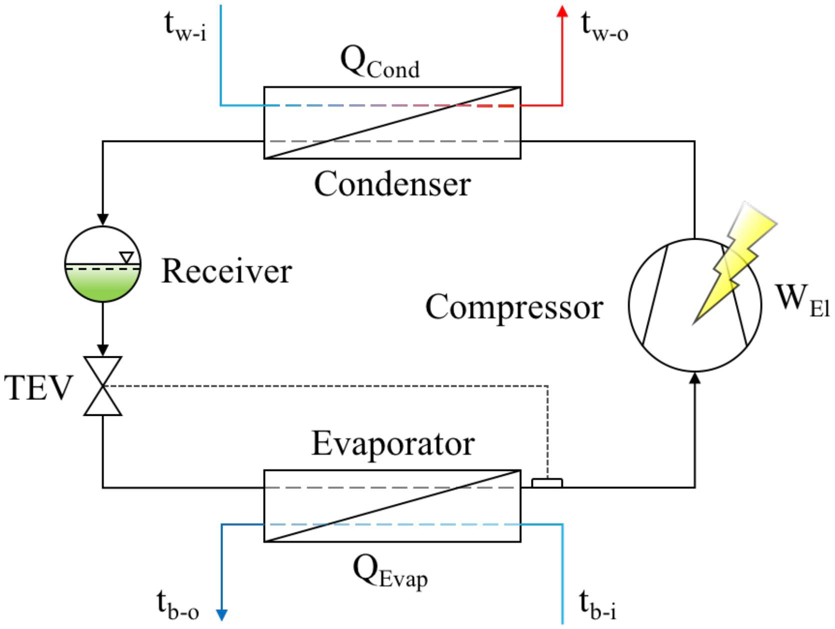

Figure 5.1: Principle flow scheme of the Calorex heat pump unit.

The compressor is compatible with evaporation temperatures ranging from -30 to +10 °C, and condensarion temperatures ranging from 25 to 65 °C. Fig. 5.2 illustrates the permissible operating range for the compressor, with R407C as the working fluid. At evaporation temperatures above -5 °C, the compressor is restricted to a maximum temperature lift of 40 K. At evaporation temperatures below -5 °C, the maximum temperature lift quickly decreases.

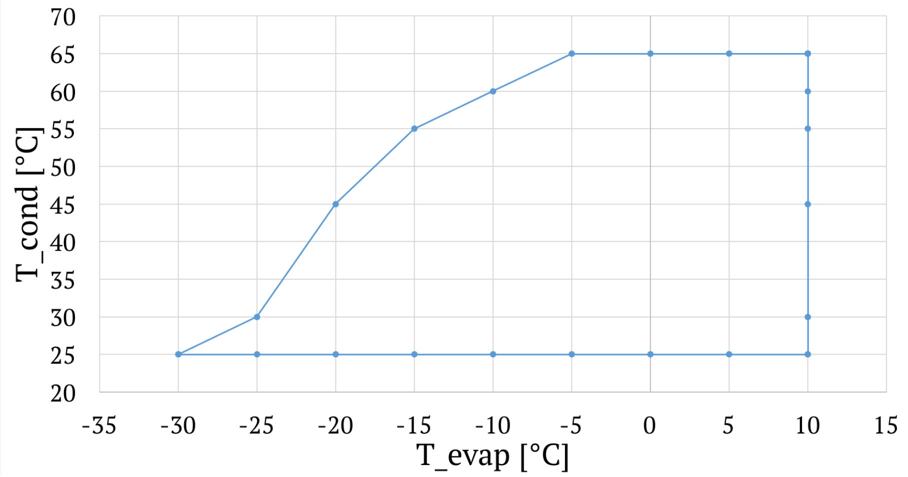

Figure 5.2: Operating range for the scroll compressor.

5.1.2 Ground Collector Circuit

The heat collector system comprises a horizontal ground source heat exchanger, which is buried at 1-1.5 m depth on the north side of the building. The heat exchanger is a smooth PN6.3 ø40x2.4 mm PE tube, with an approximate length of 105 m and a heat transfer surface of 26.4 m^2. The total area of the surface collector field is approximately 100 m^2. Fig. 5.3 illustrates the projected layout of the ground heat exchanger. A mutual distance of approximately 1.5 m is used in order to minimize thermal influence between parallel tubes.

Heat is extracted from the ground by cooling the surrounding soil. Depending on the moisture content in the ground, a share of the heat absorption occur as latent heat transfer when the water in the soil freezes. During parts of the year, the temperature on the heat carrier fluid drops below the normal freezing point of water. Consequently, an antifreeze brine is utilized.

At the Living Lab an aqueous solution propylene glycol is applied. The use of propylene glycol is motivated from environmental and safety concerns, as well as the fact that the PG mixture contains a favorable corrosion inhibitor. The substance is ecologically benign, and the consequences in case of leakage are negligible [64]. With respect to hydrodynamic and thermodynamic performance, however, an aqueous solution of ethyl alcohol would be preferable.

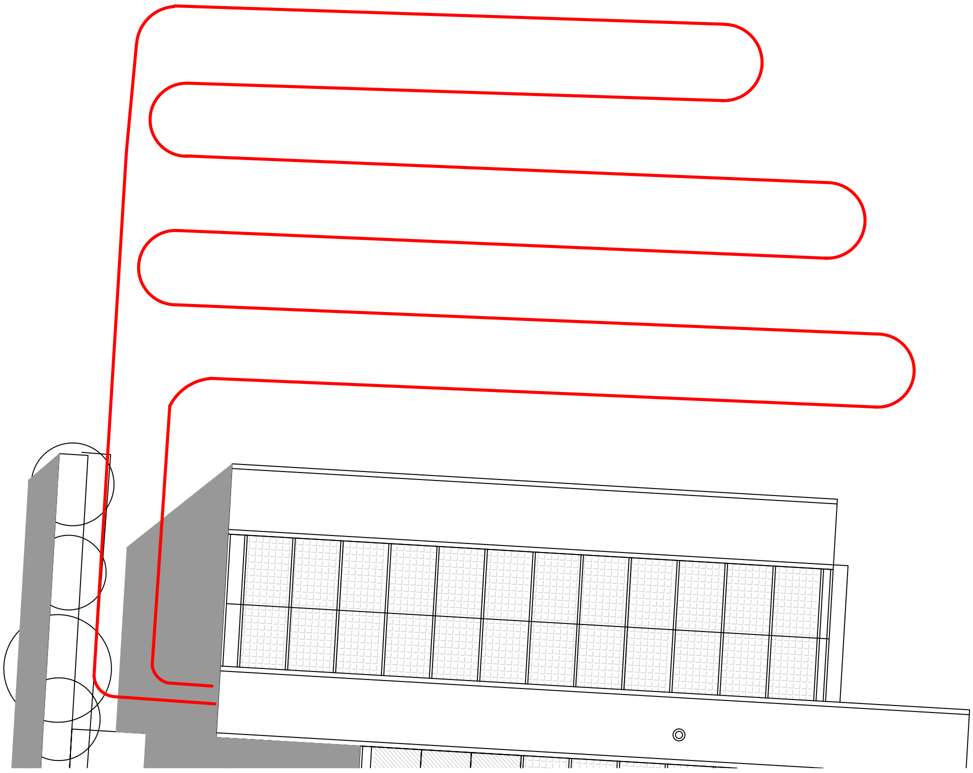

Figure 5.3: Principle layout of the horizontal collector circuit.

5.2 Solar Thermal Circuit

The solar thermal circuit (STC) is designed as a combined DHW and space heating system, comprising two façade-mouted *Hewalex KS2000 SLP* glazed flat plate collectors. The combined aperture area is 3.63 m^2. Fig 5.4 depicts a cross-sectional view of the solar collectors, and unveils a relatively simple design. The construction comprises copper tubes, attached to the back of an absorber plate. These are thermally insulated underneath and on the sides. A glass cover plate is mounted on the outside of the absorber plate, with an air gap in between. The absorber plate is coated by a black chrome film, which gives a high absorption coefficient, durability and corrosion resistance [17].

As for the ground collector circuit, sub-zero temperatures will prevail in the STC during the wintertime. Consequently, an antifreeze solar fluid is used. Unlike the ground collector loop, however, the solar fluid must be able to resist excessive stagnation temperatures in the range 150-160 °C. Due to this requirement, the same aqueous propylene glycol solution is used in the STC, as in the ground loop.

Solar heat can be utilized by the thermal energy system in one of two ways. The first option is heat rejection to the bottom section of the integrated water tank (IWT), by means of a 0.7 m^2 coil, see fig. 5.5 in section 5.3. This enables pre-heating of DHW

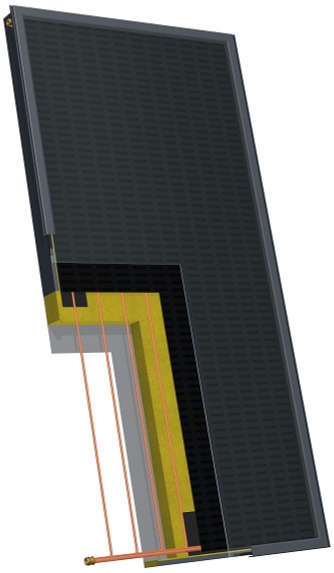

Figure 5.4: Cross sectional view of the Hewalex KS2000 SLP solar thermal collector [17].

and low-temperature space heating. The second option is to exchange heat with the ground collector circuit, by means of a compact brazed plate heat exchanger (BPHX). For optimal heat transfer efficiency a counter-flow arrangement is used for the two streams.

5.3 Heat Accumulation and Storage

The heart of the hydronic system is an OSO EPTRC 400 integrated space heat (SH) accumulation and domestic hot water (DHW) storage tank. This is a tank-in-tank configuration with the two sections physically separated by a metal wall. Conduction heat transfer from one side to the other is thus allowed. The IWT has four main temperature zones, namely, pre-heating of DHW, space heating, re-heating of DHW with the heat pump, and top-up DHW heat by electrical heating. The tank is very compact and therefore well-suited for small spaces, which is the case for the technical room at the Living Lab. Exterior dimensions of the tank are ø580x2250H mm. Fig. 5.5 shows the principle construction of the IWT.

The SH tank has a volumetric capacity of 160 liters and serves as temporary heat storage for the hydronic heating systems, and functions as a buffer for the GSHP due to ON/OFF control. The hydronic system may draw heat from the tank until the average

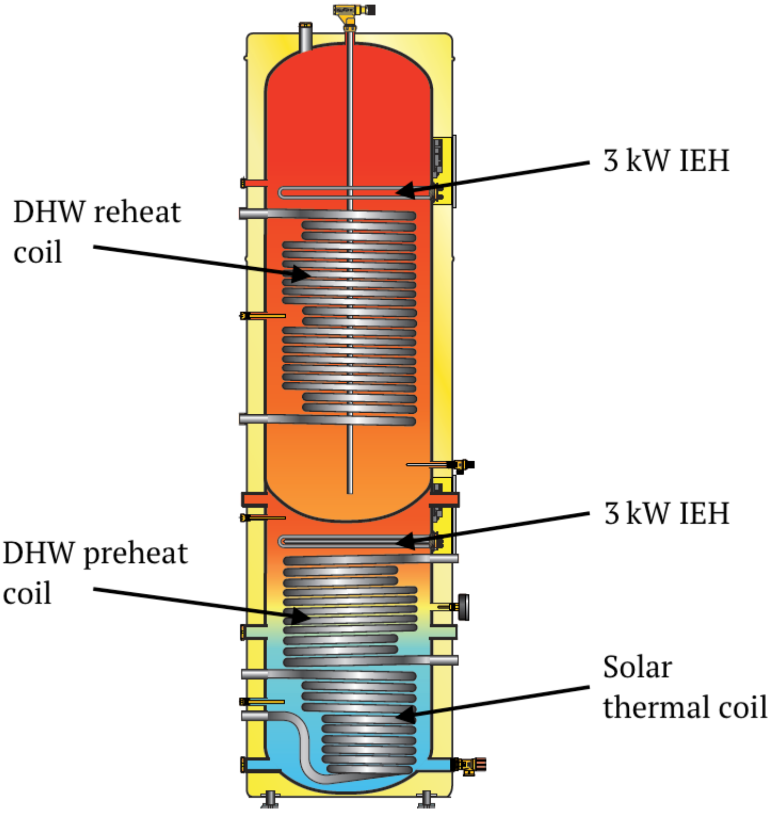

Figure 5.5: Principle flow scheme of the thermal energy system at the Living Lab [4]

temperature reaches a pre-set value, before any of the heat sources are activated. This reduces the intermittency of operation for the heat pump, as well as the operation time for the 3 kW immersed electric heater (IEH), which is located in the upper region of the tank. The set-point temperature of the IEH is presently 40 °C, but may be adjusted within the range of 30-60 °C. If needed, the capacity of the coil can be increased to 6 or 9 kW. A DHW preheating coil with 0.8 m^2 heat transfer area is located above the solar thermal coil, in the middle section of the tank.

The top section of the IWT comprises a 240 liter DHW storage volume. It integrates a 3 kW IEH, located in the top region of the tank, which is activated automatically according to a pre-set temperature requirement. The current setting for the thermostat is 70 °C, although a range between 60 and 90 °C is possible. To minimize the risk of bacterial growth (legionella) a minimum set-point temperature of 65 °C is recommended by the manufacturer. A large coil with a heat transfer surface of 1.8 m^2 occupies the middle and lower region of the tank. This coil is coupled with the ground source heat pump, and is activated when there is a DHW load. That is, when the average temperature in the tank drops below the set-point.

5.4 Heat Distribution

The heat distribution system is designed to be flexible with respect to heating strategies. Specifically, four options are available: 1) underfloor heating in several zones, 2) heating by means of a single interior wall-mounted radiator, 3) heating by means of a ventilation heating battery, or 4) a combination of the previous options. In the subsequent sections the overall system is dissected, and presented as separate subsystems.

5.4.1 Primary Circuit

The heat distribution system has been designed to supply heat at medium temperatures for space heating by means of a **radiator** circuit, and for ventilation heating by means of a duct-mounted **heating battery**. Fig. 5.6 and 5.7 illustrate the principle layout of the circuits.

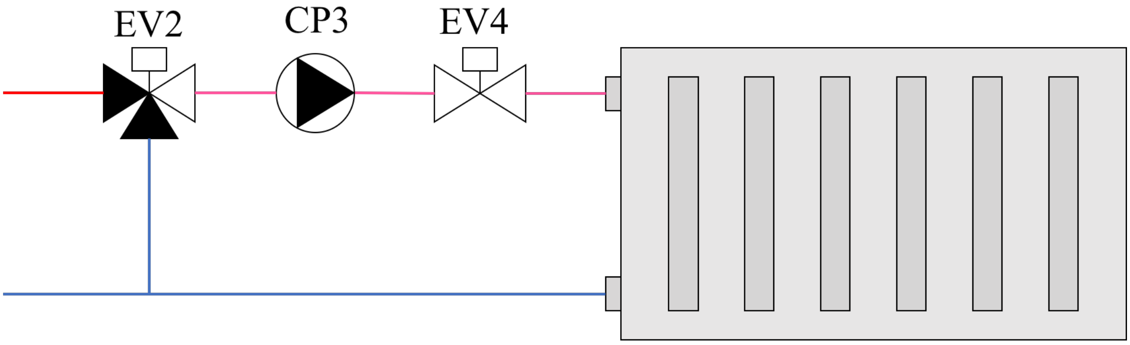

Figure 5.6: Capacity control of the radiator circuit.

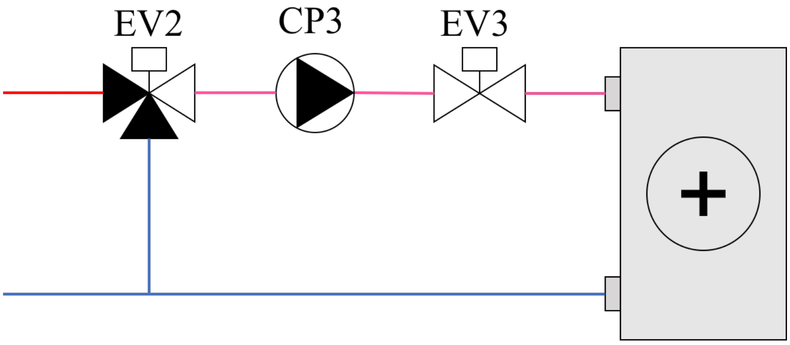

Figure 5.7: Capacity control of the heating battery.

At design conditions, the supply and return temperatures are 55/50 °C. Design volumetric flow rates are 436 l/h for both the radiator and heating battery circuits, with resulting heating power of 2.5 kW. At higher ambient temperatures the supply and return temperatures should be controlled according to the actual power demand, preferably according to and outdoor compensation curve. Keeping the distribution temperatures as low as possible is beneficial with respect to the COP and heating capacity of the Calorex heat pump.

5.4.2 Secondary Circuit

From a thermodynamic point of view it is more advantageous to supply heat at lower temperature levels, especially for a heat pump. A low-temperature underfloor heating (UFH) system is coupled with the primary circuit by means of an OSO MX pump central, as illustrated in fig. 5.8. The pump central integrates a *Grundfos Alpha2 L* pump, a shunt valve and a deaerator, and can optionally be fitted with an 18 liter expansion vessel. The latter has been omitted since the hydronic system has an expansion vessel integrated at the SH tank. The combination of the primary circuit pump, CP3, and the OSO pump central may be recognized as a "Norwegian coupling", according to [20, p. 426].

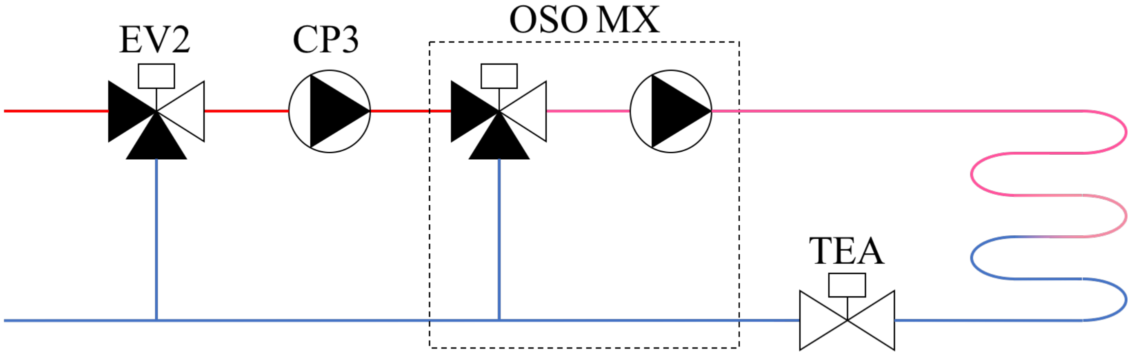

Figure 5.8: Capacity control of the floor heating circuits.

Supply and return water is mixed to achieve temperature control of the underfloor heating system. Depending on the actual demand, heat is delivered to maximum eight underfloor heating circuits. Zoning of these circuits is illustrated in fig. 5.9. Design temperature levels for the supply and return lines are 33/28 °C, with a volumetric flow rate of 601 l/h and heating power of 3.5 kW.

5.5 Monitoring and Data Acquisition

Monitoring, data aqcuisition (DAQ) and control of the Living Lab technical systems is an integrated solution, based on the National Instruments LabVIEW platform. This software is specifically designed for advanced measurements, enabling user interfaces and functionality to be tailored for the specific experiment [65].

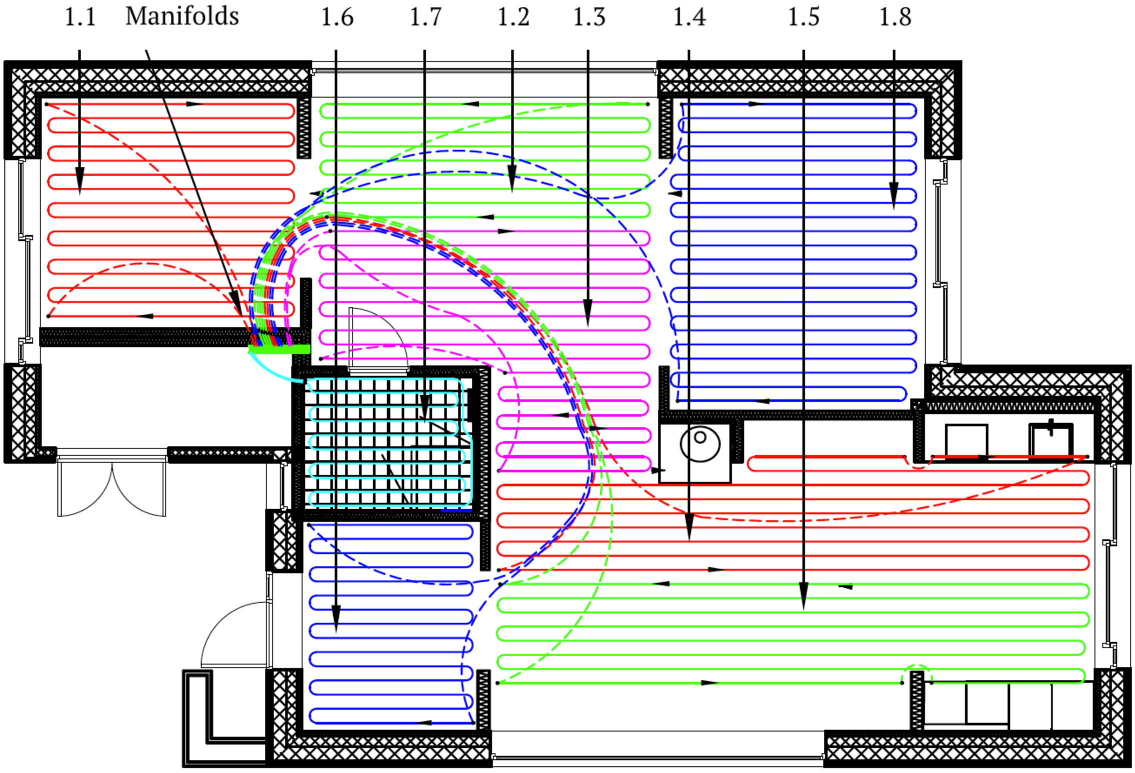

Figure 5.9: Zoning of the underfloor heating circuits.

Table 5.2: Overview of underfloor heating circuits and zones.

Closing valve	Circuit	Length [m]	Zone
TEA1	1.1	68	Bedroom, west
TEA2	1.2	54	Living room, north
TEA3	1.3	79	Living room, north
TEA4	1.4	96	Living room, south + kitchen
TEA5	1.5	92	Living room, south + kitchen
TEA6	1.6	63	Entrance
TEA7	1.7	28	Bathroom
TEA8	1.8	98	Bedroom, east

The hardware is a National Instruments CompactRIO platform, to which signals from sensors and transducers are routed. Like the LabVIEW software, this system can be customized for the particular purpose [3]. It combines controllers, input/output modules and expansion slots, which is flexible with respect to future expansions or modifications. Presently, the system includes one controller, two expansion slots, and a total of 19 different input/output signal modules. Transducers and components communicate with the monitoring and control system through a Modbus communication protocol. Different equipment and sensors use different control signals. Among these are 0-10 V analogue signals, 24 V digital signals, and Modbus serial communication.

An example of the latter is the serial connection of circulator pump signals.

The DAQ system has been designed with a certain compromise between measuring accuracy, and the number and type of sensors. Hence, the measuring accuracy is lower compared to typical laboratory standards, and primarily commercialized measurement equipment is used. With respect to the Living Lab as a test facility, more sensors are used than what would be required for a typical single-family house. These sensors are nevertheless integrated as would be expected for a real-life scenario.

While the monitoring and DAQ system is fairly comprehensive, the following presentation is limited to relevant functionality for monitoring and control of the systems for thermal energy supply. A complete schematic of the MAC system is provided in appendix A.

5.5.1 Thermal Energy Metering in Hydronic Circuits

Thermal energy production and use is monitored by means of thermal energy meters (TEMs) at five separate locations in the hydronic circuits. The TEMs are of the type *Kamstrup Multical 602*, which have functionality to calculate thermal energy and power, based on measured quantities of temperature and volumetric flow. The latter is measured by *Kamstrup Ultraflow 54* ultrasonic sensors, while temperatures are measured by means of Pt500 probes. The combined accuracy of energy measurements when used in combination with pure water is ± 2 %.

Table 5.3 gives an overview of the installed thermal energy meters, their locations and connected sensors. The thermal energy output from the heat pump unit, as well as the thermal energy use for DHW, radiator and heating battery, underfloor heating in the living rooms, and underfloor heating in the bedrooms and bathroom are measured.

Table 5.3: Overview of thermal energy meters and connected sensors.

Location	TEM	Temperature	Volumetric flow
Heat pump output	TEM1	RTD4, RTD5, RTD6	UFS1, UFS2
Domestic hot water use	TEM2	RTD13, RTD14, RTD15	UFS3, UFS4
Radiator and heating battery	TEM3	RTD17, RTD18, RTD19	UFS5, UFS6
UFH, living rooms	TEM4	RTD20, RTD21	UFS7
UFH, bedrooms and bathroom	TEM5	RTD22, RTD23, RTD24	UFS8, UFS9

5.5.2 Thermal Energy Metering in Brine Circuits

Thermal energy quantities in the ground collector and solar thermal brine circuits are monitored by means of separate Pt100 probes and volumetric flow sensors. Hence, thermal the energy flows in these circuits must be calculated manually, which contributes to a lower measuring accuracy.

In the ground collector circuit, the volumetric flow rate is measured by means of an *Omega FMG94-PVDF* full-flow electromagnetic flow meter (EFS1). It has a range of 2...120 l/h and an accuracy of ± 5 %. The supply brine temperatures, before (RTD1) and after (RTD2) the heat exchanger, and the return brine temperature (RTD3), are measured by means of Pt100 probes. These have a range of -50...180 °C, and an accuracy of ± 0.1 °C.

In the solar collector circuit, the volumetric flow is measured by an *Omega FMG93-PVDF* electromagnetic sensor (EFS2). This sensor has a range of 1...60 l/h and an accuracy of ± 5%. Solar panel inlet (RTD25) and outlet (RTD26) temperatures are measured by means of Pt100 probes. These have a range of -50...180 °C, and an accuracy of ± 0.1 °C.

5.5.3 Electric Energy Metering

Electric energy use for operation of the heat pump unit, circulation pumps and actuators, as well as auxiliary heat for the IEHs are monitored by means of *C18WS* electrical energy meters (EEMs) by *Frer*. The measured quantities have a resolution of 1 Wh, and an accuracy of ± 1%.

5.5.4 Temperature Metering in the Main Ventilation Ducts

The temperatures and relative humidities in the main ventilation ducts are measured by *Delta Ohm HD4917ET01* multi-sensors. The sensors are placed in the outdoor air supply duct (TRHT1), exhaust air duct (TRHT2), main supply duct before the hydronic coil (TRHT3), main supply duct after the hydronic coil (TRHT4), and in the main extract duct (TRHT5). Temperature sensors are Pt100 probes, with a range of -40...+150 °C and an accuracy of ± 0.3 K. Relative humidity is measured by capacitive probes, with a range of 0...100 % and an accuracy of ± 1.5%.

5.5.5 Temperature Metering in the Integrated Water Tank

The water temperatures in the IWT are measured by means of *S+S Regeltechnik HTF-200* 4-wire probes, that have an accuracy of ± 0.1 K. In the SH tank, the temperature is measured near the bottom at the solar coil (RTD9) and at the top above the lower IEH, near the the tank outlet (RTD10). In the DHW tank the temperatures are measured at the middle, near the heat pump coil (RTD11), and at the top between the heat pump coil and the upper IEH (RTD12). These temperatures are used for thermostat settings for the solar panels, heat pump and IEHs.

5.5.6 Indoor Environmental Quantities

For control and operation of the thermal energy system, the indoor air temperatures are the most relevant quantities. They are measured in the occupied zone at 1.6 m height, by means of *S+S Regeltechnik* multi-sensors. Temperatures are measured in the range of 0...50 °C, at an accuracy of ± 0.8 °C. These temperatures are used as *actual* values for controlling the heating and ventilation system. An overview is given in table 8.5. Relative humidity is measured by capacitive probes, with a range of 0...100 % and an accuracy of ± 3%.

Table 5.4: Indoor temperature control sensors.

Zone	Sensor
Living room south	TRHT13
Kitchen	TRHT14
Living room north	TRHT15
Bedroom west	TRHT16
Bedroom east	TRHT17
Bathroom	TRHT18

5.5.7 Outdoor Environmental Quantities

With respect to variations in the thermal energy demand and production, the most important quantities are the **outdoor air temperature** and the **global solar irradiance** on the south façade. The latter (SIM2) is measured by means of a *LP Pyra 03 AC* pyranometer by *Hukseflux*. The measured quantity is in W/m^2, which is measured within the range of 0...2000, with an accuracy of ± 5 %. The sensor is façade-mounted at 3.2 m height. The outdoor ambient air temperatures on the north (RTD28) and south (RTD27) façades are recorded by means of *AFT-2 Pt100* 4-wire probes by *S+S Regeltechnik*. This sensor has a range of -50...90 °C, and an accuracy of ± 0.1 K. Both sensors are mounted at 3.2 m height. It should be noted that the south façade sensor is exposed to solar irradiation.

Additionally, a *HD52.3DP147R* rooftop weather station (WS1) by *Delta Ohm* measures the outdoor air temperature and global solar irradiance on the horizontal surface. Temperature is measured by a Pt100 probe, with a range of -40...60 °C and ± 0.3 % accuracy. Global solar irradiance is measured in the range of 0...2000 W/m^2, with ± 5 %. Other quantities measured by the weather station include the relative humidity, barometric pressure, wind velocity and illuminance. The global solar irradiation on the PV surface, at a 30°angle, is measured by a pyranometer *Hukseflux* pyranometer, idetical to that on the south façade.

Chapter 6

Analytical Approach

The incentives for investing in a combined GSHP and solar thermal system are both environmental and economical. From the builders perspective the latter is decisive, and as such, the pay-back time and return on investment determines the viability of the system. These parameters are closely coherent with capital costs due to the initial investment, as well as energy and maintenance costs due to operation of the system. A profitable system is characterized by energy savings that surpass the costs for investment and maintenance.

This chapter presents the theoretical and experimental approach used to analyze the energy efficiency, operation, dimensioning and design of the thermal energy system at the ZEB Living Laboratory.

6.1 Operation and Control

The overall goal for operation of the GSHP and solar thermal heating system is to cover the annual heating demand at the lowest possible electrical energy input. Specifically, the largest annual savings go hand-in-hand with optimum system performance. It is therefore important that the heat source, which results in the lowest overall electrical energy input, is operated consecutively. Prioritization of the heat sources should be as following:

1. STC.
2. GSHP.
3. IEHs.

The singular electricity user in the STC is the pump, CP4. Heat production via the STPs should have first priority, provided that the thermal input potential is not restricted by the temperature level in the system.

Compared to the STC, operation of the GSHP requires a significantly higher electrical power input. This includes, at least, electric power input to the HP compressor, the brine circuit pump, CP1, and the hydronic pumps, CP2, CP3 and OSO MX. The GSHP should not be operated unless the thermal power output from the STC is insufficient to cover the demand.

The IWT IEHs are the least efficient thermal energy sources. Their operating time should be as short as possible, and they should only be activated to ensure that the minimum temperature requirements for DHW and space heating are maintained. Preferably, the GSHP should be controlling the auxiliary heat input from the IEHs. Based on these considerations, the following methodologies apply when operating strategies are analyzed:

- Minimize the overall electricity use (compressor, IEHs, pumps, actuators).
- Maximize the operating time and performance for the STC.
- Maximize the operating time and performance for the GSHP.
- Minimize the operating time for the IEHs.

Optimum energy efficiency is achieved when the (annual) thermal energy demand is covered at the lowest possible electrical energy input. This includes electrical energy use to the GSHP, IEHs, pumps and actuator valves. For the Living Laboratory optimization problem may be represented by eq. (6.1).

$$\min E_{tot} = E_{HP} + E_{IEH} + E_{CP1} + E_{CP2} + E_{CP3} + E_{CP4} + E_{OSOMX} \tag{6.1}$$

subject to:

$$Q_{HP} + Q_{IEH} + Q_{sol} \geq Q_{TEM2} + Q_{TEM3} + Q_{TEM4} + Q_{TEM5} + Q_{losses}$$

6.2 Performance and Control

The main parameters applied when assessing the performance and control of the combined GSHP and STC system are presented in table 6.1. The parameters are explained subsequently.

Table 6.1: Parameters addressing system performance.

	Performance parameter	Symbol	Analyzed	Approach
1.	HP Coefficient of Performance	COP	✓	Experimental
2.	HP Carnot efficiency	η_C	✓	Experimental
3.	HP volumetric heating capacity	VHC	✓	Theoretical
4.	HP Seasonal performance factor	SPF	✓	Experimental
5.	HP relative energy saving potential	ΔE	✓	Experimental
6.	Solar panel efficiency	η_{sol}	✓	Experimental

6.2.1 GSHP System

The coefficient of performance (COP) is used to evaluate the instantaneous performance of the heat pump unit. The relation is given by (6.2) as the ratio of the condenser heating capacity, to the electric power input of the compressor.

$$COP = \frac{\dot{Q}_{HP}}{\dot{W}_{HP}} \approx \frac{\dot{Q}_w}{\dot{W}_{ad}} [-] \tag{6.2}$$

where:

$\dot{Q}_{HP}$ = condenser heating capacity $[kW]$

$\dot{W}_{HP}$ = compressor electric input power $[kW]$

$\dot{Q}_w$ = heat delivered to the water $[kW]$

$\dot{W}_{ad}$ = adiabatic compressor power $[kW]$

The Carnot efficiency (η_C) is given by eq. (6.3) as the ratio of the actual COP and ε_C. It expresses the actual heat pump performance in relation to the ideal cycle. Hence, it provides a measure of the internal losses of the heat pump unit, such as heat exchange, compression and throttling losses.

$$\eta_C = \frac{COP}{\varepsilon_C} [-] \tag{6.3}$$

The Carnot COP (ε_C) is given by eq. (6.4), and expresses the performance of the ideal cycle. It is defined as the ratio between the heat sink temperature, T_{sink}, and the temperature lift, ΔT_{lift}.

$$\varepsilon_C = \frac{T_{sink}}{T_{sink} - T_{source}} = \frac{T_{sink}}{\Delta T_{lift}} = \frac{t_{w-o} + 273,15}{t_{w-o} - t_{b-i}} [-] \tag{6.4}$$

where:

T_{sink} = heat sink temperature $[K]$
T_{source} = heat source temperature $[K]$
ΔT_{lift} = temperature lift $[K]$
t_{w-o} = water outlet temperature $[°C]$
t_{b-i} = brine inlet temperature $[°C]$

The volumetric heating capacity (VHC) is given by eq. (6.5), and is specific to the performance of the working fluid. It is defined as the product of the vapor density at the compressor inlet, ρ_{vap}, and specific enthalpy difference in the condenser, Δh_{cond}. A constant VHC can be observed if ρ_{vap} decreases while Δh_{cond} increases, and vice versa.

$$VHC = \rho_{vap} \cdot \Delta h_{cond} [kJ/m^3] \tag{6.5}$$

where:

ρ_{vap} = the vapor density at the outlet of the evaporator $[kg/m^3]$
Δh_{cond} = the enthalpy change from inlet to outlet of the condenser $[kJ/kg]$

The VHC expresses the condenser heating capacity per unit volume of working fluid leaving the evaporator. This implies that for a constant condenser heating capacity the volumetric flow rate increases when ρ_{vap} decreases. A high VHC increases the system compactness, and reduces the necessary volumetric displacement capacity of the compressor. In turn, this implies a smaller working fluid charge and cheaper components. This performance measure is used to compare the benignity of different working fluids.

The seasonal performance factor (SPF) is used to evaluate the long-term performance of the heat pump system. The SPF is defined as the ratio of the supplied heat and the electrical energy input. This includes the thermal energy output from the HP and IEHs, and the electrical energy used by the HP, circulation pumps, and IEHs. The SPF is dependent on the use of auxiliary heat and decreases rapidly for undersized heat collector systems [59]. Ideally, the whole year performance of the system should be included. For the present analysis, however, only a fraction of the annual demand is included.

$$SPF = \frac{Q_{HP} + Q_{sol} + Q_{IEH}}{E_{HP} + E_{sol} + E_{IEH} + E_{aux}} [-] \tag{6.6}$$

The relative energy saving potential (ΔE), is used to display the energy saving benignity of the HP and HP system in relation to an electric heating system. It may be calculated on the basis of either the SPF or COP, and is described by eq. (6.7). Using the SPF as basis for the calculation is generally more representative to the annual savings.

$$\Delta E = \left(1 - \frac{1}{SPF}\right) \cdot 100\% \approx \left(1 - \frac{1}{SCOP}\right) \cdot 100\% [\%] \tag{6.7}$$

6.2.2 Heat Pump Cycle

The thermodynamic performance of different working fluids is evaluated for operation in a single-stage vapor compression cycle in Coolpack [66]. The following underlying assumptions apply when modeling the cycle:

1. Each component is treated as an individual control volume to which mass and energy rate balances apply.
2. Steady state operation.
3. Kinetic and potential energy effects are neglected.
4. The outlet state of one component equals the inlet state of the next.
5. All components have one inlet and one outlet.
6. Superheating at the evaporator outlet: $\Delta T_{sh} = 5$ K.
7. Subcooling at the condenser outlet: $\Delta T_{sc} = 2$ K.
8. Compressor heat losses: $\xi = 10$ % of the electrical input power.
9. Isentropic efficiencies are dependent only on the pressure ratio.
10. Pressure drops are neglected.

The transient mass and energy rate balance is given in its general form by eq.(6.8) [67, p. 157].

$$\frac{dE_{cv}}{dt} = \dot{Q}_{cv} - \dot{W}_{cv} + \sum_i \dot{m}_i \cdot (h_i + \frac{{V_i}^2}{2} + gz_i) - \sum_o \dot{m}_o \cdot (h_o + \frac{{V_o}^2}{2} + gz_e) \tag{6.8}$$

When assumptions 1, 2, 3 and 5, it reduces to eq. (6.9). This general equation applies to the each component of the HP cycle.

$$0 = \dot{Q}_{cv} - \dot{W}_{cv} + \dot{m}_R \cdot (h_i - h_o) \tag{6.9}$$

where:

$\dot{Q}_{cv}$	= heat transfer, defined positive out of the control volume	$[W]$
$\dot{W}_{cv}$	= work input, defined positive into the control volume	$[W]$
$\dot{m}_R$	= working fluid mass flow rate	$[kg/s]$
h_i	= specific enthalpy at the control volume inlet	$[kJ/kg]$
h_o	= specific enthalpy at the control volume outlet	$[kJ/kg]$

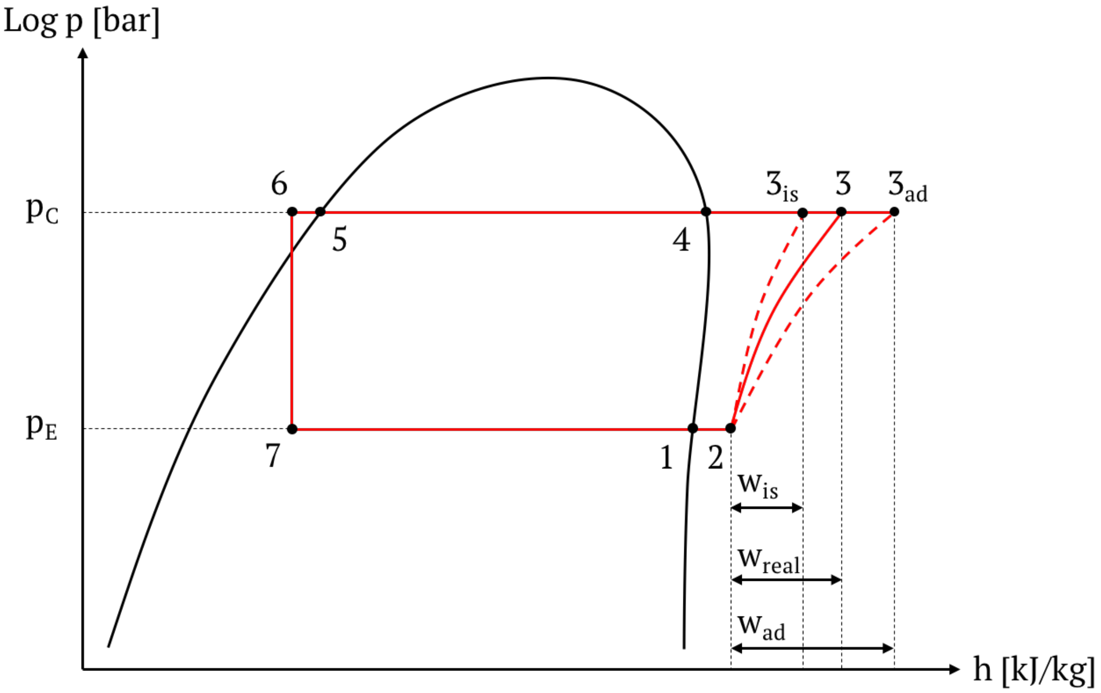

Figure 6.1: Principle Calorex GSHP vapor compression cycle.

Fig. 6.1 illustrates the principle vapor compression cycle, with seven distinct state points specified. External measurements of the water side temperatures and flow, electric power input, as well as condensing and evaporating pressures are made to complement the above assumptions. The water side flow and temperature measurements are used to determine the actual heating capacity, as given by eq. (6.10). This information is used to determine the working fluid mass flow rate, given by eq. (6.11).

$$\dot{Q}_C \approx \dot{Q}_w = \dot{V}_w \cdot \rho_w \cdot c_{p,w} \cdot (t_{w-o} - t_{w-i}) [kW] \tag{6.10}$$

$$\dot{m}_R = \frac{\dot{Q}_C}{\Delta h_{36}} \approx \frac{\dot{Q}_w}{\Delta h_{36}} [kg/s] \tag{6.11}$$

The thermodynamic work input, w_{real} in fig. 6.1, is determined my means of DAQ recordings of the compressor input power, w_{ad}, in combination with the isentropic efficiency and heat loss factor. The measured compressor work input is assumed adiabatic, as indicated by w_{ad} in fig. 6.1. While the inlet state (2) is specified by p_E and ΔT_{sh}, the outlet state (3) is given by eq. (6.12).

$$h_3 = h_2 + \left[\frac{h_{3,is} - h_2}{\eta_{is}}\right] \cdot \left[1 - \left(\frac{\xi}{100}\right)\right] [kJ/kg] \tag{6.12}$$

where:

h_2 =	compressor inlet specific enthalpy	$[kJ/kg]$
$h_{3,is}$ =	isentropic compressor outlet specific enthalpy	$[kJ/kg]$
η_{is} =	overall isentropic efficiency	$[-]$
ξ =	heat loss relative to the electric input power	$[-]$

The volumetric efficiency of the compressor is calculated by means of eq. (6.13), as the working fluid mass flow rate divided by the product of the displacement volume, $\dot{V}_s$, and the vapor density at the compressor inlet. The volumetric displacement is specified as 7.4 m^3/h at 2950 rpm [68].

$$\lambda = \frac{\dot{m}_R}{\dot{V}_s \cdot \rho_2} [-] \tag{6.13}$$

6.2.3 STC System

The panel efficiency, given by eq. (6.14), is an important consideration during the design phase of solar thermal systems. At optimal conditions, the efficiency of the flat plate STP is given as η_0. That is, with zero temperature difference between the circulated liquid average temperature and the ambient air temperature. At non-optimal conditions the panel efficiency is deteriorated due to convection, conduction and radiation heat losses. The magnitude of these losses increase as the temperature difference between circulated liquid and the surroundings increase.

$$\eta_{sol} = \eta_0 - a_1 \frac{(\bar{T}_m - T_a)}{G} - a_2 \frac{(\bar{T}_m - T_a)^2}{G} \tag{6.14}$$

where:

η_0 =	thermal efficiency with no ΔT between liquid and air	$[-]$
a_1 =	heat loss coefficient (convection and conduction)	$[W/(m^2 \cdot K)]$
a_2 =	heat loss coefficient (radiation)	$[W/(m^2 \cdot K)]$
$\bar{T}_m$ =	average liquid temperature in the STC	$[°C]$
T_a =	ambient air temperature	$[°C]$
G =	global solar irradiance	$[W/m^2]$

Eq. (6.14) indicates that the temperature dependent losses are dominating when the global solar irradiation is low. In this case, both thermal efficiency and power output is reduced. In order to achieve highest possible annual panel efficiency, the average liquid temperature in the collectors should be restricted. Hence, a low return temperature from the accumulation tank should be maintained. It turn, this requires efficient heat rejection to the accumulation tank.

6.3 Design and Dimensioning

The main parameters applied when assessing the design and dimensioning of the combined GSHP and STC system are presented in table 6.2.

Table 6.2: Parameters addressing system design and dimensioning.

	Design parameter	Symbol	Analyzed	Approach
1.	HP power coverage factor	β	✓	Theoretical
2.	HP energy coverage factor	α	✓	Theoretical
3.	Heat source temperatures	T_{source}	✓	Experimental
4.	Heat sink temperatures	T_{sink}	✓	Experimental
5.	Solar fraction	SF	✓	Theoretical
6.	Solar panel area	A_{STP}	✓	Theoretical
7.	Solar panel tilt angle	ψ	✓	Theoretical
8.	DHWT volume	V_{DHWT}	✗	-
9.	SHT volume	V_{SHT}	✗	-

6.3.1 GSHP System

The cost effectiveness of the heat pump system is determined by its capability to cover the annual heating demand at a lower cost than the alternatives. Heat pump systems are characterized by relatively high investment costs (NOK/kW), relatively low operating costs (NOK/kWh). Consequently, correct dimensioning with respect to installed heating power is decisive to obtain a positive balance between investment-related financial costs and operation-related energy savings.

The design point of the heat pump is determined by the share of the total annual heating demand to be covered. This is a matter of optimization, which depends on both capital costs and operational costs. The power coverage factor, β, is given by eq. (6.15). Brine-water system are traditionally designed for a β between 50 and 60 %. This typically results in an annual energy coverage factor, α, in the range of 80-95 % [20]. The energy coverage factor is given by eq. (6.16).

$$\beta = \frac{\dot{Q}_{HP}}{\dot{Q}_N} \tag{6.15}$$

where:

$\dot{Q}_{HP}$ = Heat pump design heating capacity $[kW]$
$\dot{Q}_N$ = Net power demand for space heating and ventilation $[kW]$

$$\alpha = \frac{Q_{HP}}{Q_N} \tag{6.16}$$

where:

Q_{HP} = Heat pump energy coverage $[kWh]$
Q_N = Net annual heating demand $[kWh]$

The heat pump system should be designed according to the building's net thermal power demand. This is because over-dimensioning results in a higher investment, marginally higher heat coverage, and reduced COP at part load. By contrast, under-dimensioning results in a lower investment, however, combined with a lower heat coverage and therefore reduced savings [41].

6.3.2 STC System

Residential solar thermal systems for DHW heating only, may achieve an annual solar fraction (SF) between 0.5 and 0.6 [20, 54]. Combined systems may achive an SF of 0.5 for DHW heating, and 0.1 - 0.3 for space heating. Table 6.3 provides an overview of recommended dimensioning values for STPs and accumulator tanks.

Table 6.3: Recommended dimensioning of solar thermal systems for single-family houses [20, p. 138].

	DHW system	Combined system
Solar collector area	$[m^2]$	$[m^2]$
Per person	1 - 2	2 - 3
Per single-family house	4 - 6	8 - 12
Accumulator tank volume	$[l]$	$[l]$
Per m^2 STP area	50 - 75	75 - 125
Per single-family house	250 - 300	400 - 750

Solar collector systems for space heating are recommended as support heating systems for buildings characterized by low thermal demands. For this purpose, a low heat distribution temperature, T_{sink}, is essential [54].

In combined systems, the accumulation tank should provide sufficient thermal stratification between the top and bottom. Hence, both high and low temperature solar heat input is made possible. Coverage of low-temperature heating demands, such as DHW preheating or low-temperature space heating, should be a first priority [20]. Higher temperature demands, such as space heating or DHW reheating may be covered as a second priority.

Chapter 7

Thermal Power and Energy Demands

The thermal energy supply at the Living Lab is a combined system, designed to cover the entire heating demand for space heating, heating of ventilation air and domestic hot water. In order to evaluate the dimensioning of the system, the theoretical heating power and energy demand has been calculated.

With respect to the thermal power demand, a distinction is made between the the **gross power demand** and the **net power demand**. A similar distinction is made between the demand for **delivered energy** to the building, and the **net energy use**. Subsequent calculations are made with respect to the net power demand and energy use. Hence, the efficiency of the thermal supply system is omitted.

7.1 Gross vs. Net Power Demand

The gross heating power demand, P_G, is the sum of space heating and ventilation air heating demands at nominal conditions. That is, the maximum heat loss rate at the prevailing design outdoor temperature (DOT). The net heating power demand, P_N, is determined as the gross demand, subtracted internal heat gains from artificial lighting, equipment, persons and solar irradiation.

The Internal heat gains from lighting and equipment are dependent on the electrical efficiency of these installations. Increasingly stringent efficiency requirements, set by EU Directives, contribute to reduced internal heat gains from electrical appliances. The magnitude of the internal gains from persons are dependent on their number, activity level and physique. Passive solar heat gains are dependent on geographical location and orientation of the building, absorption and emission characteristics of exterior building components and glazed surfaces, and also shading characteristics of nearby buildings and vegetation.

7.2 Domestic Hot Water Demand

The DHW demand is added to the space and ventilation heating demand, and is highly dependent on user behavior. Specifically, the demographic profile and number of building residents influences the energy use for daily tasks, such as showering and washing. According to [69, p. 268] the average DHW use in residential buildings is ~65 liters per day per person. Variations from the average are distinguished as:

- Low demand: 40 - 60 l/day/person
- Medium demand: 60 - 100 l/day/person
- High demand: 100 - 150 l/day/person

The energy use for DHW is further dependent on the temperature requirement, and average temperature levels in the DHWT. Typical requirements range between 38 and 55 °C, where the latter is most relevant to residential buildings [69, p. 273]. This further determines the effective volume and dimensioning of the DHWT.

7.3 Simulation Input Data

The net thermal energy use is calculated according to the dynamic procedure described in NS3031 [23]. Calculations are carried out using the validated simulation software SIMIEN [70]. Input data for the Living Lab building envelope and technical systems are selected according to documented specifications [2], and are as shown to the right in table 7.1.

Table 7.1: Overview of building performance input data [21, 22, 2]

		TEK10	Low energy	Passive house	Living Lab
U-value wall	W/m^2K	0.22	0.16	0.12	0.11
U-value floor	W/m^2K	0.18	0.12	0.08	0.10
U-value roof	W/m^2K	0.18	0.12	0.09	0.10
U-value windows	W/m^2K	1.6	1.2	0.80	0.77
Norm. thermal bridge	W/m^2K	0.05	0.05	0.03	0.03
Infiltration	h^{-1}	3.0	1.0	0.6	0.5
g-value	-	0.5	0.5	0.5	0.5
η_T heat recovery	%	70	70	80	85

The theoretical thermal power and energy demands for the Living Lab are compared to those of equivalent single-family houses, built according to the prevailing building codes and standards. Table 7.1 lists the minimum requirements for residential buildings according to the Norwegian building code TEK10, as well as for *Class 1 Low Energy Buildings* and *Passive House Buildings*, according to NS3700 [21, 22]. Where minimum requirements are non-existent, values are chosen as equal to the higher standards. This applies, for instance, to normalized thermal bridge values, g-values and heat recovery rates. Evidently, the building standard of the Living Lab closely matches the Norwegian Passive House requirements.

While space heating and ventilation heating demands are dictated by meteorological conditions, building design and heat recovery rates, the DHW demand is user dependent, inconsistent and unpredictable. Consequently, the DHW demand is calculated on the basis of normalized input data [23]. Table 7.2 presents normalized input data for operating hours, net power and energy demands, as well as internal heat gains for DHW, lighting, equipment and persons.

Table 7.2: Overview of net specific power and heat gain input data [23]

		Lighting	Equipment	DHW	Persons
Operating hours	hh/dd/ww	16/7/52	16/7/52	16/7/52	24/7/52
Net power demand	W/m^2	1.95	3.0	5.10	-
Net energy demand	$kWh/(m^2 year)$	11.4	17.5	29.8	-
Heat gain	W/m^2	1.95	1.80	0.0	1.50

7.4 Calculated Net Thermal Power and Energy Demand

The net thermal power duration curve for the Living Lab is plotted in fig. 7.1. This includes the demand for space heating and heating of ventilation air, as well as for DHW production. The building performance is clearly affecting the thermal power demand. A winter simulation indicate a gross power demand for space and ventilation heating, P_G, of 6.10 kW. By comparison, **the nominal net power demand, P_N, is 5.69 kW**.

As is seen from fig. 7.1, the duration of power demands greater than 3 kW is approximately 175 hours. Consequently, a large part of the heating demand may be covered with a low-capacity heat source. It should be noted that fig. 7.1 is based on a year simulation. Hence, a slighty lower peak power demand is indicated, compared to the winter simulation.

Results from the SIMIEN simulation are presented as area-specific values in table 7.3. The total net annual heating, Q_N, is estimated to ~6690 kWh, based on a heated floor

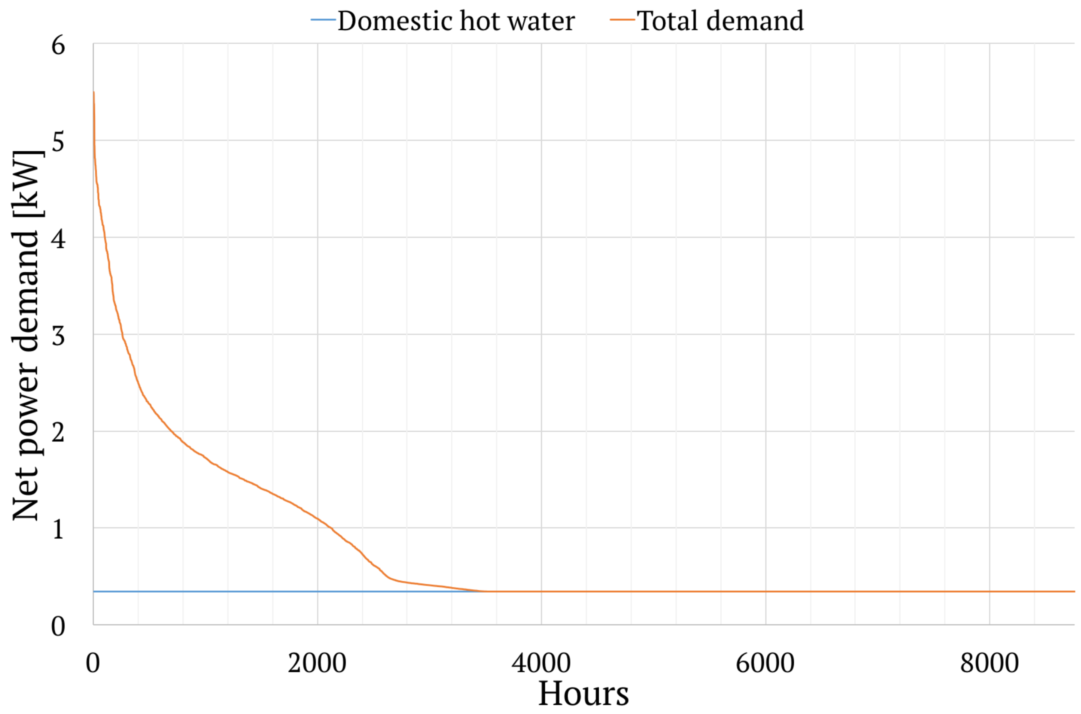

Figure 7.1: Net thermal power-duration curve for the Living Lab.

area of 102 m^2. The distribution of the thermal energy demands is presented as relative values in fig. 7.2.

Table 7.3: Calculated thermal energy and power demand.

		TEK10	Low energy	Passive house	Living Lab
Space heating	kWh/m^2	122.3	63.3	33.5	33.7
Ventilation	kWh/m^2	8.0	7.6	3.4	2.1
DHW	kWh/m^2	29.8	29.8	29.8	29.8
Tot. net power	W/m^2	96.56	73.8	58.8	58.0

It is evident that thermal power and energy demands for space heating diminishes as the insulation thickness and the tightness of the building envelope is improved. This also applies to the ventilation heating demand as the heat recovery efficiency is improved. By contrast, the DHW heating demand is user dependent, and remains constant regardless of building standard. As can be seen from fig. 7.2 the characteristics of the Living Lab closely matches those of a comparable Passive house building. The normalized net thermal energy demand is divided almost equally between space heating and DHW heating.

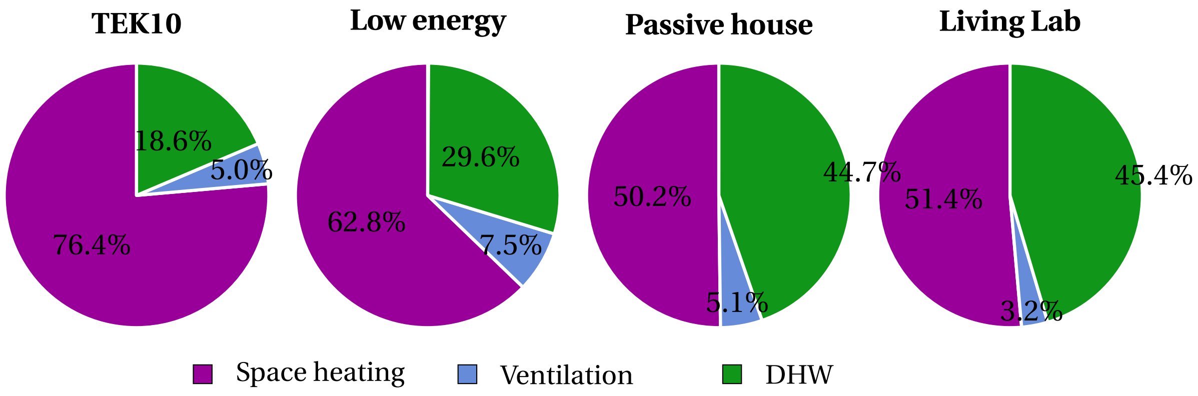

Figure 7.2: Thermal energy demand of the Living Lab relative to the prevailing standards.

7.5 Relating Theoretical and Actual Thermal Demands

The theoretical power and energy demands presented in this chapter are calculated according to standardized methods and normalized input data. As a result, the actual thermal demands at the Living Lab are likely to deviate from the calculated values.

At Miljøbyen Granås in Trondheim, the actual energy use in passive house residential buildings was measured throughout 2013 [71]. The buildings included 45 row-houses and 17 single-family houses, each with 138 and 181 m^2 living area, respectively. Bathrooms and ventilation air were electrically heated. District heating was used as the primary heat source, which covered the energy demand DHW heating, and space heating by means of a single radiator. During calculation of the specific space heating demand, the area of the bathrooms were subtracted. Consequently, the calculated specific heating demand was increased. Nevertheless, measurements indicated that the actual thermal energy demand was 10-20 % higher than the calculated values.

Table 7.4: Comparison of calculated and measured energy use at Miljøbyen Granås.

		Electricity	District heating	Total
Calculated demand	[kWh]	5 869	10 869	16 737
Lowest reduction	[%]	-9.9	-35.7	-14.2
Highest increase	[%]	+150.3	+39.7	+75.2
Average deviation	[%]	+91.0	-3.6	+29.6

In the same residential area, the delivered quantities of electricity and district heating energy was measured specifically for 16 single-family passive houses [72]. For these buildings, the calculated demand for **delivered** energy and deviations in actual energy use are given in table 7.4. Since only a part of the heating demand was covered by electrical heating, any conclusions regarding increased electricity use for heating are ambiguous. Meanwhile, there was a good correlation between the calculated demand for district heating and the average actual use. These findings suggest that the actual thermal demands for delivered energy are 10 - 30 % higher than the calculated demands.

Chapter 8

Preliminary Performance and Control

The heat pump system was put into operation on March 18^{th} 2016, and has been running virtually uninterrupted until the building was vacated, on April 22^{nd}. This period represents the residual part of the heating season, and as such, the corresponding measuring data form an incomplete picture of the actual thermal demands. DAQ recordings are nevertheless delimited to two ten-day periods.

The first DAQ period constitutes the period between March 22^{nd} and 31^{st}. It coincides with the Easter holidays, and also overlaps two resident periods. Consequently, the building was only partially inhabited, resulting in an unnaturally low DHW use. The average ambient temperature, however, was highest during the first period. Driving parameters for the thermal energy use are listed in table 8.1.

The second DAQ period stretches between April 8^{th} and 17^{th}. This represents 40 % of the last resident period, during which the building was inhabited by an elderly couple throughout. Hence, the DHW use during this period is regarded representable to the demographical profile of the residents. The thermal energy demand for space heating was also higher during the second period, due to a lower ambient temperature. **Measurements from this period are emphasized in the subsequent analysis.**

8.1 Energy Performance Measurements

8.1.1 Driving Factors

Table 8.1 lists the main quantities governing the thermal energy use during the two DAQ periods. A complete overview is given in appendix I. Indoor temperatures are represented as average values for the entire occupied zone. That is, as average values for stratified air temperatures in the living areas, and for all zones combined. Due to continuous occupancy during the second period, and presumably higher set-point temperatures, a higher indoor temperature was observed.

Table 8.1: Quantities governing the thermal energy use.

			22.03-31.03	08.04-17.04
Indoor air	$T_{i,avg}$	$[°C]$	21.3	22.8
Ambient air	$T_{a,avg}$	$[°C]$	4.3	3.4
Outdoor air duct	TRHT1	$[°C]$	5.7	4.9
Exhaust air duct	TRHT2	$[°C]$	11.1	11.0
Main supply duct	TRHT3	$[°C]$	22.1	21.9
Main extract duct	TRHT5	$[°C]$	21.8	23.8
Water main, inlet	RTD13	$[°C]$	3.8	5.3
Hot water tank, top	RTD12	$[°C]$	68.1	68.6
DHW	UFS3/4	$[m^3]$	0.27	1.07

Due to a warm March and a cold April, the recorded ambient temperature was lowest during the second DAQ period. Temperatures are calculated as average values between the weather station and north façade measurements. South façade temperatures are omitted, due to influence from direct solar irradiation. A larger ΔT between the indoor and ambient air translated to a higher energy use for space heating during the second period.

Average temperatures for the main ventilation ducts are also given. These resulted in average thermal heat recovery efficiencies, η_T, of 102 and 90 % for the first and second periods, respectively. An η_T which exceeds 100 %, is highly unlikely. It should be noted that the TRHT sensors have an accuracy of ± 0.3 K, and that actual η_T values thus may deviate significantly from the calculated values. Fig. 8.1 illustrates the variation in the heat recovery rate during the second DAQ period.

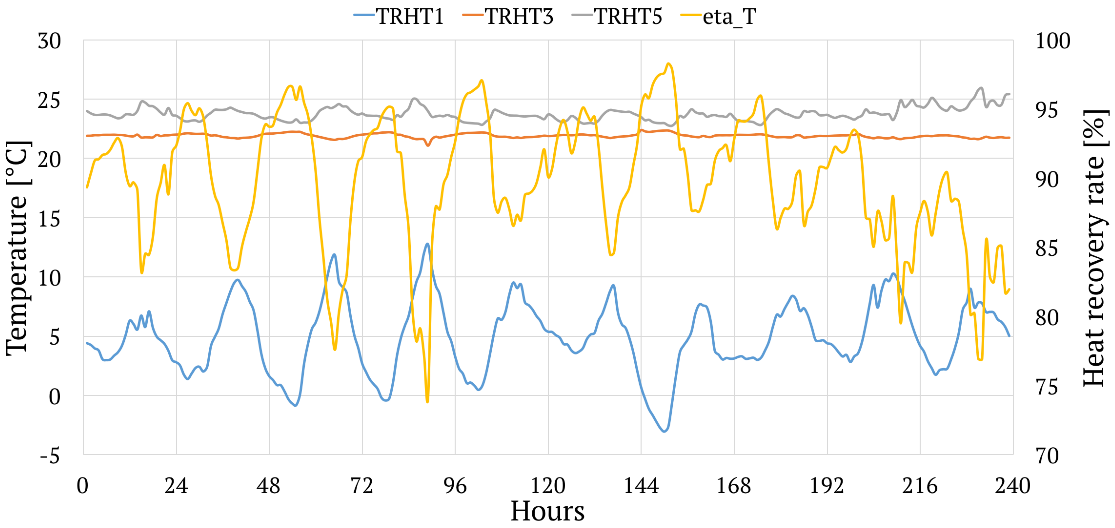

Figure 8.1: Thermal heat recovery efficiency during the second DAQ period.

8.1.2 Energy Supply and Use

Table 8.2 summarizes the overall performance of the thermal energy system during the two DAQ periods. Due to faulty configuration of TEM1 and TEM2, neither the heat pump thermal energy delivery nor the DHW energy use have been recorded.

The DHW energy has been approximated from the accumulated water volume, as well as IWT inlet and outlet temperatures, cf. table 8.1. Inlet temperatures were taken as the minimum water main temperatures in each period, to offset the error of stand-still measurements. The outlet temperatures were taken as the average DHWT top temperatures. The calculated DHW heating demand of 77.9 kWh for the second period corresponds to 27.9 $kWh/(m^2 year)$, which is slightly lower than the normalized value of 29.8 $kWh/(m^2 year)$.

The overall system performance may be evaluated on the basis of the electrical energy use. A comparison is made in fig. 8.2. During the first period the electrical energy use to the IEHs was 46 % of the corresponding use during the second period. At the same time, the electrical energy use to the heat pump unit was almost twice as high, indicating a longer operating time. This is because the estimated thermal energy use for space and DHW heating was almost 100 kWh lower, compared to the second period.

A comparable electrical energy use to hydronic pumps and actuator valves, CP2/3/OSO MX, may be seen during both periods. For the ground circuit circulator pump, CP1, the electricity use was almost identical during both periods. This is because it was running continuously. Consequently, it contributes to an excessive parasitic loss, comparable to the energy use to the DHWT IEH, or all hydronic actuators combined. Hence, there

Table 8.2: Energy use during the selected DAQ periods.

		22.03-31.03	08.04-17.04
Thermal energy		$[kWh]$	$[kWh]$
TEM1	GSHP condenser output	-	-
TEM2	Domestic hot water use	**20.0**	**77.9**
TEM3	Ventilation hydronic coil and radiator	0	0
TEM4	UHP Living areas, kitchen and entrance	181.0	219.0
TEM5	UHP Bedrooms and bathroom	7.0	9.0
EPTRC 400	Nominal thermal losses	33.0	33.0
Electrical energy - heating		$[kWh]$	$[kWh]$
EEM22	GSHP compressor input	79.2	42.8
EEM18	IEH SHT	9.5	24.8
EEM19	IEH DHWT	23.2	45.6
EEM21	AHU electric coil	0	0
Electrical energy - auxiliaries		$[kWh]$	$[kWh]$
EEM17	CP2, CP3, OSO MX and EV valves	28.4	29.1
EEM23	CP1	32.2	32.1
EEM24	CP4	0.27	0.48

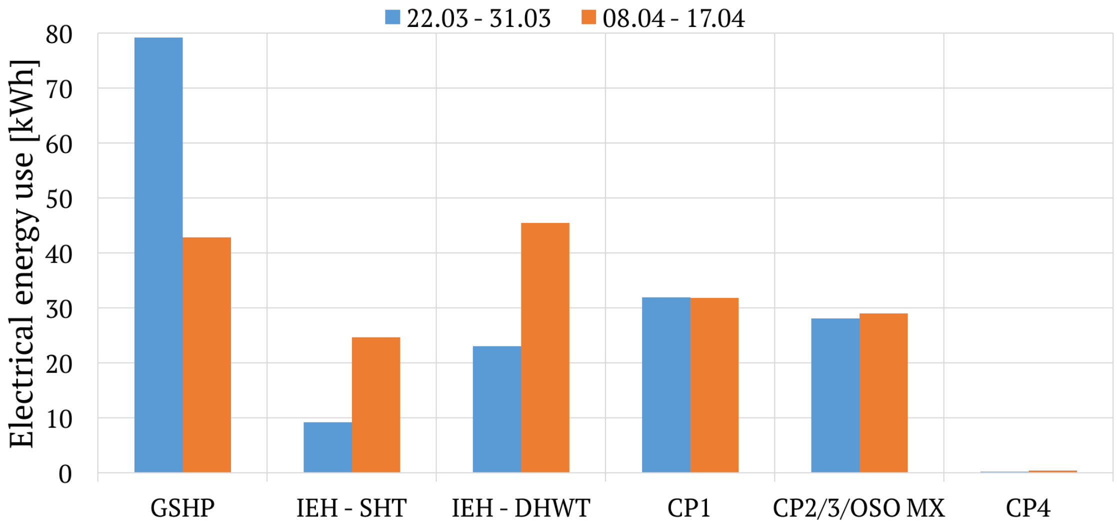

Figure 8.2: Comparison of electrical energy use.

is a significant potential for improvement, if proper control is introduced. For CP4 the electrical energy input increased by almost 80 % from the first to the second period. This indicates a longer operating time for the STC in April. The total electricity use is nevertheless negligible. These measurements show that the electric energy input to both the brine circuit pump, CP1, and hydronic pumps and actuators, CP2/3/OSO MX, represent a significant share of the total use. An improvement in system performance can thus be achieved by restricting pump operation to a minimum.

8.2 SPF Calculations

The SPFs for the heat pump unit and system have been calculated on the basis of data provided in table 8.2. Operating conditions for the GSHP was -1.0/40.9 °C and -0.3/39.4 °C, during the first and second DAQ periods, respectively. There are however a number of uncertainties involved, and hence the following assumption are made:

1. The thermal energy use to DHW is approximated based on data in table 8.1.
2. It is assumed that the combined thermal input from the GSHP and STC is equal to the total thermal energy use to space heating and DHW, minus the electricity use to the IEHs.
3. A conversion efficiency from electrical to thermal energy of 1 is assumed for the IEHs.
4. Thermal losses from pipes, storage vessels and other components are neglected.
5. Thermal gains from pumps are neglected.

Comprehensive assessments of residential heat pump systems, based on field measuring data, have previously been carried out in Sweden, Germany, Denmark and Norway [73, 74, 75, 76]. All of these studies suggest a step-wise SPF calculation, by applying increasingly wider system boundaries. This allows the significance of different electricity consumers to be evaluated, while a conformity in measuring methods is maintained. Specifically, four boundary conditions are recommended. These are listed in table 8.3. The electricity input to CP4 (EEM24) is particular to the present case.

Table 8.3: SPF input data at different system boundaries.

	$Q[kWh]$	$E[kWh]$
SPF_0	TEM: (2+4+5) - EEM: (18+19)	EEM: 22
SPF_1	TEM: (2+4+5) - EEM: (18+19)	EEM: (22+23+24)
SPF_2	TEM: (2+4+5) + EEM: (18+19)	EEM: (18+19+22+23+24)
SPF_3	TEM: (2+4+5) + EEM: (18+19)	EEM: (17+18+19+22+23+24)

The numerator of SPF_0 includes only the delivered heat from the GSHP and STC, while the denominator includes only the electricity use to the GSHP. SPF_1 is defined similarly, however, also including the electricity use to the brine pumps in the denominator. SPF_2 and SPF_3 includes the delivered heat from the IEHs in the numerator. The denominator of SPF_2 includes the electricity use to the compressor, the IEHs and the

Table 8.4: SPF values at different system boundaries.

	22.03-31.03			08.04-17.04			
	$Q[kWh]$	$E[kWh]$	SPF	$Q[kWh]$	$E[kWh]$	SPF	SPF_{AVG}
SPF_0	175.3	79.2	2.21	235.5	42.8	5.50	3.86
SPF_1	175.3	111.7	1.57	235.5	75.4	3.12	2.34
SPF_2	240.7	144.4	1.67	376.3	145.8	2.58	2.12
SPF_3	240.7	172.8	1.39	376.3	174.9	2.15	1.77

brine circulators. SPF_3 additionally accounts for the electricity use to hydraulic circulator pumps and valves. The results are given in table 8.4.

Relatively large deviations in the calculated SPF values between the first an second periods are observed by studying table 8.4. While the calculated SPF values during the first period are unnaturally low, the opposite is true for the second period. In particular, SPF_0 during the second period is much higher than the nominal COP at the prevailing conditions. This is likely a result of inaccurate estimations of the supplied heat from the heat pump unit. It should also be mentioned that larger loads for DHW and space heating during the second period are cause for more stable operating conditions. The largest difference in SPF values are, as expected, between SPF_0 and SPF_1. Evidently, the electrical energy use to the ground collector pump, CP1, has a large influence on the overall performance. It is thus crucial that this pump is deactivated simultaneously with the GSHP.

8.3 System Control Strategies

The control logic of the thermal energy system was tested on the 26^{th} of April 2016, by inducing virtual space heating and DHW loads. Specifically, the zone set-point temperatures were raised to 28 °C for a 30 minute period, while the DHWT was discharged. At this point, however, not all of the intended control logics had been implemented. One example is the brine cicuit pump, CP1, which was running continuously. Another example is the heat pump circuit 3-way valve, EV1, which had not been programmed to switch position in the event of a DHW load.

The following presentation is thus based partially on actual and intended control strategies. These are basic **two-position control** strategies, developed within the Research Centre on Zero Emission Buildings [77]. Table 8.5 lists the sensors and corresponding physical quantities used as *actual* values for control. The *error* is calculated as the deviation between *set-point* and actual values. Fig. 8.3 illustrates the principle scheme of the thermal energy supply system.

Table 8.5: Overview of sensors used for the preliminary control scheme.

Sensor	Measured quantity
RTD9	Lower temperature SHT
RTD10	Upper temperature SHT
RTD11	Lower temperature DHWT
RTD12	Upper temperature DHWT
RTD26	Outlet temperature solar thermal panels
TRHT13	Air temperature living room south
TRHT14	Air temperature kitchen
TRHT15	Air temperature living room north
TRHT16	Air temperature bedroom west
TRHT17	Air temperature bedroom east
TRHT18	Air temperature bathroom

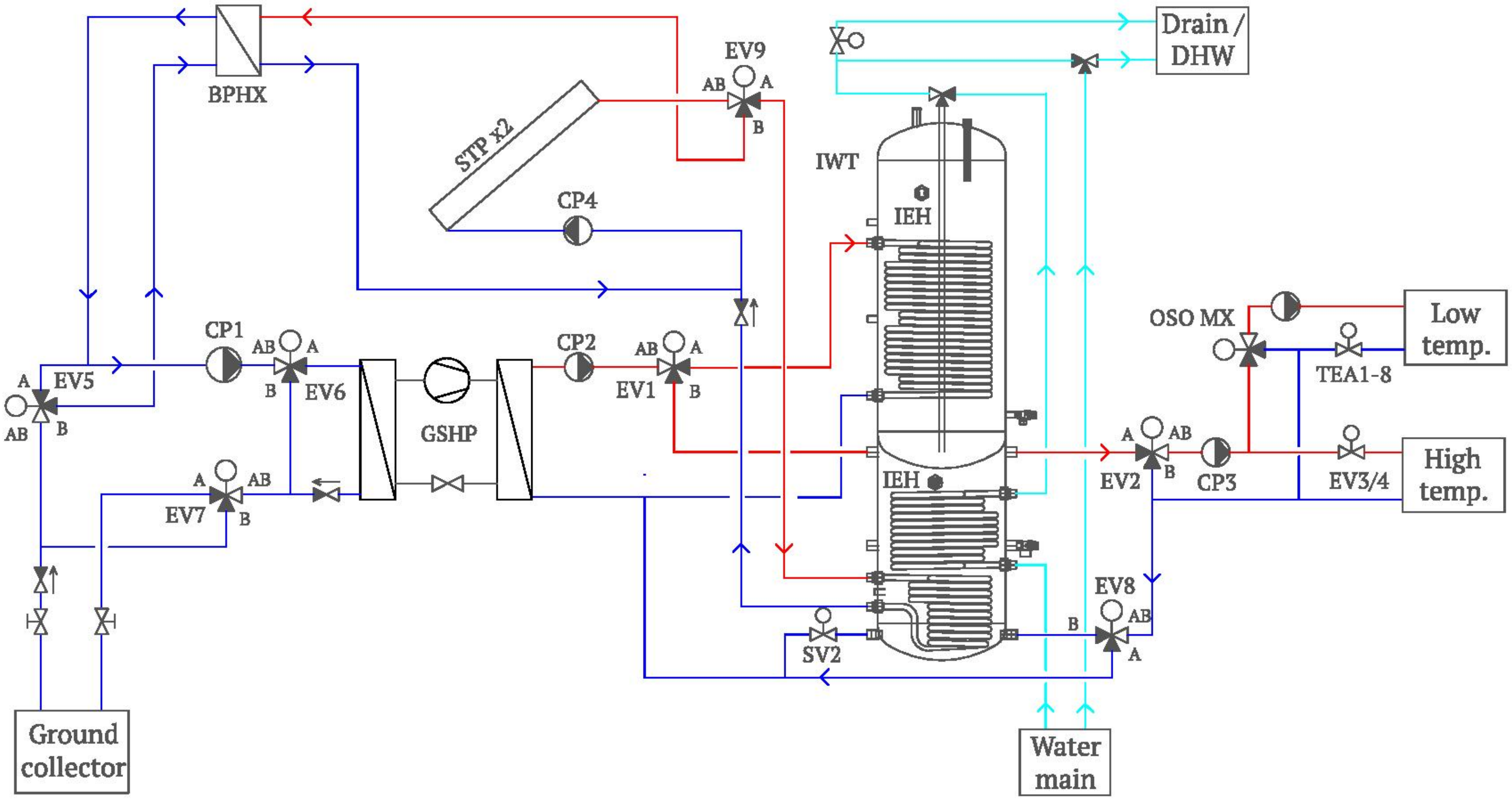
BPHX
EV9
AB
A
B
Drain /
DHW
STP x2
IWT
CP4
IEH
IEH
CP1
AB
A
B
EV6
CP2
AB
A
EV1
B
A
EV5
AB
B
GSHP
OSO MX
Low
temp.
TEA1-8
A
AB
EV2
B
CP3
EV3/4
High
temp.
A
EV7
AB
B
EV8
B
AB
A
SV2
Ground
collector
Water
main

Figure 8.3: Principle flow-scheme of the thermal energy system.

8.3.1 GSHP: Space Heating

Because the heat pump compressor is controlled intermittently, external capacity modulation is necessary in order to maintain a balance with the load. ON/OFF control of the GSHP is thus determined by the error between its set-point temperature, and the accumulation tank temperature. The present control strategy only integrates the underfloor heating system, and, assumes a constant set-point temperature of 35 °C.

SHT Average Temperature > 35 °C

The average temperature in the SHT is calculated as the arithmetic average between RTD9 and RTD10, (RTD9 + RTD10)/2. If there is a space heating load and the average temperature is **above 35 °C**, the heat pump is switched off. Subsequently, accumulated heat is discharged from the tank to cover the space heating load.

During this mode of operation the modulating valve EV2 is set to flow direction A-AB (100 % open), to let the water flow from the tank to the distribution system. EV8 is set to flow direction AB-A (100 % open) to let return water back to the bottom of the tank. It should be noted that the opposite flow direction (AB-B) was specified in the initial flow scheme. A correction was made due to opposite coupling of pipes and valve connections.

Unnecessary thermal losses from the IWT are avoided by setting EV1 to AB-A (100 % open), thus closing port B. For the same reason the shut-off valve SV2 is closed at all times. CP3 provides circulation of water between the tank and the primary circuit, while the OSO MX pump central maintains circulation of water in usecondary circuit.

The underfloor heating circuits are controlled according to a ± 1 K **deadband** between the user-defined set-points and the actual zone air temperatures. Table 8.6 lists the five zones of the floor heating system, with the corresponding control sensors and closing valves. The TEA valve(s) are opened when the corresponding zone air temperature(s) drop(s) below the(ir) set-point value(s). Fig. 8.4 illustrates the opening of the TEA valves as all set-point temperatures are raised to 28 °C.

The TEA valves remain open until the zone air temperatures have reached their set-point values. Then, the corresponding TEA valves are closed. If all set-point temperatures are reached and all the TEA valves are closed, the OSO MX pump central and CP3 are switched off. To avoid thermal losses from the accumulation tank, valves EV2 and EV8 are set to flow directions B-AB and AB-B, respectively.

Preferably, there should be a tolerance of ± 1-2 K, to reduce the intermittency of the

Table 8.6: Overview of floor heating zones, control sensors and valves.

Zone	Sensor(s)	Valve(s)
Living room south + kitchen	TRHT13 + TRHT14	TEA4 + TEA5
Living room north	TRHT15	TEA2 + TEA3
Bedroom west	TRHT16	TEA1
Bedroom east	TRHT17	TEA8
Bathroom	TRHT18	TEA7

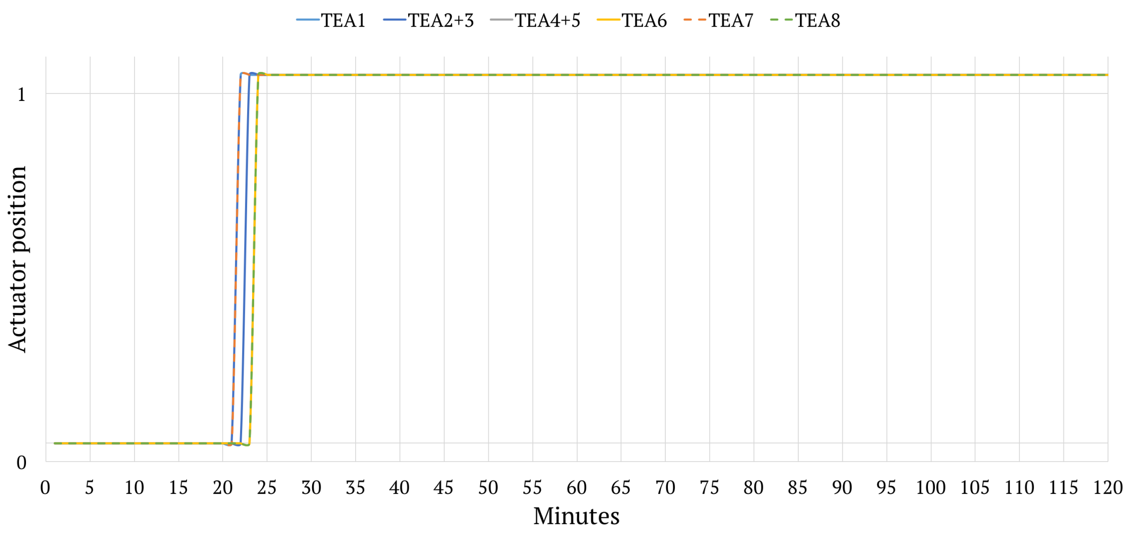

Figure 8.4: TEA closing valve positions during testing.

control. This is because there is some time delay between the measured air temperature and the actual heat output from the floor heating system. Specifically, the TEA valves should open when the actual air temperatures are 1-2 K below the set-point, and close 1-2 K above it.

SHT Average Temperature < 35 °C

When there is a space heating demand, and the average temperature in the tank is **lower than 35 °C**, the heat pump is switched on. Heat is delivered from the heat pump, via the accumulation tank (SHT), to the distribution system. The accumulation tank thus acts as a two-port control volume through which the hot water flow passes, without any significant decrease in enthalpy. Hence, heat accumulation is negligible.

Fig. 8.5 illustrates, as an example, the development in brine and water temperatures, as well as the heat pump input power. Comparing the compressor power curve with the SHT average temperature curve, it may appear that the heat pump starts as the temperature drops below 35 °C. In reality, the heat pump is controlled according to its built-in thermostat setting, which in this case is 35 °C. Meanwhile, the inlet and outlet temperatures, RTD6 and RTD4, are both lower than the set-point. At 5 minutes, the heat pump was activated manually, before CP2 gave any circulation. The significant increase in the compressor input power is due to an increase in the condensing pressure, as virtually no heat rejection took place.

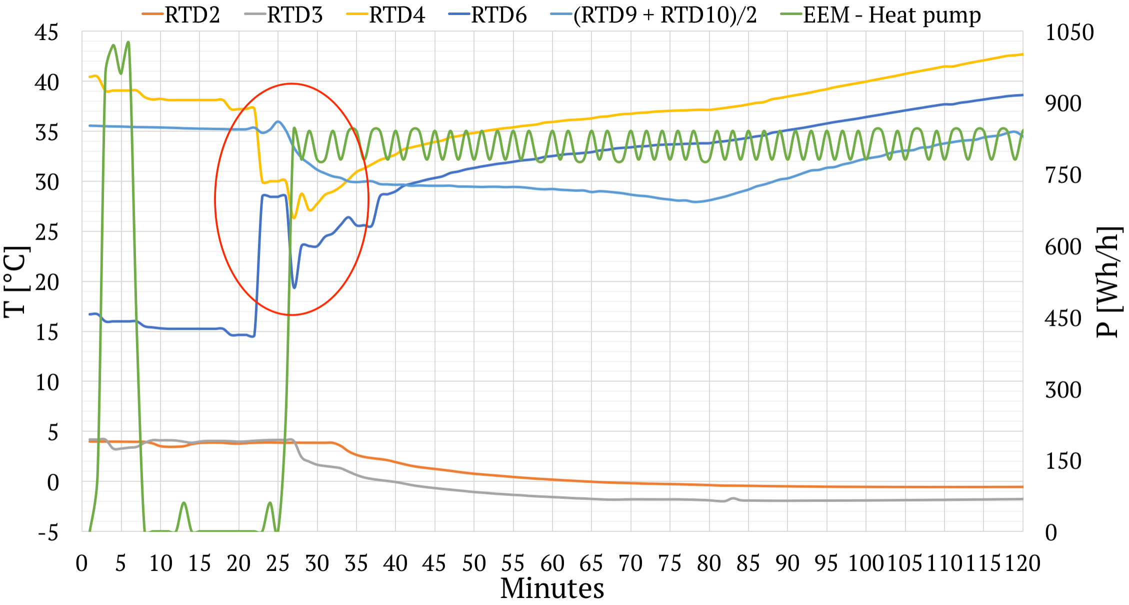

Figure 8.5: Heat pump operation during testing.

During this mode of operation valve EV2 was set to 100 %, with flow direction A-AB, to let water flow from the tank to the distribution system. EV8 was set to 0 %, with flow direction AB-B, to let return water flow directly to the heat pump. Switching of the valve set-point values is illustrated in fig. 8.6. SV2 was closed in order to avoid unintended thermal losses from the tank. Valve EV1 was set to 0 %, with flow direction AB-B, to let water flow from the heat pump to the accumulation tank. In the ground collector circuit the valves EV5, EV6 and EV7 were all set to 100 %, with flow directions AB-A, to allow brine circulation between the SCF and the heat pump. The set-point values for pumps CP1, CP2, CP3 and the OSO MX pump central, were then set to ON.

The underfloor heating circuits were controlled as described above, however, with one alteration. With the heat pump unit activated, the TEA valves remained in the open position for 15 minutes. Subsequently, the zone air temperatures were compared to their corresponding set-point values. As the set-points had not yet been reached, the 15 minute period was re-initiated. An advantage of this strategy is that operation of the heat pump unit becomes more stable, and the number of start-ups is restricted to a maximum of 2 to 3 per hour. This is beneficial with respect to wear and tear of the compressor.

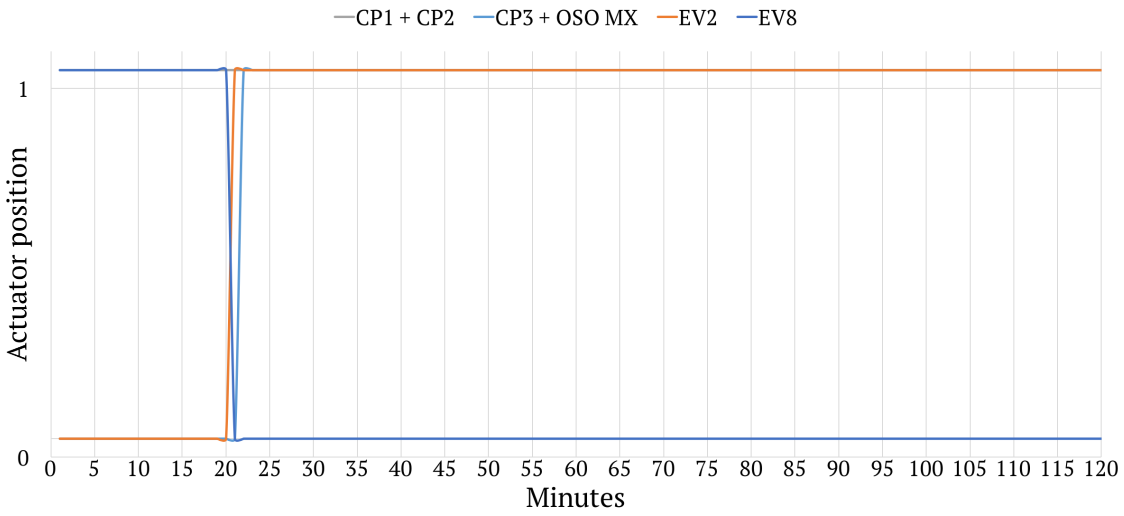

Figure 8.6: Modulating valve positions during testing.

Upon comparison of a zone air temperatures and set-point values, the corresponding TEA valves close if the desired values are reached. Once all TEA valves are closed, the GSHP unit and OSO MX pump central is switched off, followed by CP1, CP2 and CP3. EV1 is set to position AB-A, while the valves EV2, EV6 and EV8 are set to 0 %, or B-AB, AB-B and AB-B, respectively. Currently, however, CP1 remains on regardless if the GSHP is switched off.

8.3.2 GSHP: Domestic Hot Water Heating

The heat pump system has been designed for alternate operation between space and DHW heating. Consequently, when there is a DHW load, the GSHP needs to be set to DHW heating mode, for the outlet water temperature to increase. Additionally, the heat pump circuit 3-way valve, EV1, has to be set to position AB-B, to let water flow to the DHWT coil. Presently, however, no control signals are produced to make these changes.

This issue demonstrates an unreliable design, which complicates the implementation of control functionalities. In order to make the DHW heating mode functional, adequate communication between the LabVIEW controller and the GSHP unit is compulsory. **The malfunctioning DHW heating mode is a serious issue with respect to the overall thermal energy use in the Living Lab**. By not being able to supply DHW by means of the GSHP, the load is shifted towards the DHWT IEH. Hence, the electricity use increases, which translates to a decrease in the overall system SPF.

The *intended* control strategy is described in the subsequently. Heat delivery from the GSHP to the DHWT is controlled according to the DHWT average temperature, which is determined as the arithmetic average between RTD11 and RTD12, (RTD11 + RTD12)/2. RTD11 measures the temperature at the middle of the DHWT, while RTD12 measures the temperature at the top. Fig. 8.7 illustrates the temperature development of the DHW flow prior to preheating in the SHT (RTD15), after preheating (RTD14), and the DHWT outlet temperature)RTD13). Between 20 and 65 minutes only the bathroom faucet was used. At 65 miutes the kitchen faucet was opened addtionally. The DHWT temperature development is demonstrated in fig. 8.9, in subsection 8.3.4.

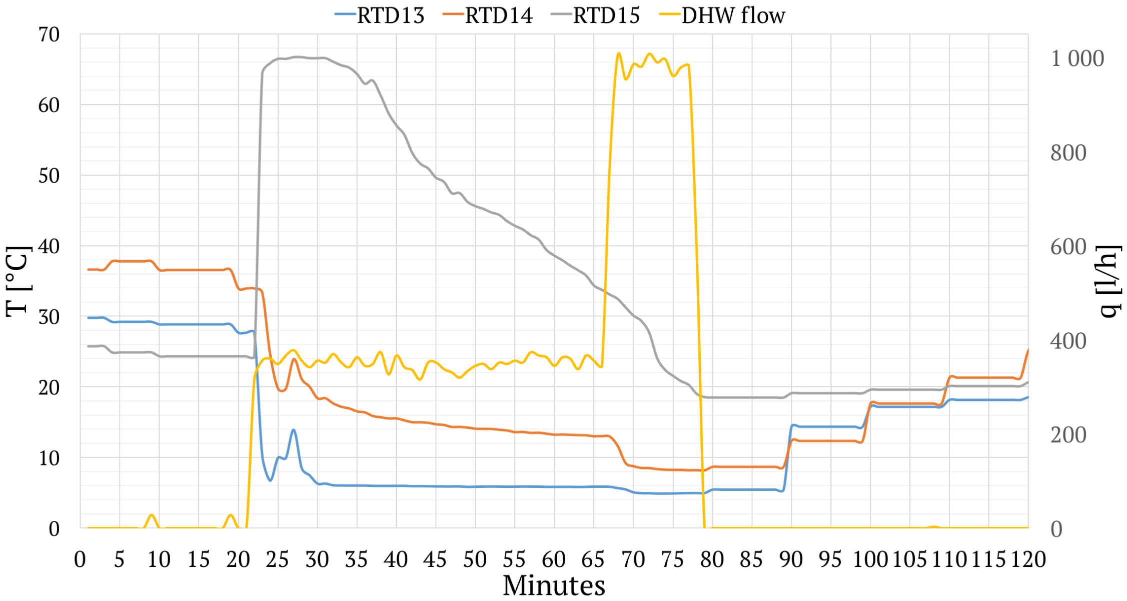

Figure 8.7: DHW temperature and flow development during testing.

The intended set-point temperature for activation of the heat pump during a DHW load is 55 °C. That is, if (RTD11 + RTD12) < 55 °C, the heat pump unit is switched on. EV1, EV5, EV6 and EV7 are then set to flow directions AB-A, while circulation pumps CP1 and CP2 are activated. This allows circulation of water between the GSHP and the DHWT, and brine flow between the SCF and the GSHP. Operation is maintained for 15 minutes, before the DHWT average temperature is re-checked. If the value still is < 55 °C, the cycle is repeated. Otherwise, the GSHP, CP1 and CP2 are stopped, before EV6 is set to position AB-B (0 % open).

8.3.3 STC: Water Heating

The STC pump, CP4, and 3-way valve, EV9, are controlled according to a differential temperature thermostat. Specifically, EV9 is set to position AB-A and CP4 is activated when the temperature at the STP outlet, RTD26, exceeds the SHT average temperature, (RTD9 + RTD10)/2. The activation and deactivation logics are as following:

- STC ON: RTD26 > (RTD9 + RTD10)/2
- STC OFF: RTD26 < (RTD9 + RTD10)/2

Fig. 8.8 illustrates the weakness of this control strategy. Because there is no deadband, CP4 is activated momentarily after the panel outlet temperature exceeds the SHT average temperature. It is thus allowed to run only for 2 to 4 minutes, before the logical condition fails.

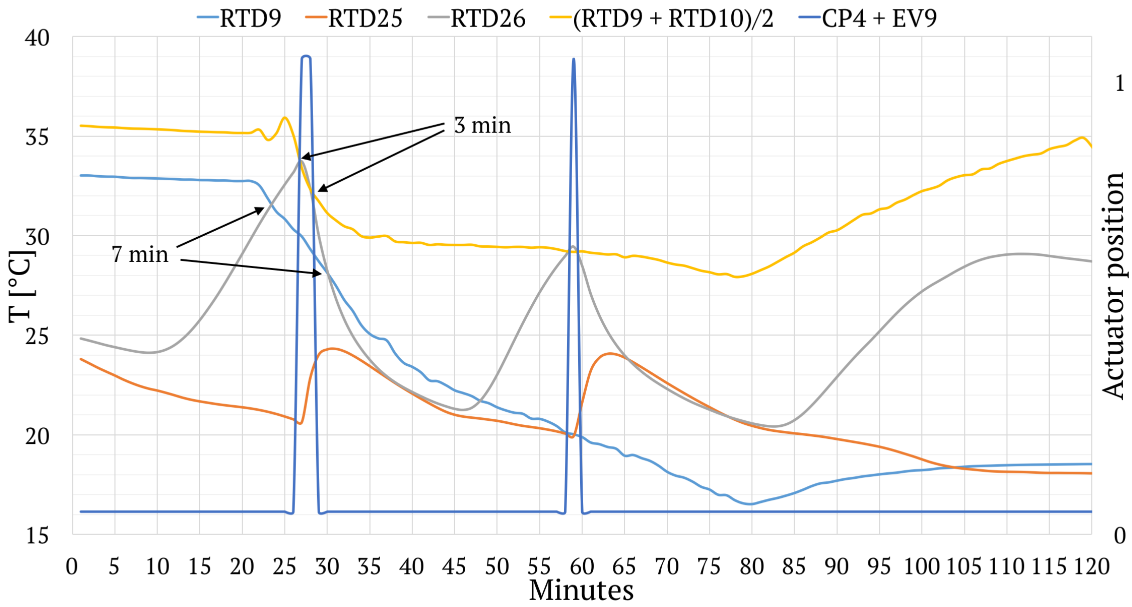

Figure 8.8: Variation of the STP inlet and outlet temperatures during testing.

By investigating the intersections between the STP outlet temperature (RTD26) and the SHT bottom temperature (RTD9), a potential for improvement is observed. **The measurements indicate that, by omitting the SHT top temperature (RTD10) from the control scheme, the operating time for the STC can be improved significantly**. In the present case, the operating time would have been extended from 3 to 7 minutes, if the followng control logic had been applied:

- STC ON: RTD26 > RTD9
- STC OFF: RTD26 < RTD9

The SHT bottom temperature is measured directly at the solar coil, and is thus a much more suitable control condition for the STC, compared to the SHT average temperature. Another consideration is that circulation in the STC must be avoided if the STP outlet temperature (RTD26) is lower than the inlet temperature (RTD25). Otherwise, heat would be rejected from the SHT to the ambient.

8.3.4 IWT IEHs: Peak Load Heating

Peak load heating by means of the IWT IEHs is controlled according to pre-defined thermostat set-points. During the test period only the SHT was heated directly by the GSHP, while the DHWT was heated by the upper IEH. Fig. 8.9 illustrates the how the upper and lower IEHs are activated when the average tank temperatures drop below 55 and 35 °C, respectively. These temperatures are calculated as the arithmetic averages between the upper and lower tank temperatures, as (RTD11 + RTD12)/2 and (RTD9 + RTD10)/2, respectively. Fig. 8.9 illustrates a rapid temperature decrease in the upper part of the DHWT, as hot water is drained to the bathroom sink. The actual flow rate is illustrated in fig. 8.7, with a sudden increase at 65 minutes, as the kitchen tap was opened.

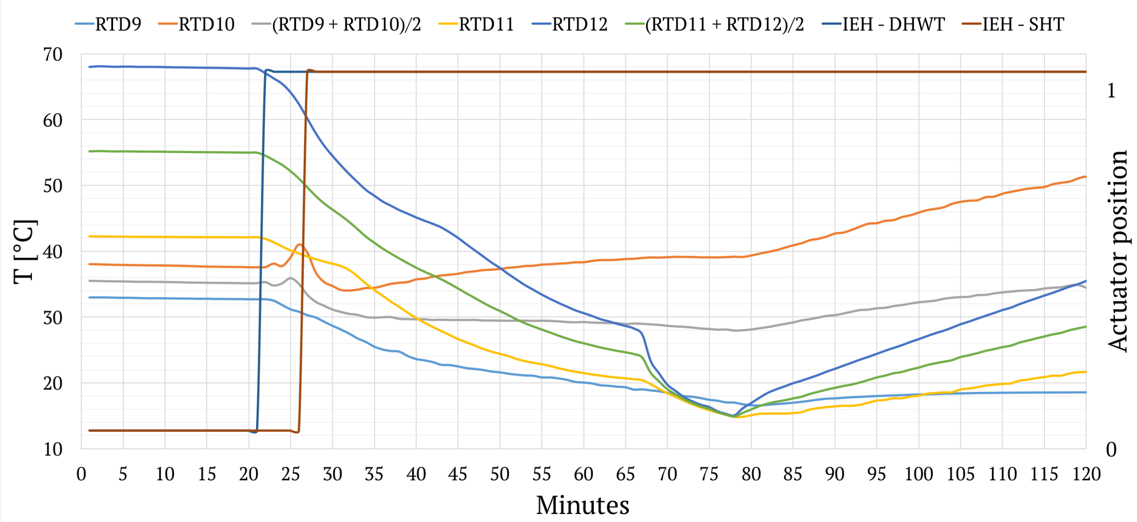

Figure 8.9: Temperature development in the IWT during testing.

As figs. 8.5 and 8.9 suggest, the thermostat setting for the heat pump and the SHT IEH are identical. Consequently, both heat sources are activated simultaneously. This is because the present setting for the IEHs is intended for electrical heating only, not for the heat pump as the base load heat source.

With this setting, the energy coverage potential for the heat pump unit is restricted. In order for the heat pump to achieve a high energy coverage factor, the IEHs should supply peak load heating only. Hence, the IEHs should be activated only when the demand supersedes the heat pump power output. For instance, the IEH thermostat set-points could be given as the upper water layer temperatures alone (RTD10 and RTD12), and not as average temperatures for the tank sections.

Chapter 9

Complementary Field Measurements

As a result of inconclusive measuring data from the normal operating period, a series of experimental tests were carried out, in an attempt to circumvent some of the problems encountered. Modifications to the operation of the system had to be adopted, in order to facilitate proper data acquisition. Due to limited access, lack of control functionalities and collision with experiments assessing the indoor environment in the building, these measurements were postponed until late May. Consequently, the amount of available time for detailed investigations was limited. The advance of the summer period also had an effect on operating conditions.

9.1 Measuring Devices

The instantaneous performance of the GSHP, STC and IWT has been tested as a means to validate or disprove the measuring data from the two DAQ periods, as discussed above. In this relation, external measuring equipment has been utilized for control purposes, as well as to supplement the system-integrated equipment. Unfortunately, measurements could not be performed until a month after the building was vacated. Due to higher ambient temperatures and global solar irradiance, the operating conditions during testing were improved, compared to the prevailing conditions in March and April.

The water flow rate was measured with the combination of two different meters. One calculating the water flow rate based on in-the-flow differential pressure measurements, and the other calculating the flow rate based on non-intrusive ultrasound technology. The latter is also used for brine flow measurements. These meters are presented subsequently.

9.1.1 IMI Hydronics TA-SCOPE

This is a multi-function device, which may be used for temperature, pressure, flow and thermal power measurements. The actual pipe flow is calculated on the basis of the pressure drop, which is measured between the two ports of a TA valve, as shown in fig. 9.1a. In the thermal energy system at the Living Lab, three TA valves have been installed for the purpose of system balancing. Two are found on the radiator and heating battery return pipes, while a third is mounted near UFS2 on the return pipe to the heat pump. The latter has been used for control measurements of the water flow to the heat pump.

9.1.2 Ultraflux UF 801-P

This is a clamp-on flow meter, which measures internal pipe flow rate by means of sound waves in the ultrasonic range. Two transducers alternately transmit and receive ultrasonic sound waves through the external surface of the pipe, both in the upstream and downstream directions. Fig. 9.1b illustrates the transducer setup on a 28x1.5 mm water circuit steel pipe.

The basic theory is that waves induced in a flow move faster in the flow direction, and slower upstream. For each direction, the travel time of the sound is measured accurately, before the difference in travel time is calculated [78, p. 389]. The average velocity of the pipe flow may then be calculated, since it is proportional to the difference in travel time. By specifying the pipe external diameter and thickness, the internal diameter and cross-sectional area is given. Correct determination of the volumetric flow rate also require that the properties of the fluid, as well as pipe material, are specified. Measurements are sensitive to the distance between the transducers.

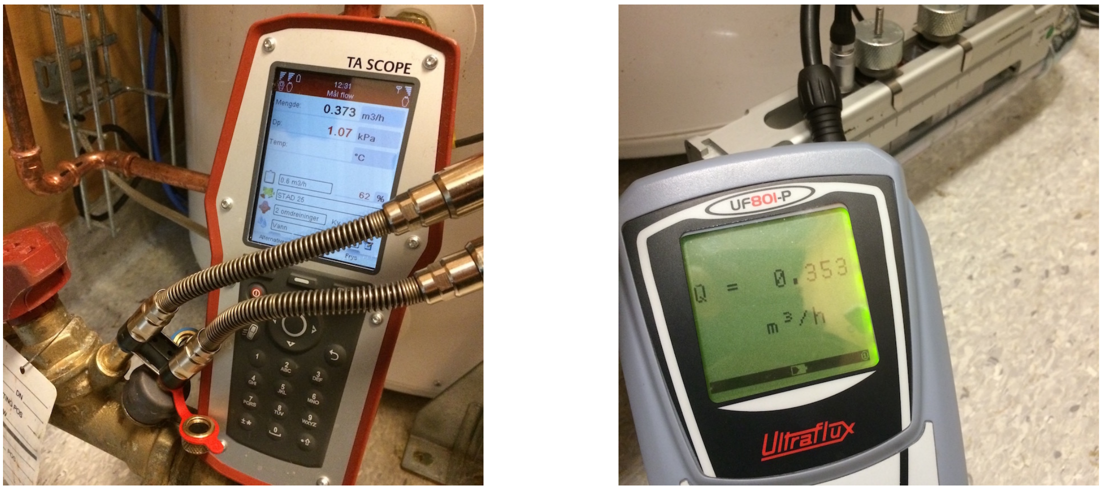

(a) TA-SCOPE valve connection.

(b) UF 801-P pipe connection.

Figure 9.1: Setup of volumetric flow meters.

9.1.3 Analog Manometers

To measure the evaporating and condensing pressures of the Calorex heat pump, manometers were fitted to the high and low pressure Schrader service valves. Combined with the electric input power to the compressor, as well as and water circuit temperature and flow rate measurements, these allow evaluation of the units thermodynamic performance. The manometers are depicted in fig. 9.2. The low pressure gauge has .05 bar divisions, while the divisions on the high pressure gauge are .1 bar. Both instruments have an accuracy of 0.5 %.

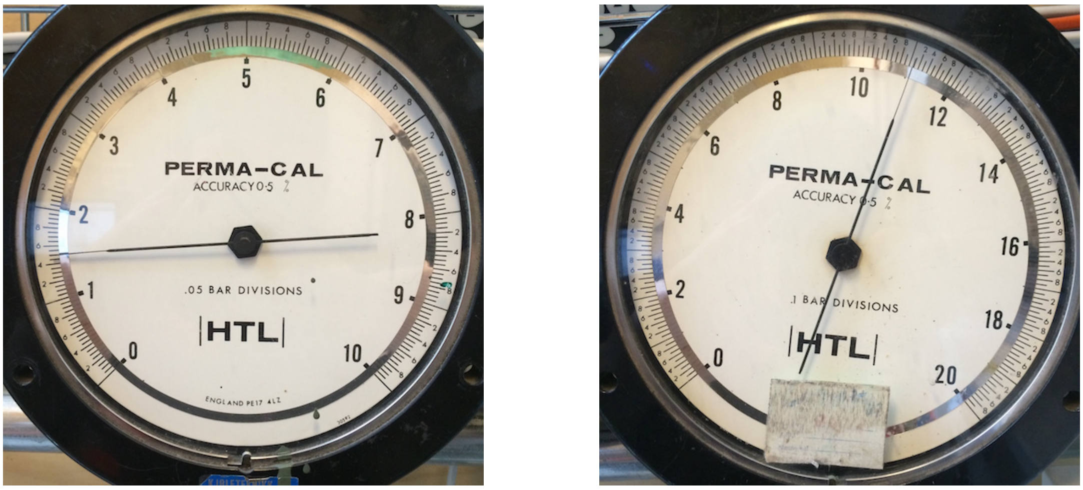
PERMA-CAL
ACCURACY 0·5 %
.05 BAR DIVISIONS
HTL
PERMA-CAL
ACCURACY 0·5 %
.1 BAR DIVISIONS
HTL

(a) Evaporating pressure gauge.

(b) Condensing pressure gauge.

Figure 9.2: Manometer measurements.

9.1.4 Handheld Analog Refractometer

The composition of the aqueous propylene glycol solution, was determined on the basis of its refractive index. Fig. 9.3 shows the refractometer used to perform this measurement. A sample droplet was extracted from the ground circuit refill valve, and placed between the measuring prism and the cover glass. A freezing point of -25 °C was then read from the scale, which corresponds to a propylene glycol concentration of approximately 44 weight-%. It was not possible to obtain a sample from the STC, and hence the brine mixtures were assumed identical.

Reichert
7182 °C
Duo-Chek
MADE IN U.S.A.
COOLANT AND BATTERY TESTER
AUTOMATICALLY TEMPERATURE COMPENSATED

Figure 9.3: Handheld refractometer used to determine the PG concentration.

9.2 Test 1 and 2: GSHP and STC Performance

The instantaneous performance of the GSHP has been tested experimentally by measuring the heating capacity and electrical power input for two operating conditions. Test 1 addresses standalone operation, that is, for heat rejection without influence from other heat sources. Test 2 addresses combined operation with the STC, which was operated in order to elevate the evaporator brine inlet temperature.

Because of flawed configuration of TEM1, the flow was directed to the radiator circuit in order to obtain satisfactory measuring data from TEM3. During these tests, only CP2 and CP3 was operated in the hydronic circuit. Hence, the flow rate at TEM3/UFS6 could be assumed equal to the flow rate at TEM1/UFS2. Temperature measurements for the supply and return flow was attained from TEM1.

External measurements were carried out in 5 minute intervals. These include water circuit flow measurements by means of the UF 801 and TA-SCOPE field measuring devices. The UF 801 was fixed to a horizontal 28x1.5 mm steel pipe close to the TA valve, cf. fig. 9.1b. Evaporating and condensing pressures were read from the LP and HP gauges, respectively, cf. 9.2, while input power to Magneta circulator pumps were read from their respective displays.

9.2.1 Test 1: GSHP Standalone Operation

During this test the GSHP temperature set-point was adjusted to 55 °C, in order to allow uninterrupted operation. The total duration of the data acquisition period was 100 minutes, excluding the first five minutes of operation. Proportional pressure mode and a differential pressure setting of 100 % was used for circulator pumps CP1, CP2 and CP3, throughout. Temperature and flow characteristics for the brine and water circuits are shown in figs. 9.4 and 9.5, respectively.

The average operating condition during this test was 4.4/43.9 °C, which corresponds to a ΔT_{lift} of 39.5 K. This is slightly lower than the average ΔT_{lift} of 41.9 K and 39.7 K, during the first and second DAQ periods, cf. section 8.1. The higher inlet brine temperature, however, suggests a higher evaporating temperature, lower suction gas density, lower working fluid mass flow rate and reduced heating capacity.

External measuring data and DAQ recordings for the 100 minute period are presented as average values in tables 9.1 and 9.2, respectively. **For the hot water flow, an average density of 990 kg/m^3 and a specific heating capacity of 4.183 kJ/kgK, were assumed**. The average evaporation pressure of 1.74 bar_g corresponds to an evaporating temper-

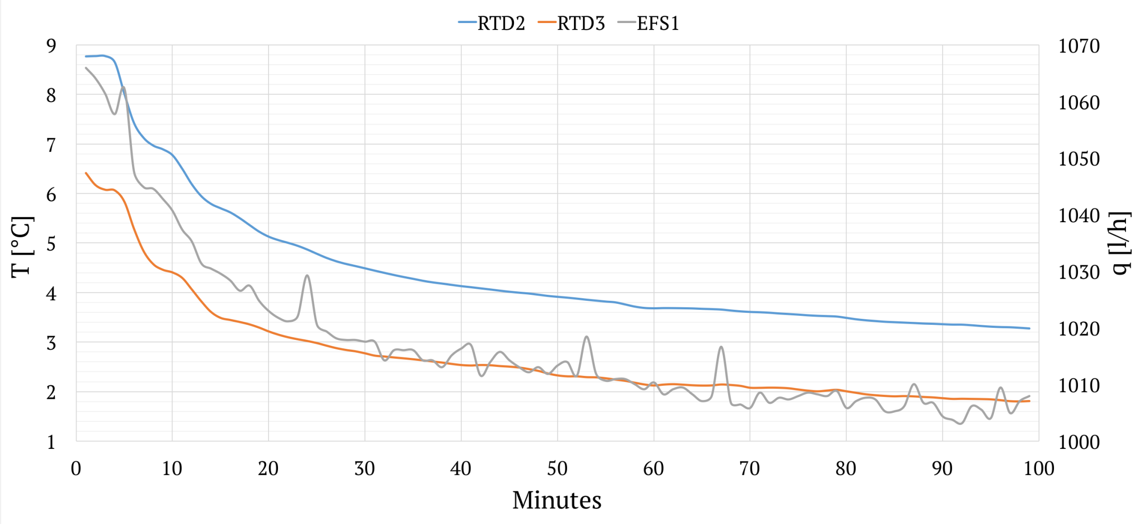

Figure 9.4: Brine circuit temperature and flow development - Test 1.

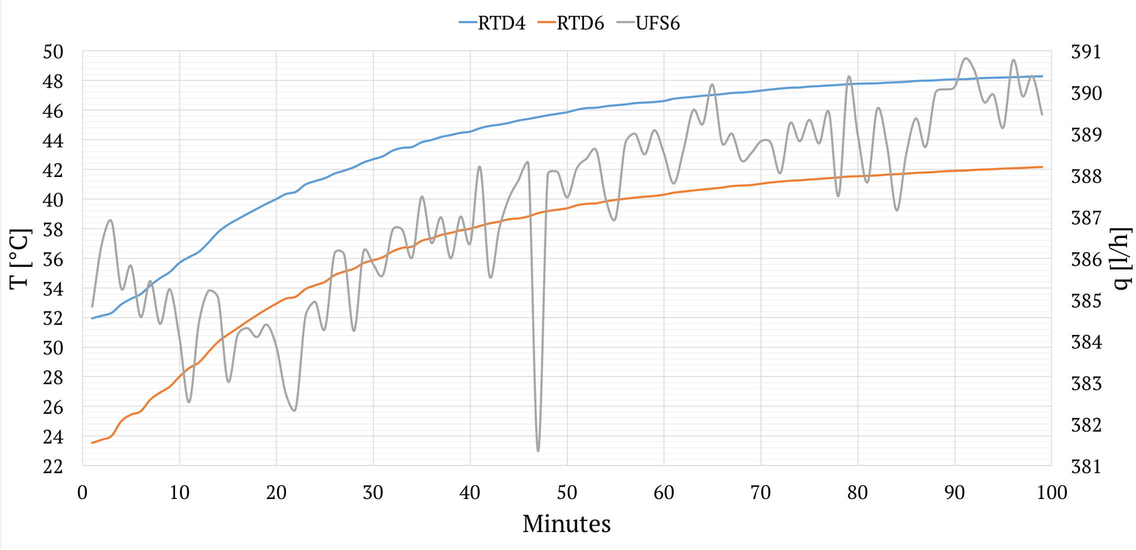

Figure 9.5: Water circuit temperature and flow development - Test 1.

ature of -1.8 °C, which gives an evaporator LMTD of 5.3 K. The average condensing pressure of 10.90 bar_g corresponds to a condensing temperature of 46.6 °C, which results in a condenser LMTD of 4.8 K. Based on the absolute evaporating and condensing pressures a pressure ratio of 4.34 was prevailing.

A good correlation was seen between the external flow measurements. Comparing external measurements to DAQ recordings, a 10 % deviation was seen. It is thus likely that the actual flow rates differ slightly from the measured values. In that case, the calculated heating capacity would also be influenced. The recorded brine flow rates ranged between 1005 and 1065 l/h, resulting in an average value of 1017.2 l/h. This was 15 % lower than the design flow rate of 1200 l/h.

External readings of the pump input power were lower, compared to the DAQ recordings. For CP1, the deviation was approximately 6 %. For CP2 and CP3 combined, the deviation was approximately 33 %. It is worthwhile mentioning that the DAQ measurements also include the power consumption for operation of actuator valve motors.

Table 9.1: External measurements and readings - Test 1.

p_E $[bar_g]$	p_C $[bar_g]$	$\dot{V}_{w,TA}$ $[l/h]$	$\dot{V}_{w,UF}$ $[l/h]$	$\dot{W}_{CP1}$ $[W]$	$\dot{W}_{CP2}$ $[W]$	$\dot{W}_{CP3}$ $[W]$
1.74	10.90	348	350	138.3	44.1	47.5

Table 9.2: DAQ system recordings - Test 1.

$\dot{V}_b$ $[l/h]$	$\dot{V}_w$ $[l/h]$	ΔT_b $[K]$	ΔT_w $[K]$	$\dot{Q}_w$ $[W]$	$\dot{W}_{HP,ad}$ $[W]$	$\dot{W}_{CP1}$ $[W]$	$\dot{W}_{CP2/3}$ $[W]$
1017.4	387.2	1.7	6.7	2973	932.9	147.3	136.4

The performance during standalone operation was evaluated on the basis of the COP. Analogous to SPF calculations in section 8.1, the COP has been calculated at different system boundaries. The first system boundary only includes the heat pump unit and electrical input power to the compressor. The second boundary includes the electrical input power to the brine circuit circulator pump, CP1, while the third also includes the hydronic circuit pumps.

The development of the COP values are plotted in figure 9.6. A sharp decrease in performance was observed during the first 40 minutes of operation. After stabilization of the brine inlet and water outlet temperatures, the decrease was less apparent. A stationary condition was not reached, however. It is evident that the electric power input to the pumps has a significant influence on the COP. CP1 has the largest influence, with a reduction of the HP COP of 13.5 %. The electric power input to the pumps represent 30.4 % of the power input to the compressor, which is significant.

Fig. 9.7 shows the relative energy saving potential, ΔE, plotted as a function of the COP. It is presumed that electrical heating, with an efficiency of 1, represents the alternative heat source. Average values presented in table 9.3.

Performance measurements are summarized in table 9.3, along with the Carnot COP, ε_C, for the average operating condition (4.4/43.9 °C). The Carnot efficiency, η_C for the heat pump unit is thus 39.8 %. This is poor compared to typical values around 50 %,

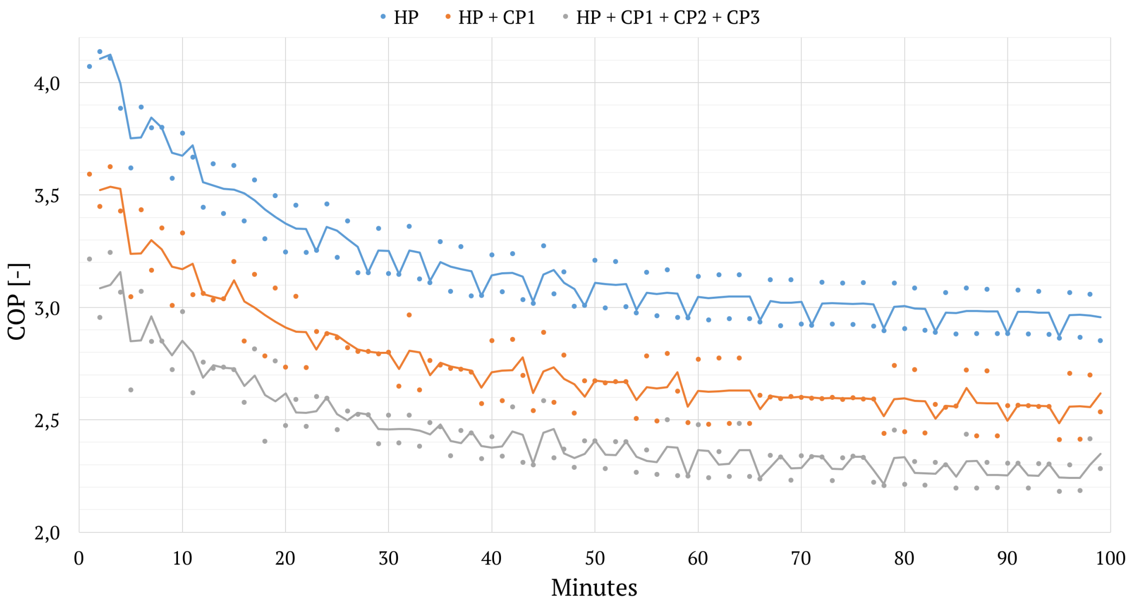

Figure 9.6: COP development - Test 1.

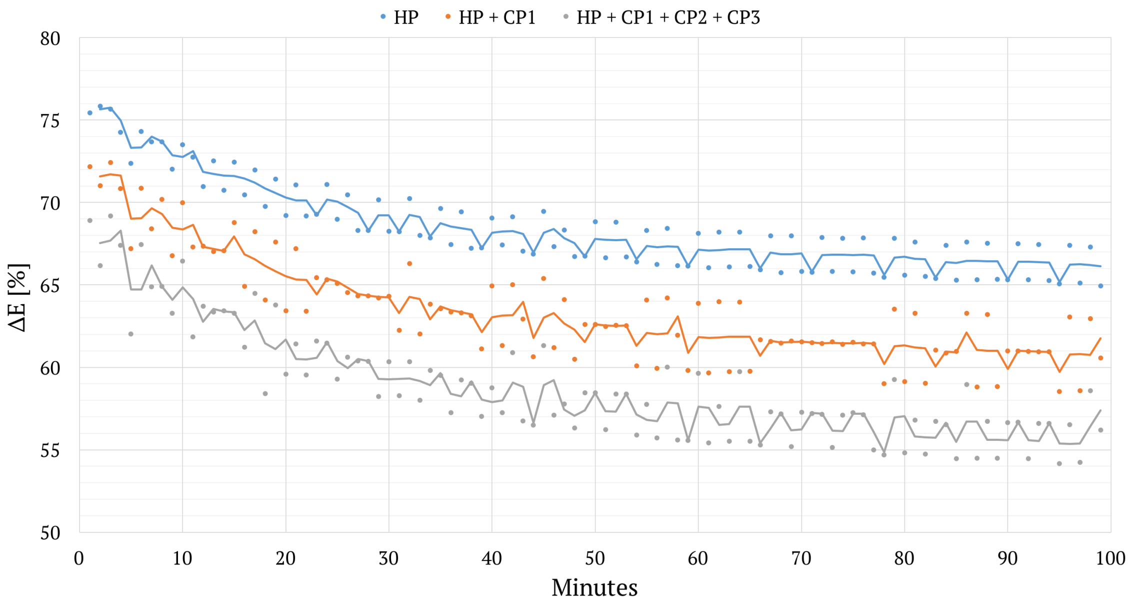

Figure 9.7: Relative energy saving potential - Test 1.

and worse than the values specified by the manufacturer, cf. chapter 5. An improved value would be obtained with larger heat transfer areas and reduced LMTDs in the evaporator and condenser.

Table 9.3: Performance measurements - Test 1.

ε_C	COP	COP_1	$COP_{1/2/3}$	ΔE	ΔE_1	$\Delta E_{1/2/3}$
8.02	3.19	2.76	2.45	68.7	63.8	59.2

The results of the present section indicate that the actual SPF values during normal operation might be lower than those presented in section 8.1. It should be noted, however, that the result are attained at different operating conditions. This difference may be offset by the fact that OSO MX pump central was inactive during the present test. The difference in ΔE is nevertheless less sensitive to differences in the input power, compared to the COP. Hence, the relative energy saving potential of the GSHP system was in the range between 59 and 69 %. For the GSHP and brine pump, an intermediate ΔE around 64 % was observed.

9.2.2 Test 2: GSHP and STC Combined Operation

During this test the STC was operated in combination with the GSHP, rejecting heat to the ground collector circuit. The GSHP set-point temperature was adjusted to 55 °C, in order to allow uninterrupted operation. The total duration of the data acquisition period was 100 minutes. In order to reach a more stable condition, a run-in period of twenty minutes was permitted. Proportional pressure mode and a differential pressure setting of 100 % was used for the pumps CP1, CP2 and CP3, throughout. For CP4, the pre-set differential pressure setting of 50 % was used.

The temperature and flow characteristics for the STC, ground collector, and water circuits are shown in figs. 9.8, 9.9 and 9.10, respectively. In the STC a peak in the flow rate was observed as the pump, CP4, was activated. In the ground collector circuit, peaks in the inlet and outlet brine temperatures were simulatenously observed.

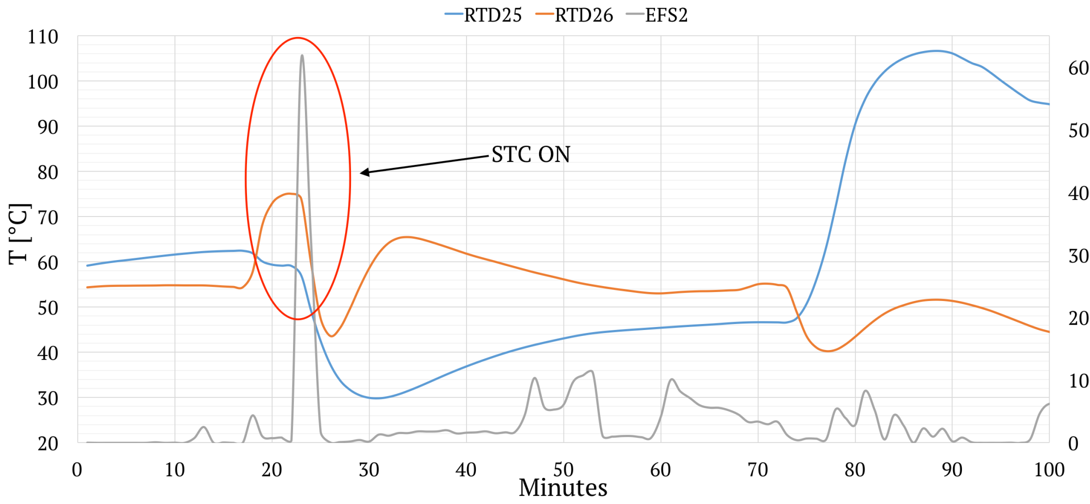

Figure 9.8: STC temperature and flow development - Test 2.

The average operating condition during this test was 4.7/47.1 °C, which corresponded to a ΔT_{lift} of 42.4 K. This was higher than the average ΔT_{lift} of 40.8 K, during normal

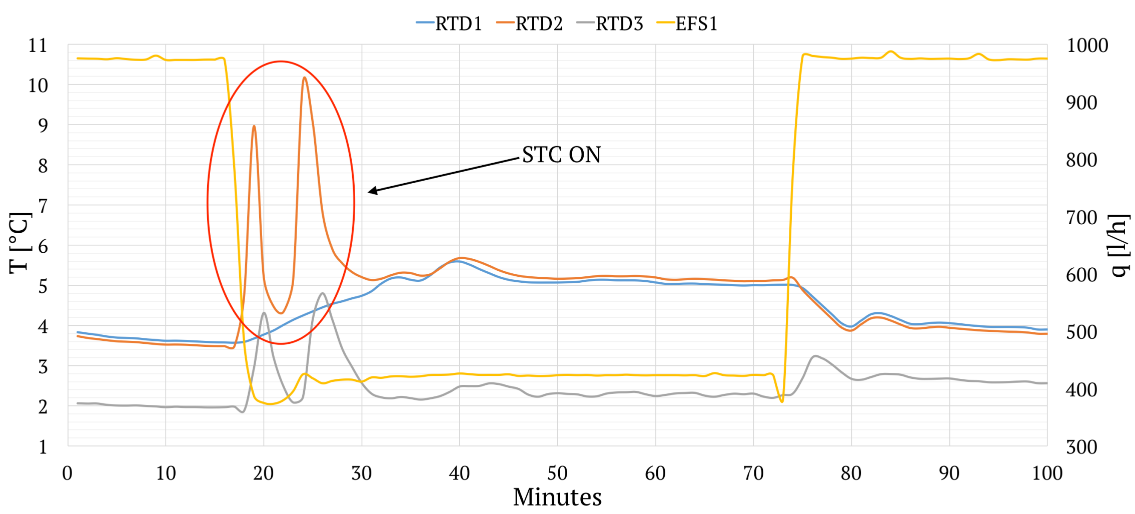

Figure 9.9: Brine circuit temperature and flow development - Test 2.

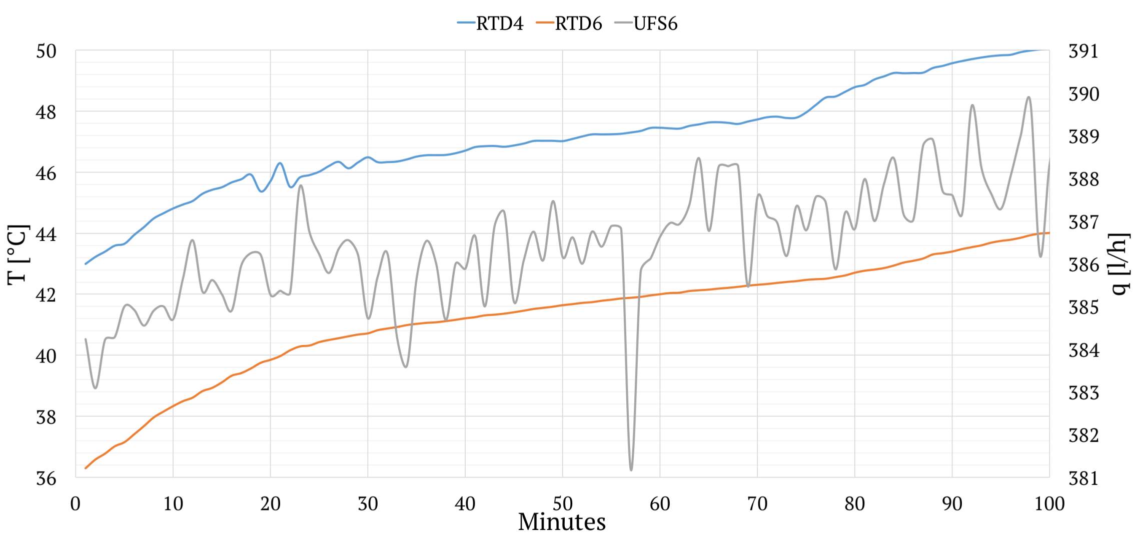

Figure 9.10: Water circuit temperature and flow development - Test 2.

operation, cf. section 8.1, and 39.5 K during the first test. The average inlet brine temperature was also higher in the present case.

External measuring data and DAQ recordings for the 100 minute period are presented as average values in tables 9.1and 9.2, respectively. For the hot water flow, an average density of 990 kg/m^3 and a specific heating capacity of 4.183 kJ/kgK, were assumed. The average evaporation pressure of 1.58 bar_g corresponded to an evaporating temperature of -3.4 °C, which gave an evaporator LMTD of 6.9 K. The average condensing pressure of 11.24 bar_g corresponded to a condensing temperature of 47.2 °C, which resulted in a condenser LMTD of 1.4 K. Based on the absolute evaporating and condensing pressures, a pressure ratio of 4.74 was prevailing.

Table 9.4 shows a good correlation between the external water flow measurements. By comparing these measurements to DAQ recordings, a deviation between 1.3 and 8.4 % is seen. This is better compared to the prior case. The recorded flow rates in the ground collector loop ranged between 1000 and 350 l/h, resulting in an average value of 662.8 l/h. A sharp decrease was observed as heat exchange via the BPHX was initiated. Whith the heat exchanger operational, the average STC flow rate was 47.4 l/h. Heat input from the STC resulted in a significant increase in ΔT_b. As a consequence, the pressure-controlled CP1 responded by reducing the brine flow rate.

Table 9.4: External measurements and readings - Test 2.

p_E $[bar_g]$	p_C $[bar_g]$	$\dot{V}_{w,TA}$ $[l/h]$	$\dot{V}_{w,UF}$ $[l/h]$	$\dot{W}_{CP1}$ $[W]$	$\dot{W}_{CP2}$ $[W]$	$\dot{W}_{CP3}$ $[W]$	$\dot{W}_{CP4}$ $[W]$
1.58	11.24	381.3	354.1	119.3	43.4	45.9	20.0

The large difference in LMTDs for the evaporator and condenser was due to the higher ΔT_b and reduced brine flow rate. This gave a lower evaporating temperature and suction gas density. Consequently, working fluid mass flow rate dropped, which gave a lower evaporator capacity. As a result, the evaporator LMTD increased, in order to maintain an energy rate balance. For the condenser, the opposite effect occured. The reduction in heating capacity meant that the LMTD had to decrease, in order to maintain an energy rate balance.

External readings of the pump input power are lower compared to the DAQ recordings. For CP1 and CP4, the deviations are 7.9 and 37.5 %, respectively. By contrast to the other units, the recorded values for CP4 are lower, compared to the external readings. For CP2 and CP3 combined, the deviation is 33 %, as in the prior case.

Table 9.5: DAQ system recordings - Test 2.

$\dot{V}_b$ $[l/h]$	$\dot{V}_w$ $[l/h]$	$\dot{V}_{sol}$ $[l/h]$	ΔT_b $[K]$	ΔT_w $[K]$	ΔT_{sol} $[K]$	$\dot{Q}_w$ $[W]$	$\dot{W}_{HP,ad}$ $[W]$	$\dot{W}_{CP1}$ $[W]$	$\dot{W}_{CP2/3}$ $[W]$	$\dot{W}_{CP4}$ $[W]$
662.8	386.5	47.4	2.3	5.8	15.3	2592	898	129.6	133.1	12.5

The development of the COP at different system boundaries is plotted in figure 9.11. A sharp decrease in performance was observed after 20 minutes, as the BPHX was put into operation. As the BPHX was deactivated at 75 minutes, the COP values increased to the normal condition. Comparing figs. 9.6 and 9.11, it is seen that similar conditions were prevailing at the end of each run. A stationary condition was not reached.

Fig. 9.12 shows the relative energy saving potential, ΔE, plotted as a function of the COP.

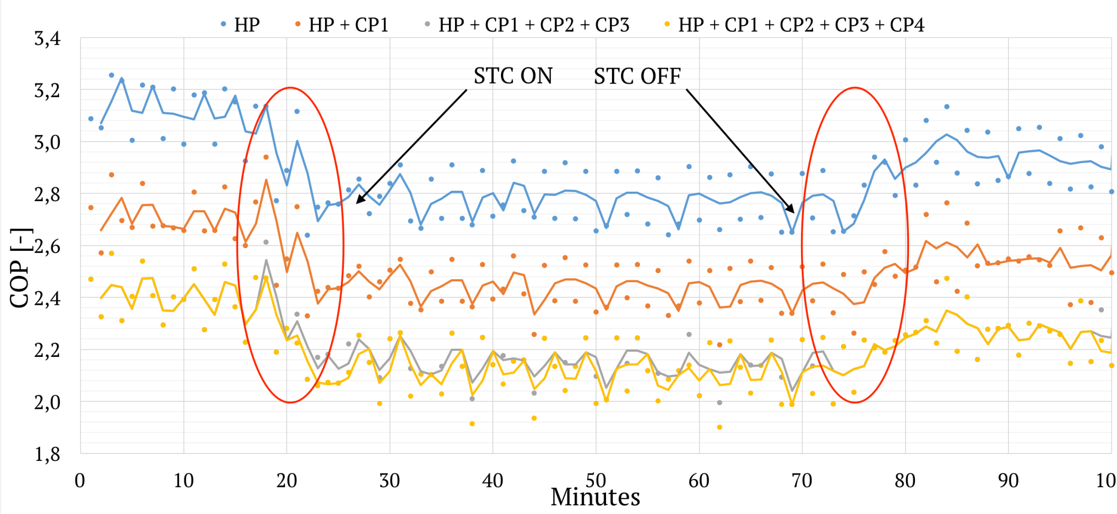

Figure 9.11: COP development - Test 2.

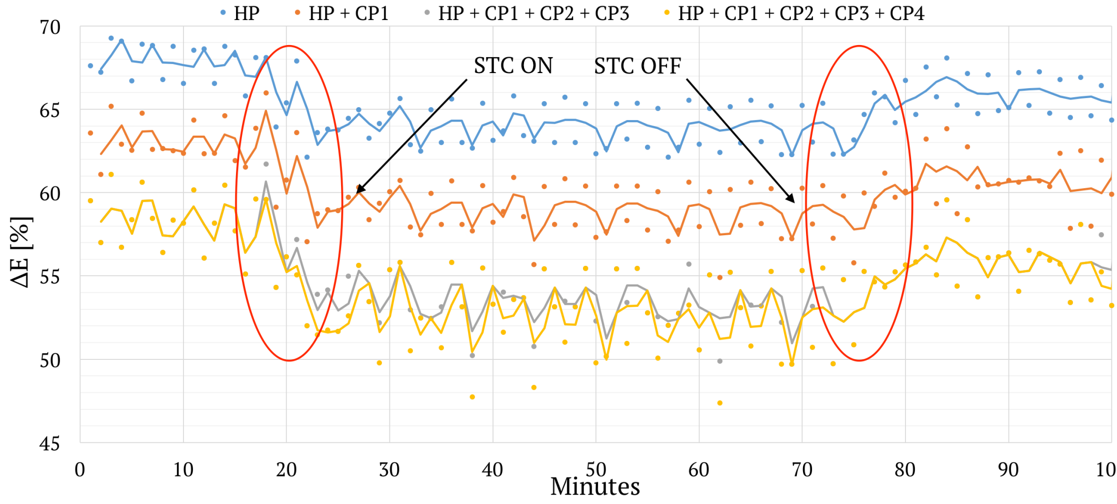

Figure 9.12: Relative energy saving potential - Test 2.

Performance measurements are summarized in table 9.3, along with the Carnot COP, ε_C, for the average operating condition (4.7/47.1 °C). The Carnot efficiency, η_C for the heat pump unit was thus 38.1 %. This is worse compared to a value of 39.8 % during the first test.

Against the intention to increase the evaporating temperature and COP, by means of the STC, the reverse effect was observed. Because the brine circuit pump is controlled according to a differential pressure setting, the flow rate is reduced dramatically as the brine temperature and ΔT_b is increased. This culminates in a larger LMTD and thus

Table 9.6: Performance measurements - Test 2.

ε_C	COP	COP_1	$COP_{1/2/3}$	$COP_{1/2/3/4}$	ΔE	ΔE_1	$\Delta E_{1/2/3}$	$\Delta E_{1/2/3/4}$
7.58	2.89	2.53	2.24	2.22	65.4	60.5	55.4	55.0

a lower evaporating temperature. Consequently, the specific enthalpy of evaporation and vapor density are reduced, which leads to a lower working fluid mass flow rate and evaporator capacity. Consequently, the heating capacity and COP are reduced. During this test COP values ranging between 2.22 and 2.89 were observed, which is 8 - 10 % lower than the corresponding results of the first test. This culminated in lower energy saving potentials, ranging from 55 to 65 %. **Increasing the evaporator inlet brine temperature by means of solar heat, is thus not a recommended strategy, in combination with the Δp-controlled pumps.**

9.3 Test 3 and 4: IWT and STC Performance

9.3.1 Test 3: IWT Discharging

The effective volume of the IWT has been tested for an extreme DHW load. With total volume of 400 l, and a DHWT volume of 240 l, the potential energy storage capacity is large. The effective energy content, however, is dependent on the overall temperature level and temperature stratification in the tank, as well as the minimum required DHW temperature. This test was carried out simply by draining the tank via the kitchen sink, and recording the temperature development at the top and bottom of each tank section. The kitchen faucet was set to its maximum position, with respect to both temperature and flow.

Fig. 9.13 illustrates the temperature development in the SHT, as well as the water flow rate through the preheating coil. The initial tank bottom temperature, measured by RTD9 was 22 °C. The initial tank top temperature is measured by RTD10 as 40 °C. Within 3 minutes of draining, a constant water main temperature of 8 °C was measured by RTD13. Upon investigation of the ΔT between RTD14 and RTD13, it is seen that the initial temperature increase from preheating was approximately 7 °C. After 20 minutes the temperature increase from preheating was reduced by approximately 50 %. This illustrates the influence of the SHT temperature level on the DHW preheating potential. While a lower temperature level is beneficial with repect to GSHP and STC performance for space heating, it has a negative influence on the DHW production.

Fig. 9.14 illustrates the temperature development in the DHWT, as well as the flow rate

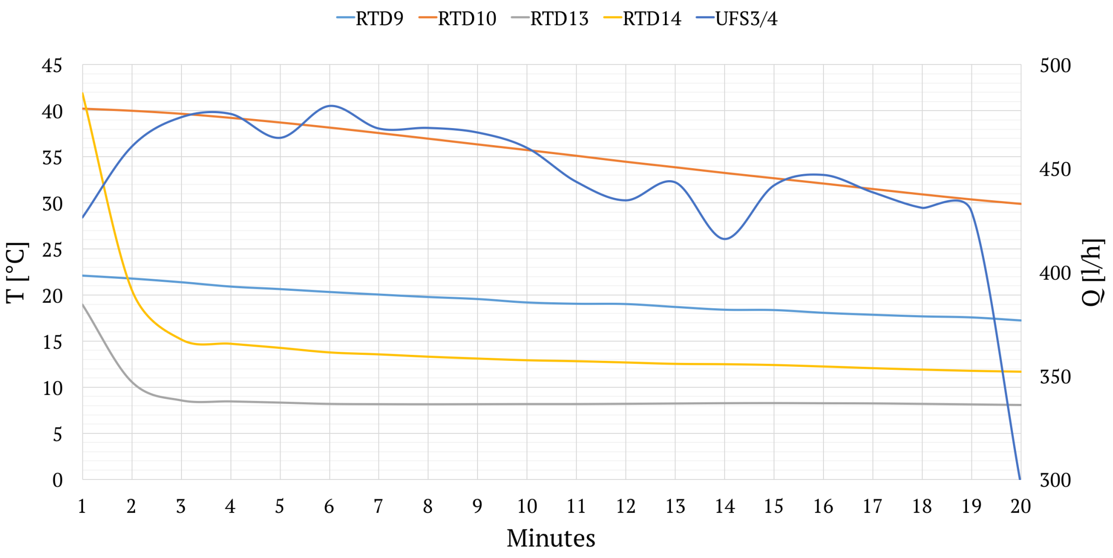

Figure 9.13: SHT temperature and flow development - Test 3.

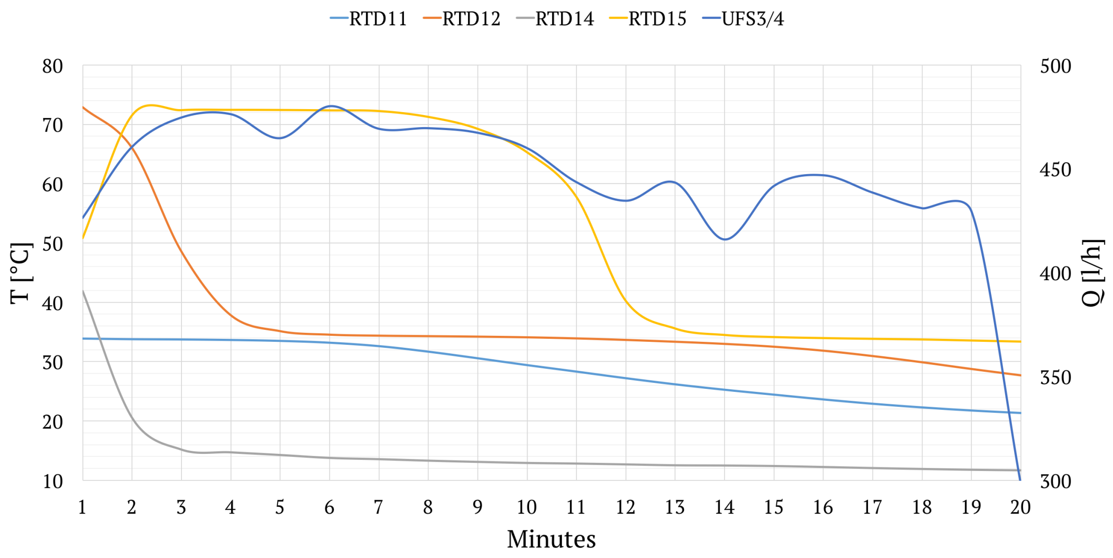

Figure 9.14: DHWT temperature and flow development - Test 3.

of the water passing through the tank. The initial tank bottom temperature, measured by RTD11, was 34 °C. The initial tank top temperature was measured by RTD12 as 73 °C. Within 2 minutes of draining, an outlet water temperature identical to the tank top temperature, was measured by RTD15. This value was maintained for 5 minutes, before a decrease in temperature was observed. The tank top temperature, meanwhile, dropped much more rapidly. This is because the temperature probe RTD12 is located a distance below the tank outlet. By examination of RTD11, a constant temperature of 35 °C was observed during the first 6 minutes. This is because the probe is located near the middle of the tank, mid-way down the reheating coil. The delay between the drop in RTD12 and RTD11 measurements, indicate a favorable stratification performance during simultaneous hot water extraction and cold water refilling.

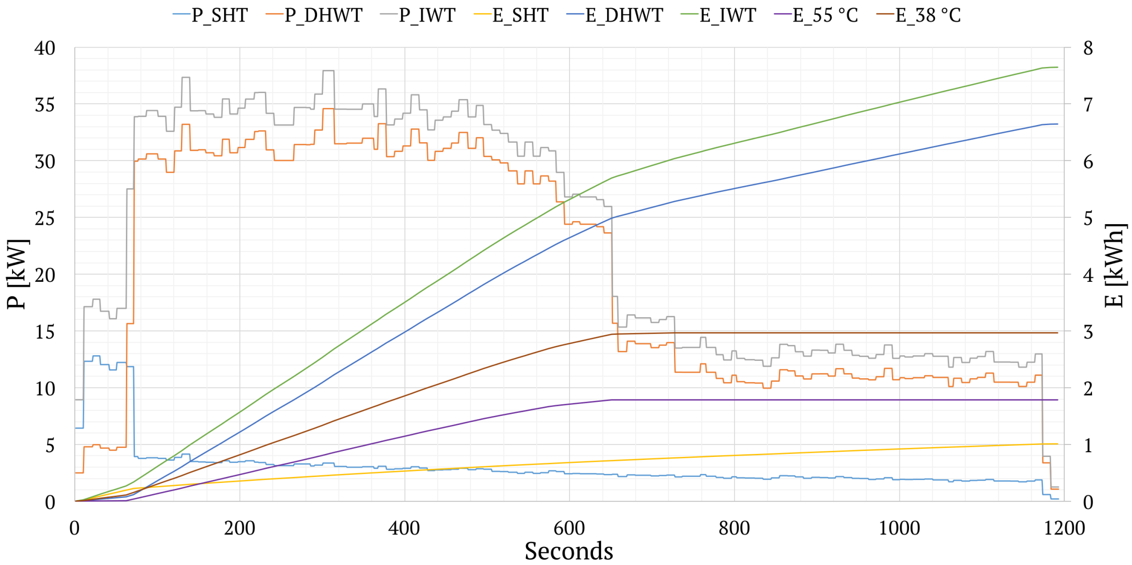

Figure 9.15: IWT power and energy development - Test 3.

The power duration and accumulated extracted heat is plotted in fig. 9.15. The graph indicate a total instantaneous power demand between 35 and 25 kW during an 8 minute period. A sharp decrease in heating power was seen as the outlet water temperature dropped below 60 °C. The total accumulated heat extraction from the IWT during the 20 minute period, was 7.6 kWh. This amount to an average power demand of 23 kW. **By imposing minimum outlet water temperature requirements of 55 or 38 °C, the maximum heat extraction was reduced to 1.8 and 3.0 kWh, respectively**. IWT temperature levels and DHW minimum temperature requirements are thus heavily affecting the available heat quantity. In case of larger DHW demands it is favorable to increase the IWT set-point temperatures, although this contributes to increased heat losses and lower energy coverage for the GSHP and STC.

9.3.2 Test 4: STC Standalone Operation

Solar thermal water heating was tested for a 5 hour period between 10 AM and 15 PM, on a partly cloudy day in May. The STC was operated as a stand-alone system, without any form of auxiliary heating. Specifically, both the GSHP and the IEHs were deactivated before and during the test period. Both the DHWT and SHT were initially discharged, in order to improve the potential for thermal recharging. Pump CP4 was operated continuously in proportional pressure mode, with the differential pressure set-point at 50 %.

Fig 9.16 illustrates the development of the south façade ambient temperature, as well as the global solar irradiance on the south facade and PV surface. Average values were 551 and 782 W/m^2, respectively. Hence, the intensity of the solar irradiation was about 29.6 % higher at a tilt angle of 30°, compared to 90°. The average ambient temperature was 28.5 °C. Fig. 9.17 illustrates the development of the STP supply and return temperatures, RTD25 and RTD26. An average ΔT of 5.9 K between the STP inlet and outlet, and an average fluid temperature of 35.1 °C, were measured. **At these conditions, the average panel thermal efficiency, η, was 75.6 %. This is close to the optimum panel efficiency, η_0, which is 81.1 %, cf. appendix F**. It may be noted, however, that a low ΔT between the solar fluid and ambient air contributes to favorable operating conditions. A low accumulation tank temperature is contributing as well.

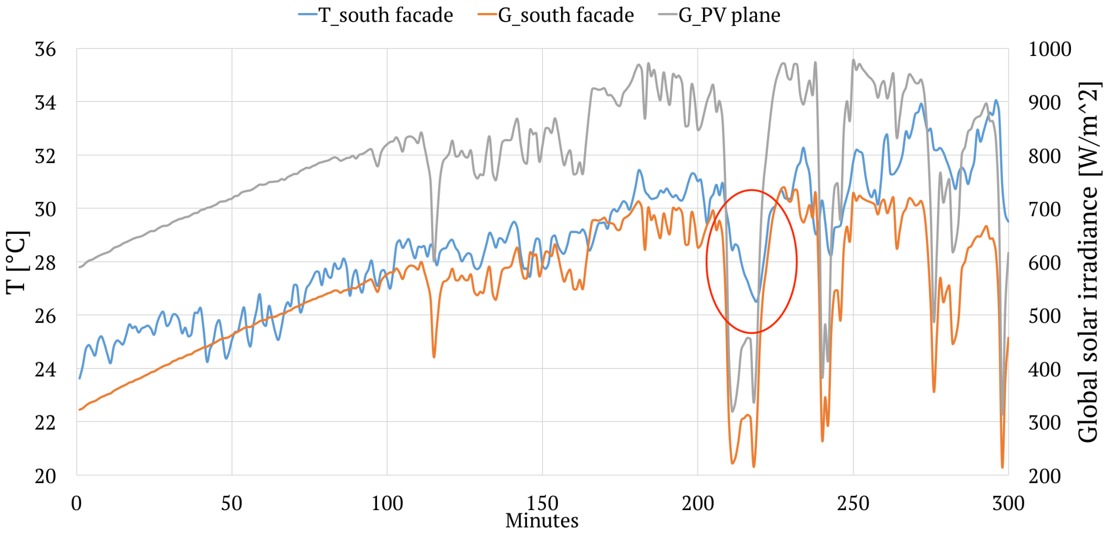

Figure 9.16: Outdoor environmental quantity development - Test 4.

The average water temperatures in the SHT and DHWT are plotted in fig. 9.17. Temperatures are given as arithmetic average values between RTD9 and RTD10, and between RTD11 and RTD12, respectively. The solar fluid flow rate, measured by the electromagnetic flow meter, EFS2, is also plotted. By comparing the global solar irradiance and ambient temperature with the solar fluid flow rate, a certain time delay was observed. The flow rate was relatively steady at 200 l/h, until the irradiation and temperature reached about 700 W/m^2 and 31 °C, respectively. At this point, CP4 produced an increase in the flow rate to 600 l/h. The subsequent drop in the irradiation was due to a passing cloud. Fig 9.16 indicates a **distinct influence of the solar irradiation on the south facade temperature measurements. This is a partial explaination to the unrealistically high panel efficiency**.

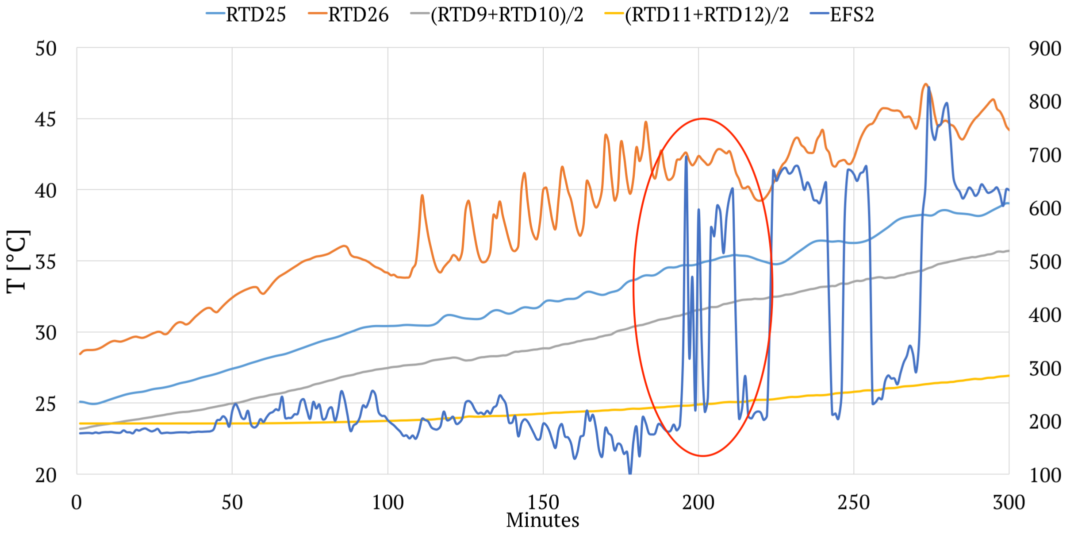

Figure 9.17: STC temperature and flow development - Test 4.

The power and energy output from the STPs, and the energy input to the IWT are plotted in fig. 9.18. The theoretical power input of the solar irradiation, P_{STP}, is plotted as the product of the global solar irradiation and the active panel area of 3.63 m^2. This quantity has an average value of 2.8 kW, and is lower than the average power of 2.0 kW for the solar circuit fluid, P_{STC}. **A PG density of 1025 kg/m^3 and specific heating capacity of 3.7 kJ/kgK, were assumed**. The ratio of these values corresponds to an efficiency of 71.4 %, which is lower than the thermal efficiency given earlier, and closer to a realistic value. It is readily seen that the while the accumulated energy transported by the solar fluid, E_{STC}, is 10 kWh, the accumulated energy in the IWT is just 3.7 kWh. The bulk of this energy is delivered to the SHT. These observations suggest losses between the STPs and the IWT of 63 %, which is highly unlikely.

9.4 Summary of Measurements

Test 1: GSHP Standalone Operation

The GSHP was operated in space heating mode, rejecting heat via the SHT to the radiator circuit. An average operating condition of 4.4/43.9 °C was observed, giving a ΔT_{lift} of 39.5 K. Based on an evaporating pressure of 1.74 bar_g, an evaporating temperature of -1.8 °C was prevailing. This indicated an evaporator LMTD of 5.3 K. For the condensing pressure a value of 10.9 bar_g was observed, which implied a condensing temperature of 46.6 °C, and a condenser LMTD of 4.8 K. A pressure rato of 4.34 was calculated, based on absoulute pressures.

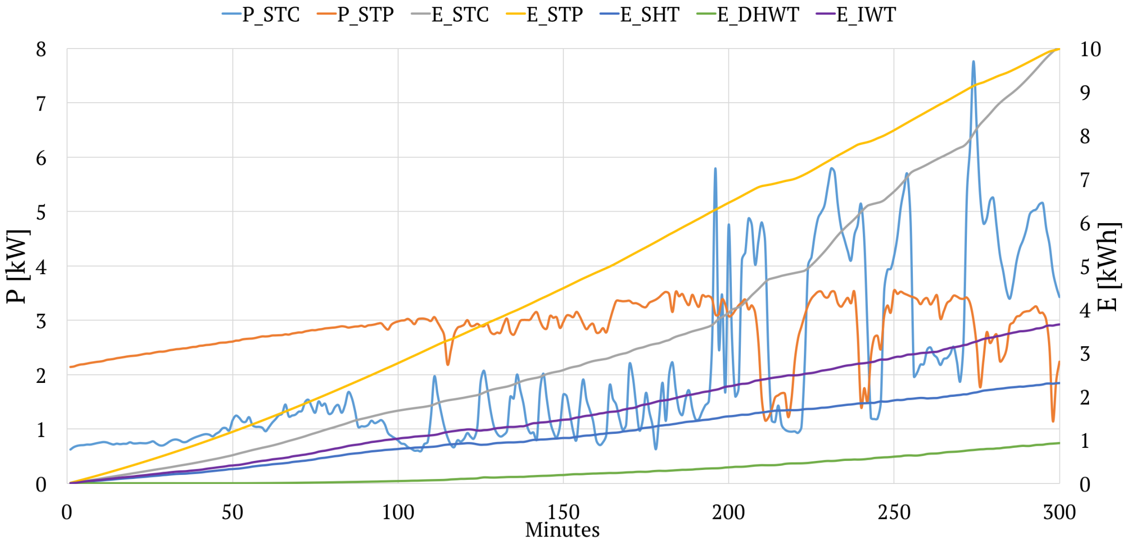

Figure 9.18: STC power and energy development - Test 4.

The average heating capacity for the GSHP was measured to 2973 W, at an electric input input power (adiabatic) of 932.9 W. This resulted in a COP for the HP unit of 3.19, and a poor Carnot efficiency, η_C, of 39.8 %. The electric input power to CP1 was nevertheless 147.3 W, and should be included in the COP calculation. Hence, the was reduced by 13.5 % to 2.76. By further including the 136.4 W electric power consumption to the hydronic pumps, CP2 and CP3, the COP dropped to 2.45. **The total electric input to pumps represented 30.4 % of the compressor input power, and thus a significant parasitic system loss**.

At these conditions, ΔE for the GSHP system ranged from 59 to 69 %, depending on the system boundary. This excluded the electric energy use to the IWT IEHs and the OSO MX pump central.

Test 2: GSHP and STC Combined Operation

The STC was operated in combination with the GSHP, rejecting heat to the ground collector circuit via the BPHX. The GSHP was rejecting heat to via the SHT to the radiator circuit. An average operating condition of 4.7/47.1 °C was observed, giving a ΔT_{lift} of 42.4 K. An evaporating pressure of 1.58 bar_g was measured, thus giving an evaporating temperature og -3.4 °C. At the condenser, a pressure of 11.24 bar_g was measured, giving a condensing temperature of 47.2 °C. The low eavporating temperature was due to a reduced brine flow rate, which gave a larger ΔT_b. Consequently, the evaporator LMTD increased to 6.9 K, resulting in a reduced capacity. The condenser LMTD dropped to 1.4 K, in order to compensate for a lower heating capacity.

The average heating capacity was measured to 2592 W, at an electric input power of 898 W. This gave a COP of 2.89, and an η_C, of 38.1 % for the GSHP unit. For CP1 a noticable reduction in electric input power was observed. Compared to the first test, a reduction from 147.3 to 129.6 W was observed. This was largely due to a lower brine flow rate. For CP2 and CP3 the electric power input was 133.1 W, and 12.5 W for CP4. The combined electric input power to the pumps represented 30.6 % of the compressor input power, and was almost equivalent to the first test.

Poor COP values, ranging from 2.22 to 2.89, were observed. Consequently, relative energy savings ranged from 55 - 65 %. This is a reduction compared to the normal operation in test 1. **Hence, direct increase the evaporator brine inlet temperature, by means of solar heat, is not recommended with the current pump design.**

Test 3: IWT Discharging

The effective DHWT volume was assessed by discharging the tank, in order to simulate an extreme DHW load. Initial temperature conditions in the SHT were 22 °C at the bottom and 40 °C at the top. For the DHWT, an initial top temperature of 73 °C, and a bottom temperature of 35 °C, was measured.

With a water main temperature of 8 °C, the DHW preheating potential for the SHT was initially 7 °C, and 3 - 4 °C after 20 minutes. The power output for preheating ranged from 4 - 2 kW. For the DHWT, the power output ranged from 30 kW initially, to 10 kW at the end. The DHWT top temperature decresed much more rapidly, compared to the tank middle temperature, thus indicating good thermal stratification.

These results show that the potential for water preheating is heavily influenced by the SHT average temperature, (RTD9 + RTD10)/2. **A higher temperature level in the SHT will increase the DHW preheating potential, but will deteriorate the operating conditions for the GSHP and STC**. DHW preheating by means of the SHT coil, may thus be a less optimum solution.

Test 4: STC Standalone Operation

After discharging the IWT, the STC was operated in water heating mode during a 5 hour period between 10 AM an 15 PM. During this period, an average global solar irradiation of 551 W/m^2, was measured on the south façade. This was almost 30 % lower than the corresponding value on the PV surface. Hence, a panel tilt angle of 90° resulted in a lower solar energy potential, compared to an angle of 30°.

The measured thermal efficiency of the STPs was 75.6 %, which was close to the theoretical maximum value of 81.1 %, specified in the Solar Keymark documentation. The STP thermal efficiency is dependent on the ΔT between the ambient temperature and the avaerage temperature of the solar fluid. A south façade temperature measurement, which is influenced by direct solar irradiaton, may affect the efficinecy calculation, and result in a high value. **The south façade temperature sensor should be protected against direct solar irradiation, in order to minimize the error**.

Similar anomalies were experienced with the calculated thermal energy quantity transported by the STC, E_{STC}, and the thermal energy input to the IWT. Specifically, the results suggested a 10 kWh solar thermal input to the STC, while the calculated increase in IWT energy content was 3.7 kWh. This deviaton is too large to be explained as thermal losses from pipes alone. **Possible errors include wrong estimations of the density and specific heat of the STC PG solution and IWT water, as well as measuring errors in flow rates (EFS2) and temperatures (RTD25 and RTD26).** Further investigations are advised.

9.5 Error Sources and Comments

Initially, an attempt was made to calculate the evaporator capacity on the basis of measurements on the ground collector circuit. Specifically, the the supply (RTD2) and return (RTD3) brine temperatures, the volumetric flow rate (EFS1), and thermopysical properties for the 44 % PG solution were used. It was observed, however, that small inaccuracies in temperature measurements translated to large inaccuracies in the evaporator capacity. With a typical ΔT_b of 2 K, and an accuracy of ± 0.2 K, the error was ± 10 %. Instead, measurement were carried out at the water side of the GSHP.

For all calculations, the thermophysical properties of water were assumed constant throughout, with negligible deviations is the temperature range 20-50 °C. The density and specific heating capacity were set to 990 kg/m^3 and 4.183 kJ/kgK, respectively.

The heat pump performance was calculated according to the water side heating capacity, and the compressor power input. The heat pump thermal energy meter, TEM1, has not been configured to record flow rate measurements. Consequently, TEM3/UFS6 in the radiator circuit was used for this purpose. Comparisons between these measurements and external measurements suggested an error of ± 10 %. Supply and return temperatures for the heat pump was taken from TEM1, as RTD4 and RTD6, respectively. These measurements have an accuracy of ± 0.1 K. With a typical ΔT_w of 6.3 K, the error amounts to ± 3.2 %.

The electrical power input to the heat pump compressor was calculated on the basis of its energy use. The heat pump EEM records this quantity with an accuracy of 1 Wh. By dividing the electrical energy use by time, the electrical power input (W) was estimated. Due to the ON/OFF compressor control, the error is expectedly small.

During combined operation of the GSHP and STC, the temperatures in the STC was above the temperature range suggested in the literature. Observations indicated a reduction in the COP, as opposed to the desired increase. Significant contributors to this effect were the proportional pressure-controlled circulator pumps, CP1 and CP2. Different results may be expected if the volumeric flow rate is maintained constant. With the present design, however this is not an option. Testing at lower STC temperatures is nevertheless advised.

While testing the STC in water heating mode, the accumulated energy input to the water tank (3.7 kWh) was considerably lower than the accumulated energy input to the STC (10 kWh). This difference is significant, although there are several uncertainties involved. Firstly, the STC energy input is calculated from the STP inlet and outlet temperatures, RTD25 and RTD26, respectively. Hence, pipe losses are excluded. These losses might be significant, as the STPs and accumulation tank are located at opposite sides of the building. Secondly, the solar fluid mixture was assumed equal to that of the ground circuit brine (PG at 44 %). Deviations may thus result from wrong thermophysical properties. In order to accurately assess this difference, STC temperature measurements should be made at the coil, and the PG solution should be measured.

Chapter 10

System Design and Dimensioning

For passive house and ZEB buildings, the net peak power demand for space and ventilation heating is generally low, compared to traditional buildings. Meanwhile, the availability of low-capacity brine-water heat pump units is limited. Thus, keeping with traditional design criteria, avoiding over-dimensioning is an apparent challenge.

Paradoxically, combined space and water heating systems achieve longer operating hours than systems designed for space heating only. Hence, equivalent energy coverage factors may be obtained with a lower power coverage factor. In combined heat pump and solar thermal systems, the required energy coverage for the heat pump is further challenged by the solar thermal energy input. This chapter addresses the design and dimensioning of the combined GSHP and solar thermal system at the Living Lab.

10.1 GSHP Power and Energy Coverage Potential

The thermal power and annual energy coverage factors has been estimated on the basis of normalized weather data, and Calorex technical data. The SIMIEN simulation resulted in a net peak power demand, P_N, of 5.69 kW for space heating and heating of ventilation air. This excludes the power demand for DHW production, which is regarded a continuous process. The average power demand for DHW heating is estimated to 0.35 kW, based on a normalized energy demand of 29.8 kWh/m^2day. The theoretical annual heating demand for space heating, ventilation heating and DHW production, Q_N, is 6691 kWh.

Heating capacities for the Calorex heat pump are listed in table 10.1 for two different operating conditions. It is readily seen that the heating capacity drops significantly as the temperature lift increases. Typically, the heating capacity is reduced by 3-4 % per K decrease in the evaporating temperature, and by 0.5 % per K increase in the condensing temperature. Hence, it is most advantageous with a high inlet brine temperature, combined with a low outlet water temperature. The lower the temperature lift, the higher the heat pump heating capacity and COP. This translates to a higher energy coverage factor, α, and relative energy saving, ΔE.

Table 10.1: Heating capacities for the WW3500 at different operating conditions.

	Outlet water: 35 °C	Outlet water: 55 °C
Inlet brine: 0 °C	3.17 kW	2.61 kW
Inlet brine: 15 °C	5.49 kW	4.65 kW

With the ideal, but unlikely, condition of 15 °C inlet brine temperature and 35 °C outlet water temperature (15/35 °C), a power coverage factor, β, of 92.9 % could be achieved. For the more likely condition of 0/35 °C, a β of 53.6 % would be prevailing, and at 0/55 °C the value drops to 44.2 %. Consequently, the need for IEH top-up heat is increasing as the heat pump operating conditions are deteriorated. **With respect to these data the dimensioning of the GSHP is within the recommended values**.

The heat sink temperature, T_{sink}, and relative energy saving potential, ΔE, are largely determined by the chosen strategy for heat distribution. Whether heat is distributed at 33/28 °C via the underfloor heating panels, or at 55/50 °C via the radiator or heating battery is decisive to the performance. Fig. 10.1 illustrates the annual theoretical energy coverage potential for the heat pump and IEHs, at 35 °C supply water temperature. A DHWT top temperature of 68 °C is used, and the combined temperature delivery from preheating and reheating with the heat pump is set to 50 °C, from 5 °C to 55 °C. The remaining 13 °C are covered by the IWT IEHs. Well-functioning switching between space heating and DHW heating modes is assumed.

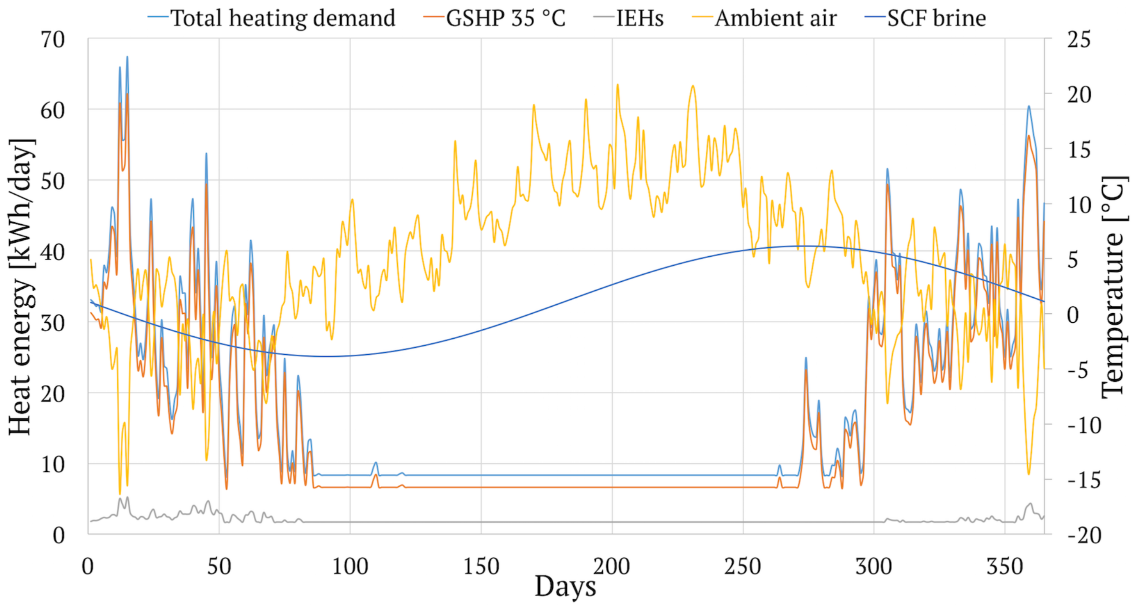

Figure 10.1: Theoretical energy coverage at t_{w-o} = 35 °C.

The heat source temperature is dependent on climatic conditions and the thermal properties of the ground. As an approximation, a cosine variation is used, with the temperature swinging around the annual mean ambient temperature of 5.1 °C. In accordance with the experimental results of Eggen [8], an amplitude of 5 K and a phase shift of 2 months is used. ΔT between the soil and the brine inlet temperature to the evaporator is set to 4 K, in close accordance with Nielsen [7].

For a supply temperature of 35 °C, the total energy coverage of the GSHP amounts to 5731.1 kWh, corresponding to an α of 85.7 %. The annual SPF for combined operation at this condition is 2.56. By increasing the output temperature to 55 °C, the energy coverage drops to 5626.5 kWh, corresponding to an α of 84.1 %. In this case the annual SPF is 2.31. Relative energy saving potentials are 60.9 and 56.7 %, respectively. According to NS3700, the minimum required renewable energy coverage for DHW heating is 50 % [22]. This requirement is maintained in both cases, with an α for DHW heating of 71.4 %. Table 10.2 summarizes the results. It should be noted that, while a lower heat distribution temperature improved the operating conditions for the GSHP, it reduces the potential for DHW preheating in the SHT.

Table 10.2: Theoretical performance of the GSHP system.

		DHW heating	Space heating		Total	
		55 °C	55 °C	35 °C	55 °C	35 °C
E_{HP}	$[kWh]$	711.3	1125.3	945.2	1836.6	1656.5
Q_{HP}	$[kWh]$	2171.1	3455.4	3560.0	5626.5	5731.1
E_{IEH}	$[kWh]$	868.5	197.4	92.8	1065.9	961.3
Q_{IEH}	$[kWh]$	868.5	197.4	92.8	1065.9	961.3
SPF_{HP}	$[-]$	3.05	3.07	3.77	3.06	3.46
ΔE_{HP}	[%]	67.2	67.4	73.5	67.3	71.1
SPF_{system}	$[-]$	1.92	2.76	3.52	2.31	2.56
ΔE_{system}	[%]	47.9	63.8	71.6	56.7	60.9

10.2 GSHP Unit

The Calorex heat pump unit has a simple design, and is based on the single-stage vapor compression cycle. Its main components are the evaporator, hermetic scroll compressor, condenser, liquid receiver and TEV. Process improving components, such as a DSH or SGHX, are not part of this design. The unit is charged with 2.5 kg of HFC-134a, and uses a polyolester (POE) compressor lubricant. Fig. 10.2 shows a principle flow scheme of the heat pump unit. A manufacturer-provided flow scheme may also be found in appendix B. Regarding heat pump technical information, several requests has been made to the manufacturer. Feedback on this matter, however, has been scarce.

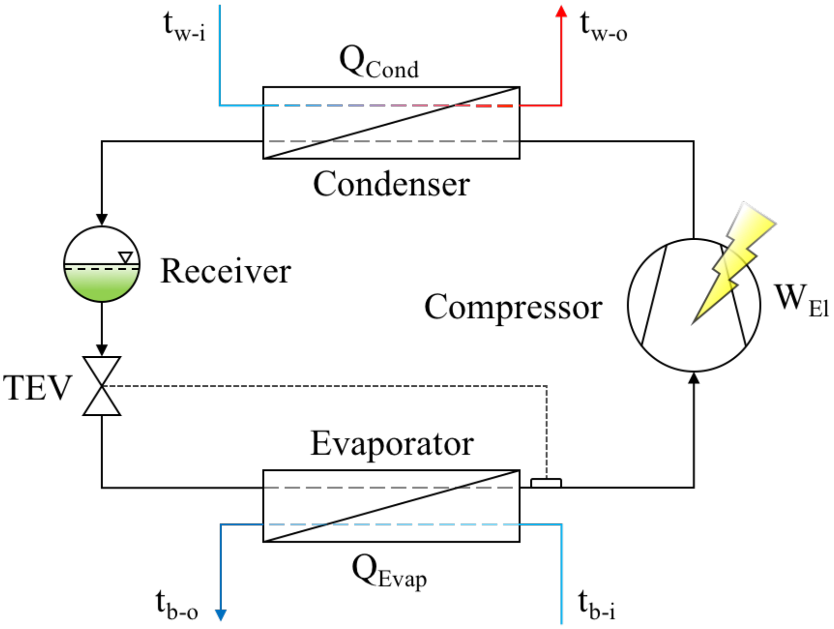

Figure 10.2: Principle flow scheme of the Calorex heat pump unit.

Operation of the heat pump unit is divided between two modes; space heating and DHW heating. Outlet water temperature limitations are 55 and 65 °C, respectively. At present, however, the GSHP has been operated in space heating mode only. Consequently, only DHW preheating is covered by the heat pump, while the rest of the demand is covered by the IEHs. Well-functioning switching between modes is hence necessary in order to approach the theoretical energy coverage factor for the heat pump. Poor allocation of heating loads between the HP and peak load equipment is a known cause for deteriorated performance [76]. HP-integrated peak load heaters is a more favorable design, which reduces the risk of errors.

CP2/JP43 has a differential pressure-controlled design value of 601 l/h at Δ p 25 kPa, compared to the recommended 450 l /h ± 10 %. Field measurements, presented in chapter 9, indicated that the actual flow rates at 100 % differential pressure settings are approximately 390 l/h, which is close to the recommended value. At the operating condition 4.4/43.9 °C the condenser temperature difference, $LMTD_C$, was 4.8 K. combined with a heating capacity of 2973 W, the resulting U·A-value is 619 W/K.

Design flow rates for the brine and water circuit circulator pumps are somewhat larger than recommended by the HP manufacturer. CP1/JP42, has a constant flow design value of 1200 l/h, compared to the recommended 720 l/h ± 10 %. Measurements have indicated flow rates in between these values, with an average of 1017 l/h. At the operating condition 4.4/43.9 °C, $LMTD_E$ was measured to 5.3 K. With an evporator capacity of approximately 2100 W, the resulting U·A-value is 403 W/K.

The heat pump compressor is a scroll-type, which is produced by *Bristol Compressors*, according to the serial number, H71J223ABK, cf. appendix B. It desiged for HFC working fluids and has been tested for R407C. According to the test data its evaporator temperature range is between -30 and +10 °C. In the Calorex technical data, lower and upper limits for the evaporator brine inlet temprature are specified as -5 and +20 °C, respectively. Hence, there is an inconsistency, which might affect the performance at elevated brine temperatures.

Fig. 10.3 illustrates the overall volumetric efficiency for the R407C compression process. Efficiencies are plotted for constant condensing temperatures and for 5 K increments in the evaporating temperature, ranging from +10 to -10 °C. This clearly illustrates a decreasing volumetric efficiency with an increasing temperature lift.

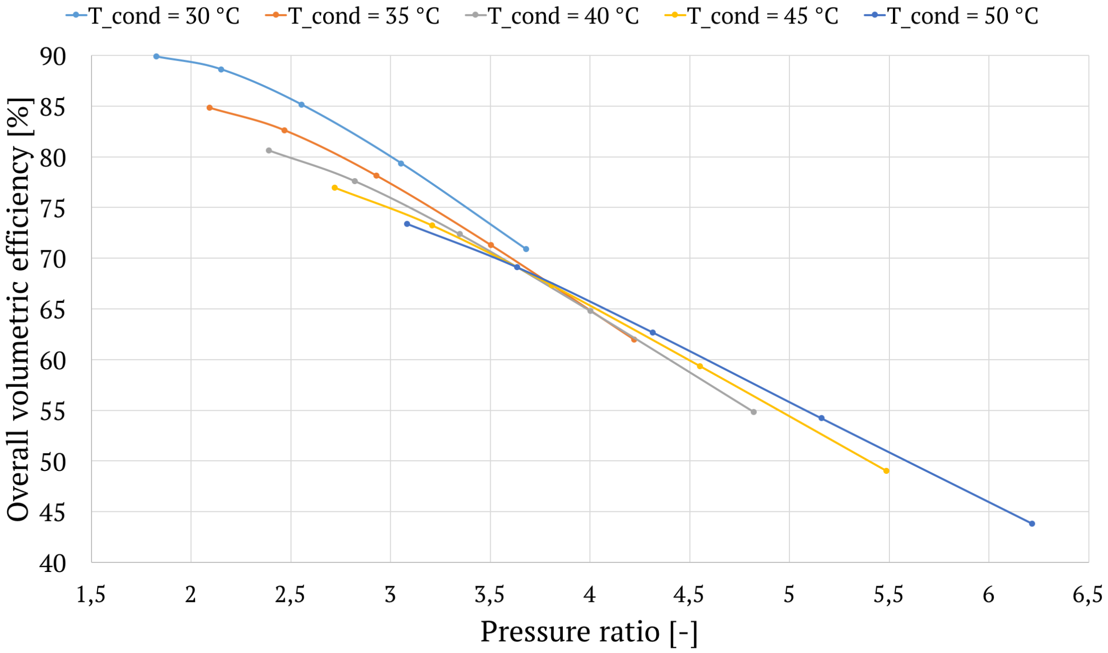

Figure 10.3: Overall volumetric efficiency curves for the R407C compression process.

Overall isentropic efficiency curves for the R407C compression process are plotted in fig. 10.4 for constant condensing temperatures. For each condensing temperature, the isentropic efficiency is plotted against the pressure ratio, when the evaporating temperature decreases in 5 K increments from +10 to -10 °C. The reduction in isentropic efficiency is clear as the temperature lift and pressure ratio increases.

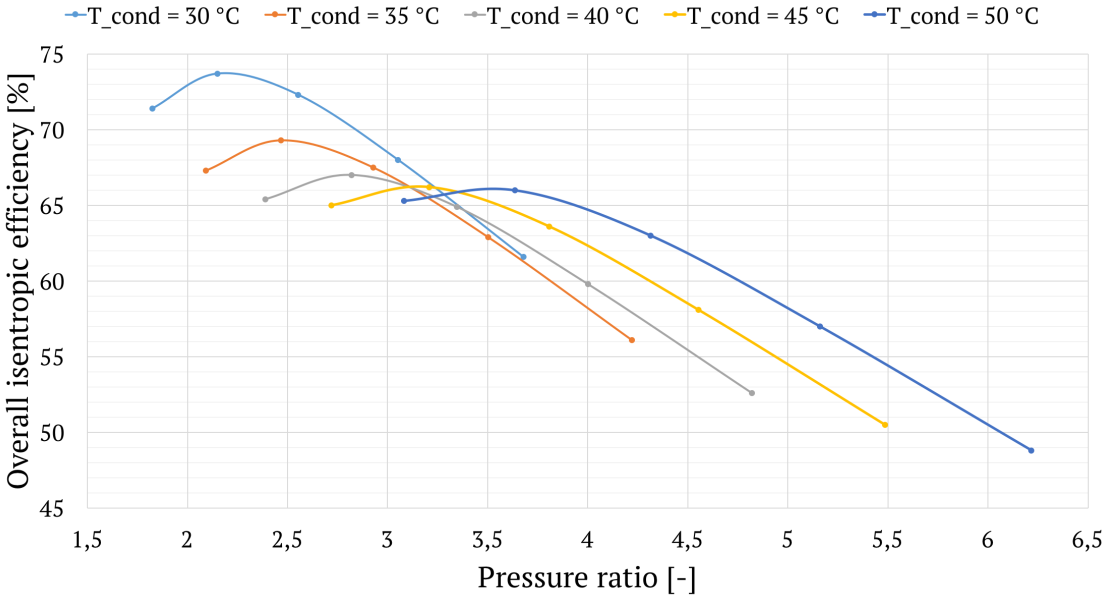

Figure 10.4: Overall isentropic efficiency curves for the R407C compression process.

Mass flow and pressure control is provided by a **thermostatic expansion valve** (TEV). The valve opening is adjusted on the basis of *feedback control* from a phial, which measures the degree of superheat at the evaporator outlet. The pressure inside the phial increases or decreases according to the variations in temperature. The pressure force acts on the spring loaded valve, which in turn increases or decreases the valve opening and the working fluid mass flow rate. This valve design might not be suitable for elevated evaporating temperatures, as the Δp over the valve is reduced. Specifically, the valve authority might be an issue.

A significant disadvantage of the Calorex heat pump design, is that only condenser heat is utilized for DHW heating. This increases the average condensation temperature, which results in a lower COP and heating capacity. Consequently, this leads to reduced energy savings. A more suitable design should at least include a DSH and SGHX. Additional design features should include VSD capacity control and an electronic expansion valve (EEV).

10.2.1 Cycle Comparison with Alternative Working Fluids

The Calorex heat pump uses HFC-134a as working fluid, which is a less common option for low capacity residential units. Its thermodynamic performance is therefore compared to alternative working fluids. Operating conditions are taken as 4.4/43.9 °C, corresponding to test 1 in chapter 9. The evaporating temperature of -1.8 °C, and condensing temperature of 46.6 °C is set constant for all working fluids. Table 10.3 list the properties of the R134a cycle, compared those of five potential alternatives.

Table 10.3: Comparison of cycle characteristics for alterneative working fluids.

Parameter	Unit	R134a	R1234yf	R407C	R410A	R32	R290
PR	$[-]$	4.408	4.040	4.224	4.224	3.782	3.541
COP	$[-]$	3.88	3.87	3.86	3.86	3.97	4.10
$x_{throttle}$	$[-]$	0.329	0.387	0.324	0.346	0.278	0.334
ΔE	[%]	74.2	74.2	74.1	74.1	74.8	75.6
η_C	[%]	48.3	48.2	48.1	48.1	49.4	51.0
η_{is}	[%]	59.3	62.2	60.8	64.1	63.9	65.2
λ	[%]	58.9	62.8	39.1	25.5	22.9	44.2
x_{DSH}	[%]	15.0	9.2	19.9	27.3	28.9	13.4
$\dot{W}_{real}$	$[W]$	771.5	772.3	774.4	774.9	754.0	729.7
VHC	$[kJ/m^3]$	2470	2314	3721	5706	6357	3294
Δh_E	$[kJ/kg]$	138.7	105.9	153.3	151.7	235.7	260.2
T_{dg}	$[°C]$	71.5	57.6	80.4	84.3	107.6	66.4
ρ_2	$[kg/m^3]$	13.2	16.2	18.0	27.9	20.2	9.6
$\dot{m}_R$	$[kg/s]$	0.0160	0.0209	0.0144	0.0146	0.00948	0.00869

Although equivalent with respect to COP and ΔE, the performance of R134a is superior to R1234yf in most other areas. The latter is thus discarded as an alternative, unless the GWP is of governing relevance. R407C and R410A exhibits similar properties, although inferior to R134a. R410A rejects a larger fraction of heat in the superheated vapor area, x_{DSH}. Combined with a higher discharge gas temperature, R410A is thus more suitable for water heating applications than both R407C and R134a. Its GWP is nevertheless higher than for R407C, and much higher than for R134a. On these terms it is discarded as a suitable option.

R32 is superior to the other HFC working fluids, including R134a. Its GWP value is also 50 % lower than that of R134a. At these conditions its volumetric efficiency is nevertheless the lowest of all alternatives, which is due to a high vapor density, combined with a low mass flow rate. Introducing an SGHX could be a possible means to offset this disadvantage, although that would further increase its already high discharge gas temperature.

As the only natural working fluid subject to this comparison, R290 exhibits performance characterisitcs that are superior to the HFC fluids. It offers a higher COP and ΔE, and a much higher specific heat of evaporation, Δh_E. Consequently, the required filling charge is low, which is favorable consodering its flammability. Its GWP value is only surpassed by that of R1234yf, although its environmental benignity is unhampered by uncertain ecological effects. R290 is thus regarded the best alternative to R134a. Barring its flammability, the low T_{dg} may be the only disadvantage for water heating applications. This may be offset by introducing a SGHX. The above discussion does not consider the different heat transfer properties of the working fluids. In practical applications, these have a major impact on the performance. Propane, for instance, has thermal conductivities and specific heating capacities that are superior to the other fluids. Tanking these differences into account, the practical performance will increase significantly. A comparison of properites is provided in appendix D.

10.3 Ground Collector Circuit

At the prevailing conditions during test 1, 4.4/43.9 °C, the GSHP heating capacity was 2973 W. With an input power of 932.9 W and an adiabatic efficiency of 90 %, the real compressor work was estimated to 0.84 kW. Consequently, there was a 2 kW heat extraction from the SCF. The horizontal ground collector tube is 105 m long, which results in an average specific heat extraction of 38.1 W/m. This outside the range of recommended values, and the value increases further at improved operating conditions. Hence, the ground collector is under-dimensioned.

Furthermore, the freezing point of the aqueous propylene glycol solution has been measured to -25 °C, which corresponds to a concentration of 44 weight-%. This is more than sufficient at the prevailing conditions, and a negative effect is observed on the thermophysical properties of the fluid. These are also dependent on the operating temperature, as illustrated in table 10.4 for three operating temperatures. Table 10.5 lists the properties and two standard PN 6.3 tube dimensions.

Table 10.4: Thermophysical properties of propylene glycol-water.

T	ρ	c_p	k	μ	Pr
[°C]	$[kg/m^3]$	$[J/kg\cdot K]$	$[W/m\cdot K]$	$[kg/m\cdot s]$	[-]
10	1041	3604	0.378	0.008246	78.65
0	1046	3569	0.372	0.01446	138.6
-10	1051	3534	0.367	0.02784	268.2

The hydrodynamic and thermodynamic performance of the ground collector circuit are largely affected by the collector tube design and dimensioning, as well as the brine

Table 10.5: Collector tube properties.

PN 6.3	D_o mm	t_{wall} mm	D_i mm	λ $W/m \cdot K$
DN32	32	2.0	28	0.42
DN40	40	2.4	35.2	0.42

composition. Relevant parameters include the tube inner diameter and length, tube wall thickness and roughness, average flow velocity and thermophysical properties of the brine mixture. The latter include fluid density, dynamic viscosity, specific heat and thermal conductivity. These parameters dictate the Reynolds and Prandtl numbers, given by eqs. (10.1) and (10.2), and therefore determine the magnitude of friction losses and convection heat transfer.

$$Re = \frac{\rho \cdot V_{avg} \cdot D_i}{\mu} \tag{10.1}$$

$$Pr = \frac{c_p \cdot \mu}{k} \tag{10.2}$$

Field measurements have indicated that the brine pump, CP1, account for the largest parasittic loss in the heat pump system. Specifically, the electric input power to CP1 is comparable to the total input power of CP2, CP3, and OSO MX. Consequently, a noticeable increase in the overall system performance is expected if the input power to CP1 is reduced. This could be achieved by means of modifications to the heat transfer fluid and/or the collector tube.

Due to the indirect design of the ground collector circuit, an extra temperature difference is added between the heat source and the evaporator. The magnitude of this temperature difference is dependent on the average overall heat transfer coefficient, $\bar{U}$, between the soil and the secondary fluid. Eq. (10.3) gives Newton's law of cooling as a function of $\bar{U}$, the collector tube external surface area, A_s, and the logarithmic mean temperature difference, ΔT_{lm}, between the secondary fluid and the soil. The higher the U-value, the lower the temperature difference, and the higher the evaporation temperature. The heat flux between the soil and the circulated brine is assumed uniform along the tube length.

$$\dot{Q} = \bar{U} \cdot A_s \cdot \Delta T_{lm} \tag{10.3}$$

The U-value is given by eq. (10.4) as a function of the internal heat transfer coefficient, the conductivity of the tube material, the wall thickness, as well as the properties of the soil or any ice formation on the tube exterior [79, p. 138, ch. 3.3]. In the current analysis the convection heat transfer coefficient is regarded the most imporant variable. Investigation of the conduction heat transfer in the soil is thus reserved for a further investigation.

$$\bar{U} = \frac{1}{\frac{1}{h_b} + \frac{r_i}{k_t} ln\frac{r_o}{r_i} + \frac{r_i}{k_s} ln\frac{r_s}{r_o}} \tag{10.4}$$

The internal convection heat transfer coefficient, h_b, is determined from the local Nusselt number of the flow. For **fully developed laminar flow** in a circular tube, the Nusselt number is a constant, which is independent on the Reynolds number, Prandtl number, and axial location [79, p. 538, ch. 8.4]. For a uniform surface heat flux, the Nusselt number is given by eq. (10.5). The brine conductivity, k_b, is evaluated at the arithmetic average temperature between brine inlet and outlet.

$$Nu = \frac{h_b \cdot D_i}{k_b} = 4.36 \tag{10.5}$$

For turbulent flow in a smooth circular tube, the Nusselt number is calculated by means of the Gnielinski correlation. It is valid for a wide range of Reynolds numbers, including the transitional region between laminar and turbulent flow. This correlation, given by eq. (10.6), is roughly valid for $0.5 \leq \mathrm{Pr} \leq 2000$, $3000 \leq \mathrm{Re} \leq 5 \times 10^6$ and $L/D_i \geq 10$ [79, p. 545, ch. 8.5].

$$Nu = \frac{h_b \cdot D_i}{k_b} = \frac{(f/8)(Re - 1000)Pr}{1 + 12.7(f/8)^{1/2}(Pr^{2/3} - 1)} \tag{10.6}$$

The friction factor is determined from the Petukhov correlation, given by eq. (10.7). This correlation is valid for smooth pipes and $3000 \leq \mathrm{Re} \leq 5 \times 10^6$.

$$f = (0.790 lnRe - 1.64)^{-2} \tag{10.7}$$

Fig. 10.5 illustrates the ground collector performance as the U·A-value, divided by the pump work due to friction losses. The current design (PG 44 %, ø40x2.0) is encircled in red. Both propylene glycol (PG) and ethyl alcohol (EA) solutions are investigates. Tube dimensions are set to the present ø40x2.4, and a smaller ø32x2.0. Fig. 10.5a illustrates the performance as a function of the brine concentration, while fig. 10.5b presents the performance as a function of the flow rate. Further reducing the flow rate would result in a reduced evaporator capacity. Increasing the flow rate both increases friction losses and reduces convection heat transfer.

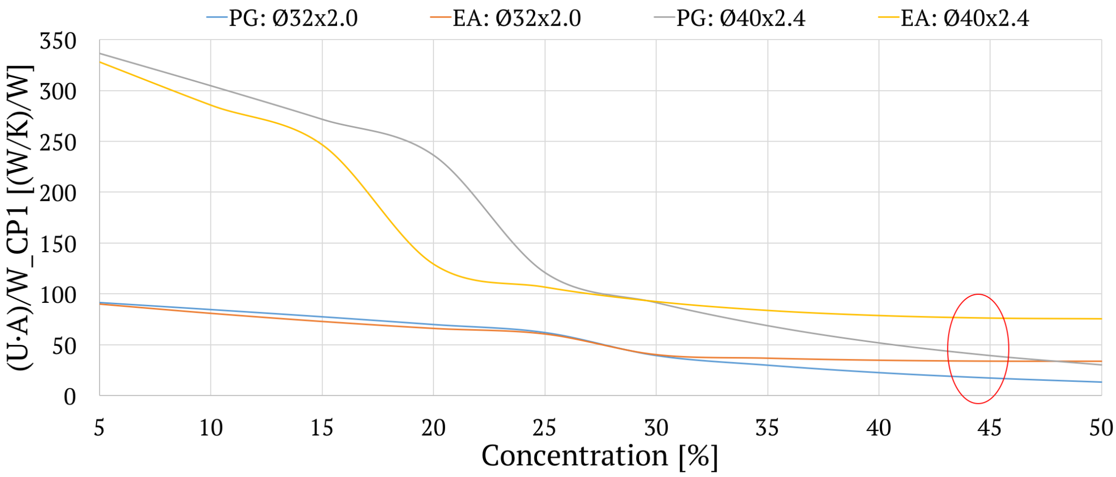

(a) Performance as a function of brine concentration.

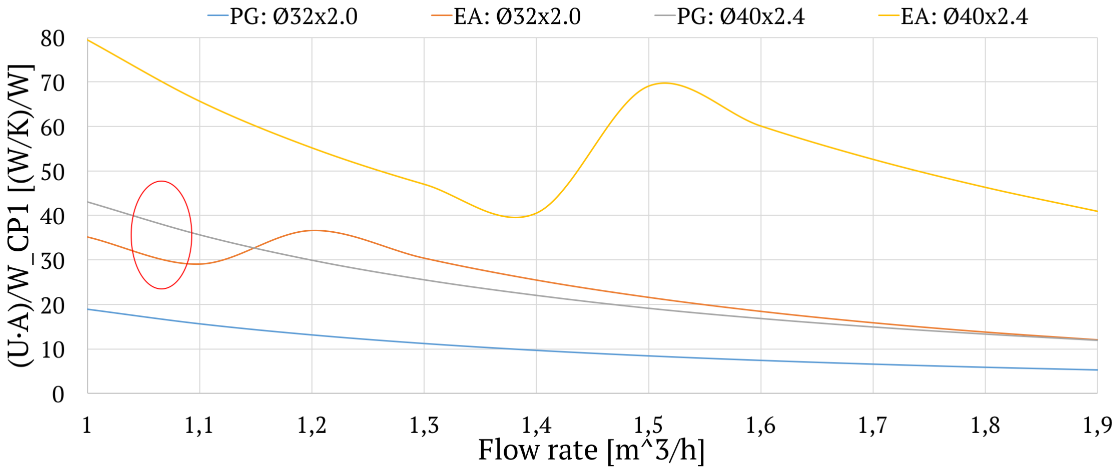

(b) Performance as a function of brine flow rate.

Figure 10.5: Hydrodynamic and thermodynamic performance of the collector tube.

The performance may be improved by reducing the PG concentration, or replacing it for an aqueous EA solution. The latter provides better performances, particularly at lower concentrations. A 25 % EA solution would maintain a freezing point of -15.5 °C, and almost triple the performance. At the same concentration, PG would only provide a freezing point of - 9.8 °C. In this case, however, the performance is slightly better. Due to a reduced heat transfer surface, it is not advised to reduce the tube diameter.

Heat transfer may be further enhanced by increasing the surface roughness of the tube, and hence the turbulence. A standard solution for ground collector tubes is to introduce internal spiral grooves, which increases both the convection heat transfer coefficient, and the convection surface area. These grooves introduce centrifugal forces within the fluid, that may increse both heat trasfer and friction losses [79, p. 557, ch. 8.7]. A commercially available solution is the MuoviTech AB Turbulence Collector®

[80, 81]. The hydrodynamic and thermodynamic performance of the collector tube has been tested experimentally [39, 82]. Pressure drops are claimed to be reduced up to 17 %, while the ground heat extraction may be improved with 16 %. By utilizing this type of collector tubes the operating conditions and required circulator pump work input will be improved significantly.

10.4 Hydronic Heat Accumulation and Distribution

10.4.1 Space Heat Accumulation Tank

The accumulation tank acts as a buffer between the GSHP and the heat distribution system. A consequence of ON/OFF compressor control is that the HP is either fully off, or operated at maximum heating capacity. At off-design conditions, when the space heating demand is lower than the HP heating capacity, operation of the unit becomes increasingly more intermittent as the heating demand deminishes. This is illustrated by fig. 10.6 for the second DAQ period.

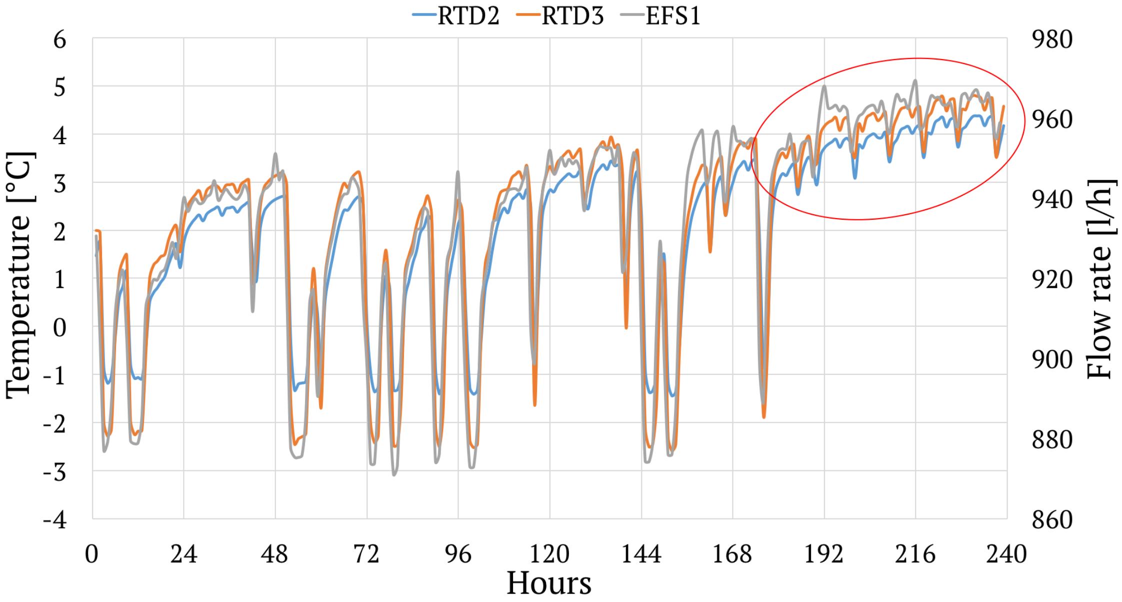

Figure 10.6: Ground collector circuit during the second DAQ period.

RTD2 and RTD3 are the hourly average evaporator inlet and outlet brine temperatures, respectively. During the last 2-3 days the inlet temperature is lower than the outlet temperature, which indicates many short operating periods. This is also reflected by increasing temperatures from the beginnin to the end of the period. Meanwhile, wear and tear of the compressor increases proportionally with the number of start-ups. Scroll compressors should not be operated with more than 2-4 start-ups per hour.

With 3 as a maximum limit, a total of 72 start-ups are permitted per day. The cycle duration, which is the time between two start-ups, is given by eq. (10.8) [20].

$$t = \frac{V \cdot C_p \cdot \Delta T}{\dot{Q}} [hours] \tag{10.8}$$

V =	total water volume	$[dm^3]$
C_p =	specific heating capacity	$[kWh/(dm^3K)]$
ΔT =	temperature difference between start and stop	$[K]$
$\dot{Q}$ =	net extracted heating power	$[kW]$

Assuming the design condition of 0/35 °C, and heat rejection by means of the underfloor heating system, a nominal heating capacity of 3.17 kW is prevailing. This corresponds to 55.7 % of the net peak power demand. Hence, when the heating demand drops below 3.17 kW, intermittent operation of the heat pump is initiated. According to the present operating strategy, the heat pump is activated or deactivated according to an accumulation tank temperature of 35 ± 1 °C, or a ΔT of 2 K. The total water volume of the heating system is approximated to 240 liters, distributed between 80 liters in the underfloor heating circuits, and 160 liters in the accumulation tank. Other components are neglected. With a water density of 0.990 kg/dm^3 and a specific heat of 4,183 kJ/kgK, the latter is expressed as $1.17 \cdot 10^{-3}$ $kWh/(dm^3K)$.

Table 10.6 illustrates that the current tank volume and heat pump control setting, the number of compressor start-ups per day may exceed the recommended value by 48. This inconvenience can be offset by allowing an effective ΔT of 4 K between cycles. It should be noted, however, that these issues are only relevant to intermittently controlled units, and are largely offset by introducing VSD capacity control.

Table 10.6: Intermittency of operation for the GSHP.

	$\Delta T = 2K$		$\Delta T = 4K$	
Heating demand	Cycle duration	Start-ups	Cycle duration	Start-ups
[kW]	[hours]	#/day	[hours]	#/day
0.5	1.17	21	2.34	10
1.0	0.59	41	1.17	21
1.5	0.39	62	0.78	31
2.0	0.29	83	0.59	41
2.5	0.23	104	0.47	51
3.0	0.20	120	0.39	62

10.4.2 Hydronic Heating System

Compared to a typical residential installation, the hydronic heat distribution system at the Living Lab is comprehensive. It integrates subsystems for both underfloor and radiator space heating, as well as a hydronic heating battery. Consequently, the extent of components, such as heat emitters, pumps and modulating valves is significant. The complexity not only contributes to added investment costs and hampered reliability, but also influences the thermodynamic performance as well.

The combination of heat emitters with different design temperatures (55/50 °C and 33/28 °C) results in a split system design, in which the highest temperature level governs the heat source temperature requirement. Combined operation of primary and secondary circuits, necessitates mixing of supply and return water in order to reach the temperature requirement of the latter. Heat is thus generated at higher temperature level than the requirement for the underfloor heating system. This aggravates the operating conditions, and affects the heat pump heating capacity. Consequently, the demand for IEH energy coverage increases.

With respect to the GSHP and STC system performance and energy coverage, the low-temperature underfloor heating system is favorable. It allows utilization of low temperature heat, and thus longer operating times for both systems. Fig. 10.7 illustrates a disadvantage of the current design. Specifically, that operation of the underfloor heating system requires operation of CP3, in addition to the OSO MX pump central. CP3 represents a parasitic loss, which could be avoided if the system was designed for underfloor heating only. Additional benefits would be reduced investment costs due to fewer components and a simpler design.

The primary and secondary circuits are designed for combined temperature and mass flow capacity control. This is ensured by the OSO MX pump central in the floor heating

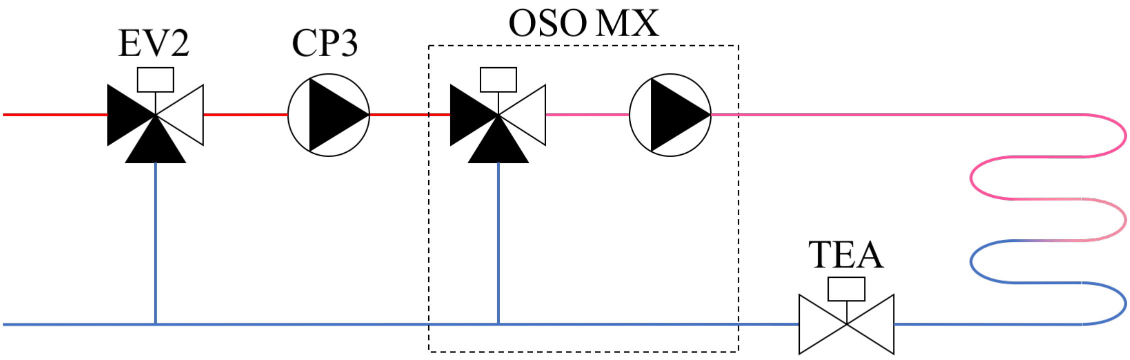

Figure 10.7: Capacity control of the floor heating circuits.

system. For the radiator and heating battery ciruits, however, capacity control has not been implemented in the LabVIEW control system. The mixing valve EV2 is either in position AB-A (100% open) during operation, or AB-B (0 % open) otherwise. Capacity control is thus provided only by CP3, which prodices a variable mass flow, proportional to its differential pressure.

Pressure variations in the primary circuit may result in momentarily low mass flow rates to the heating battery. This is not a recommended condition, as the risk of freezing in the heating battery is imminent [20, p. 290]. Temperature control is thus a favored alternative, although it requires mixing of supply and return water by means of EV2. With respect to overall system performance, however, temperature control of the GSHP outlet water temperature is a better alternative. Preferably, the GSHP outlet water temperature is controlled according to the demand, by means of an outdoor compensation curve.

10.5 Actuators

10.5.1 Circulator Pumps

Three distinct pumps are found in the five main hydraulic circuits. Two of these are of the type *Smedegaard Magneta*, while the OSO MX integrated pump is of the type *Grundfos Alpha2 L*. As seen from table 10.7, all circulation pumps except CP1 are of the same size. The first number, 25 or 32, indicates the dimension of the pipe connections, in millimetres. The second number, 60 or 120, indicates the pump lifting height in meters, multiplied by ten. Pump characterisrics for the Magneta pumps are found in appendix E.

Energy efficiency requirements for circulation pumps with an hydraulic output power between 1 and 2500 W are specified in the Directive 2005/32/EC of the European Par-

Table 10.7: Overview of circulator pumps.

Pump	Make	Model	Size	Circuit
CP1	Smedegaard	Magneta	32-120	Heat pump ground collector
CP2	Smedegaard	Magneta	25-60	Heat pump water side
CP3	Smedegaard	Magneta	25-60	Distribution primary
CP4	Smedegaard	Magneta	25-60	Solar thermal
OSO MX 18	Grundfos	Alpha2 L	25-60	Distribution secondary

liament, otherwise known as the **Ecodesign Directive** [83]. The directive addresses standalone and product-integrated glandless circulators, which per definition are circulators with the rotor directly coupled to the impeller, and the impeller immersed in the pumped medium. As of August 1^{st} 2015, all such circulators are obliged to comply with an Energy Efficiency Index (EEI) < 0.23. Both the Grundfos and Smedegaard circulator pumps installed at the Living Lab fulfil this requirement.

Figure 10.8: Illustration of the Smedegaard Magneta circulation pump [18].

The Smedegaard Magneta circulators have four distinct control settings. These include proportional-pressure, open-loop, constant-pressure and ECO mode [84]. Presently, all pumps are controlled according to the **proportional pressure** setting. With this setting the flow rate is adjusted linearly according to the differential pressure set-point, which is increased or decreased between 50 and 100 % of the selected value. The differential pressure is dependent on system characteristics, and is more or less constant during normal operation.

With the **open-loop** setting the pump is operated at fixed speed. There are ten set-points, ranging from 10 to 100 %. The pump head and flow rate are adjusted continuously to fit the characteristic curve. In **constant-pressure** mode a constant pump head is maintained according to its set-point value. The differential pressure set-point is independent of the flow rate. In **ECO mode** the pump characteristic curve is quadratic, as opposed to the linear control in proportional-pressure mode. The start-up differential pressure set-point is 25 % of the selected value. Compared to proportional-pressure control, energy savings up to 20 % may be achieved. As opposed to design conditions, neither of the pump settings allow constant flow rates. This was proved as a disadvantage during test 2, in chapter 9.

10.5.2 Modulating Valves

Three-way and two-way modulating valves are widely installed in the system and are key components to allow flexibility in operation and control. *Siemens* valves and electromotoric actuators are used [85]. An overview of the valves is given in table 10.8. The *Activax*™ electromotoric actuators allow step-less adjustment of valve positions in the range between 0 and 100 %. Control signals are 0...10 V DC.

Table 10.8: Overview of actuator valves in the system.

Control valve	Type	Construction	Application
EV1	VXP45.15-2.5	3-way	Distribution
EV2	VXP45.20-4	3-way	Mixing
EV3	VVP45.15-2.5	2-way	Control
EV4	VVP45.15-2.5	2-way	Control
EV5	VXP45.25-6.3	3-way	Distribution
EV6	VXP45.20-4	3-way	Distribution
EV7	VXP45.20-4	3-way	Distribution
EV8	VXP45.20-4	3-way	Distribution
EV9	VXP45.15-2.5	3-way	Distribution

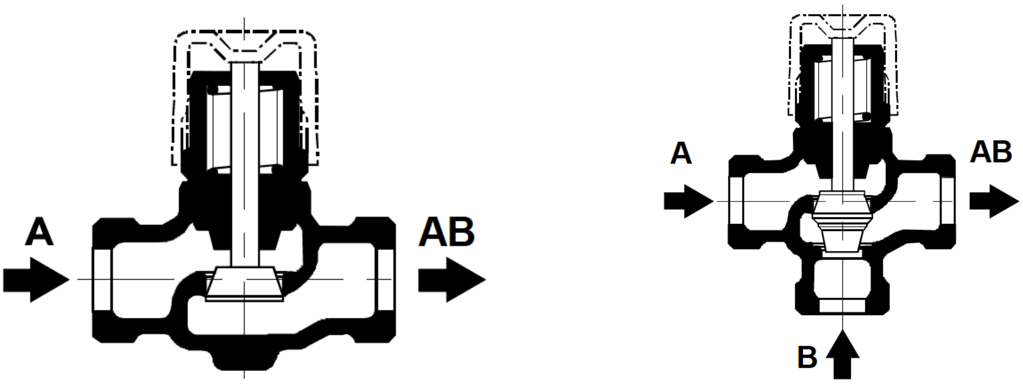

(a) VVP45...

(b) VXP45...

Figure 10.9: Flow direction of the Siemens 2-port and 3-port valves.

Although constructed as mixing valves, all three-way valves, with the exception of EV2, are used for flow distribution. This application of mixing valves is regarded acceptable at design conditions. In combination with higher flow rates, however, a disadvantage may be identified by studying fig. 10.9b. When a 3-way mixing valve is used in a distribution application, the flow direction is reversed. In direction AB-B, a low pressure region will occur at port B. In a worst case scenario the valve seat may be sucked into valve port B, thus changing the flow direction from AB-B to AB-A. Using purpose-made distribution valves is therefore advised.

10.6 Solar Thermal Circuit

For combined space and DHW heating systems, the recommended dimensioning of the STP area is 2-3 m^2 per person, or 8-12 m^2 per single-family house [20, p. 138]. Recommended accumulation tank volumes range between 75 and 125 l per m^2 STP area, or between 400 and 750 l per single-family house.

With an active absorber area of 3.63 m^2, and a total accumulator tank volume of 400 l, the STC system at the Living Lab thus appears to be under-dimensioned. This coincides with findings from a preliminary study, in which an optimum panel area of 12-20 m^2 was recommended [86]. Moreover, the direct volume at the coil is just 160 l.

The STC is a liquid filled system, in which the solar fluid remains in the STPs when the circulator pump is stopped. The solar fluid is an aqueous propylene glycol solution, identical to the ground collector fluid. The freezing point of the latter has been measured to -25 °C, which corresponds to a weight-% of 44. Propylene glycol is used because it is compatible with excessive stagnation temperatures, that may prevail in the STP during the summertime. Pure PG has an auto-ignition temperature (AIT) of 420 °C and a high flame point. Its boiling point interval is 102-170 °C [64].

10.6.1 Energy Coverage Potential

The dimensioning of the STC has been evaluated on the basis of the theoretical solar energy yield, based on the installed active STP area and tilt angle. The annual energy coverage and solar fraction (SF) was simulated on a monthly basis, by means of Polysun® [55].

The STC is modeled as a standalone DHW heating system, thus omitting the GSHP and space heating systems. Due to limited flexibility in software functionality and library components, the system boundary was set to the STPs. The calculations therefore represent the solar energy transferred from the STPs to the PG solution.

Thermal losses from copper pipes and additional components are omitted from the current evaluation. Transport losses in the range 7-10 % are nevertheless suggested by Polysun. Hence, the actual thermal input to the IWT is lower. Fig. 10.10 illustrates the Polysun flow scheme.

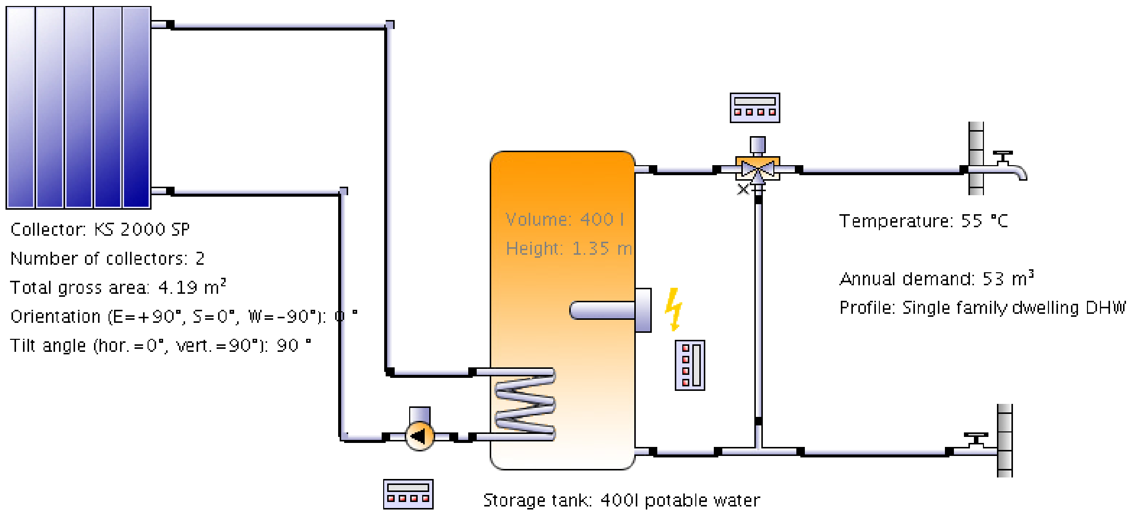
Collector: KS 2000 SP
Number of collectors: 2
Total gross area: 4.19 m^2
Orientation (E=+90°, S=0°, W=-90°): 0 °
Tilt angle (hor.=0°, vert.=90°): 90 °
Volume: 400 l
Height: 1.35 m
Temperature: 55 °C
Annual demand: 53 m^3
Profile: Single family dwelling DHW
Storage tank: 400l potable water

Figure 10.10: Schematic drawing of the Polysun model.

The following input data apply to the model:

- System configuration: DHW heating.
- Annual DHW demand: 53 m^3 at 55 °C
- DHWT: 400 l.
- Pump cut-in ΔT: 1 K
- Pump cut-off ΔT: 1 K
- Specific flow rate: 40 $l/h/m^2$

The DHW demand is based on a normalized energy use of 29.8 $kWh/m^2 year$, a ΔT of 50 K between the water main and DHW plant, and specific heat and density for water of 4,183 kJ/kgK and 990 kg/m^3, respectively. The pump is operated according to a ΔT of 1 K between the panel oulet and water temperature at the solar coil.

Technical data for the Hewalex KS 2000 SP collector is used as input data. The performance is equivalent to that of the KS 2000 SLP. Solar Keymark certification data, provided by *Solartechnik Prüfung Forschung*, may be found in appendix F. Table 10.9 lists the constants η_0, a_1 and a_2.

Table 10.9: Hewalex KS 2000 series technical data.

Panel type	η_0 [-]	a_1 $[W/m^2 \cdot K]$	a_2 $[W/m^2 \cdot K]$
KS 2000 SP/SLP	0.812	4.46	0.0096

Fig. 10.11 illustrates the duration of the annual solar energy yield. The annual DHW and space heating demands from the SIMIEN simulation are also given. The results indicate an **annual energy input to the STC of 1505 kWh**, excluding losses. This corresponds to an SF of 0.37. By including a 10 % loss factor, the annual energy yield and SF drop to 1355 kWh and 0.34, respectively.

The results indicate that the STC is undersized with respect to coverage of the entire normalized DHW demand during the summertime, between March and October. Meanwhile, only a fraction of the demand may be covered during the wintertime, between November and February. With respect to space heating, the results clearly show that the solar energy potential is at a minimum when de demand is highest. Consequently, the energy saving potential for DHW heating during the summertime, is much higher than for space heating during the wintertime.

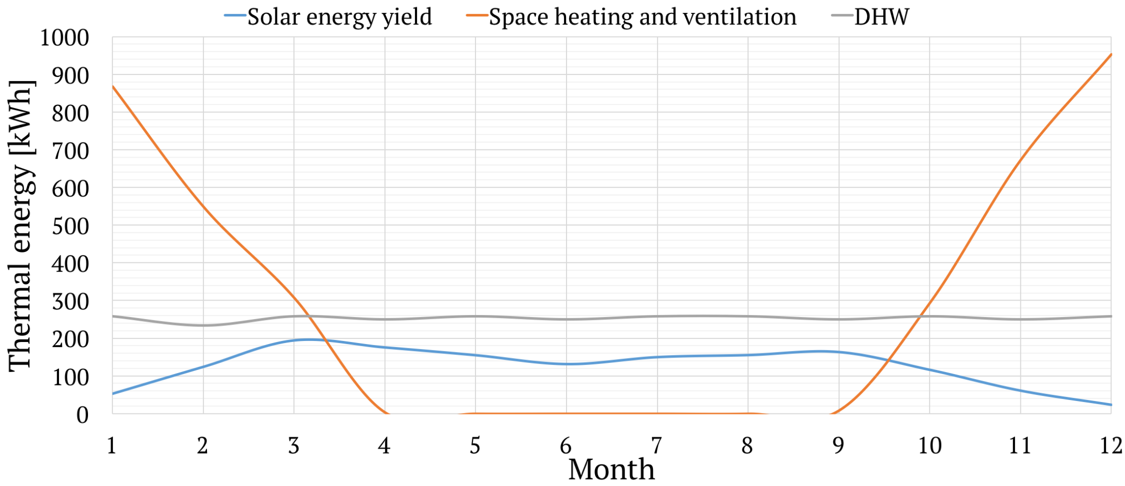

Figure 10.11: Solar thermal energy coverage potential.

The sensitivity of the solar fraction on the panel area has been studied by varying the number of installed panels, in increments of 1, while maintaining a constant tilt angle of 90°. Fig. 10.12 compares the SF of the current design, to configurations with one to seven panels in total. With the current design, an SF of approximately 0.60 is otained during the summertime. By doubling the number of panels, an SF a value of 1 is achievable by doubling the number of panels. This results in an increase of the annual SF from 0.40 to 0.60.

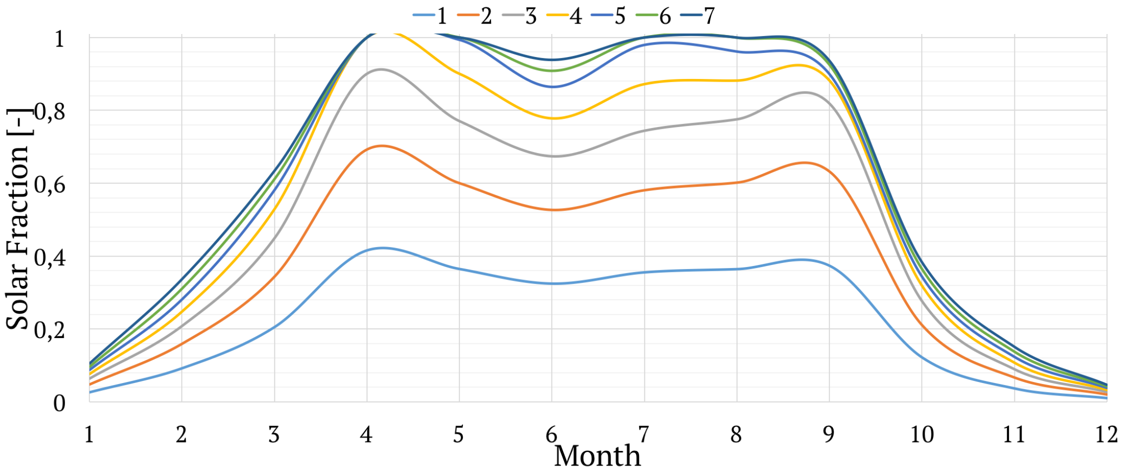

Figure 10.12: Solar fraction at different panel areas.

Table 10.10: Annual SF for 1 to 7 panels mounted at 90°.

Panels	#	1	2	3	4	5	6	7
SF	[−]	0.22	0.37	0.48	0.55	0.60	0.62	0.63

Fig. 10.13 compares the SF of the current design, to configurations with varying tilt angles. By reducing the angle from 90° to 60°, the annual SF may increase from 0.40 to 0.53. The SF during the summertime is increased from 0.60 to 0.90. Further reducing the tilt angle gives no significant increase in the annual SF, but will increase its value during the summertime.

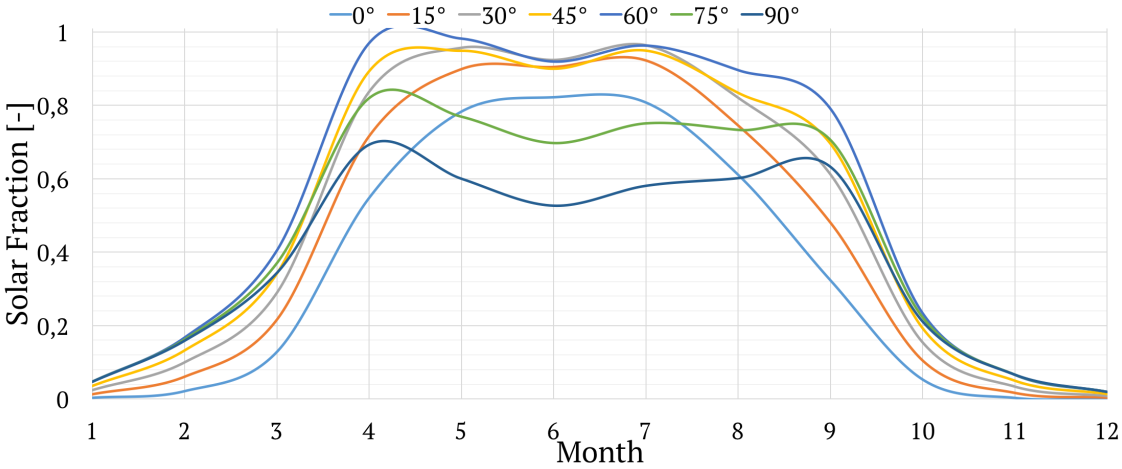

Figure 10.13: Solar fraction at different panel tilt angles.

Table 10.11: Annual SF for 2 panels mounted at 0 to 90 °.

ψ	[°]	0	15	30	45	60	75	90
SF	[−]	0.34	0.42	0.48	0.50	0.54	0.45	0.37

Comments

The results presented above are based on a simplified system design, in which the space heating load is omitted. Consequently, the amount of heat extracted from the accumulation tank between November and February is reduced, compared to a combined system design. The potential heat input from the STC to the tank is therefore hampered during this period.

Between March and October, however, the space heating demand is low, compared to the space heating demand. The model is thus expected to provide a close estimation of the energy yield and SF for DHW heating during this period. It should also be mentioned that the potential energy yield increases slightly with an incresing demand. This is because a larger heat extraction increases the potential input from the STC.

10.6.2 Heat Accumulation

The IWT is designed for compatibility with STP areas up to 12 m^2, which means that in the event of future expansion, the current 3.63 m^2 may be tripled. With respect to the location of the solar coil, low-temperature heating is prioritized. This faciltates both preheating of DHW and low-temperature space heating. Simultaneously, the STP return temperature is minimized, which has a positive effect on the panel efficiency.

Compared to the active STP area, the solar coil heat transfer area of 0.7 m^2 is low. The heat transfer rate is thus dependent on the U-value and LMTD between the coil and the SHT. Due to lack of temperature measurements at the coil inlet and outlet, it has not been possible to quantify the LMTD. A large LMTD is necessary to maintain sufficient heat transfer to the tank. This reduces potential heat input when the global solar irradiation and ΔT between the solar fluid and the water tank is low. A lower LMTD can be achieved by increasing the size of the coil. The solar coil heating power may be expressed by eq. (10.9).

$$\dot{Q}_{sol} = U \cdot A \cdot LMTD[kW] \tag{10.9}$$

In addition to limited heat transfer area, the location of the solar coil may also be a weakness of the IWT. Because of the limited panel area, the solar energy potential for space heating is low during the wintertime, between October and February. The summertime, comprising the period between March and September, thus becomes more important. During this period, however, the DHW demand is governing. Simultaneously, the STP outlet temperatures are higher. In order to improve the performance and potential for DHW heating it should be possible to provide reheating, as well as preheating. Additionally, the coil heat transfer area should be increased. Fig. 10.14 presents hourly average values for the global solar irradiance, G, and outdoor temperature measurements during the second DAQ period. Four distinct peaks in G-values between 550 and 800 W/m^2 are observed.

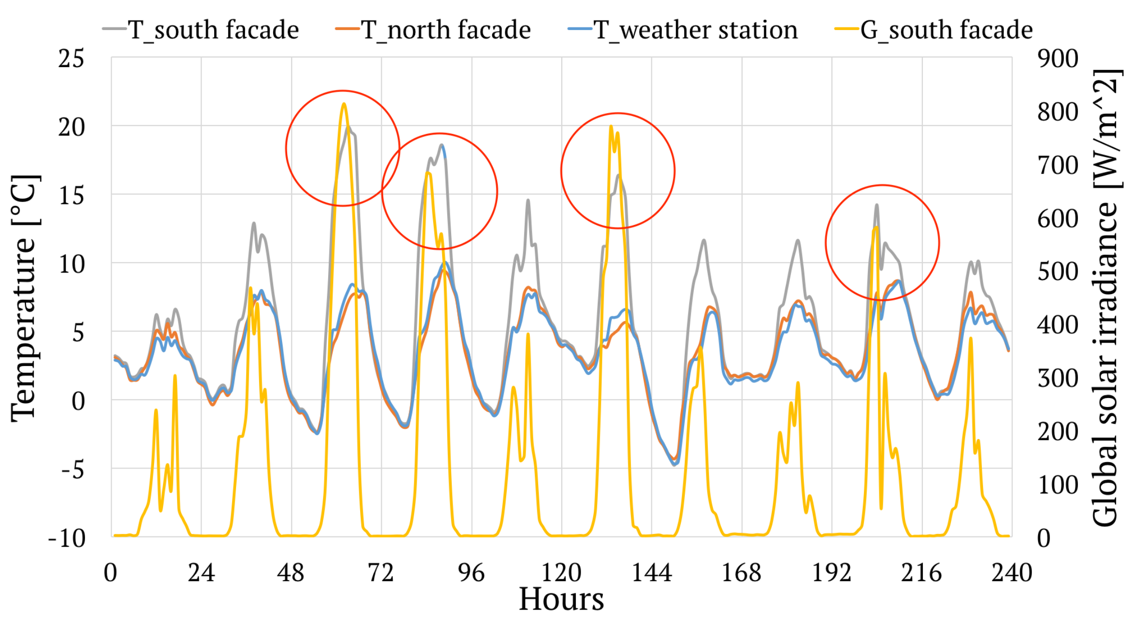

Figure 10.14: Outdoor environmental quantities during the second DAQ period.

As illustrated by fig. 10.15, the operation of the STC is closely correlated to the intensity of the solar irradiation. STP inlet (RTD25) and outlet (RTD26) temperatures are plotted together with the average electric input power to CP4. Panel outlet temperatures range from 30 to 65 °C.

The heat input from the STC to the IWT is illustrated by elevated SHT temperatures in fig. 10.16. The largest contibution is observed when the G-values and coherent STP outlet temperatures are highest. Between 48 and 72 hours, an STP outlet temperature of 55 °C is observed. In this case the SHT bottom temperature is elevated by 10 K, from 35 to 45 °C. The peak in the DHWT temperature is due to heat input from the IEH.

Between 120 and 144 hours, a panel outlet temperature of 50 °C is observed. In this case RTD9 is elevated by 13 K, from 30 to 43 °C. A uniform SHT temperature, slightly

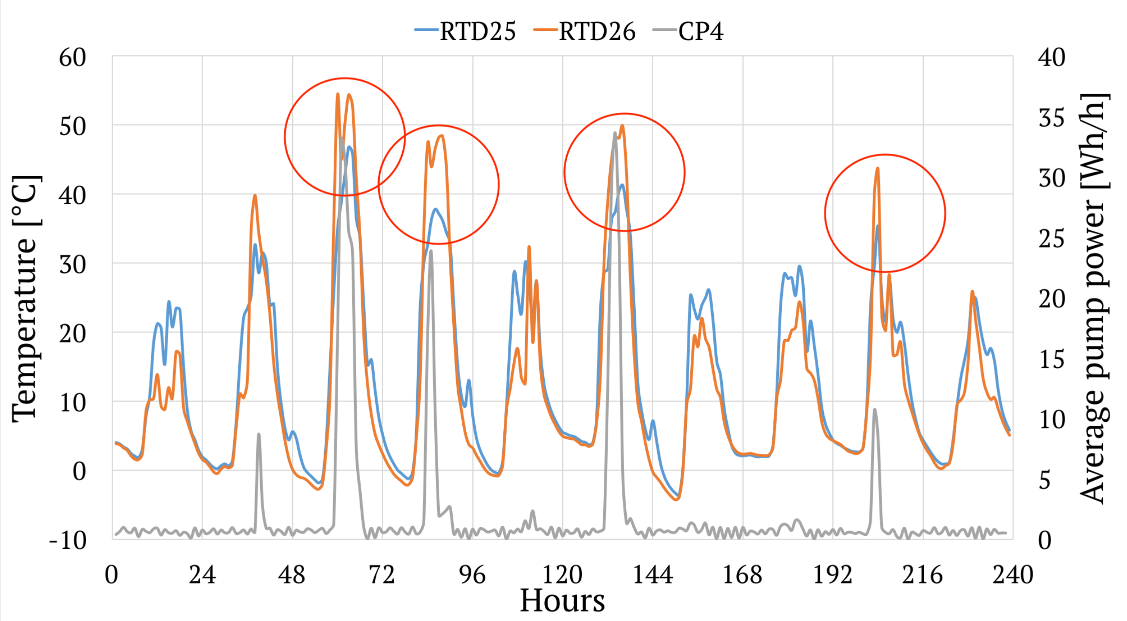

Figure 10.15: STC operation during the second DAQ period.

higher than the DHWT bottom temperature, RTD11, is reached in both cases.

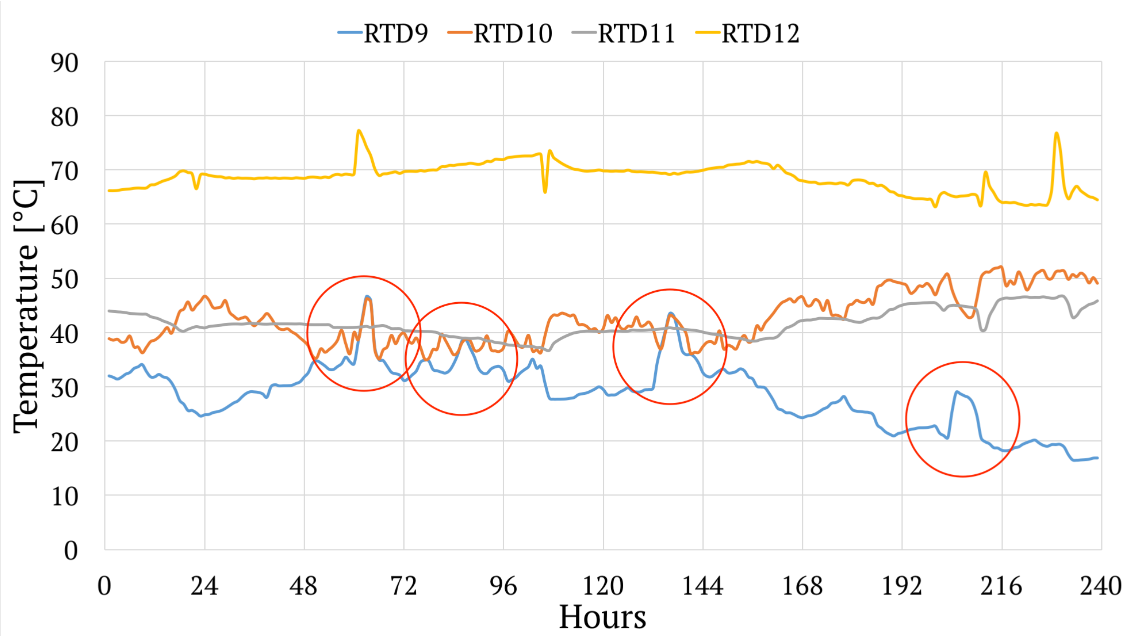

Figure 10.16: STC heat input to the IWT during the second DAQ period.

During each operating period for the STC, the DHWT bottom temperture, RTD11, is virtually uaffected. Evidently, a higher ΔT between the IWT sections is required, in order to improve the heat transfer. This was also verified by measurements in chapter 9. High solar intensities, above 800 W/m^2, are thus required in order to achieve effective charging of the DHWT.

10.7 Domestic Hot Water Tank

Besides an efficient heat pump and solar thermal collectors, the design and sizing of the thermal storage tank is of great importance for achieving a high system efficiency. From the moment the heat supply from the heat pump or solar collectors stop, thermal energy is stored in the tank. Meanwhile, space heating or DHW loads may occur, in which case the bulk of hot water is gradually replaced by cold water. The design of the tank not only affects its thermal storage capacity, but also its thermal efficiency during refilling.

The accumulation capacity and utilization of the DHWT is therefore highly dependent on the stratification performance during simultaneous hot water discharge and cold water refilling [20]. In the OSO EPTRC tank, pre-heated cold water is injected near the bottom of the tank as hot water is withdrawn from the top. This is advantageous, as mixing of cold and hot water is reduced to a minimum. Ideally, the velocity of the cold water is also reduced by increasing the cross-sectional area of the inlet pipe.

Chapter 11

Suggested Improvements

The present chapter presents suggested improvements for, or alternatives to, operation and design of the systems for thermal energy supply at the ZEB Living Laboratory. The overall goal is to reduce the intermittency of operation, especially for the GSHP and STC, while reducing the electrical energy input to the IEHs and pumps.

11.1 Alternative Operation

This section provides suggestions for alternative control logics for the main components; GSHP, STC and IWT.

11.1.1 GSHP

LabVIEW control functionality for the GSHP is limited. While start/stop functionality is operational, automated switching between space and DHW heating modes is currently not working. As a consequence, most of the DHW demand is covered by the DHWT IEH. Resolving this issue is a **minimum requirement** to improve the system performance.

Space Heating Mode

Currently, the GSHP is activated only in combination with a space heating load, that is, when the underfloor heating system is operational. An activation signal (ON) is received by the GSHP from the LabVIEW control system when the average SHT temperature drops below 35 °C. That is, according to the following logic:

- GSHP ON: if (Underfloor heating = ON) and (RTD9 + RTD10) < 35 °C
- GSHP OFF: if (Underfloor heating = OFF)

Recharging of the SHT thus occurs by means of the IEH. There should be an additional condition checking whether the SHT temperature is sufficiently high, before the GSHP is deactivated. In addition, temperature deadband should be implemented. For instance, the following logic could be applied:

- GSHP ON: if (Underfloor heating = ON) and (RTD9 + RTD10) < 33 °C
- GSHP OFF: if (Underfloor heating = OFF) and (RTD9 + RTD10) > 37 °C

The GSHP unit allows manual adjustment of the outlet water set-point temperature in steps of 0.1 K between 10 and 55 °C. By implementing this as a LabVIEW control functionality, the set-point temperature could be adjusted according to an outdoor compensation curve.

DHW Heating Mode

Discharging of the DHWT indicated a good thermal stratification during simultaneous hot water extraction and cold water refilling. A decrease in the tank top temperature, RTD12, occurred sooner and was much more rapid, compared to the tank middle temperature, RTD11. Quick response with respect to the top temperature is thus important to maintain the effective DHW volume.

According to the preliminary operating strategy, the heat pump is activated in DHW heating mode, when (RTD11 + RTD12) < 55 °C. The setting is to be maintained for 15 minutes, before re-evaluating the error. During the present analysis the GSHP was tested in space heating only, with a temperature set-point of 55 °C. In this case, the increase in the outlet water temperature was slow. In DHW heating mode, however, a quicker response is expected, due to better utilization of high-temperature discharge gas.

The effective DHWT volume, as well as the response and operating time for the GSHP, can be improved by implementing a temperature deadband. The suggested logic for operation of the GSHP in DHW heating mode is as following:

- GSHP ON: RTD12 < 65 °C
- GSHP OFF: (RTD11 + RTD12) > 55 °C.

11.1.2 STC

Water Heating

In order to reduce the temperature requirement for activation of the STC, it is highly recommended to ommit RTD10 from the control logic. RTD10 is located in the space heating zone of the SHT, where the temperature is higher than at the solar coil. Hence, the potential for low temperature heat input is restricted. Presently, the following condition applies:

- STC ON: (RTD9 + RTD10)/2 < RTD26

It is also essential that the panel outlet temperature (RTD26) is higher than the panel inlet temperature (RTD25). Otherwise, heat is rejected from the SHT to the ambient. The following conditions are suggested in order to increase the operating time for the STC, and reduce the intermittency of operation:

- STC ON: [(RTD25 + RTD26)/2 and (RTD26 > RTD25)] > (RTD9 + 5 K)
- STC OFF: (RTD25 + RTD26)/2 < (RTD9 + 2 K)

Brine Temperature Increase

Direct heat exchange between the STC and ground collector circuit via the BPHX, is not recommended as a means to improve the GSHP performance. This is because the Smedegaard pumps are differential pressure controlled in all operating modes. As a consequence, the brine flow rate and evaporator capacity are reduced when this strategy is applied.

In order to achieve the desired effect, it might be necessary with purpose-made equipment. This includes a compressor designed for high evaporation temperatures, and a throttling valve designed for lower differential pressures (larger authority). Further investigations are advised.

11.1.3 IWT: Peak Load Heating

Set-point temperatures for activation of the SHT and DHWT IEHs are currently 35 and 55 °C, respectively. Tank temperatures are taken as average values, as following:

- SHT: (RTD9 + RTD10)/2
- DHWT: (RTD11 + RTD12)/2

These are identical to the current activation temperatures for the GSHP. Meanwhile, there is no communication between the IEHs and the GSHP. This results in parallel operation, and and a shift in energy coverage from the GSHP to the IEHs. The latter should only provide top-up heat, and activation should thus be goverened by the tank top temperatures. As a suggestion, the following set-points can be applied:

- SHT IEH: RTD10 = 40 °C
- DHWT IEH: RTD12 = 65 °C

11.1.4 Seasonal System Operation

In order to gain maximum benefit from the combined GSHP and STC system, it is important maintain consequtive operation according to the maximum renewable energy coverage potential and energy efficiency. In particular, the following considerations apply:

- DHW heating demand: constant throughout the year.
- Primary space heating demand: November-February.
- Residual space heating demand: March-April and September-October.
- Low solar energy potential and temperature output: November-February.
- Medium solar energy potential and temperature output: October and March.
- High solar energy potential and temperature output: April-September.

Because the thermal demands and solar energy potential change according to the seasons, so does the optimal operation of the system. Suggested seasonal operation modes are presented in subsequently.

Winter

Winter operation should constitute the period between November and February (4 months). The bulk of the demands for space and DHW heating are to be covered by the GSHP. Alternate operation between space and DHW heating modes is thus essential. Top-up heat is supplied by the IWT IEHs. During this period, the solar energy potential is virtually non-existent. Hence, the power supply to the STC pump, CP4, could be disconnected in order to avoid stand-by electricity use.

Only the low-temperature underfloor heating system should be operated, in order to maintain a high heating capacity for the GSHP. Operation of the high-temperature radiator and ventilation heating battery should be avoided. Instead, the AHU electric coil should be used for supply air heating. Winter operation is summarized as following:

- November - February.
- Base load DHW and space heating: GSHP
- DHW and space top-up heating: IWT IEHs
- Space heat distribution: UHP
- Ventilation heating: electric coil

Spring and Fall

During the transition between winter and summer, and vice versa, there are periods with simultaneous space heating demands and solar energy potentials. These periods are roughly constitute March - April and September - October. During these periods the solar heat should be used to cover the demands for space heating and DHW preheating.

The GSHP is primarily operated in DHW mode to cover the DHW reheating demand, but may also support the STC to cover larger space heating demands. Due to low thermal power demands, the radiator and/or ventilation heating battery may be used for space heat distribution. Both circuits should be temperature controlled, according to an outdoor compensation curve. Spring and fall operation is summarized as following:

- March - April and September - October.
- Space heating and DHW preheating: STC.
- Space heating and DHW reheating: GSHP.
- DHW and space top-up heating: IWT IEHs
- Space heat distribution: radiator and/or heating battery.

Summer

Summer operation should constitute the period between May and August, when the space heating demand is non-existent. During this period the STC is covers the entire DHW preheating demand, and as much as possible of the DHW reheating demand. The SHT IEH should be deactivated to prevent unnecessary electric heat input. In the event of surplus solar heat production, the BPHX is used to reject heat to the SCF. The GSHP is operated in DHW mode only, to provide DHW reheating. Summer operation is summarized as following:

- May - August.
- DHW preheating: STC.
- DHW reheating: GSHP and STC.
- DHW top-up heating: DHWT IEH.
- STC surplus heat: rejected to SCF via BPHX.
- SHT top-up heat: none (IEH deactivated).

11.2 Alternative Designs

In the following, alternative designs that can improve the system performance are discussed. Principle flow schemes are provided in appendix J.

11.2.1 Heat Pump Unit

Replacement of the Calorex GSHP unit might be a relevant measure if the intended functionality and energy performance is to be achieved, especially in relation to DHW heating. The saving potential is nevertheless dependent on the actual demand.

During the last resident period, the DHW heating demand was estimated to 7.79 kWh/day, or 3.90 $kWh/person \cdot day$. This is close to the normalized area-specific demand of 29.8 kWh/m^2year. If the number of residents doubles from 2 to 4, the DHW demand is expected to double as well. Hence, the actual DHW demand may constitute between 44.8 and 60.9 % of the annual thermal energy demand. Efficient DHW heating is thus important.

The Calorex unit is badly suited for DHW heating because it primarily utilizes the heat of condensation. This results is a higher average condensation temperature, a lower COP and reduced energy coverage. By introducing a DSH, and preferably also a SGHX, DHW heating becomes much more efficient. This also circumvents the problem of alternate DHW and space heating, as both demands can be covered simultaneously.

A DHW-optimized unit should integrate a DHWT and electrical heaters for both DHW and space heat. Better part-load efficiency can be achieved by introducing VSD capacity control, which is a highly recommended improvement. This also reduces the dependency of the SHT. The most important design criteria for an alternative GSHP unit are listed below:

- DHW heating by means of a separate DSH.
- SGHX
- VSD capacity control.
- Electronic expansion valve.
- Integrated DHWT.
- Integrated electrical heater.

Enhanced performance may be achieved by selecting an R290-based combined DHW and space heating unit. For larger DHW demands, a transcritical CO_2 HPWH may be beneficial. The space heating demand is still significant, and the unit should be applicable for combined operation [48].

11.2.2 Ground Collector Circuit

The prevailing conditions in the ground collector loop indicate that there is a potential for both hydrodynamic and thermodynamic performance improvements. Specifically, the 44 % aqueous PG solution provides a freezing point of -25 °C, which is 10-15 K lower than the expected minimum brine temperature. This greatly influences the dynamic viscosity, thermal conductivity and specific heating capacity. Combined with a smooth collector tube surface, the resulting flow regime is laminar. Due to a collector tube length of 105 m, the typical specific heat extraction is > 40 W/m, which is too high.

The electric power input to the circulator pump, CP1, can be reduced by reducing the tube pressure drop due to friction. Coherent measures may simultaneously result in a larger UA-value and thus a reduced LMTD between the brine and soil. Increasing the collector tube length will result in reduced specific heat extraction, a larger heat transfer surface and a lower LMTD. Relevant measures that will improve the ground collector performance are summarized as following:

1. Dilute the aqueous propylene glycol solution to 30-35 % (t_{freeze} -12.8 to -16.5 °C).
2. Replace with a 25 % aqueous ethyl alcohol solution (t_{freeze} -15.5 °C).
3. Replace the 40x2.4 mm smooth collector tube with a rifled turbulence collector.
4. Replace the 105 m collector tube with a longer tube.

It is not recommended to reduce the collector tube dimension, as this increases the friction pressure drop. A reduced heat transfer area also results in a lower UA-value. Replacing the PG solution with an EA solution is higly recommended. Installing a longer collector tube is also advised.

Pipe Insulation

Insulation of pipes in heating and cooling systems is important in order to avoid unintended heat transport between the circulated fluid and the surroundings. While hot pipes should be insulated to minimize heat losses to the surroundings, cold pipes should be insulated to avoid heat transport in the reverse direction. Fig. 11.1, illustrates the corrosion damage, which is a consequence of omitting the latter. The low-temperature brine cools the ground circuit pipes, valves and connections. Condensation occurs as the surface temperature of components drops below the dew-temperature of the air inside the technical room.

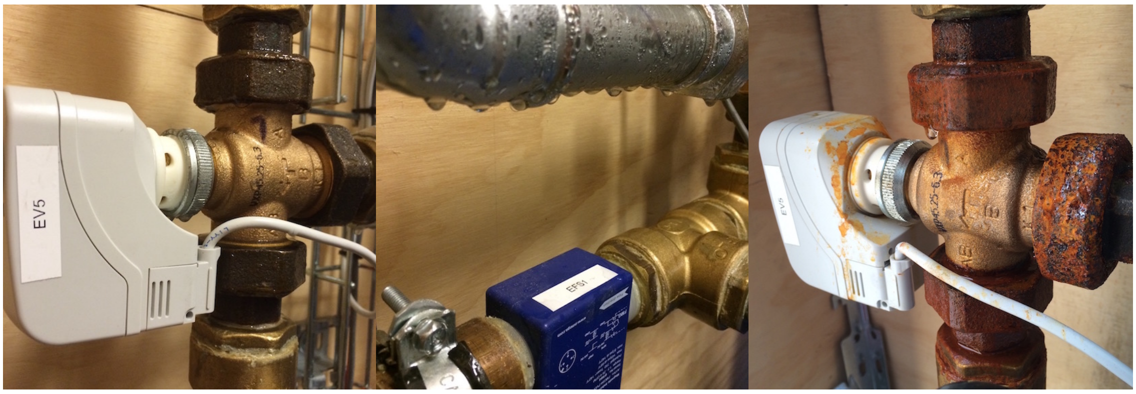

(a) 18.03.2016. (b) 18.03.2016 (c) 03.05.2016

Figure 11.1: EV5 condition before and after 6 weeks of operation.

In this case, different materials and alloys have been used for the valves, connections and pipes. Specifically, valves are made of brass, connections of black steel and pipes of standard steel. This causes galvanic corrosion, which enhances the effect of corrosion due to condensation. It is hence recommended that pipe connections are replaced for a higher quality material or different alloy. For instance, brass could be used, thus avoiding the black steel to act as sacrificial anodes for the standard steel pipes. All steel pipes should also be insulated. The insulation should not be deteriorated over time, for instance due to moisture of mechanical strain. Cellular rubber is the standard insulation type for this application. With a pipe exterior diameter of 35 mm, an insulation thickness of 30-40 mm is recommended [20].

11.2.3 Heat Distribution System

High temperature heat distribution is should be avoided in heat pump systems, due to the negative impact on both heating capacity and COP. Moreover, due to the temperature limitation of the STC during the spring and fall, the potential solar heat input for space heating is deteriorated as well.

Consequently, the design temperatures of 55/50 °C for the radiator and heating battery circuits result in a higher dependency on the SHT IEH, and thus reduced energy savings. Design temperatures of 45/40 °C and larger radiator surfaces would be a more optimum solution. For these heat emitters to be relevant, the supply water temperatures need to be temperature controlled, preferably according to an outdoor compensation curve. The annual ventilation heating demand is low, compared to space and

DHW heating demands. Supply air heating by means of the electrical coil may thus be a more favorable option.

Heat distribution via the underfloor heating system is the preferred alternative with the current design. This strategy, however, requires operation of CP3 in addition to the OSO MX pump central. The design thus contributes to unnecessary additional pump work. Underfloor heating only would be a simpler and more favorable design.

11.2.4 Solar Thermal System

The results from Polysun® simulations suggest that the system is under-dimensioned with respect to the intended design as a combined system. Recommended design values support this opinion [20, p. 138]. The system comprises two façade-mounted flat plate collectors with a total active area of 3.63 m^2.

Consequently, the SF for DHW heating between May and August is affected by the 90° STP tilt angle. Simultaneously, the SF for space heating during the spring and fall is affected by the limited panel area. Because the solar energy potential is largest during the summer, it is recommended to focus on improved performance and energy coverage for DHW production. Possible improvements are summarised as following:

- Reduced panel tilt angle from 90° to 60°.
- Increase the number of panels to 3 or 4.
- Install **glazed** PV/T panels on the roof. Consequently, the PV electricity production is unaffected, while the solar thermal energy production is increased. Roof-mounting of additional panels reduces the average tilt angle.

Heat Accumulation

A disadvantage of the current design, is that solar heat is delivered to the SHT. Conduction heat transfer between the SHT and DHWT is slow, meaning that utilization of high temperature solar heat for DHW reheating is limited. The solar coil has a heat transfer area of 0.7 m^2, which corresponds to just 17 % of the active absorber area.

Consequently, the ΔT between the solar fluid and the water is relatively large. Measurements have indicated a ΔT of 10 K between the STP outlet, RTD26, and the SHT, (RTD9 + RTD10)/2. As a result, the potential for low-temperature solar heat utilization is reduced. Possible improvements are summarized as following:

- Serial connection of the DHWT coil and and SHT solar coil. Requires separate DHWT for the GSHP.
- Separate DHWT for high-temperature solar heating.

11.2.5 Monitoring and DAQ System

The thermal energy system is extraordinarily equipped with thermal probes, volumetric flow meters and energy meters. During the present analysis, however, external measurements were necessary in order to obtain and verify the reqired data. This resulted from incorrect configuration of the GSHP thermal energy meter, TEM1. Consequently, the DAQ log data included no information about following quantities:

- Water flow rate, $q[l/h]$.
- Thermal power, $\dot{Q}[kW]$.
- Thermal energy, $Q[kWh]$.

Due to a communication error with the DAQ system, similar issues were experienced with the DHW thermal energy meter, TEM2. Consequently, the DAQ log data included no information about following quantities:

- Thermal power, $\dot{Q}[kW]$.
- Thermal energy, $Q[kWh]$.

While the above measuring data is missing, it should also be noted that a large quantity of available log data is corrupted. Possible explainations include communication errors between sensors, energy meters and DAQ hardware, momentary loss of internet connection, wiring issues or defect equipment. The following sensors are particularly prone to unreasonably high or zero values:

- TEM1 - RTD6 (GSHP return temperature)
- TEM2 - RTD13 (DHW supply temperature)
- TEM2 - UFS3/4 (DHW flow rate)
- TEM5 - RTD24 (UFH return temperature)

Accuracy and time resolution of DAQ measurements is also an important matter. For instance, the temperature probes in the ground collector circuit have an accuracy of ± 0.1 K. With a typical ΔT_b of 2 K, the measuring error is potentially 10 %. This makes determination of the GSHP evaporator capacity and SCF heat extraction. Similar uncertainties are observed when calculating η_T for the heat recovey unit. Values > 100 % are observed, due to a ± 0.3 K accuracy in temperature measurements.

Summing up, there is little use of an elaborate monitoring and DAQ system, if the recorded data is littered with flaws and errors. It is essential to define the goal and application of the measurements, and make sure that a certain standard is met. With energy performance assessments as a main priority, it is crucial that at least all TEMs are functioning. The following measures are hence recommended:

- Recalibration of sensors and probes.
- Reconfiguration of TEMs.
- Installation of TA valves in all pipes where measurements are made.
- Installation of temperature probes at the solar coil inlet and outlet.

Chapter 12

Recommendations for Future Installations

The current chapter provides recommendations for design, dimensioning and operation of combined heat pump and solar thermal systems for single-family houses of passive house or ZEB standard. The recommendations are largely based on observations and findings related to the installation at the Living Lab.

12.1 System Design and Dimensioning

- It is important to acknowledge that the solar energy potential is lowest between November and February, when the space heating demand is highest. Meanwhile, there are residual space heating demands in October and March, when the solar energy potential is intermediate. With a combined solar thermal system design, these demands are partially covered. The gain in space heat coverage may nevertheless be offset by the deficit in DHW heat coverage during the summertime, between March and October. **A DHW system design is recommended**.

- In order to provide optimum DHW coverage between March and October, **facade-mounted solar panels should be avoided**. This is because the angle of the sun is higher during this part of the year. As an example for Trondheim, a panel tilt angle around 60° results in the highest SF during the summertime. For façade-mounting, the panel area needs to be 2-3 times as high, in order to obtain an equvalent SF during the summertime.

- In order to maintain effective heat transfer between the solar thermal circuit and accumulation tank, large heat transfer surfaces are recommended. Preferably, **the accumulation tank should facilitate both high-temperature DHW heating, and low-temperature space heating**. Hence, thermal stratification in the tank, as well as cooling of the solar fluid, are maximized. This also increases the solar panel thermal efficiency.

- The heat pump system should be designed to cover the bulk of the thermal energy demands for space and DHW heating between November and February, when the solar energy potential is negligible. In order to achieve the highest possible heating capacity and energy coverage during this period, it is essential to minimize the average temperature of condensation. Selecting **a HP unit which integrates a DSH, and preferably also a SGHX, is recommended**. With respect to DHW heating, **it is recommended that both the DHWT and IEH are integrated in the HP unit**. With this design, an energy coverage factor for DHW heating of 100 %, can be obtained.

- The heat pump system should be designed to cover the thermal energy demands for space and DHW heating during the spring and fall, when the thermal power demand is low. Consequently, achieving a high part-load COP is essential. Selecting **a HP unit which integrates VSD capacity control is recommended**.

- Horizontal ground collector systems offer high and stable temperatures between November and February. Simultaneously, the initial investment costs are moderate. It is recommended to design the system for a specific heat extraction of no more than 30 W/m. It is important to recognize that the effective length of the collector tube is only 50 % of the total length. **Turbulence collector tubes are highly recommended**. A, 25 % ethyl alcohol aqueous solution is recommended for optimum heat transfer and minimum pump work.

- The space heat distribution temperature determines the HP condensation temperature and temperature lift. In order to achieve the highest possible heating capacity and COP, **the heat distribution temperature should be minimized**. In this regard, **underfloor heat distribution is recommended**. Optional hydronic **radiator circuits should have temperature control according to an outdoor temperature compensation curve**. Design temperatures should not exceed 45/40 °C. Large heat transfer surfaces are thus reccomended.

- In order to minimize parasitic losses to pump operation, **it is essential to select high-efficiency pumps, and minimize their operation time**. According to the EcoDesign Directive [87] an energy efficiency index (EEI) < 0.23 is required. It is advised to select pumps that superceed this requirement. Permanent magnet motor-driven (IE4) pumps are preferred.

- Due to high heat recovery rates, the annual demand for ventilation air heating is low, compared to space and DHW heating demands. **Unless the ventilation system is designed as the main heat distribution system, it might be preferable to utilize direct-acting electricity for ventilation heating purposes.** This simplifies the design and operation of the hydronic heat distribution system, and contributes to lower investment costs.

12.2 System Operation

- The solar thermal energy potential is largest between March and October, when the space heating demand is lowest. The DHW heating demand is nevertheless constant throughout the year. Hence, during this period, the solar thermal system should be operated to cover the majority of the DHW heating demand. The remainder should be covered by the heat pump. Surplus solar heat production should be directed to the ground.

- The space heating demand is highest between November and February, when the solar thermal energy potential is low. During this period, the heat pump should be operated to cover the majority of the demands for both space and DHW heating. Top-up heat from electrical heaters, should always be controlled by the heat pump.

- Optional use of solar heat should be possible during the spring and fall, when the temperature level is too low for direct heat exchange with the accumulator tank. During this period, solar heat may be used for thermal recharging of the ground, or to increase the evaporator brine inlet temperature.

12.3 Comments

In order to achieve the highest possible SPF and energy saving, it is essential to prioritize an integrated system design. All components, including the heat pump, solar panels, electrical heaters, accumulation tank, pumps and heat distribution system must be dimensioned and operated according to a mutual optimum.

Although separate design of subsystems may culminate in an auspicious overall system, the prospect of unreliability and poor efficiency is more likely. This approach also complicates the definition and implementation of control strategies, and presupposes in-depth knowledge of the system.

In this regard, plug-and-play systems, such as the HYSS [14] may be preferable. With this design, utilization of solar heat is optimized to obtain the highest possible annual SPF. For 4-6 months of the year, high temperature solar heat is used directly to cover the majority of DHW and space heating demands. Low-temperature solar heat is otherwise used to improve the operating conditions for the heat pump.

Chapter 13

Conclusions

The systems for thermal energy supply at the ZEB Living Laboratory have been investigated both experimentally and theoretically. Badly configured or inactive measuring equipment, and coherent missing DAQ data, have complicated the analysis of the energy performance and design of the system. The most important discoveries from the analysis are nevertheless summarized as following:

- Significant deviations and errors in DAQ measuring data were observed. In particular, this applied to TEM1 and TEM2, including the connected temperature probes and flow sensors. In order to acculately determine the energy performance of the combined GSHP and solar thermal system, these instruments have to be reconfigured or recalibrated.

- SPF calculations were carried out with DAQ measuring data for two ten day periods in March and April, respectively. Depending on the system boundary and measuring period, SPF-values ranged between 1.39 and 5.50. Average values for the two periods ranged between 1.77 and 3.86. The deviation in these results is so extreme that any conclusions regarding the actual system performance are inexpedient.

- During normal operation, the brine circuit pump, CP1, was operated continuously. Consequently, this pump contibuted to a significant electric energy use. This was, on average, equivalent to ~58 % of the electricity input to the GSHP compressor, and slightly higher than the combined input to the three hydronic pumps. It thus concluded that operation of CP1 must be aborted whenever the GSHP is inactive.

- Field measurements of the system COP confirmed significant parasitic losses due to pump operation. At 4.4/43.9 °C an average COP of 3.19 was measured for the GSHP unit alone. By including the electric power input to CP1, the average COP dropped by 13.5 % to 2.76. By further including the electric power input to CP2 and CP3, the COP dropped by 11.2 % to 2.45. While CP1 account for the largest individual loss, the hydronic pumps also greatly influence the system performance. An improvement may be achieved by operating CP2 and CP3 in *Eco Mode*, rather than *Proportional Pressure Mode*.

- The electric power input to CP1 and U·A-value of the collector tube, are closely related to the thermophysical properties of the 44 % PG solution, and the smooth collector tube. By repacing the PG solution with a 25 % EA solution, the ratio UA/W_{CP1}, can achieve a theoretical improvement of 270 %, from 39.4 to 106.9. A further increase can be achieved by replacing the the smooth collector tube with a turbulence collector.

- Automated switching between the GSHP space and DHW heating modes is non-functional. Consequently, most of the DHW demand is covered by direct-acting electric heating, by means of the IEHs. To impove the energy saving for DHW heating, it is essential that the DHW mode is made operational. This is essential in order to fulfill the Norwegian passive house requirement of 50 % renewable energy coverage for DHW heating.

- The GSHP is designed for alternate operation between space and DHW heating. Consequently, only condenser heat is utilized in DHW heating mode, which will results in a higher average condensation temperature. As a result, the heating capacity, COP and relative energy saving are reduced. In conclusion, this design is non-optimal for DHW heating, and energy coverage factors well below 100 % are expected.

- The STC is operated according to a two-point control setting, with a ± 1 K bandwidth. Hence, there is appreciable intermittency in operation of the pump, CP4, which in turn reduces the STC operating time and heat input to the IWT. DAQ data furthermore indicate that, as a result of the current operation strategy, the solar thermal input to the system is marginal.

- Polysun® simulations suggest that the STC is under-dimensioned. Specifically, the active panel area of 3.63 m^2 is too low to provide any significant space heating during the spring and fall. Moreover, the panel tilt angle is too steep to provide sufficient DHW heating during the summer. Hence, it is concluded that the current system design is non-optimal, both as a combined system and as a DHW heating system only.

- The radiator and ventilation heating battery circuits have a nominal temperature level og 55/50 °C. This a poor design, considering that the primary heat sources, the GSHP and the STC, supply low-temperature heat. Temperature control, according to an outdoor compensation curve, is thus essential for this design to be relevant. Heat distribution via the underfloor heating system is regarded the best alternative, with respect to energy performance.

Bibliography

[1] I. Sartori, A. Napolitano, and K. Voss, “Net zero energy buildings: A consistent definition framework,” *Energy and Buildings*, vol. 48, pp. 220 – 232, 2012.

[2] L. Finocchiaro, F. Goia, S. Grynning, and A. Gustavsen, “The ZEB Living Lab: a multi-purpose experimental facility,” 2014. Available from `http://www.zeb.no/index.php/conference/item/537-the-zeb-living-lab-a-multi-purpose-experimental-facility` [Accessed (08.02.2016)].

[3] F. Goia, L. Finocchiario, and A. Gustavsen, “The ZEB living laboratory at the norwegian university of science and technology: a zero emission house for engineering an social science experiments,” *Passive House Nordic - Sustainable Cities and Buildings*, 2015.

[4] E-mail correspondence. Terje Larsen, Sales Engineer, OSO Hotwater [16.02.2016].

[5] Nibe, 2016. Attained from `http://www.nibe.no/Produkter/` [Downloaded (18.04.2016)].

[6] Nilan, “Compact solutions,” 2016. Available from `http://www.nilan.dk/en-gb/frontpage/solutions/domestic-solutions/compact-solutions` [Accessed (09.03.2016)].

[7] G. Nielsen, “Borehole Installations or Air to water Heat Pumps. What to Use and Where,” tech. rep., Multiconsult A/S, 2015.

[8] G. Eggen, “Heimdalsprosjektet - Varmepumpesystemer for småhus,” tech. rep., Sintef Kuldeteknikk, 1986.

[9] acr chiller rent, 2016. Attained from `http://www.ac-rent.de/english/images/faq/faq_funktionsprinzip.jpg` [Downloaded (18.04.2016)].

[10] Fornybar, “Solenergiressursen i Norge,” 2016. Available from `http://www.fornybar.no/solenergi/ressursgrunnlag/solenergiressursen-i-norge` [Accessed (26.04.2016)].

[11] F. Mauthner, W. Weiss, and M. Spörk-Dür, “Solar Heat Worldwide - Markets and Contribution to the Energy Supply 2013,” 2015. Available from `http://www.iea-shc.org/data/sites/1/publications/Solar-Heat-Worldwide-2015.pdf` [Accessed (05.02.2016)].

[12] C. Good, I. Andresen, and A. G. Hestnes, “Solar energy for net zero energy buildings – a comparison between solar thermal, {PV} and photovoltaic–thermal (pv/t) systems,” *Solar Energy*, vol. 122, pp. 986 – 996, 2015.

[13] V. Trillat-Berdal, B. Souyri, and G. Achard, “Coupling of geothermal heat pumps with thermal solar collectors,” *Applied Thermal Engineering*, vol. 27, no. 10, pp. 1750 – 1755, 2007. Heat transfer and sustainable energy technologies.

[14] Free Energy, “HYSS - Hybrid Solar System.” Available from `http://www.free-energy.com/no/produkter/hyss-hybrid-solar-system` [Last checked (14.05.2016)].

[15] N. Nord, L. H. Qvistgaard, and G. Cao, “Identifying key design parameters of the integrated energy system for a residential zero emission building in norway,” *Renewable Energy*, vol. 87, Part 3, pp. 1076 – 1087, 2016. Sustainable energy utilization in cold climate zone (Part II).

[16] E-mail correspondence. Harald Amundsen, Brødrene Dahl AS [09.03.2016].

[17] HEWALEX Solar Collectors, “Solar Collector KS2000 SLP.” Available from `http://www.hewalex.eu/en/offer/flat-plate-collectors/solar-collector-ks2000-slp.html` [Accessed (11.02.2016)].

[18] Smedegaard, “Smedegaard Magneta 32-120.” Available from `http://www.sirkulasjonspumper.no/products/smedegaard-magneta-32-120` [Accessed (07.05.2016)].

[19] The Research Centre on Zero Emission Buildings, “ZEB - Zero Emission Buildings,” 2016. Available from `hhttp://zeb.no/index.php/about-zeb/zeb-definitions` [Accessed (29.02.2016)].

[20] D. Zijdemans, *Vannbaserte oppvarmings- og kjølesystemer.* Skarland Press, 2014.

[21] *Veiledning om tekniske krav til byggverk - Kapittel 14. Energi*, 2014.

[22] *NS3700:2013 Criteria for passive houses and low energy buildings - Residential buildings*, 2013.

[23] *NS3031:2014 Calculation of energy performance of buildings - Method and data*, 2014.

[24] Statistics Norway, “This is Norway 2015,” 2015. Available from `http://ssb.no/en/befolkning/artikler-og-publikasjoner/_attachment/237252?_ts=1516c73e3a8` [Accessed (05.02.2016)].

[25] I. Sartori, B. J. Wachenfeldt, and A. G. Hestnes, "Energy demand in the norwegian building stock: Scenarios on potential reduction," *Energy Policy*, vol. 37, no. 5, pp. 1614 – 1627, 2009.

[26] A. C. Bøeng, B. Halvorsen, and B. M. Larsen, "Space heating in dwellings," 2014. Available from `http://webby.nve.no/publikasjoner/rapport/2014/rapport2014_85.pdf` [Accessed (04.02.2016)].

[27] A. C. Bøeng, "Hvordan kan Norge nå sitt mål om fornybar energi i 2020?," tech. rep., Statistisk Sentralbyrå, 2011. Attained from `https://www.ssb.no/a/publikasjoner/pdf/oa_201106/boeng.pdf` [Last checked (07.06.2016)].

[28] Directive 2010/31/EU of the European Parliament and of the Council of 19 May 2010 on the energy performance of buildings (recast), "EPBD recast," 2010. Available from `https://ec.europa.eu/energy/en/topics/energy-efficiency/buildings/nearly-zero-energy-buildings` [Accessed (29.02.2016)].

[29] The Research Centre on Zero Emission Buildings, "Living Lab," 2016. Available from `http://zeb.no/index.php/living-lab-trondheim` [Accessed (01.02.2016)].

[30] A. Marszal, P. Heiselberg, J. Bourrelle, E. Musall, K. Voss, I. Sartori, and A. Napolitano, "Zero energy building – a review of definitions and calculation methodologies," *Energy and Buildings*, vol. 43, no. 4, pp. 971 – 979, 2011.

[31] M. R. Inman and A. H. Wiberg, "Life Cycle GHG Emissions of Material Use in the Living Laboratory," 2015. Available from `http://www.zeb.no/index.php/news-and-events/219-zeb-report-nr-24-life-cycle-ghg-emissions-of-material-use-in-the-living-` [Accessed (08.02.2016)].

[32] J. Stene, "Oppvarmingssystemer for boliger av lavenergi- og passivhusstandard," tech. rep., SINTEF Energiforskning AS, 2008.

[33] J. Stene, "Heat Pumps in Passive House Buildings - Residential Buildings." Lecture Slides in Spcialization Course TEP16, October 2015.

[34] UNEP, "2014 Report of the Refrigeration, Air Conditioning and Heat Pumps Technical Options Committee - Montreal Protocol on Substances that Deplete the Ozone Layer," 2015.

[35] D. Adamovsky, P. Neuberger, and R. Adamovsky, "Changes in energy and temperature in the ground mass with horizontal heat exchangersâthe energy source for heat pumps," *Energy and Buildings*, vol. 92, p. 92, 2015.

[36] ABK AS, "Varmeopptak. Energikollektorer og tilbehør." Available from `http://www.abkklima.no/globalassets/global/markedsmateriell-brosjyrer-priskataloger-annonser-etc/kataloger-uten-priser/katalog-varmeopptak---energikollektorer-og-tilbehor.pdf` [Accessed (09.05.2016)].

[37] P. Congedo, G. Colangelo, and G. Starace, "CFD simulations of horizontal ground heat exchangers: A comparison among different configurations," *Applied Thermal Engineering*, vol. 33 - 34, pp. 24 – 32, 2012.

[38] International Institute of Refrigeration, "Thermophysical Properties of Liquid Secondary Refrigerants," Undated.

[39] J. Acuña, *Distributed thermal response tests - New insights on U-pipe and Coaxial heat exchangers in groundwater-filled boreholes*. PhD thesis, KTH Industrial Engineering and Management, 2013.

[40] J. Stene, *Varmepumper - Grunnleggende varmepumpeteknikk*. SINTEF Energiforskning AS, 4 ed., 1997.

[41] J. Stene, "Dimensioning of Heat Pumps for Heating and Cooling." Lecture Slides in Course TEP4260, 2016.

[42] GK Konsern AS, "Inneklima 2015," 2015. Available from `http://www.gk.no/filestore/Filer_Norge_-_2010/Om_GK/Media/Inneklima/GK_Inneklima_2_2015_NO.pdf` [Accessed (05.04.2016)].

[43] P. Nekså, H. Rekstad, G. R. Zakeri, and P. A. Schiefloe, "CO2-heat pump water heater: characteristics, system design and experimental results," *International Journal of Refrigeration*, vol. 21, pp. 172–179, May 1998.

[44] G. Lorentzen, "Revival of carbon dioxide as a refrigerant," *International Journal of Refrigeration*, vol. 17, no. 5, pp. 292 – 301, 1994.

[45] J. Stene, "Carbon Dioxide (R744) as a Working Fluid in Heat Pumps." Lecture Slides in Spcialization Course TEP16, September 2015.

[46] T. M. Eikevik and I. Tolstorebrov, "Review of Standards for Hydrocarbons and co2," tech. rep., Norwegian University of Science and Technology, 2014.

[47] P. Nekså, "CO2 heat pump systems," *International Journal of Refrigeration*, vol. 25, pp. 421–427, June 2002.

[48] J. Stene, "Residential CO2 heat pump system for combined space heating and hot water heating," *International Journal of Refrigeration*, vol. 28, no. 8, pp. 1259 – 1265, 2005.

[49] J. Stene, “IEA Annex 22 - Compression Systems with Natural Working Fluids - Guideline for Design and Operation of Compression Heat Pump, Air Conditioning and Refrigeration Systems with Natural Working Fluids,” tech. rep., SINTEF Energy Research, 1998.

[50] A. Cavallini, E. D. Riva, and D. D. Col, “Performance of a large capacity propane heat pump with low charge heat exchangers,” *International Journal of Refrigeration*, vol. 33, no. 2, pp. 242 – 250, 2010.

[51] E. Granryd, “Hydrocarbons as refrigerants — an overview,” *International Journal of Refrigeration*, vol. 24, no. 1, pp. 15 – 24, 2001.

[52] D. D. Col, M. Azzolin, G. Benassi, and M. Mantovan, “Energy efficiency in a ground source heat pump with variable speed drives,” *Energy and Buildings*, vol. 91, pp. 105 – 114, 2015.

[53] F. Karlsson and P. Fahlen, “Capacity-controlled ground source heat pumps in hydronic heating systems,” *International Journal of Refrigeration*, vol. 30, no. 2, pp. 221 – 229, 2007.

[54] HEWALEX, “Solar technology. Product catalogue 2015. Edition I.” Available from `http://www.hewalex.pl/pliki/pobierz/Hewalex_KATALOG_TS_EN_2015_www.pdf` [Accessed (11.02.2016)].

[55] Vela Solaris AG, “Polysun.” Available from `http://www.velasolaris.com/english/downloads.html` [Accessed (29.02.2016)].

[56] V. Trillat-Berdal, B. Souyri, and G. Fraisse, “Experimental study of a ground-coupled heat pump combined with thermal solar collectors,” *Energy and Buildings*, vol. 38, no. 12, pp. 1477 – 1484, 2006.

[57] E. Kjellsson, *Solar Collectors Combined with Ground-Source Heat Pumps in Dwellings*. PhD thesis, Lund University, 2009.

[58] VVS aktuelt, “HYSS-gjennombrudd,” 2015. Available from `http://www.vvsaktuelt.no/hyss-gjennombrudd-84901/nyhet.html` [Last checked (14.05.2016)].

[59] E. Kjellsson, G. Hellström, and B. Perers, “Optimization of systems with the combination of ground-source heat pump and solar collectors in dwellings,” *Energy*, vol. 35, no. 6, pp. 2667 – 2673, 2010. 7th International Conference on Sustainable Energy Technologies7th International Conference on Sustainable Energy Technologies.

[60] Solar Energy Laboratory, University of Wisconsin-Madison, “Trnsys.” Available from `http://sel.me.wisc.edu/trnsys/index.html` [Accessed (04.04.2016)].

[61] The Research Centre on Zero Emission Buildings, “Multikomfort Larvik,” Undated. Available from `http://zeb.no/index.php/pilot-projects/157-multikomfort-larvik` [Accessed (09.03.2016)].

[62] Harald Amundsen, “Energiregnestykke Multikomforthus Larvik.” E-mail correspondence. Harald Amundsen, Brødrene Dahl AS [09.03.2016].

[63] Calorex, “Ground source heat pumps.” Available from `http://www.calorex.com/heat-pumps-domestic/ground-source-domestic-gshp` [Accessed (11.02.2016)].

[64] Univar AS, “Sikkerhetsdatablad Dowcal 200,” 2013. Available from `http://www2.renkulde.no/MKDokume.nsf/e16209c1d01a68f6c125732a00375b1c/2411c320f6769768c1257c1900477429?OpenDocument` [Accessed (20.03.2016)].

[65] National Instruments, “NI LabVIEW,” 2016. Available from `nationalinstrumentslabviewcommunications` [Accessed (21.04.2016)].

[66] Department of Mechanical Engineering, Technical University of Denmark, “CoolPack.” Available from `http://www.en.ipu.dk/Indhold/refrigeration-and-energy-technology/coolpack.aspx` [Last checked (13.06.2016)].

[67] M. J. Moran, H. N. Shapiro, D. D. Boettner, and M. B. Bailey, *Principles of Engineering Thermodynamics.* John Wiley and Sons, Inc., 7th ed., 2012.

[68] “Product Specifications for H71J223ABK,” 2016. Available from `http://search.bristolcompressors.com/BCWC02.aspx?ModelNo=H71J223ABK&CylRunning=2&Frequency=50&System=E` [Accessed (16.03.2016)].

[69] V. Novakovic, S. O. Hanssen, J. V. Thue, I. Wangensteen, and F. O. Gjerstad, *ENØK i bygninger - Effektiv energibruk.* Gyldendal Norsk Forlag AS, 3. utgave ed., 2007.

[70] Programbyggerene, “Simien v.5.504.” Available from `http://www.programbyggerne.no/` [Accessed (29.02.2016)].

[71] Åmund Utne, “Bruk av fjernvarme i passivhus - Erfaringer fra Trondheim,” 2014. Available from `http://docplayer.no/5212545-Bruk-av-fjernvarme-i-passivhus.html` [Accessed (20.05.2016)].

[72] E-mail correspondence. Kristian Stensrud, Project manager, Heimdal Bolig [20.04.2016].

[73] P. Tiljander, C. H. Stignor, P. Lidbom, M. Viktorsson, M. Lindahl, and M. Axell, “Fältmätningar för att demonstrera ny teknik för värmepumpesystem,” tech. rep., SP Sveriges Tekniska Forskningsinstitut, 2010.

[74] M. Miara, “Heat Pump Efficiency - Analysis and Evaluation of Heat Pump Efficiency in Real-life Conditions,” tech. rep., Fraunhofer ISE, 2011.

[75] A. Zottl, R. Nordman, M. Miara, and H. Huber, “System Boundaries for SPF Calculation,” *10th IEA Heat Pump Conference*, 2011.

[76] L. P. Haugerud and I. Lien, “Analyse av feltmålinger av varmepumper i boliger,” tech. rep., Enova SF, 2015.

[77] E-mail correspondence. Fransesco Goia, Post doctoral Research Fellow, The Reserch Centre on Zero Emission Buildings [08.04.2016].

[78] Y. A. Çengel and J. M. Cimbala, *Fluid Mechanics, Fundamentals and Applications*. Mc Graw Hill, 2nd ed., 2010.

[79] F. P. Incropera, D. P. Dewitt, T. L. Bergman, and A. S. Lavine, *Principles of Heat and Mass Transfer*. John Wiley and Sons, Inc., 7th ed., 2013.

[80] MuoviTech AB, “Turbo kollektor.” Produktdatablad.

[81] ABK Klimaprodukter, “Turbokollektor.” Produktdatablad.

[82] Fredrik Hansson, “Experimentell jämförelse av Turbokollektor och slät energikollektor.” Produktdatablad.

[83] E. Union, “COMMISSION REGULATION (EC) No 641/2009,” 2015. Available from `http://eur-lex.europa.eu/legal-content/EN/TXT/PDF/?uri=CELEX:32009R0641&from=EN` [Last accessed (28.04.2016)].

[84] Smedegaard, “Magneta. High-efficiency Circulator Pump. Installation/Operating Manual.” Available from `http://smedegaard.co.uk/wp-content/uploads/Magneta-O-and-M----English.pdf` [Accessed (07.05.2016)].

[85] Siemens, “2-port and 3-port valves PN16,” 2011. Available from `https://www.downloads.siemens.com/download-center/Download.aspx?pos=download&fct=getasset&id1=10488` [Accessed (07.05.2016)].

[86] M. Lorentsen, “Optimization of technical solutions for heating system in low emission residential buildings,” Master’s thesis, Norwegian University of Science and Technology, 2015.

[87] E. Union, “COMMISSION REGULATION (EU) No 622/2012,” 2015. Available from `http://eur-lex.europa.eu/legal-content/EN/TXT/PDF/?uri=CELEX:32012R0622&from=EN` [Last accessed (28.04.2016)].

Appendices

A Thermal System Monitoring and Control

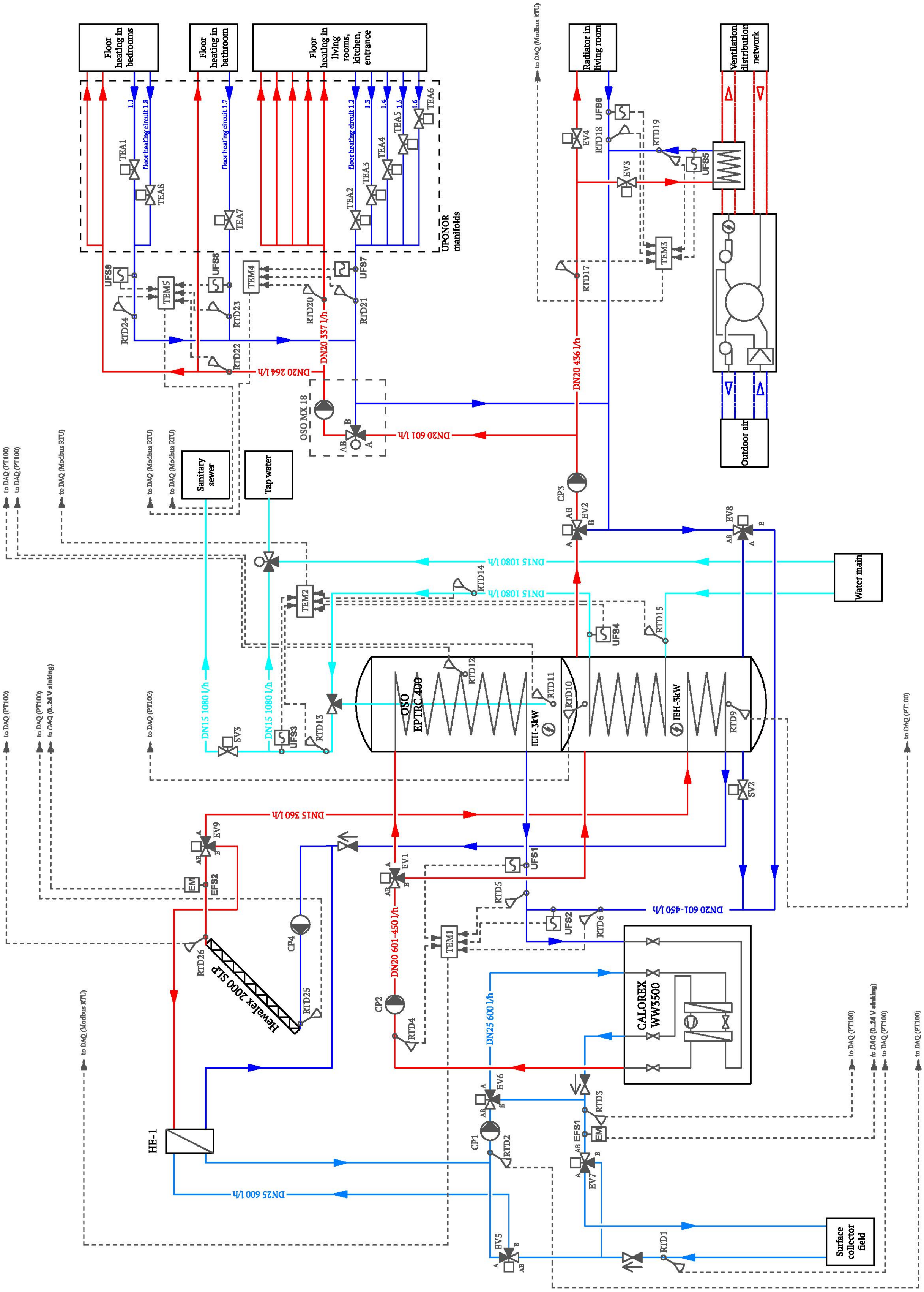
Floor heating in bedrooms
Floor heating in bathroom
Floor heating in living rooms, kitchen, entrance
Radiator in living room
Ventilation distribution network
UPONOR manifolds
floor heating circuit 1.1
floor heating circuit 1.8
floor heating circuit 1.7
floor heating circuit 1.2
1.3
1.4
1.5
1.6
TEA1
TEA2
TEA3
TEA4
TEA5
TEA6
TEA7
TEA8
UFS1
UFS2
UFS3
UFS4
UFS5
UFS6
UFS7
UFS8
UFS9
TEM1
TEM2
TEM3
TEM4
TEM5
RTD1
RTD2
RTD3
RTD4
RTD5
RTD6
RTD9
RTD10
RTD11
RTD12
RTD13
RTD14
RTD15
RTD17
RTD18
RTD19
RTD20
RTD21
RTD22
RTD23
RTD24
RTD25
RTD26
DN20 264 l/h
DN20 337 l/h
DN20 601 l/h
DN20 436 l/h
OSO MX 18
AB
A
B
Sanitary sewer
Tap water
Water main
Outdoor air
DN15 1080 l/h
OSO EPTRC 400
IEH-3kW
CP1
CP2
CP3
CP4
EV1
EV2
EV3
EV4
EV5
EV6
EV7
EV8
EV9
SV2
SV3
DN15 360 l/h
EFS1
EFS2
EM
Hewalex 2000 SLP
HE-1
CALOREX WW3500
DN25 600 l/h
DN20 601-450 l/h
DN20 601-450 l/h
Surface collector field
to DAQ (Modbus RTU)
to DAQ (PT100)
to DAQ (0..24 V sinking)

B Calorex WW3500 Ground Source Heat Pump

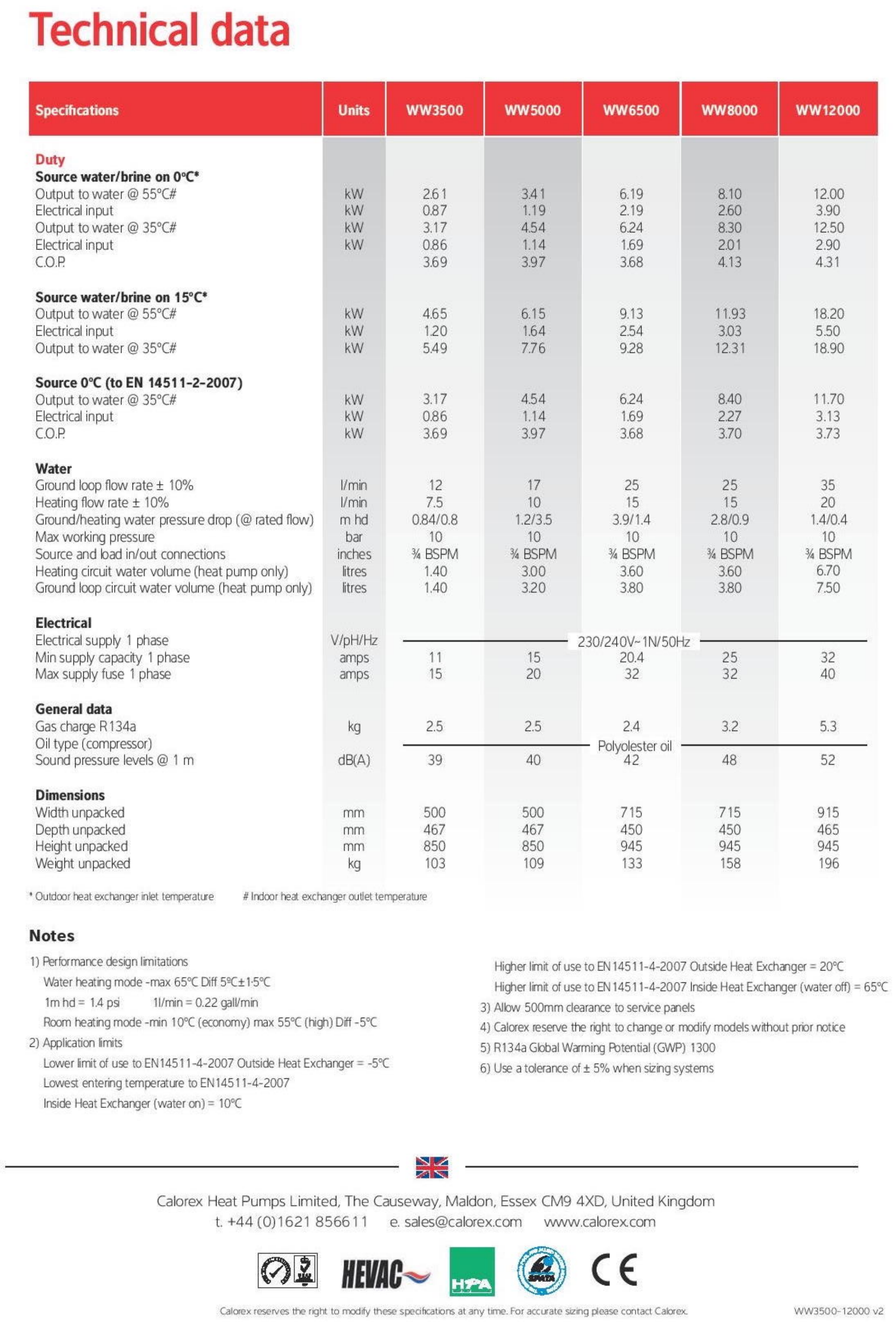

Technical data

Specifications	Units	WW3500	WW5000	WW6500	WW8000	WW12000
Duty						
Source water/brine on 0°C*						
Output to water @ 55°C#	kW	2.61	3.41	6.19	8.10	12.00
Electrical input	kW	0.87	1.19	2.19	2.60	3.90
Output to water @ 35°C#	kW	3.17	4.54	6.24	8.30	12.50
Electrical input	kW	0.86	1.14	1.69	2.01	2.90
C.O.P.		3.69	3.97	3.68	4.13	4.31
Source water/brine on 15°C*						
Output to water @ 55°C#	kW	4.65	6.15	9.13	11.93	18.20
Electrical input	kW	1.20	1.64	2.54	3.03	5.50
Output to water @ 35°C#	kW	5.49	7.76	9.28	12.31	18.90
Source 0°C (to EN 14511-2-2007)						
Output to water @ 35°C#	kW	3.17	4.54	6.24	8.40	11.70
Electrical input	kW	0.86	1.14	1.69	2.27	3.13
C.O.P.	kW	3.69	3.97	3.68	3.70	3.73
Water						
Ground loop flow rate ± 10%	l/min	12	17	25	25	35
Heating flow rate ± 10%	l/min	7.5	10	15	15	20
Ground/heating water pressure drop (@ rated flow)	m hd	0.84/0.8	1.2/3.5	3.9/1.4	2.8/0.9	1.4/0.4
Max working pressure	bar	10	10	10	10	10
Source and load in/out connections	inches	¾ BSPM	¾ BSPM	¾ BSPM	¾ BSPM	¾ BSPM
Heating circuit water volume (heat pump only)	litres	1.40	3.00	3.60	3.60	6.70
Ground loop circuit water volume (heat pump only)	litres	1.40	3.20	3.80	3.80	7.50
Electrical						
Electrical supply 1 phase	V/pH/Hz	230/240V~1N/50Hz				
Min supply capacity 1 phase	amps	11	15	20.4	25	32
Max supply fuse 1 phase	amps	15	20	32	32	40
General data						
Gas charge R134a	kg	2.5	2.5	2.4	3.2	5.3
Oil type (compressor)		Polyolester oil				
Sound pressure levels @ 1 m	dB(A)	39	40	42	48	52
Dimensions						
Width unpacked	mm	500	500	715	715	915
Depth unpacked	mm	467	467	450	450	465
Height unpacked	mm	850	850	945	945	945
Weight unpacked	kg	103	109	133	158	196

* Outdoor heat exchanger inlet temperature # Indoor heat exchanger outlet temperature

Notes

1) Performance design limitations
   Water heating mode -max 65°C Diff 5°C±1·5°C
   1m hd = 1.4 psi 1l/min = 0.22 gall/min
   Room heating mode -min 10°C (economy) max 55°C (high) Diff -5°C
2) Application limits
   Lower limit of use to EN14511-4-2007 Outside Heat Exchanger = -5°C
   Lowest entering temperature to EN14511-4-2007
   Inside Heat Exchanger (water on) = 10°C
   Higher limit of use to EN 14511-4-2007 Outside Heat Exchanger = 20°C
   Higher limit of use to EN 14511-4-2007 Inside Heat Exchanger (water off) = 65°C
3) Allow 500mm clearance to service panels
4) Calorex reserve the right to change or modify models without prior notice
5) R134a Global Warming Potential (GWP) 1300
6) Use a tolerance of ± 5% when sizing systems

Calorex Heat Pumps Limited, The Causeway, Maldon, Essex CM9 4XD, United Kingdom
t. +44 (0)1621 856611 e. sales@calorex.com www.calorex.com

Calorex reserves the right to modify these specifications at any time. For accurate sizing please contact Calorex.

WW3500-12000 v2

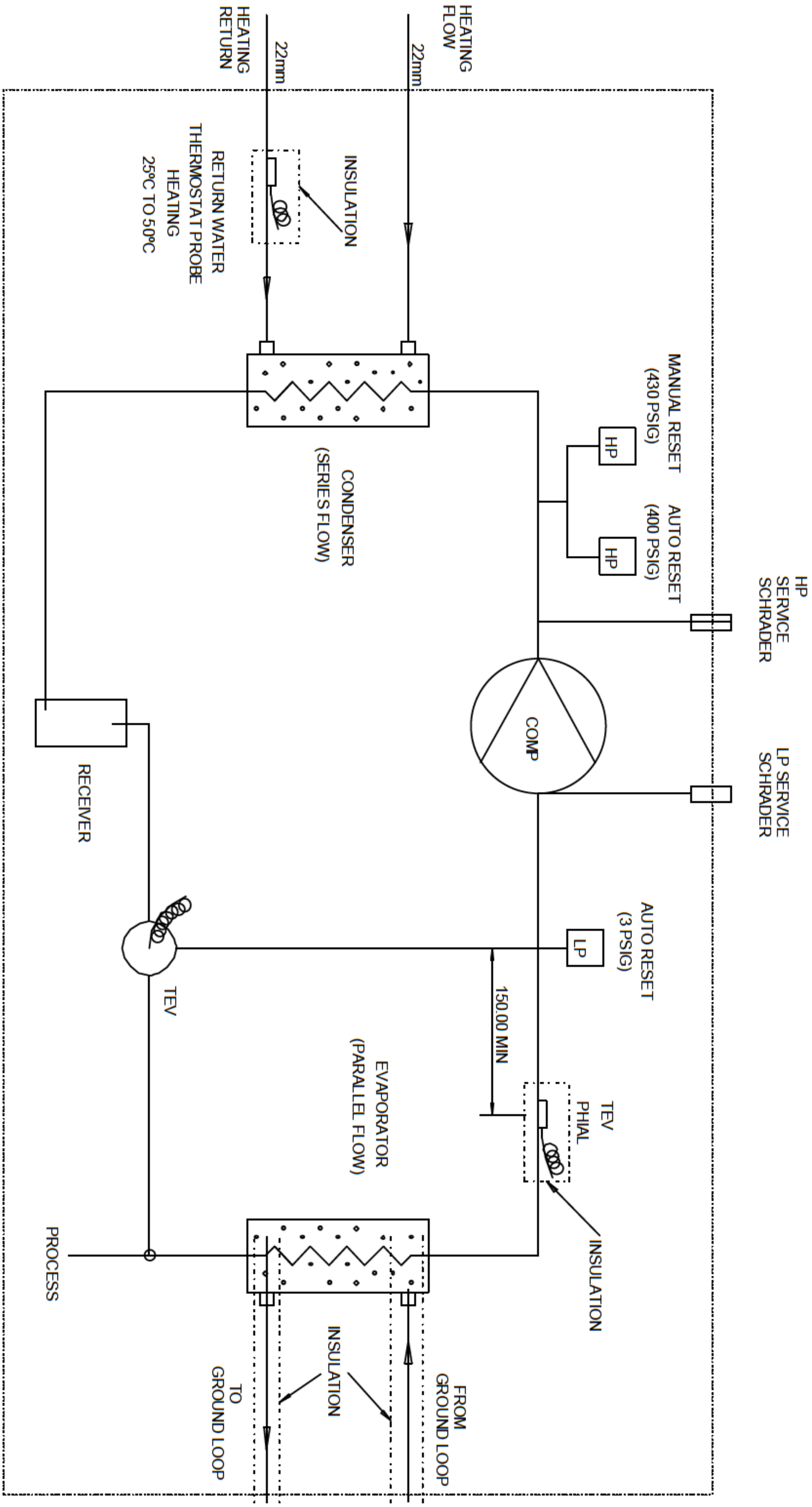
HEATING FLOW
22mm
HEATING RETURN
22mm
INSULATION
RETURN WATER THERMOSTAT PROBE HEATING 25°C TO 50°C
MANUAL RESET (430 PSIG)
HP
AUTO RESET (400 PSIG)
HP
HP SERVICE SCHRADER
CONDENSER (SERIES FLOW)
COMP
LP SERVICE SCHRADER
RECEIVER
AUTO RESET (3 PSIG)
LP
TEV
150.00 MIN
TEV PHIAL
EVAPORATOR (PARALLEL FLOW)
INSULATION
PROCESS
INSULATION
FROM GROUND LOOP
TO GROUND LOOP

3500 MAIN ASSEMBLY

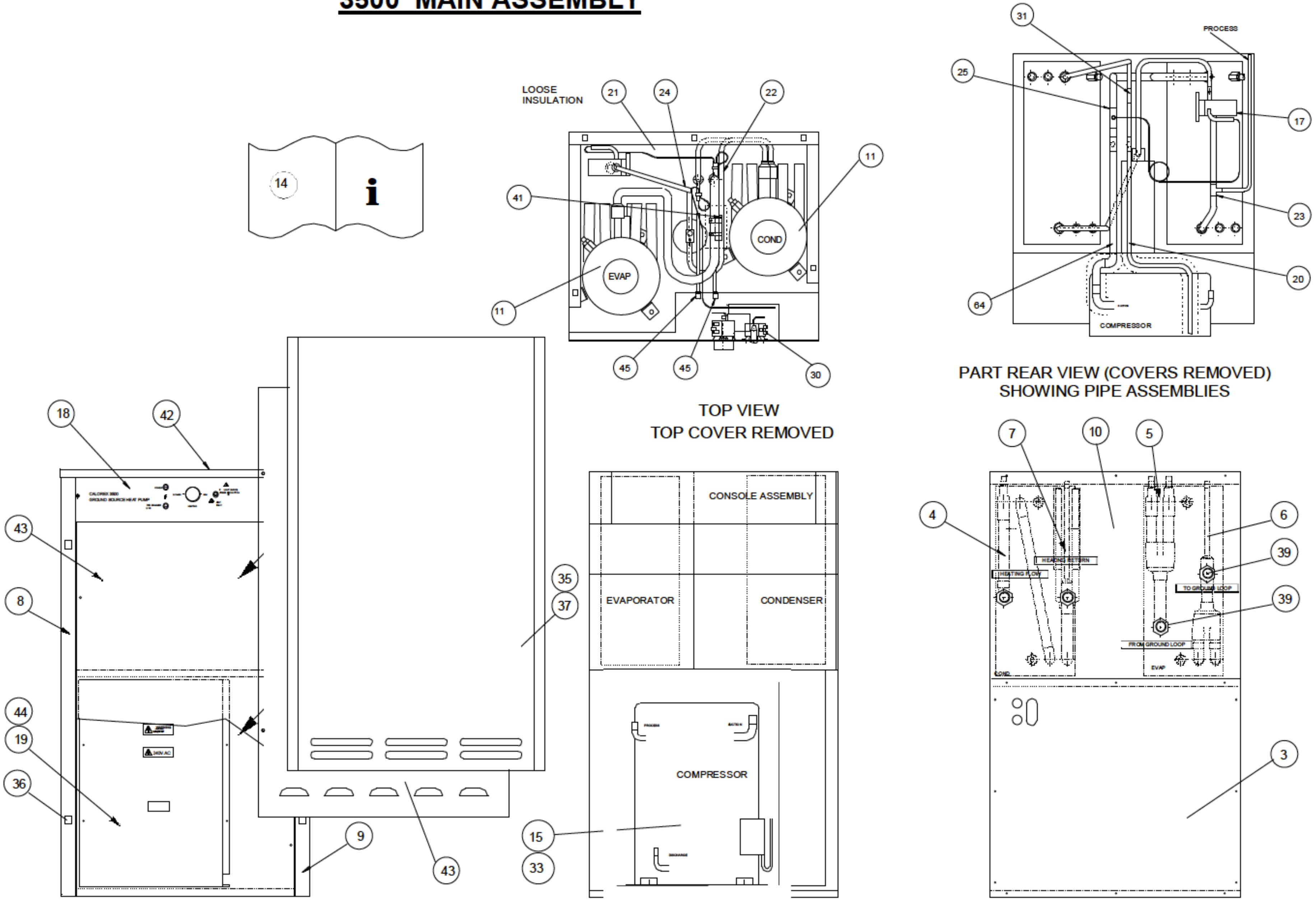
14
i
LOOSE INSULATION
21
24
22
11
41
COND
EVAP
11
45
45
30
PROCESS
31
25
17
23
20
64
COMPRESSOR
18
42
CALOREX 3500 GROUND SOURCE HEAT PUMP
43
8
44
19
36
240V AC
35
37
9
43
CONSOLE ASSEMBLY
EVAPORATOR
CONDENSER
COMPRESSOR
15
33
7
10
5
4
6
39
39
HEATING RETURN
HEATING FLOW
TO GROUND LOOP
FROM GROUND LOOP
EVAP
COND.
3

TOP VIEW
TOP COVER REMOVED

PART REAR VIEW (COVERS REMOVED)
SHOWING PIPE ASSEMBLIES

PART FRONT VIEW

REAR VIEW

A449403 ISSUE 12 MAIN ASSEMBLY 3500

ITEM NO.	PART No.	DESCRIPTION	QUAN	UNITS
3	SD442750	BACK PANEL BOTTOM	1	off
4	SD519912	PIPE ASSEMBLY WITH BLEED VALVE	1	off
5	SD519911	PIPE ASSEMBLY WITH BLEED VALVE	1	off
6	SD519903	PIPE ASSEMBLY WITH BLEED VALVE	1	off
7	SD519907	PIPE ASSEMBLY WITH BLEED VALVE	1	off
8	SA442401	SIDE PANEL ASSEMBLY	1	off
9	SA442402	SIDE PANEL ASSEMBLY	1	off
10	SD442501	CONNECTION PLATE ASSEMBLY	1	off
11	SD353457	CONDENSER S6	2	off
14	SD449551	MANUAL	1	off
15	SD624451	COMPRESSOR, H71J223ABKA	1	off
16	SD149650	RECEIVER/DRIER	1	off
17	SD447350	TEV EBF JE A CP60	1	off
18	SA448601	CONSOLE ASSY	1	off
19	SA448303	ELECTRIC BOX ASSY	1	off
20	SD565850	COMPRESSOR PIPE	1	off
21	SD459550	VERMICULITE LOOSE INSULATION	4	kg
22	SP536401	CONDENSER PIPE	1	off
23	SP537101	EVAPORATOR PIPE	1	off
24	SP536550	RECEIVER PIPE	1	off
25	SD610001	COMPRESSOR PIPE	1	off
30	SD101352	HIGH PRESSURE SWITCH 430 PSI	1	off
31	SD610101	COMPRESSOR PIPE	1	off
33	SP182555	REFRIGERANT R134a	2.5	kg
35	SD462601	OUTER COVER	1	off
36	SD462750	LATCH	1	off
37	SD462751	LATCH, STRIKER	1	off
39	SD519913	TANK CONNECTOR ASSEMBLY	1	off
41	SP090150	COPPER EARTH STRAP	0.6	m
42	SD442650	TOP PANEL	1	off
43	SD443101	SERVICE PANEL	1	off
44	SD443950	ELECTRIC BOX TOP COVER	1	off
45	SP066350	SCHRADER VALVE	2	off
64	SD565750	COMPRESSOR PIPE	1	off

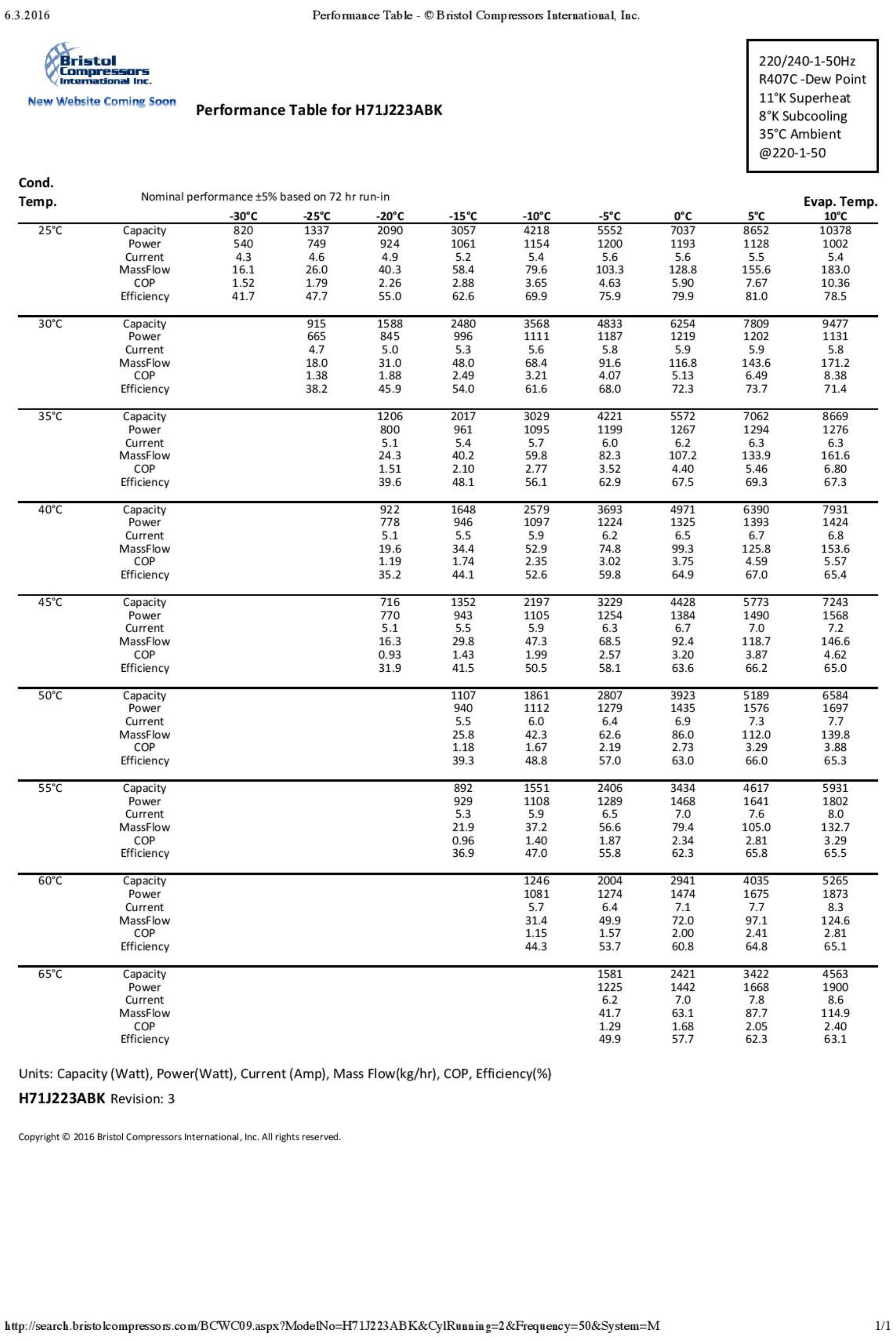

6.3.2016 Performance Table - © Bristol Compressors International, Inc.

New Website Coming Soon

Performance Table for H71J223ABK

220/240-1-50Hz
R407C -Dew Point
11°K Superheat
8°K Subcooling
35°C Ambient
@220-1-50

Nominal performance ±5% based on 72 hr run-in

Evap. Temp.

Cond. Temp.		-30°C	-25°C	-20°C	-15°C	-10°C	-5°C	0°C	5°C	10°C
25°C	Capacity	820	1337	2090	3057	4218	5552	7037	8652	10378
	Power	540	749	924	1061	1154	1200	1193	1128	1002
	Current	4.3	4.6	4.9	5.2	5.4	5.6	5.6	5.5	5.4
	MassFlow	16.1	26.0	40.3	58.4	79.6	103.3	128.8	155.6	183.0
	COP	1.52	1.79	2.26	2.88	3.65	4.63	5.90	7.67	10.36
	Efficiency	41.7	47.7	55.0	62.6	69.9	75.9	79.9	81.0	78.5
30°C	Capacity		915	1588	2480	3568	4833	6254	7809	9477
	Power		665	845	996	1111	1187	1219	1202	1131
	Current		4.7	5.0	5.3	5.6	5.8	5.9	5.9	5.8
	MassFlow		18.0	31.0	48.0	68.4	91.6	116.8	143.6	171.2
	COP		1.38	1.88	2.49	3.21	4.07	5.13	6.49	8.38
	Efficiency		38.2	45.9	54.0	61.6	68.0	72.3	73.7	71.4
35°C	Capacity			1206	2017	3029	4221	5572	7062	8669
	Power			800	961	1095	1199	1267	1294	1276
	Current			5.1	5.4	5.7	6.0	6.2	6.3	6.3
	MassFlow			24.3	40.2	59.8	82.3	107.2	133.9	161.6
	COP			1.51	2.10	2.77	3.52	4.40	5.46	6.80
	Efficiency			39.6	48.1	56.1	62.9	67.5	69.3	67.3
40°C	Capacity			922	1648	2579	3693	4971	6390	7931
	Power			778	946	1097	1224	1325	1393	1424
	Current			5.1	5.5	5.9	6.2	6.5	6.7	6.8
	MassFlow			19.6	34.4	52.9	74.8	99.3	125.8	153.6
	COP			1.19	1.74	2.35	3.02	3.75	4.59	5.57
	Efficiency			35.2	44.1	52.6	59.8	64.9	67.0	65.4
45°C	Capacity			716	1352	2197	3229	4428	5773	7243
	Power			770	943	1105	1254	1384	1490	1568
	Current			5.1	5.5	5.9	6.3	6.7	7.0	7.2
	MassFlow			16.3	29.8	47.3	68.5	92.4	118.7	146.6
	COP			0.93	1.43	1.99	2.57	3.20	3.87	4.62
	Efficiency			31.9	41.5	50.5	58.1	63.6	66.2	65.0
50°C	Capacity				1107	1861	2807	3923	5189	6584
	Power				940	1112	1279	1435	1576	1697
	Current				5.5	6.0	6.4	6.9	7.3	7.7
	MassFlow				25.8	42.3	62.6	86.0	112.0	139.8
	COP				1.18	1.67	2.19	2.73	3.29	3.88
	Efficiency				39.3	48.8	57.0	63.0	66.0	65.3
55°C	Capacity				892	1551	2406	3434	4617	5931
	Power				929	1108	1289	1468	1641	1802
	Current				5.3	5.9	6.5	7.0	7.6	8.0
	MassFlow				21.9	37.2	56.6	79.4	105.0	132.7
	COP				0.96	1.40	1.87	2.34	2.81	3.29
	Efficiency				36.9	47.0	55.8	62.3	65.8	65.5
60°C	Capacity					1246	2004	2941	4035	5265
	Power					1081	1274	1474	1675	1873
	Current					5.7	6.4	7.1	7.7	8.3
	MassFlow					31.4	49.9	72.0	97.1	124.6
	COP					1.15	1.57	2.00	2.41	2.81
	Efficiency					44.3	53.7	60.8	64.8	65.1
65°C	Capacity						1581	2421	3422	4563
	Power						1225	1442	1668	1900
	Current						6.2	7.0	7.8	8.6
	MassFlow						41.7	63.1	87.7	114.9
	COP						1.29	1.68	2.05	2.40
	Efficiency						49.9	57.7	62.3	63.1

Units: Capacity (Watt), Power(Watt), Current (Amp), Mass Flow(kg/hr), COP, Efficiency(%)

H71J223ABK Revision: 3

Copyright © 2016 Bristol Compressors International, Inc. All rights reserved.

http://search.bristolcompressors.com/BCWC09.aspx?ModelNo=H71J223ABK&CylRunning=2&Frequency=50&System=M 1/1

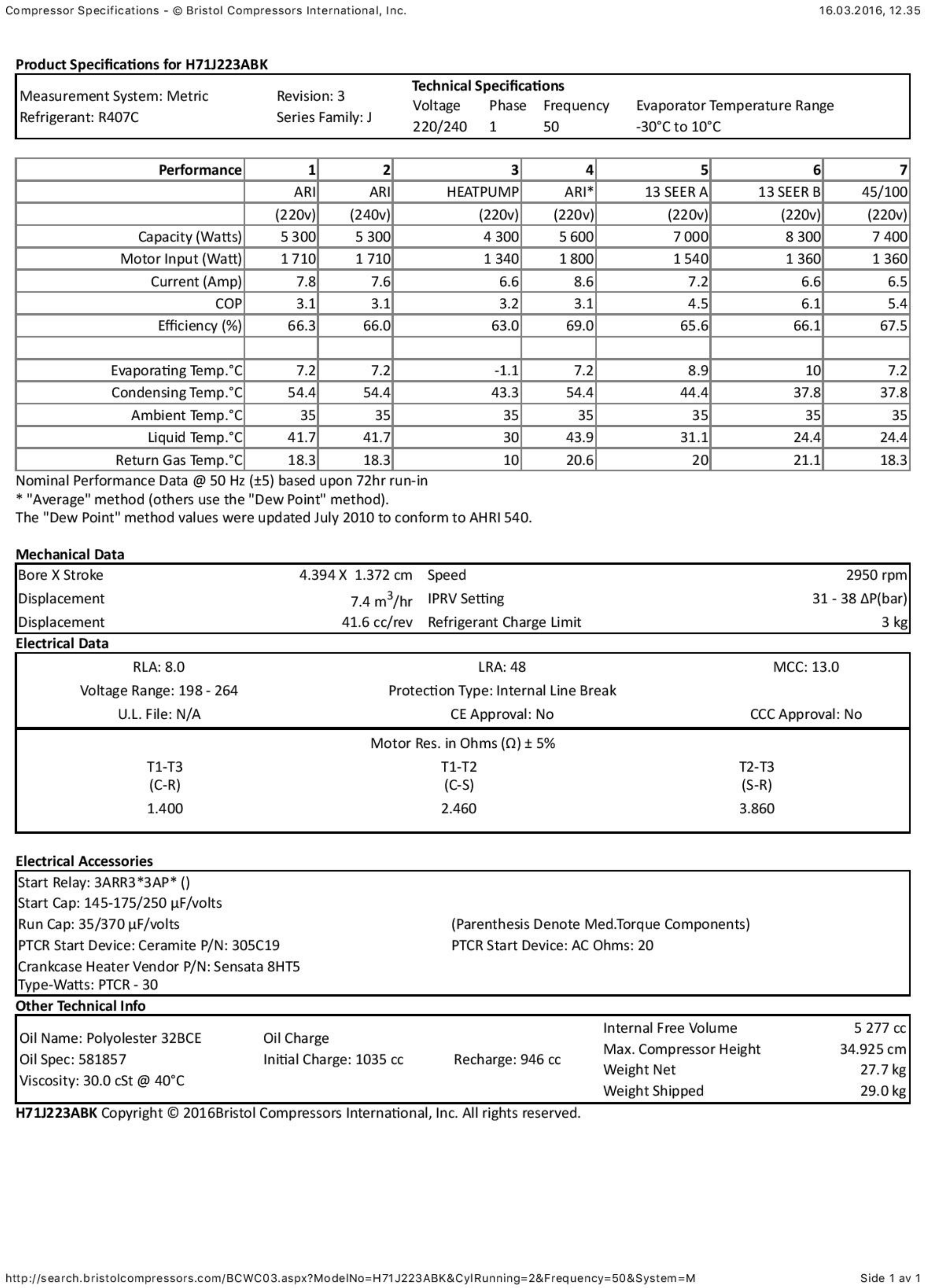

Compressor Specifications - © Bristol Compressors International, Inc. 16.03.2016, 12.35

Product Specifications for H71J223ABK

Measurement System: Metric
Refrigerant: R407C

Revision: 3
Series Family: J

Technical Specifications

Voltage	Phase	Frequency	Evaporator Temperature Range
220/240	1	50	-30°C to 10°C

Performance	1	2	3	4	5	6	7
	ARI	ARI	HEATPUMP	ARI*	13 SEER A	13 SEER B	45/100
	(220v)	(240v)	(220v)	(220v)	(220v)	(220v)	(220v)
Capacity (Watts)	5 300	5 300	4 300	5 600	7 000	8 300	7 400
Motor Input (Watt)	1 710	1 710	1 340	1 800	1 540	1 360	1 360
Current (Amp)	7.8	7.6	6.6	8.6	7.2	6.6	6.5
COP	3.1	3.1	3.2	3.1	4.5	6.1	5.4
Efficiency (%)	66.3	66.0	63.0	69.0	65.6	66.1	67.5
Evaporating Temp.°C	7.2	7.2	-1.1	7.2	8.9	10	7.2
Condensing Temp.°C	54.4	54.4	43.3	54.4	44.4	37.8	37.8
Ambient Temp.°C	35	35	35	35	35	35	35
Liquid Temp.°C	41.7	41.7	30	43.9	31.1	24.4	24.4
Return Gas Temp.°C	18.3	18.3	10	20.6	20	21.1	18.3

Nominal Performance Data @ 50 Hz (±5) based upon 72hr run-in
* "Average" method (others use the "Dew Point" method).
The "Dew Point" method values were updated July 2010 to conform to AHRI 540.

Mechanical Data

Bore X Stroke	4.394 X 1.372 cm	Speed	2950 rpm
Displacement	7.4 m^3/hr	IPRV Setting	31 - 38 ΔP(bar)
Displacement	41.6 cc/rev	Refrigerant Charge Limit	3 kg

Electrical Data

RLA: 8.0	LRA: 48	MCC: 13.0
Voltage Range: 198 - 264	Protection Type: Internal Line Break	
U.L. File: N/A	CE Approval: No	CCC Approval: No

Motor Res. in Ohms (Ω) ± 5%

T1-T3 (C-R)	T1-T2 (C-S)	T2-T3 (S-R)
1.400	2.460	3.860

Electrical Accessories

Start Relay: 3ARR3*3AP* ()
Start Cap: 145-175/250 µF/volts
Run Cap: 35/370 µF/volts
PTCR Start Device: Ceramite P/N: 305C19
Crankcase Heater Vendor P/N: Sensata 8HT5
Type-Watts: PTCR - 30

(Parenthesis Denote Med.Torque Components)
PTCR Start Device: AC Ohms: 20

Other Technical Info

Oil Name: Polyolester 32BCE
Oil Spec: 581857
Viscosity: 30.0 cSt @ 40°C

Oil Charge
Initial Charge: 1035 cc
Recharge: 946 cc

Internal Free Volume	5 277 cc
Max. Compressor Height	34.925 cm
Weight Net	27.7 kg
Weight Shipped	29.0 kg

H71J223ABK Copyright © 2016Bristol Compressors International, Inc. All rights reserved.

http://search.bristolcompressors.com/BCWC03.aspx?ModelNo=H71J223ABK&CylRunning=2&Frequency=50&System=M Side 1 av 1

C OSO Hotwater Optima Triple Coil - EPTRC 400

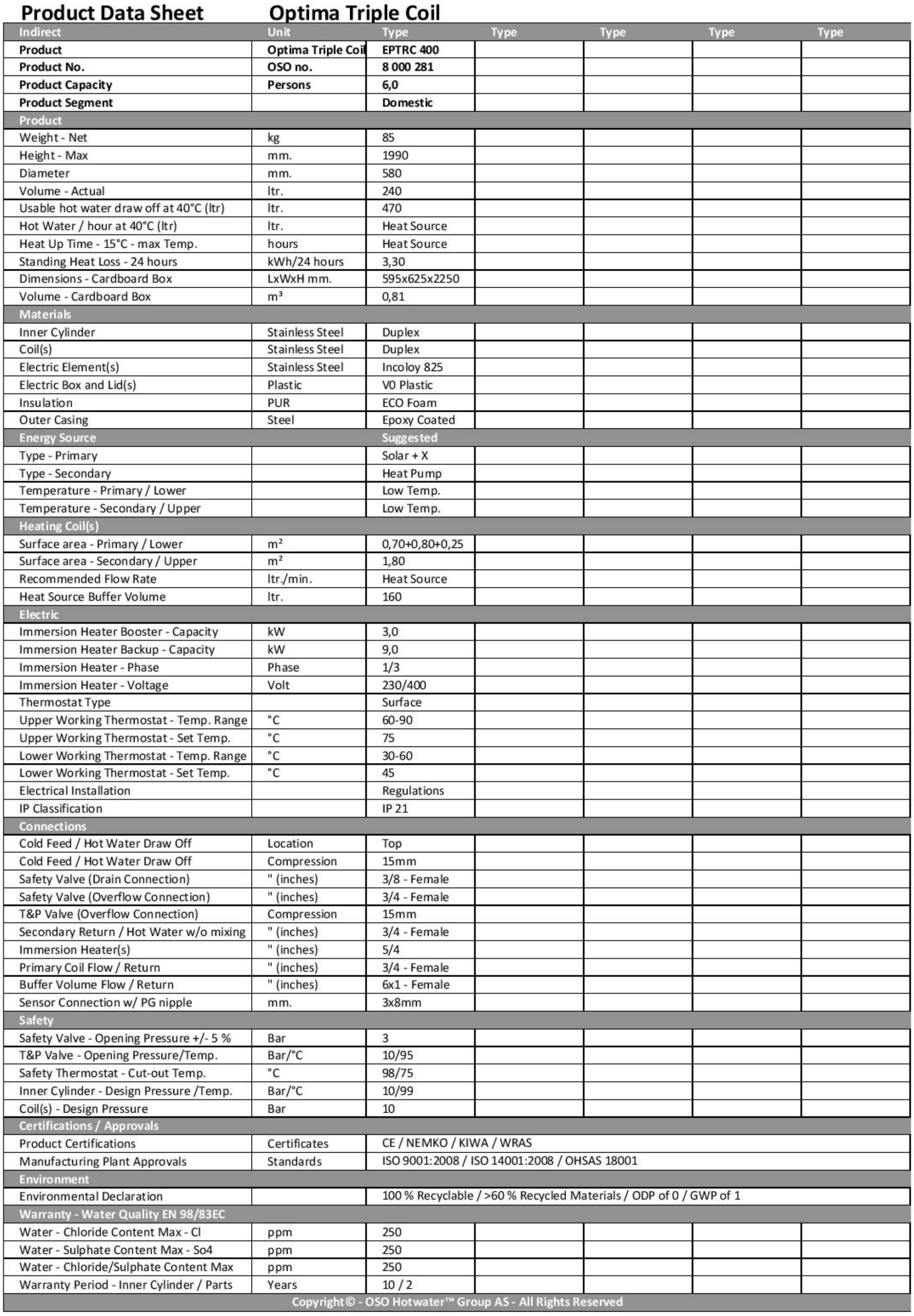

Product Data Sheet **Optima Triple Coil**

Indirect	Unit	Type	Type	Type	Type	Type
Product	**Optima Triple Coil**	**EPTRC 400**				
Product No.	**OSO no.**	**8 000 281**				
Product Capacity	**Persons**	**6,0**				
Product Segment		**Domestic**				
Product						
Weight - Net	kg	85				
Height - Max	mm.	1990				
Diameter	mm.	580				
Volume - Actual	ltr.	240				
Usable hot water draw off at 40°C (ltr)	ltr.	470				
Hot Water / hour at 40°C (ltr)	ltr.	Heat Source				
Heat Up Time - 15°C - max Temp.	hours	Heat Source				
Standing Heat Loss - 24 hours	kWh/24 hours	3,30				
Dimensions - Cardboard Box	LxWxH mm.	595x625x2250				
Volume - Cardboard Box	m^3	0,81				
Materials						
Inner Cylinder	Stainless Steel	Duplex				
Coil(s)	Stainless Steel	Duplex				
Electric Element(s)	Stainless Steel	Incoloy 825				
Electric Box and Lid(s)	Plastic	V0 Plastic				
Insulation	PUR	ECO Foam				
Outer Casing	Steel	Epoxy Coated				
Energy Source		Suggested				
Type - Primary		Solar + X				
Type - Secondary		Heat Pump				
Temperature - Primary / Lower		Low Temp.				
Temperature - Secondary / Upper		Low Temp.				
Heating Coil(s)						
Surface area - Primary / Lower	m^2	0,70+0,80+0,25				
Surface area - Secondary / Upper	m^2	1,80				
Recommended Flow Rate	ltr./min.	Heat Source				
Heat Source Buffer Volume	ltr.	160				
Electric						
Immersion Heater Booster - Capacity	kW	3,0				
Immersion Heater Backup - Capacity	kW	9,0				
Immersion Heater - Phase	Phase	1/3				
Immersion Heater - Voltage	Volt	230/400				
Thermostat Type		Surface				
Upper Working Thermostat - Temp. Range	°C	60-90				
Upper Working Thermostat - Set Temp.	°C	75				
Lower Working Thermostat - Temp. Range	°C	30-60				
Lower Working Thermostat - Set Temp.	°C	45				
Electrical Installation		Regulations				
IP Classification		IP 21				
Connections						
Cold Feed / Hot Water Draw Off	Location	Top				
Cold Feed / Hot Water Draw Off	Compression	15mm				
Safety Valve (Drain Connection)	" (inches)	3/8 - Female				
Safety Valve (Overflow Connection)	" (inches)	3/4 - Female				
T&P Valve (Overflow Connection)	Compression	15mm				
Secondary Return / Hot Water w/o mixing	" (inches)	3/4 - Female				
Immersion Heater(s)	" (inches)	5/4				
Primary Coil Flow / Return	" (inches)	3/4 - Female				
Buffer Volume Flow / Return	" (inches)	6x1 - Female				
Sensor Connection w/ PG nipple	mm.	3x8mm				
Safety						
Safety Valve - Opening Pressure +/- 5 %	Bar	3				
T&P Valve - Opening Pressure/Temp.	Bar/°C	10/95				
Safety Thermostat - Cut-out Temp.	°C	98/75				
Inner Cylinder - Design Pressure /Temp.	Bar/°C	10/99				
Coil(s) - Design Pressure	Bar	10				
Certifications / Approvals						
Product Certifications	Certificates	CE / NEMKO / KIWA / WRAS				
Manufacturing Plant Approvals	Standards	ISO 9001:2008 / ISO 14001:2008 / OHSAS 18001				
Environment						
Environmental Declaration		100 % Recyclable / >60 % Recycled Materials / ODP of 0 / GWP of 1				
Warranty - Water Quality EN 98/83EC						
Water - Chloride Content Max - Cl	ppm	250				
Water - Sulphate Content Max - So4	ppm	250				
Water - Chloride/Sulphate Content Max	ppm	250				
Warranty Period - Inner Cylinder / Parts	Years	10 / 2				

Copyright© - OSO Hotwater™ Group AS - All Rights Reserved

D Working Fluids Comparison

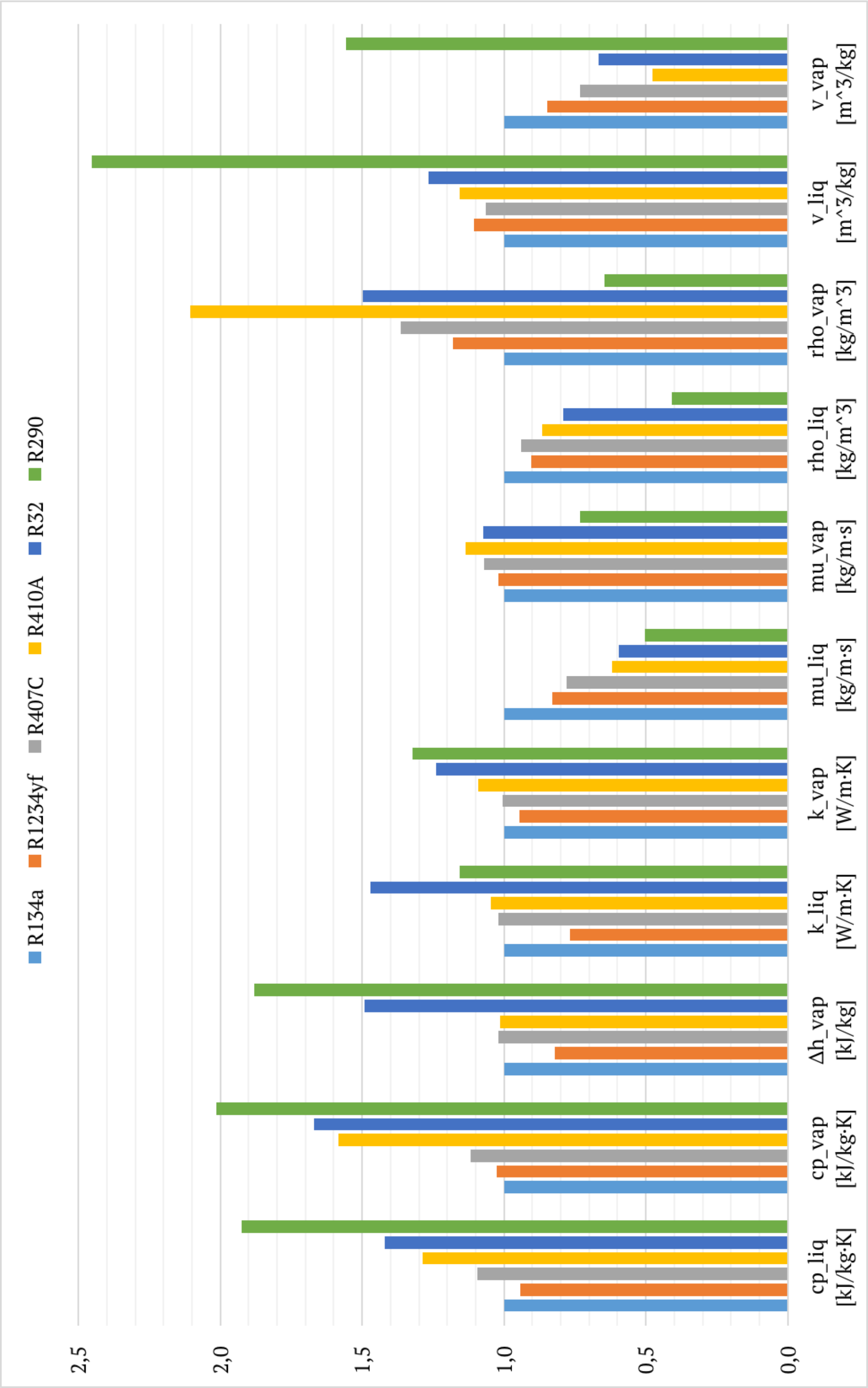

Figure 1: Relative thermophysical properties of subcritical working fluids.

E Smedegaard Pump Characteristics

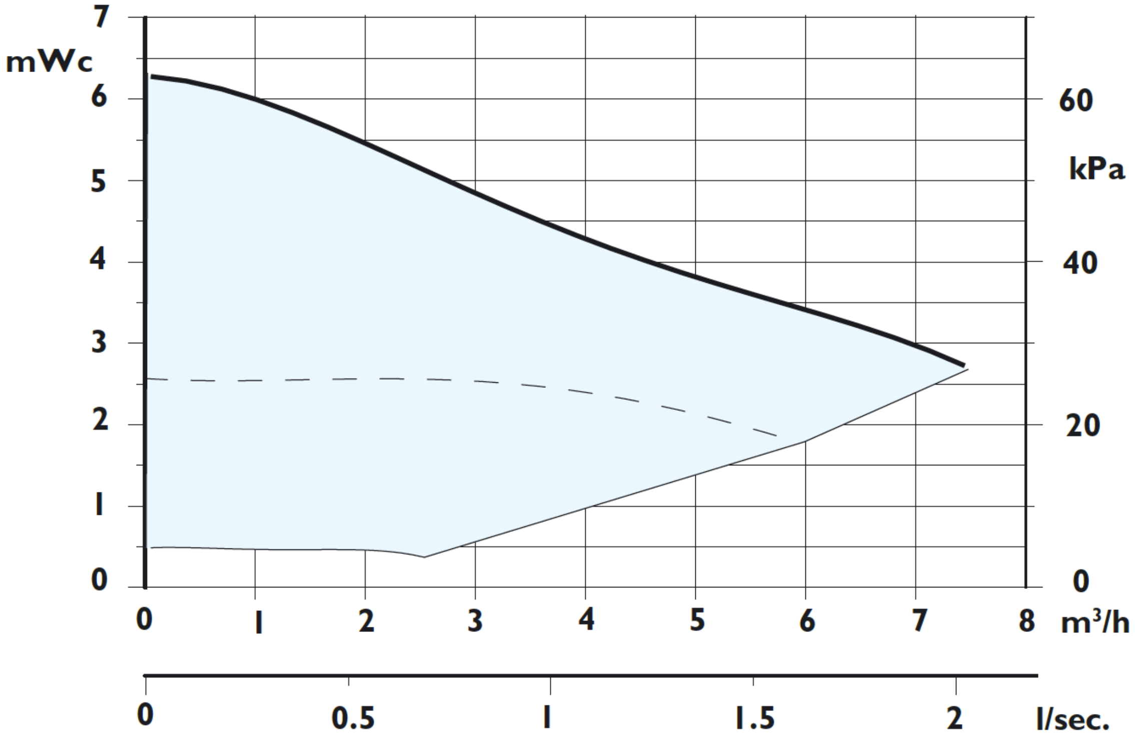

(a) Magneta 25-60.

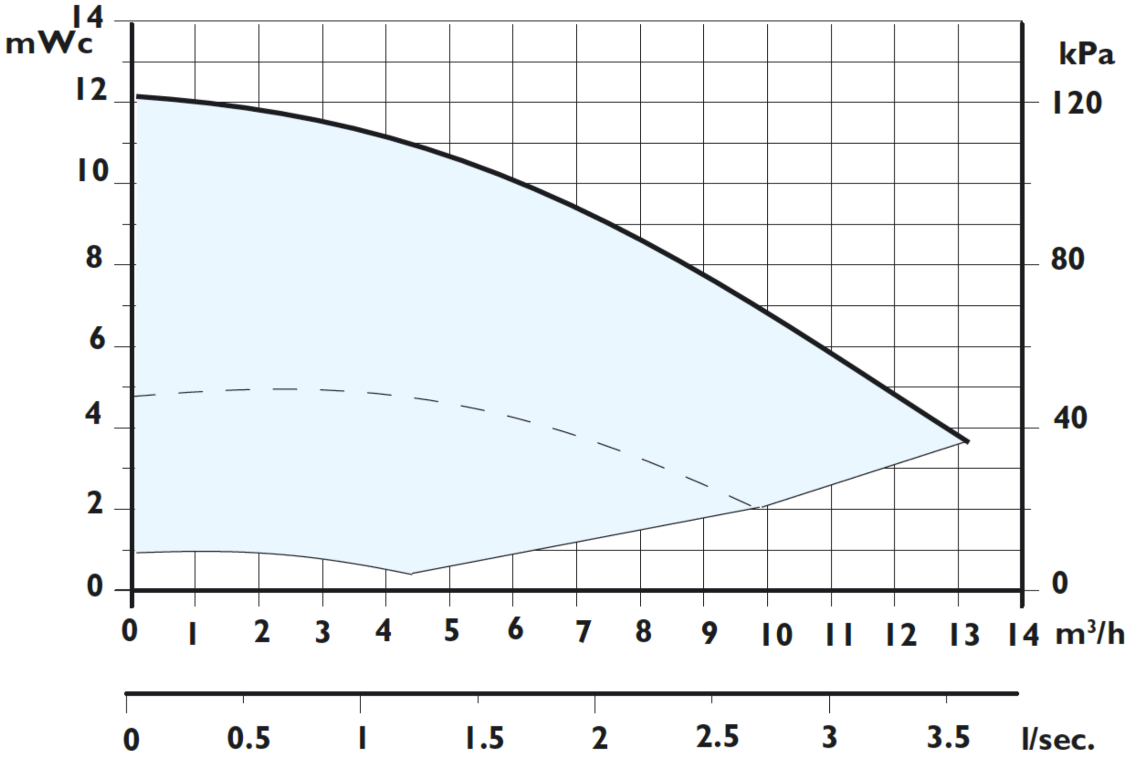

(b) Magneta 32-120.

Figure 2: Pump characteristics for the Magneta circulation pumps.

F Hewalex KS2000 SP Solar Keymark Certification

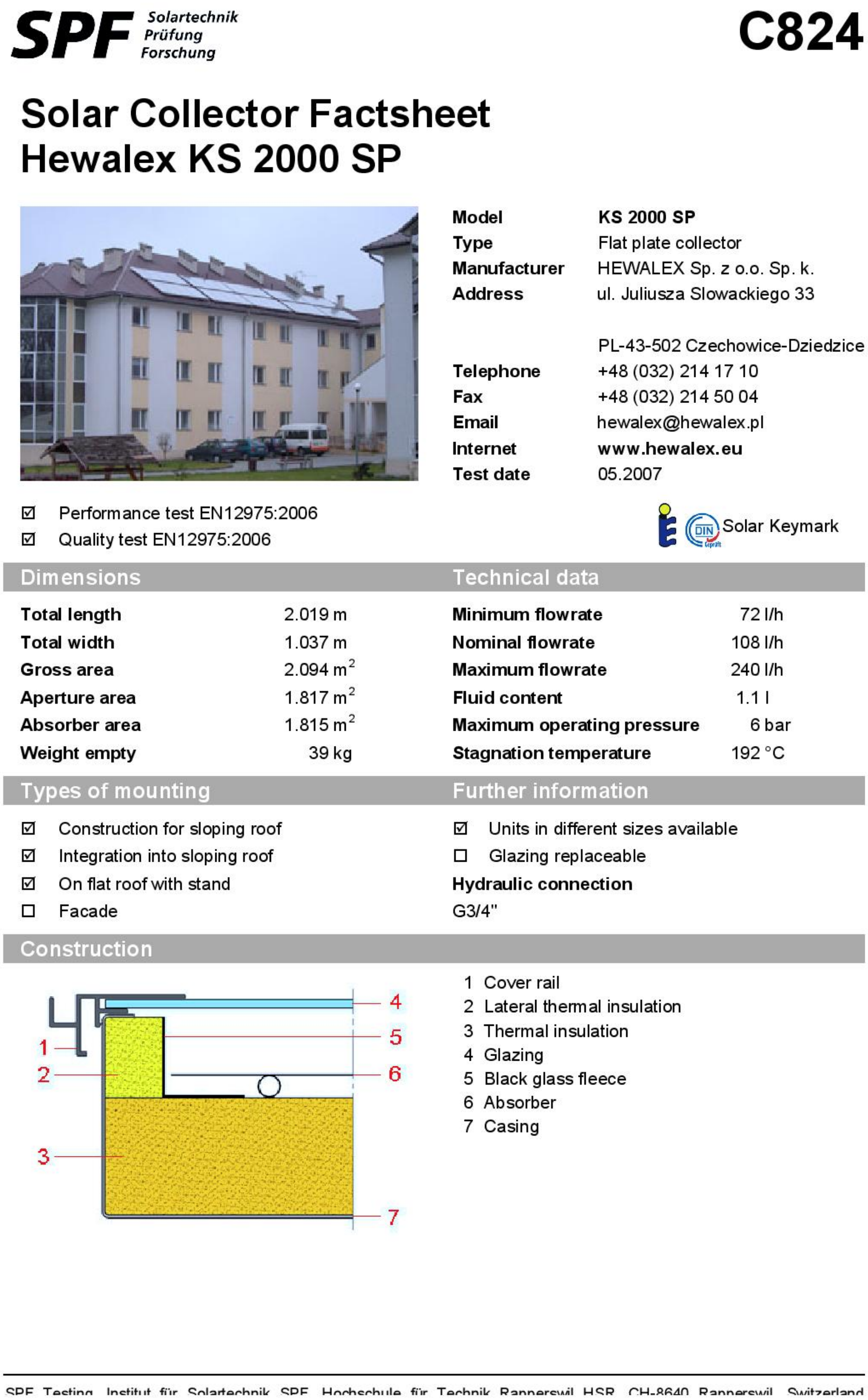

SPF Solartechnik Prüfung Forschung

C824

Solar Collector Factsheet
Hewalex KS 2000 SP

Model	**KS 2000 SP**
Type	Flat plate collector
Manufacturer	HEWALEX Sp. z o.o. Sp. k.
Address	ul. Juliusza Slowackiego 33 PL-43-502 Czechowice-Dziedzice
Telephone	+48 (032) 214 17 10
Fax	+48 (032) 214 50 04
Email	hewalex@hewalex.pl
Internet	**www.hewalex.eu**
Test date	05.2007

☑ Performance test EN12975:2006

☑ Quality test EN12975:2006

Solar Keymark

Dimensions

Total length	2.019 m
Total width	1.037 m
Gross area	2.094 m^2
Aperture area	1.817 m^2
Absorber area	1.815 m^2
Weight empty	39 kg

Technical data

Minimum flowrate	72 l/h
Nominal flowrate	108 l/h
Maximum flowrate	240 l/h
Fluid content	1.1 l
Maximum operating pressure	6 bar
Stagnation temperature	192 °C

Types of mounting

☑ Construction for sloping roof

☑ Integration into sloping roof

☑ On flat roof with stand

☐ Facade

Further information

☑ Units in different sizes available

☐ Glazing replaceable

Hydraulic connection

G3/4"

Construction

1 Cover rail
2 Lateral thermal insulation
3 Thermal insulation
4 Glazing
5 Black glass fleece
6 Absorber
7 Casing

SPF Testing, Institut für Solartechnik SPF, Hochschule für Technik Rapperswil HSR, CH-8640 Rapperswil, Switzerland

SPF Solartechnik Prüfung Forschung

C824

Solar Collector Factsheet Hewalex KS 2000 SP

Model	**KS 2000 SP**
Type	Flat plate collector
Manufacturer	HEWALEX Sp. z o.o. Sp. k.
Address	ul. Juliusza Slowackiego 33 PL-43-502 Czechowice-Dziedzice
Telephone	+48 (032) 214 17 10
Fax	+48 (032) 214 50 04
Email	hewalex@hewalex.pl
Internet	**www.hewalex.eu**
Test date	05.2007

☑ Performance test EN12975:2006

☑ Quality test EN12975:2006

Solar Keymark

Dimensions

Total length	2.019 m
Total width	1.037 m
Gross area	2.094 m^2
Aperture area	1.817 m^2
Absorber area	1.815 m^2
Weight empty	39 kg

Technical data

Minimum flowrate	72 l/h
Nominal flowrate	108 l/h
Maximum flowrate	240 l/h
Fluid content	1.1 l
Maximum operating pressure	6 bar
Stagnation temperature	192 °C

Types of mounting

☑ Construction for sloping roof

☑ Integration into sloping roof

☑ On flat roof with stand

☐ Facade

Further information

☑ Units in different sizes available

☐ Glazing replaceable

Hydraulic connection

G3/4"

Construction

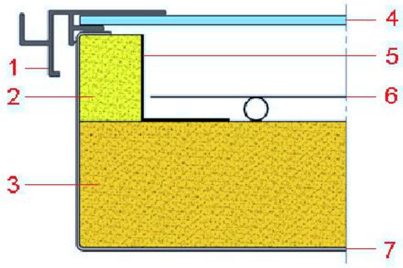

1 Cover rail
2 Lateral thermal insulation
3 Thermal insulation
4 Glazing
5 Black glass fleece
6 Absorber
7 Casing

G Additional Field Measurements

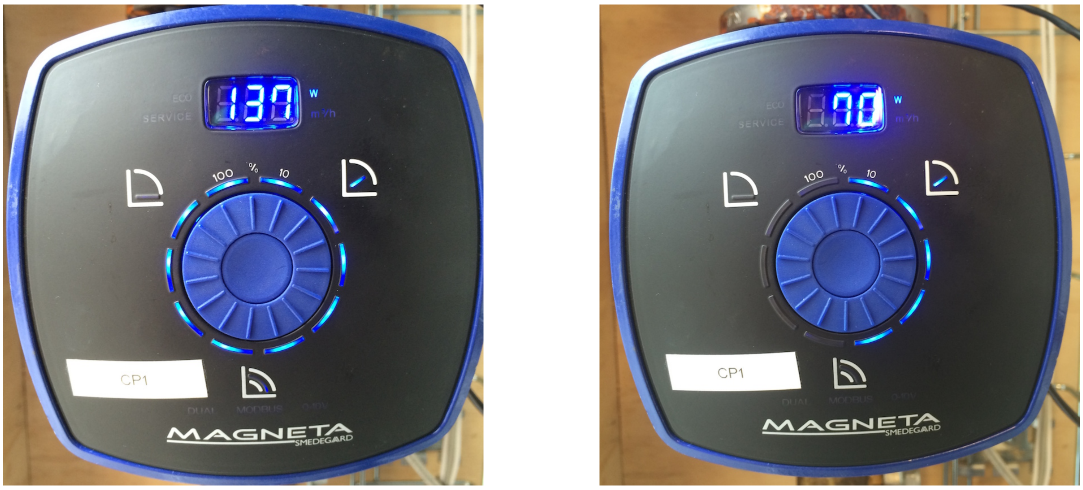
130
W
CP1
MAGNETA
90
W
CP1
MAGNETA

(a) CP1 - 100 %.

(b) CP1 - 50 %.

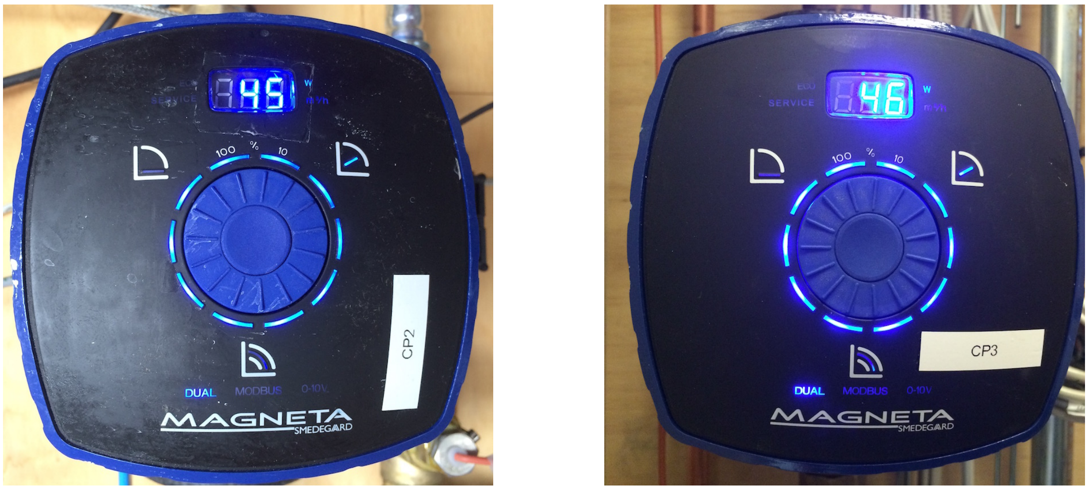
45
W
CP2
DUAL
MAGNETA
46
W
CP3
DUAL
MAGNETA

(c) CP2 - 100 %.

(d) CP3 - 50 %.

Figure 3: Circulator pump power use: 2x 60 min test.

Table 1: External measurements and readings - 2x 60 min test.

	p_E $[bar_g]$	p_C $[bar_g]$	$\dot{V}_b$ $[l/h]$	$\dot{V}_w$ $[l/h]$	$\dot{W}_{CP1}$ $[W]$	$\dot{W}_{CP2}$ $[W]$	$\dot{W}_{CP3}$ $[W]$
Series A	1.60	9.40	918	335	84.7	44.0	45.8
Series B	1.51	11.15	803	350	68.5	43.5	45.8

Table 2: DAQ recordings - 2x 60 min test.

	$\dot{V}_b$ $[l/h]$	$\dot{V}_w$ $[l/h]$	ΔT_b $[K]$	ΔT_w $[K]$	$\dot{Q}_w$ $[W]$	$\dot{W}_{HP}$ $[W]$	$\dot{W}_{CP1}$ $[W]$	$\dot{W}_{CP2/3}$ $[W]$
0 - 60 min	872	384	1.9	6.3	2591	904	115	136
60 - 120 min	636	386	2.0	5.7	2414	892	74	134

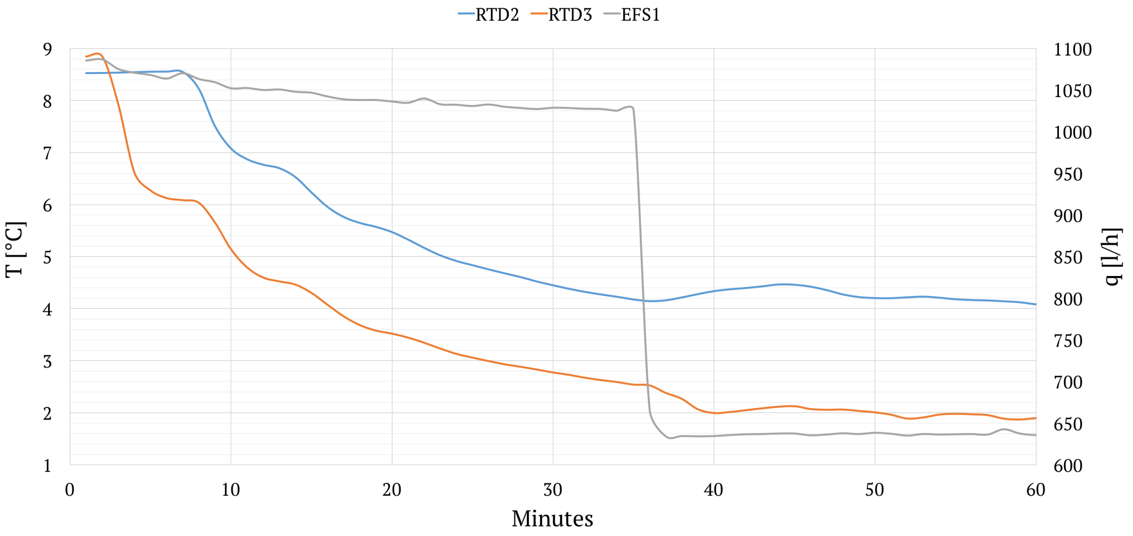

Figure 4: Brine circuit temperature and flow development: 0 - 60 min.

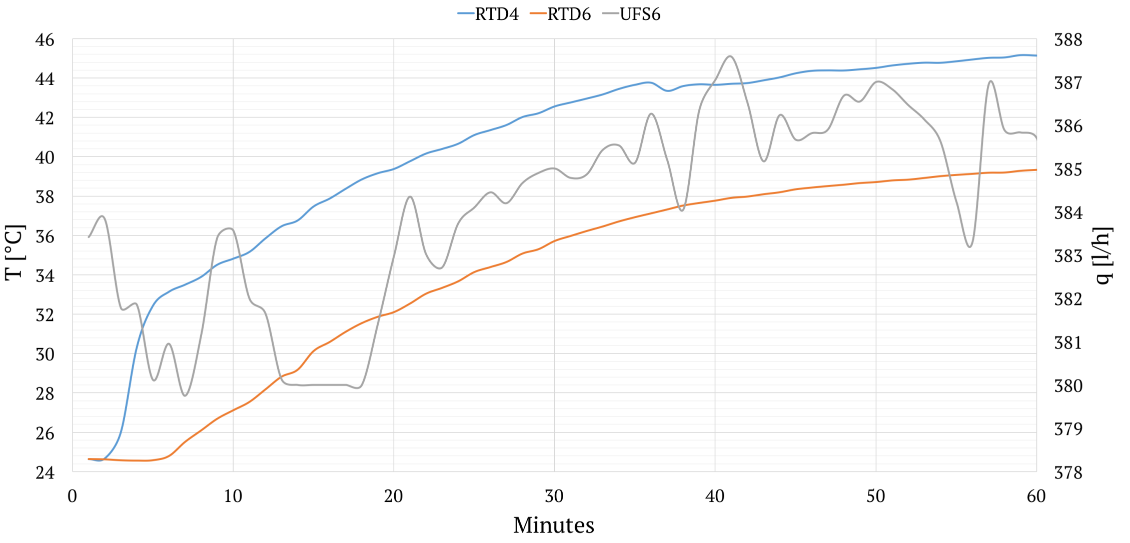

Figure 5: Water circuit temperature and flow development: 0 - 60 min.

Table 3: Performance measurements: 2x 60 min test.

	ε_{Carnot}	COP	COP_{CP1}	$COP_{CP1/2/3}$
Series A	8.93	3.07	2.73	2.41
Series B	7.41	2.70	2.35	2.19

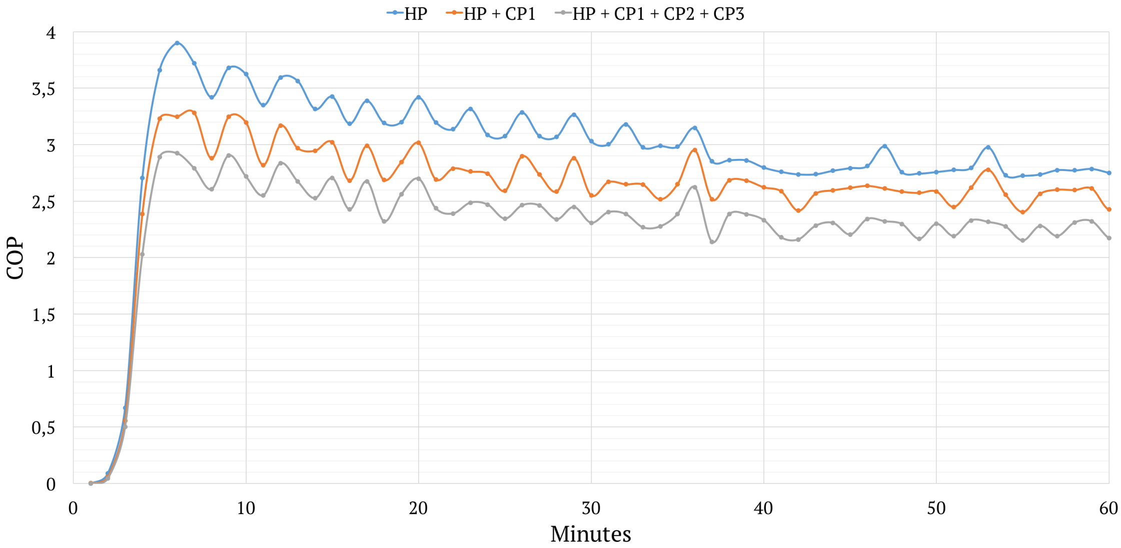

Figure 6: COP development: 0 - 60 min.

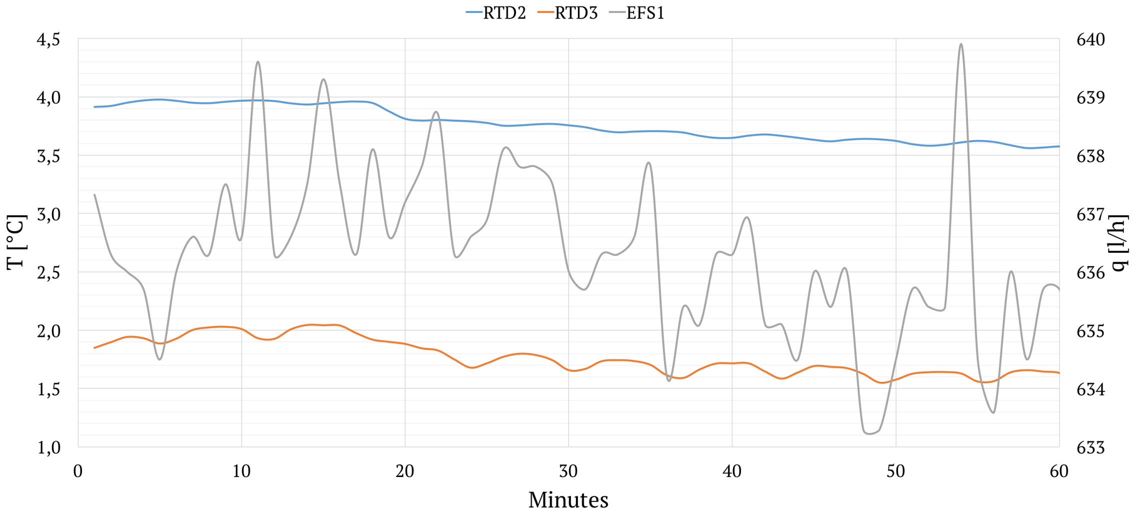

Figure 7: Brine circuit temperature and flow development: 60 - 120 min.

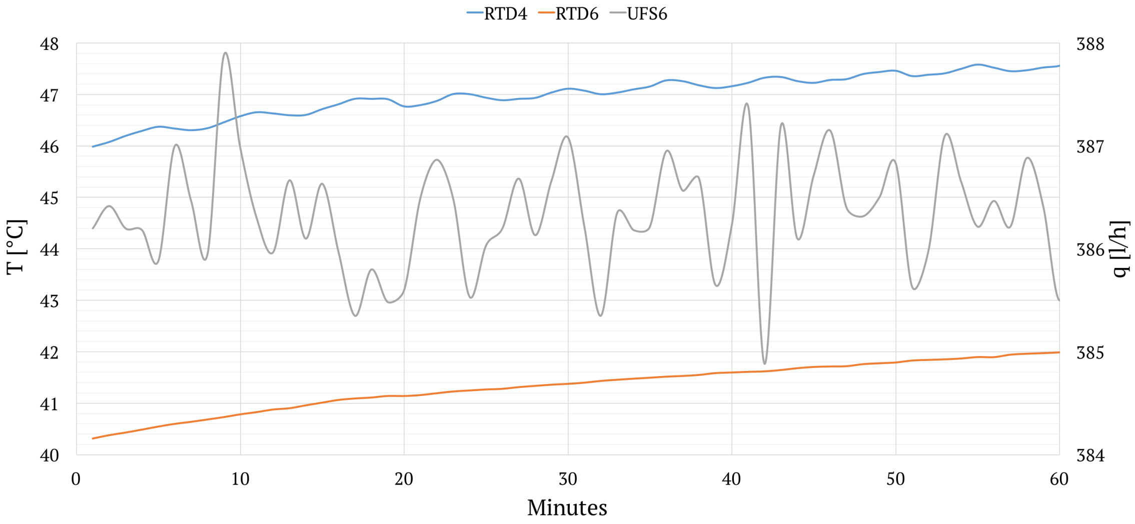

Figure 8: Water circuit temperature and flow development: 60 - 120 min.

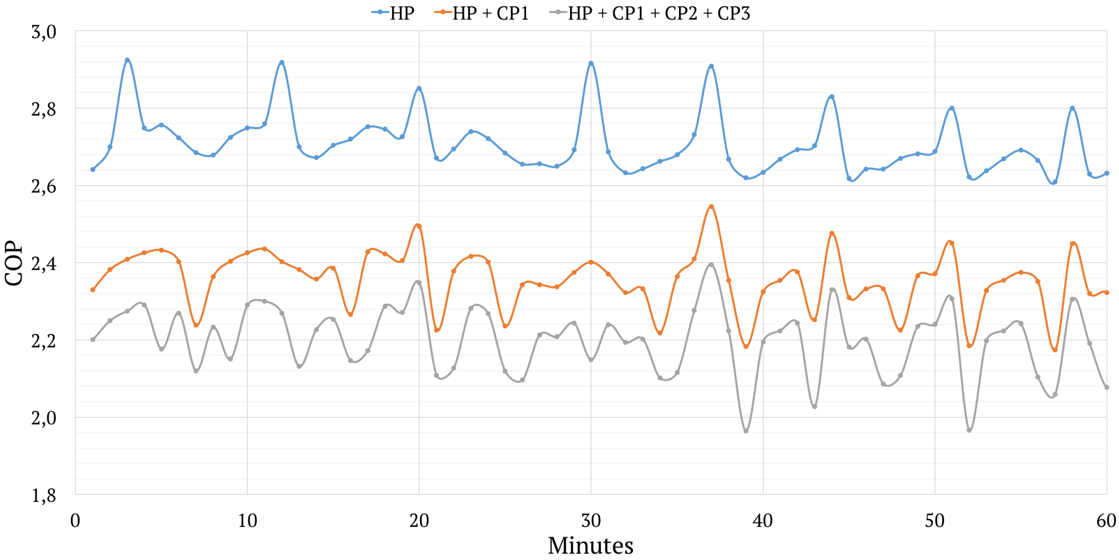

Figure 9: COP development: 60 - 120 min.

H DAQ Measuring Data

Table 4: Average temperatures and total circulated volumes.

		22.03-31.03	08.04-17.04
HP Ground Collector			
RTD2	[°C]	-1.0	-0.3
RTD3	[°C]	-1.9	-1.4
EFS1	[m^3]	211.84	223.77
HP water circuit			
RTD4	[°C]	40.9	39.4
RTD6	[°C]	36.9	35.0
UFS2	[m^3]	60.95	64.09
Integrated water tank			
RTD9	[°C]	32.4	28.6
RTD10	[°C]	41.6	42.7
RTD11	[°C]	42.2	42.0
RTD12	[°C]	68.1	68.2
Floor heating circuits			
RTD20	[°C]	36.3	38.1
RTD21	[°C]	33.4	35.5
UFS7	[m^3]	51.81	72.03
RTD22	[°C]	39.6	37.9
RTD23	[°C]	33.8	33.2
UFS8	[m^3]	4.43	4.94
RTD24	[°C]	35.3	34.6
UFS9	[m^3]	10.58	6.40
Solar thermal circuit			
RTD25	[°C]	42.1	40.4
RTD26	[°C]	49.8	47.2
EFS2	[m^3]	-	-
Ventilation			
TRHT1	[°C]	5.7	4.9
TRHT2	[°C]	11.1	11.0
TRHT3	[°C]	22.1	21.9
TRHT5	[°C]	21.8	23.8

Table 5: Outdoor and indoor thermal environment.

	22.03-31.03 [°C]	08.04-17.04 [°C]
Outdoor environment		
Weather station	4.4	3.4
South façade	5.1	5.4
North façade	4.2	3.4
Indoor environment		
Living room south and kitchen	21.7	23.7
Living room north	21.1	23.0
Bedroom west	21.7	23.5
Bedroom east	20.3	19.7
Bathroom	21.8	23.9

I Ground Collector Performance

ø32x2,0	C_PG	44	%	t_freeze	-24,64	°C		
V_dot_PG	V_avg	Re	h	U	U·A	Δp	W_CP1	(U·A)/W_CP1
[m^3/h]	[m/s]	[-]	[W/m^2K]	[W/m^2K]	[W/K]	[Pa]	[W]	[-]
1	0,5	1125,0	58,3	40,7	475,2	22673,0	25,2	18,9
1,1	0,5	1237,0	58,3	40,7	475,2	24940,0	30,5	15,6
1,2	0,5	1350,0	58,3	40,7	475,2	27208,0	36,3	13,1
1,3	0,6	1462,0	58,3	40,7	475,2	29475,0	42,6	11,2
1,4	0,6	1575,0	58,3	40,7	475,2	31742,0	49,4	9,6
1,5	0,7	1687,0	58,3	40,7	475,2	34010,0	56,7	8,4
1,6	0,7	1800,0	58,3	40,7	475,2	36277,0	64,5	7,4
1,7	0,8	1912,0	58,3	40,7	475,2	38544,0	72,8	6,5
1,8	0,8	2025,0	58,3	40,7	475,2	40812,0	81,6	5,8
1,9	0,9	2137,0	58,3	40,7	475,2	43079,0	90,9	5,2

ø32x2,0	V_dot	0,000283	m^3/s	v_avg	0,459	m/s		
C_PG	T_freeze	Re	h	U	U·A	Δp	W_CP1	(U·A)/W_CP1
[%]	[°C]	[-]	[W/m^2K]	[W/m^2K]	[W/K]	[Pa]	[W]	[-]
5	-1,2	6548,0	1355,0	122,3	1429,7	13814,0	15,6	91,5
10	-2,9	5380,0	1148,0	120,3	1406,3	14708,0	16,6	84,6
15	-4,9	4386,0	955,3	117,9	1378,3	15731,0	17,8	77,5
20	-7,2	3533,0	773,0	114,5	1338,5	16930,0	19,1	69,9
25	-9,8	2812,0	601,1	109,9	1284,7	18339,0	20,7	62,0
30	-12,8	2219,0	67,2	44,8	523,5	11740,0	13,3	39,4
35	-16,3	1745,0	63,9	43,3	506,3	15004,0	17,0	29,9
40	-20,6	1376,0	60,7	41,8	489,0	19117,0	21,6	22,6
45	-25,8	1094,0	57,7	40,4	471,8	24150,0	27,3	17,3
50	-32,2	879,6	54,7	38,9	454,7	30147,0	34,1	13,3

ø32x2,0	C_EA	44	%	t_freeze	-32,96	°C		
V_dot_EA	V_avg	Re	h	U	U·A	Δp	W_CP1	(U·A)/W_CP1
[m^3/h]	[m/s]	[-]	[W/m^2K]	[W/m^2K]	[W/K]	[Pa]	[W]	[-]
1	0,5	2033,0	52,5	37,7	441,2	11284,0	12,5	35,2
1,1	0,5	2236,0	52,5	37,7	441,2	12412,0	15,2	29,1
1,2	0,5	2439,0	431,2	102,5	1198,2	24527,0	32,7	36,6
1,3	0,6	2643,0	484,9	105,3	1231,0	28015,0	40,5	30,4
1,4	0,6	2846,0	537,6	107,5	1256,7	31696,0	49,3	25,5
1,5	0,7	3049,0	589,4	109,5	1280,1	35567,0	59,3	21,6
1,6	0,7	3252,0	640,5	111,1	1298,8	39623,0	70,4	18,4
1,7	0,8	3456,0	690,9	112,5	1315,1	43862,0	82,9	15,9
1,8	0,8	3659,0	740,6	113,8	1330,3	48282,0	96,6	13,8
1,9	0,9	3862,0	789,8	114,9	1343,2	52880,0	111,6	12,0

ø32x2,0	V_dot	0,000283	m^3/s	v_avg	0,459	m/s		
C_EA	T_freeze	Re	h	U	U·A	Δp	W_CP1	(U·A)/W_CP1
[%]	[°C]	[-]	[W/m^2K]	[W/m^2K]	[W/K]	[Pa]	[W]	[-]
5	-2,0	5997,0	1281,0	121,7	1422,7	13988,0	15,8	90,0
10	-4,4	4502,0	1008,0	118,6	1386,4	15154,0	17,1	80,9
15	-7,4	3511,0	791,1	114,9	1343,2	16303,0	18,4	72,9
20	-11,1	2871,0	626,4	110,7	1294,1	17323,0	19,6	66,1
25	-15,5	2470,0	507,2	106,3	1242,6	18122,0	20,5	60,6
30	-20,1	2231,0	62,3	42,6	497,5	10914,0	12,3	40,3
35	-24,9	2105,0	58,6	40,8	477,0	11477,0	13,0	36,8
40	-29,5	2060,0	55,1	39,1	457,0	11620,0	13,1	34,8
45	-33,8	2075,0	51,8	37,4	437,3	11416,0	12,9	33,9
50	-37,6	2138,0	48,8	35,8	418,3	10955,0	12,4	33,8

ø40x2,4	C_PG	44	%	t_freeze	-24,64	°C		
V_dot_PG	V_avg	Re	h	U	U·A	Δp	W_CP1	(U·A)/W_CP1
[m^3/h]	[m/s]	[-]	[W/m^2K]	[W/m^2K]	[W/K]	[Pa]	[W]	[-]
1	0,3	894,8	46,4	37,1	434,0	9078,0	10,1	43,0
1,1	0,3	984,3	46,4	37,1	434,0	9985,0	12,2	35,6
1,2	0,3	1074,0	46,4	37,1	434,0	10893,0	14,5	29,9
1,3	0,4	1163,0	46,4	37,1	434,0	11801,0	17,1	25,5
1,4	0,4	1253,0	46,4	37,1	434,0	12709,0	19,8	22,0
1,5	0,4	1342,0	46,4	37,1	434,0	13616,0	22,7	19,1
1,6	0,5	1432,0	46,4	37,1	434,0	14524,0	25,8	16,8
1,7	0,5	1521,0	46,4	37,1	434,0	15432,0	29,2	14,9
1,8	0,5	1611,0	46,4	37,1	434,0	16340,0	32,7	13,3
1,9	0,5	1700,0	46,4	37,1	434,0	17247,0	36,4	11,9

ø40x2,4	V_dot	0,000283	m^3/s	v_avg	0,290	m/s		
C_PG	T_freeze	Re	h	U	U·A	Δp	W_CP1	(U·A)/W_CP1
[%]	[°C]	[-]	[W/m^2K]	[W/m^2K]	[W/K]	[Pa]	[W]	[-]
5	-1,2	5209,0	851,9	153,1	1789,7	4708,0	5,3	336,2
10	-2,9	4280,0	712,6	147,9	1729,0	5024,0	5,7	304,4
15	-4,9	3489,0	582,3	141,4	1653,0	5385,0	6,1	271,5
20	-7,2	2810,0	458,5	132,7	1551,3	5810,0	6,6	236,2
25	-9,8	2237,0	56,1	43,1	504,2	3689,0	4,2	120,9
30	-12,8	1765,0	53,4	41,5	485,5	4700,0	5,3	91,4
35	-16,3	1388,0	50,8	40,0	467,0	6007,0	6,8	68,8
40	-20,6	1095,0	48,3	38,4	448,7	7654,0	8,7	51,9
45	-25,8	870,3	45,9	36,8	430,4	9669,0	10,9	39,4
50	-32,2	699,7	43,5	35,3	412,7	12070,0	13,6	30,3

ø40x2,4	C_EA	44	%	t_freeze	-32,96	°C		
V_dot_EA	V_avg	Re	h	U	U·A	Δp	W_CP1	(U·A)/W_CP1
[m^3/h]	[m/s]	[-]	[W/m^2K]	[W/m^2K]	[W/K]	[Pa]	[W]	[-]
1	0,3	1617,0	41,7	34,1	398,9	4518,0	5,0	79,5
1,1	0,3	1779,0	41,7	34,1	398,9	4969,0	6,1	65,7
1,2	0,3	1940,0	41,7	34,1	398,9	5421,0	7,2	55,2
1,3	0,4	2102,0	41,7	34,1	398,9	5873,0	8,5	47,0
1,4	0,4	2264,0	41,7	34,1	398,9	6325,0	9,8	40,5
1,5	0,4	2425,0	340,0	120,5	1408,6	12229,0	20,4	69,1
1,6	0,5	2587,0	374,1	124,5	1455,4	13612,0	24,2	60,1
1,7	0,5	2749,0	407,7	128,0	1496,3	15057,0	28,4	52,6
1,8	0,5	2911,0	440,8	131,1	1532,6	16563,0	33,1	46,3
1,9	0,5	3072,0	473,5	133,9	1565,3	18129,0	38,3	40,9

ø40x2,4	V_dot	0,000283	m^3/s	v_avg	0,290	m/s		
C_EA	T_freeze	Re	h	U	U·A	Δp	W_CP1	(U·A)/W_CP1
[%]	[°C]	[-]	[W/m^2K]	[W/m^2K]	[W/K]	[Pa]	[W]	[-]
5	-2,0	4770,0	801,4	151,4	1769,9	4772,0	5,4	328,1
10	-4,4	3582,0	616,3	143,3	1675,2	5186,0	5,9	285,7
15	-7,4	2793,0	468,7	133,5	1560,6	5596,0	6,3	246,7
20	-11,1	2284,0	55,9	43,0	502,7	3437,0	3,9	129,4
25	-15,5	1964,0	52,6	41,1	479,9	3973,0	4,5	106,9
30	-20,1	1775,0	49,5	39,1	457,5	4370,0	4,9	92,6
35	-24,9	1674,0	46,6	37,3	435,9	4595,0	5,2	83,9
40	-29,5	1639,0	43,8	35,5	415,0	4652,0	5,3	78,9
45	-33,8	1651,0	41,2	33,8	394,8	4571,0	5,2	76,4
50	-37,6	1701,0	38,8	32,1	375,4	4386,0	5,0	75,7

J Alternative System Designs

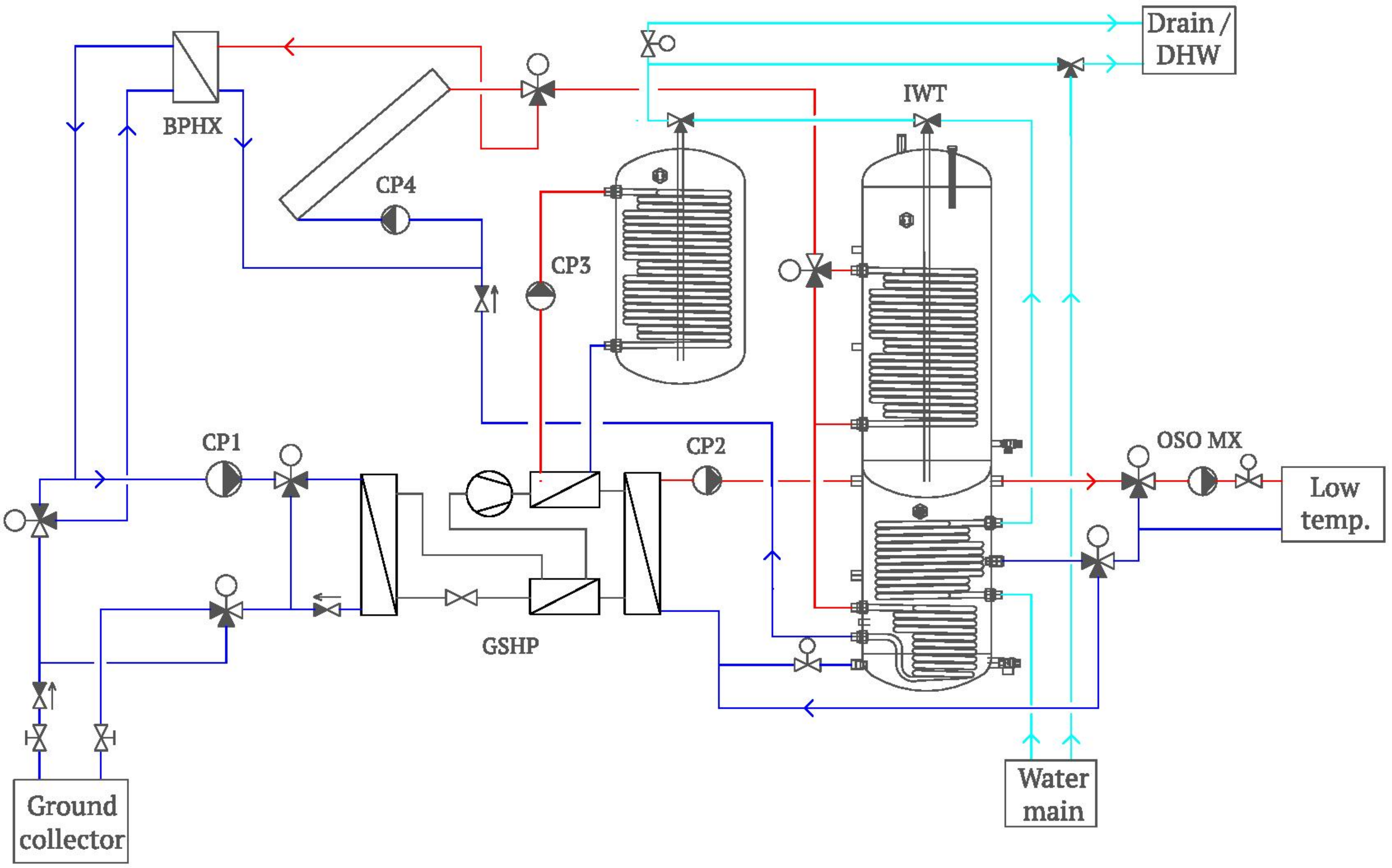
Drain /
DHW
IWT
BPHX
CP4
CP3
CP1
CP2
OSO MX
Low
temp.
GSHP
Ground
collector
Water
main

Figure 10: Principle flow-scheme of system design option 1.

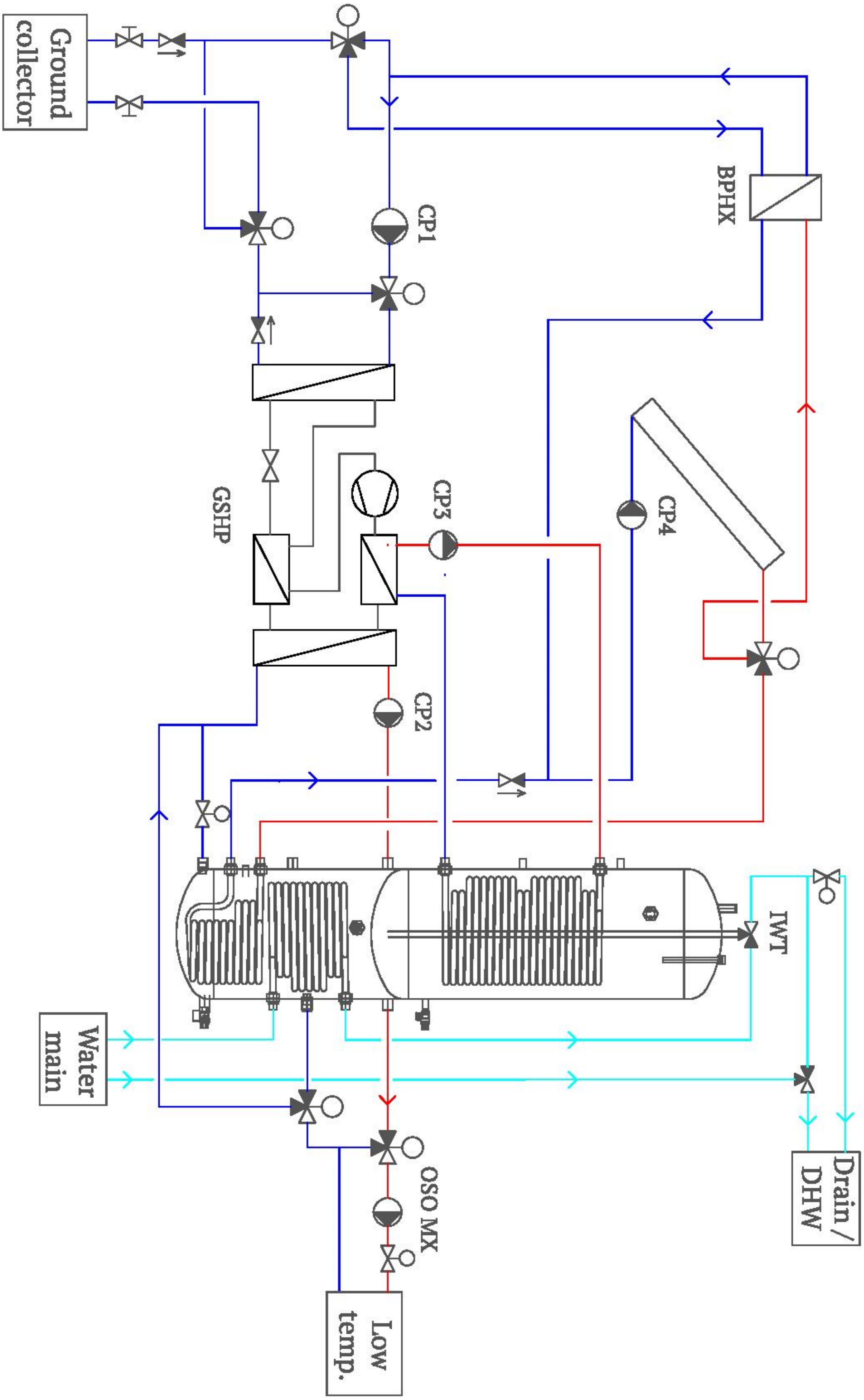
Ground collector
BPHX
CP1
GSHP
CP3
CP4
CP2
IWT
Water main
Drain / DHW
OSO MX
Low temp.

Figure 11: Principle flow-scheme of system design option 2.